INSTITUTO TECNOLÓGICO Y DE ESTUDIOS SUPERIORES
DE MONTERREY
MONTERREY CAMPUS

DOCTORATE PROGRAM IN ENGINEERING

INTELLIGENT MONITORING AND SUPERVISORY CONTROL SYSTEM IN PERIPHERAL MILLING PROCESS IN HIGH SPEED MACHINING

THESIS

PRESENTED AS A PARTIAL FULFILLMENT OF THE REQUIREMENTS
FOR THE DEGREE OF:
Ph. D. ENGINEERING SCIENCES

BY

ANTONIO JR. VALLEJO GUEVARA

MONTERREY, NUEVO LEÓN, MÉXICO, NOVEMBER 2009

INTELLIGENT MONITORING AND SUPERVISORY CONTROL SYSTEM IN PERIPHERAL MILLING PROCESS IN HIGH SPEED MACHINING

BY:

Antonio Jr. Vallejo Guevara

THESIS

Presented to the Doctorate Program in Engineering

This thesis is a partial requirement for the degree of

Doctor of Philosophy in

Engineering Sciences

INSTITUTO TECNOLÓGICO Y DE ESTUDIOS SUPERIORES DE MONTERREY

November 2009

Acknowledgements

I would first of all like to thank my advisor Dr. Rubén Morales Menéndez for permitting me opportunity to work in this interesting and motivate project.

I truly appreciate all his encouragement, guidance and the enormous and unconditional support given during the research and especially when I was writing my thesis. Working in such a challenging project under his supervision has indeed been very inspiring and enriching for my professional and academic life.

Special thanks to Dr. José Ramón Alique for all the support given during my research stance at the Instituto de Automática Industrial in Madrid, Spain. His vast experience and knowledge in the subject were fundamental for completing the project and achieving the proposed goals.

I am thankful to Dr. Arturo Nolazco and Dr. Luis Enrique Sucar Succar for their support as advisors during the experimentation and for their recommendations to apply Artificial Intelligence algorithms in the machining processes.

Also, I want to thank Dr. Ciro Rodríguez, Dr. Ricardo Ramírez, Dr. Luis Garza Castañon and Dr. Alex Elías as my professors in the graduate program in the University. The acquired knowledge in their subjects was relevant and important in my research.

I wish to express my grateful to the ITESM Campus Laguna and his director Andrés Sotomayor Reyes for the opportunity and support given to complete this graduate program.

I am really thankful to Miguel Ramírez for his knowledge and recommendations given me to develop and complete this research. Also, I want to thank my friends in Instituto de Automática Industrial, especially to Maritza, Agustín, Julian, Rodolfo, Raúl, Fernando, Adriana, Diego, and Bruno for giving me the motivation and support to finish this important project in my life.

Finally, I want to express my grateful to Good for giving me the opportunity, health and who has made all this possible.

Dedication

This thesis is dedicated to my wife Lilia, my daughter Kenia, and my sons Samir and Omar, for their support and encourage, and because they were patient during all the time that I was working in my research and thesis.

Abstract

This research is leading to solve a real problem in High Speed Machining processes (*HSM*), specifically in the peripheral milling process. Nowadays, the machining processes have increased their complexity by considering the *HSM*, because of the high dimensional precision, high surface quality, and the minimum cost in the demanded products.

The general scope of this research is: Design and implement an intelligent monitoring and supervisory control system for peripheral milling process in *HSM*. The main objectives of this research are defined as follows:

- Implement a general model to predict the surface roughness by considering several aluminium alloys, cutting parameters, geometries, and cutting tools.
- Design and implement a monitoring and diagnosis system for the cutting tool wear condition during the machining process.
- Design and develop an intelligent process planning system, which includes a merit variable to compute the optimal cutting parameters and a decision-making module to recommend some actions in agreement with the cutting tool wear condition.

The design and implementation of the system implied to make research, exhaust experiments, and write several papers to validate the proposal ideas and algorithms. The main contributions can be summarized as follows:

- A complete data acquisition system was implemented in a machining center HS-1000 Kondia. Several sensors were installed to characterize the surface roughness (R_a) and flank wear of the cutting tool with the process state variables. The Mel Frequency Cepstrum Coefficients (*MFCC*) computed from the process signals were used for modelling the R_a with *ANN* models.
- Related with the R_a modelling, the most important factors affecting the R_a were deduced by applying the screening factorial design. Also, Response Surface Methodology was applied with excellent results for modeling the R_a. The models were computed for a new, half-new, half-worn, and worn cutting tool condition. Multi-sensor and data fusion were used to build *ANN* models with excellent results.
- New ideas based in the Hidden Markov Models (*HMM*) and the *MFCC* were developed for monitoring and diagnosis the cutting tool wear condition for peripheral milling process in *HSM*. The system was implemented for recognizing on-line four cutting tool wear conditions: new, half-new, half-worn, and worn condition.
- The design and implementation of the intelligent monitoring and process planning system (*IMPPS*) represented the main module of the intelligent monitoring and supervisory control system. In this module, Genetic Algorithms with the *RSM* models were used to compute the optimal cutting parameters in *Pre-process* operating mode with excellent results. Another contribution was the implementation of the Markov Decision Process in the optimization process. This algorithm recommends optimal actions for minimizing the operation cost during the production of specific workpieces.

Contents

Nomenclature

Variable	Description	Units
A	Finite set of actions of the operator	–
$A_{i,j}$	The state transition probability distribution	–
Acc	Acceleration	m/s^2
$Acc_{x,sp}$	X-direction acceleration in the spindle	m/s^2
Acc_x	Acceleration in the $x-axis$ of the workpiece	–
$Acc_{y,sp}$	Y-direction acceleration in the spindle	m/s^2
$Acc_{z,sp}$	Z-direction acceleration in the spindle	m/s^2
$Acc_{x,wp}$	X-direction acceleration in workpiece	m/s^2
$Acc_{y,wp}$	Y-direction acceleration in workpiece	m/s^2
a	Number of levels of the factors	–
a	High of the island/box	mm
ae	Radial depth of cut	mm
ap	Axial depth of cut	mm
a_p	Axial depth of cut	mm
a_1	Minimum high of the box geometry	mm
a_2	Maximum high of the box geometry	mm
$a_{1,..,4}$	Actions of the operator	–
B	The observation symbol probability distribution	–
b	Chip width	mm
b	Width of the island/box base	mm
C	Concave path	–
C_C	Cutting conditions	–
$Coef$	Coefficients in the multiple regression	–
$Curv$	Curvature of the machined path	mm^{-1}
c	Cepstrum coefficient number	–
DF	Degrees of freedom	–
D_{tool}	Diameter of the cutting tool	mm

Variable	Description	Units
E	Absolute error	–
e_i	Represent the ith Eigenvector	–
F	Statistical F distribution	–
F_y	Force in the $y - axis$ of the workpiece	N
f	Instantaneous Cost function	–
f	Feed	mm/rev
f_{Hz}	Real frequency scale	Hz
f_{Mel}	Perceive Mel frequency scale	Mels
f_z	Feed per tooth	mm/tooth
HB	Hardness of the workpiece	BHN
I	Convex path	–
k	Number of factors	–
L	Evaluation length	mm
L_t	Length of the arc/line defined by the geometry path	mm
l	Sampling length	mm
l_c	Length of the cut	mm
M	Number of distinct observation symbols per state	–
ME	Average percentage error	$\%$
$MFCC$	Mel Frequency Cepstrum Coefficient	–
MS_E	Mean square value of the errors	$(\mu m)^2$
MS_levels	Mean square value of the levels	$(\mu m)^2$
N	Number of states considered in S	–
N	Number of samples	–
N	Total number of observations	–
N_f	Number of samples in a short frame	–
N_p	Number of filters	–
N_s	Number of states in the *HMM*	–
n	Spindle speed	rpm
n	Number of replicates	–
n_c	Number central runs in the DoE	–
n_c	Number of cycles of the cutting tool edge	–
n_F	Number of runs in the DoE	–
P	Defines the state transition probability distribution function	–
P	Principal components vector	–
P_C	Cutting parameters	–
P_G	Geometric parameters	–
p	Defines the number of components	

Variable	Description	Units
$p-value$	Probability to reject the null hypothesis	–
q_t	Represents the state at time t	–
R	Curvature radio	mm
R	Radio of the concave/convex path	mm
R	Reward function	–
R_a	Surface Roughness or arithmetic average roughness	μm
$R_a^{'}$	Predicted R_a	μm
R_a^d	Desired Surface Roughness	μm
R_a^d	Desired surface roughness	μm
$R_{a,avg}$	Average value of R_a	μm
$R_{a,measured}$	Surface roughness measured	μm
$R_{a,meas}$	Measurement of surface roughness	μm
$R_{a,min}$	Minimum surface roughness	μm
R_a^p	Predicted Surface Roughness	μm
$R_{a,pred}$	Prediction of surface roughness	μm
R_a^p	Predicted surface roughness	μm
$R_{a,obs}$	Observed surface roughness	μm
R_{path}	Radio of the geometry path	mm
R_q	Root mean square value of the Z values within a sampling length	μm
RSm	Mean value of the profile element widths (Xs)	μm
R_{sk}	Skewness	–
R_t	The maximum peak to valley height	μm
R_{tool}	Radio of the cutting tool	mm
R_t	Sum of Z_p and Z_v within the evaluation length	μm
R_z	Sum of Z_p and Z_v within the sampling length	μm
r	Interest rate	–
re	Cutter nose radius	mm
S	Finite set of states in the machining process	–
S	Defines the state space	–
SE	Estimated standard error	–
SS_R	Explained variation or the regression sum of squares	$(\mu m)^2$
SS_E	Unexplained variation or the error sum of squares	$(\mu m)^2$
SS_T	Total sum of squares	$(\mu m)^2$
S_t	Final length of the convex/concave arc	mm
T	Data set matrix to compute the PCA	–
T_c	Total cutting time of the cutting tool	min

Variable	Description	Units
$T-test$	Statistics value to evaluate the difference in means of the $Coef$	–
t_e	Cutting edge time	min
t_m	Machining time	min
$s_{1,..,4}$	Defines a specific state of the cutting tool	–
V	Defines the symbols space in the *HMM*	–
VB	Flank wear land in the cutting tool edge	mm
$VB1$	Wear land extended over the tool flanks of the active cutting tool	mm
$VB2$	Wear land with irregular width in the cutting tool edge	mm
$VB3$	Exaggerated and localized form of wear at specific part of the flank	mm
VB_{max}	Maximum wear land in the cutting tool edge and it is equal to $VB3$	mm
v_c	Cutting speed	m/min
v_f	Feed rate	mm/min
Vol	Volume of the removal metal	mm^3
VB	Flank wear in the cutting tool edge	mm
v_c	Cutting speed	m/min
v_f	Feed rate	mm/min
v_p	Vector of process state variables	–
X	Energy of the spectrum	
X, Y, Z	Milling machine axes	–
Xs	Distance between peak to peak (width)	μm
x	Amplitude of the signal	Volts
$\bar{x}$	Mean value of a specific input variable	–
Y	Scaled energy of the spectrum	
$\bar{y}$	Normalized input variable, with mean zero and $\sigma = 1$	–
Z	Absolute ordinate value within a sampling length	μm
z	Number of tooth of the cutting tool	–
$\bar{z}$	Bipolar sigmoidal input variable	–
Z_p	Height of the largest profile peak	μm
Z_v	Height of the largest profile valley	μm
α	Major cutting edge angle	Degrees
α	Distance of the axial runs from the design center.	–
β	Helix angle of the cutting tool	Degrees
$\beta^{'}$	End cutting edge angle	Degrees
ε	Residual error	–
λ_c	Cutoff value	mm
λ	Eigenvalue	–
μ	Dimensional mean vector	–

Variable	Description	Units
ϕ_i	Triangular weighted function, associated with the i^{th} filter	–
Σ	Covariance matrix	–
χ	Logarithm value of the energy spectrum	
ω_N	Constant equal to $e^{(-2\pi i)/N}$	–
ξ	Represents any value of the factors	–
$\bar{\xi}$	Normalized value of the factors	–
σ	Standard deviation of the predicted response	μm
$\Delta\phi$	Immersion angle of the cutting tool	rad
λ	Defines the representation of the *HMM*	–
π	Initial state distribution in the *HMM*	–
$\Delta Error$	Absolute percent error between the predicted and desired R_a	–
β	Vector that maps the state space into the action space	–
π	A stationary policy that can be defined by an action function	–
$\Delta Error$	Absolute percent error between the predicted and desired R_a	–
α	Discount factor	–
ν	Expected total discount cost	–

List of Figures

List of Tables

Chapter 1

Introduction

In the world, machining processes (turning, milling, and drilling) are the most widespread metal shaping processes in mechanical manufacturing. Machine tools are essential for reproducing the technologies required in an industrial economy. Currently, worldwide investment in metal-machining machine tools holds steady or continues to increase year after year, [Childs *et al.*, 2000], for the following reasons:

1. The metal machining is capable of high precision: part tolerances of $50\ \mu m$ and surface finish of $1\ \mu m$ are readily achievable.

2. The machining process is very versatile: complicated free-form shapes with many features, over a large size range, can be made more cheaply, quickly, and simply by controlling the path of a standard cutting tool rather than by investing considerable time and cost in making a dedicated moulding, forming or die casting tool.

3. Also, the mechanical micro-machining has been defined as an important and relevant process owing to its ability to fabricate micro parts out of a greater range of materials and with more varied geometry than is possible with lithography and etching.

Next-Generation Manufacturing refers to the application of new concepts, models, methodologies, and information technologies, with the goal of preparing manufacturing companies to become more competitive in a global and networked environment, [Molina *et al.*, 2005]. Then, one important characteristic of future manufacturing equipment will be its ability to adapt to changing environments and conditions. This implies the opportunity to build an intelligent machine to achieve a goal or keep the performance under stochastic process conditions. An intelligent system must posse basic features and capabilities such as sensory perception, pattern recognition, learning and knowledge acquisition, inference from incomplete information, and adaptation. For these reasons, the great economies of the world want to lead production and technology in machining centers, and during the last decades, research and development has been conducted in three areas:

- Advances in machine tools (machine technology)

- Organization of machining (manufacturing systems)
- The cutting edge (materials technology)

1.1 Motivation

Given the importance of machining to most industries, and in order to keep the competitive edge and satisfy various customer needs, innovative manufacturing techniques have to be developed by further integration of information and manufacturing technology. In summary, through different research, several opportunities areas have been identified for present and future industrial applications. These areas are related to the following items:

1. Modelling of machining operations are relevant to improve the machining performance, workpiece quality, and attaining high productivity and/or low production cost. The use of more than one sensor for monitoring the process gives more interesting features to model the process. These systems are called *multi-sensors systems*, and the information acquired will be combined in order to get a sensor fusion.

2. Monitoring of the machining processes is very important in order to achieve safety, prevent fatal damage, and prevent rejects. In [Tönshoff *et al.*, 1988] it was demonstrated that the effective machining time of the machine tool was increased from 10 % to 65 % by using a monitoring system. Then, is a great opportunity to contribute with a cutting tool condition monitoring system in order to reduce operating cost.

3. Optimization and process modelling are two important issues in the metal cutting process because the machining process is variable owing to multiple factors (e.g. cutting tool-wear, vibrations, and other disturbances). In a *CNC* machining center the selection of the optimal cutting parameters is important to reduce the costs and allow high product quality. Also, control strategies are very important in the optimization process and machining operations. Two kinds of control approach are identified, i.e. on-line and off-line control. Adaptive control is a kind of on-line control, and it is applied for time-varying systems with large uncertainty concerning the process dynamic characteristics and disturbances. The on-line control received much attention in the 1970s and 1980s, [van Luttervelt and Peng, 1999]. However, at that time, knowledge of metal cutting was not sufficient, an accurate tool wear model was not available, and sensor and computer technology was not developed far enough. Currently, successful development and implementation of process monitoring and control demands high flexibility of the machine tool controller and open architecture controls in the *CNC* machining center, [Liang *et al.*, 2004]. To date, various transducers, signal processing schemes, control strategies, and actuators have been proposed and extensively investigated. In the area of machining process sensing, research has focused primarily on the monitoring of tool condition, chatter and part quality.

Nowadays, the machining processes with high speed (*HSM*) is one of the modern technologies, which in comparison with conventional cutting enables to increase efficiency, accuracy, and quality of workpieces and at the same time to decrease costs and machining time. Major advantages of *HSM* are reported as: high material removal

rates, the reduction in lead times, low cutting forces, reduced number of technological operations, less workpiece distortion and increased precision of the part, [Cus *et al.*, 2007].

The *HSM* is being mainly used in three industry sectors owing to their specific requirements:

- The first industry sector deals with machining aluminium to produce automotive components, small computer parts, or medical devices. This industry needs fast metal removal, because the technological process involves many machining operations.
- The second sector is aircraft industry which involves machining of long aluminium parts by removing a great amount of material from prismatic block, [de Lacalle Marcaide *et al.*, 2004].
- The third industry sector is the die mould industry which requires dealing with finishing of hard materials. In this category is important to machine with high speed and to keep high accuracy.

The *HSM* is the result of numerous technical advances ensuring that milling has become faster conventional milling and has gained importance as a cutting process. This implies to define a new paradigm: *it is important to maximize the metal removal rate, minimize the cutting tool-wear rate and maintain the surface quality and dimensional precision of all the machined parts in* HSM. Also, in several researches [Liang *et al.*, 2004], [Narita *et al.*, 2004], and [Erol *et al.*, 2000] define the future of the machine tools as follows:

- The machine tool must be a smart machine with the capacity to develop intelligent functions to enhance the manufacturing process.
- The machine tool must be available to realize the effective, reliable, and superior manufacturing system.
- New development and technology must be conducted in the process level. The process level is related to the phenomena that occurs in the interaction of the cutting tool and workpiece.

To evaluate and implement these considerations in a machine tool, it is first important to define: *What does an intelligent machine mean?*

Intelligent machine, as defined by [Haber *et al.*, 1998], *is a computationally efficient procedure combining one or more intelligent techniques (ANN, fuzzy logic, etc.) and expert criteria (e.g. operator knowledge) with one or more higher resolution levels, which basically manipulate cutting conditions (spindle speed, feed, etc.) and should be monitoring tool status and finished surface quality, as well as increasing productivity through higher metal removal rate*.

1.2 Problem description

In agreement with the previous section, the following problems can be found in the industry of the metal cutting processes.

1. The *HSM* defines new concepts and strategies of the mechanical design, the design of new related frameworks with the monitoring, control, and supervision of the machining process. Furthermore, the selection of the optimal machining parameters is important for the operation of the *HSM*. Currently, for conventional machining there is enough information (e.g., machining databases, handbooks) to select the proper cutting parameters for specific cutting tools and workpiece materials. However, for *HSM* there is no available information to select the cutting parameters, so the heuristic operation is exploited based on the operator's experience. Cutting parameters based on estimations have a direct impact on the metal cutting economics. High operating costs, low productivity, and poor quality of the product result from non-optimal cutting conditions, where there is a great opportunity to develop new models that can be integrated with optimization techniques for computing optimal cutting parameters in *HSM*.

2. The quality concept implies keeping consistent tolerances in the dimensional precision and the surface finish of the parts. For this reason, the surface roughness (R_a) has received great attention in the metal cutting process. Several research works have been developed to predict the R_a and monitor the cutting tool condition *In-process* operating mode. However, the experimentation made in the majority of these works over R_a and flank wear (VB) only consider a specific combination of cutting tool and workpiece material. Therefore, several authors have pointed out the importance of building databases with information of different materials and cutting tools for a complete domain in the machining process.

3. In [Rehorn *et al.*, 2005] it is mentioned that the amount of down time owing to cutter breakage on an average machine is between 6.8 % and 20 %. Even if the tool does not break during machining, the use of dull or damaged cutters can put extra strain on the machine tool and cause a loss of quality in the workpiece. It is very much appreciated that cutting tool condition monitoring system optimizes the operating cost with the same quality of the product.

4. There is a need to design and develop an intelligent monitoring and process planning system that allows the prediction of the R_a and recommends the optimal cutting condition, *Pre-process*, and *In-process* operating mode. Also, it must be available to recommend optimal policy to operate the *CNC* with minimum cost.

1.3 State of the art

This section presents only a short description of the main research studies related with the optimization processes, surface roughness, and cutting tool wear. Chapter 2 presents a general classification of the different techniques and methodologies used to model the surface roughness and to predict the cutting tool wear condition in machining processes.

1.3.1 Optimization systems

Optimization techniques in metal cutting processes are essential to respond to serious competition and increasing demand for quality product in the market. In [Mukherjee and Ray, 2006] a review of optimization techniques in

metal cutting processes is presented, and a general framework for process parameter optimization is discussed. Some applied optimization methods are the Taguchi method, response surface methodology, mathematical iterative search algorithm, Genetic Algorithms, and simulated annealing. Furthermore, different objective functions used in the optimization of the machining conditions include: minimum production cost, maximum production rate, increase tool life, maximum profit rate, and weighted combination of several objective functions. Cutting constraints that should be considered in machining economics include: tool-life constraint, cutting force constraint, power, chip-tool interface temperature constraint, and surface finish constraint. A complete classification of the optimization techniques will be discussed in Chapter 2.

1.3.2 Surface roughness

Surface roughness (R_a) has received serious attention for many years. It has been an important design feature and quality measure in many situations, such as parts subject to fatigue loads, precision fits, fastener holes and esthetic requirements. Some geometric models to represent the surface roughness have been developed, and they take into consideration certain aspects from the theory of machining such as process kinematics, cutting tool properties, chip formation mechanism, etc.. Other research works are based on multiple regression analysis, where the obtained models allow the prediction of the R_a as a function of different factors, such as feed rate, spindle speed, depth of cut, tool nose radius, vibration, hardness, etc.. These models are applied only for a specific combination of cutting tool and workpiece material. Systematic methods, concern with the planning of experiments, collection and analysis of data are the Response Surface Methodology and Taguchi techniques. These are used for Design of Experiments (*DoE*), and they are the most wide spread methodologies for the R_a prediction problem and optimization process.

Also, a number of studies on the application of Artificial Intelligence (*AI*) have been applied in *CNC* machining for determining optimum cutting parameters and for modelling the R_a. These *AI* techniques have been used to minimize machining errors such as tool breakage, tool wear, and surface roughness.

1.3.3 Cutting tool wear

Tool wear is defined as a gradual loss of tool material at workpiece material and tool contact zones. The monitoring of cutting tool states may be classified into direct and indirect methods. Several works related with the indirect monitoring of the cutting tool wear are based on techniques such as Artificial Neural Networks (*ANN*), Bayesian networks (*BN*), multiple regression approaches, and stochastic methods. At the feature extraction level, the most frequently used techniques are the computation of average values or trends, power values in spectral bands, or statistical features. The Tool Condition Monitoring (*TCM*) system must include applications where prior knowledge or cutting data could not exist. Artificial intelligence, *ANNs*, fuzzy logic systems, and Genetic Algorithms should be some options to solve this situation.

1.4 Research objectives

HSM represents a modern technology which is used in important industry sectors, such as, automotive industry for machining aluminium components, the aircraft industry for machining aluminium parts, and the die mould industry which requires high surface finishing and high dimensional precision. relevant researches have been reported in this field with important advances in the following areas:

1. In optimization processes, applied models are based on Taguchi methods, and response surface methodology, and using Genetic Algorithms, and simulated annealing, the optimal cutting parameters are computed by considering different objective functions (i.e., minimum production cost, maximum production rate, maximum tool-life). However, there is a great opportunity to design and implement intelligent monitoring systems and process planning systems in *HSM*.

2. In surface roughness, several models have been developed (mechanistic, statistical, etc.) to estimate the R_a as function of different factors. However, they have been only applied at specific combination of workpiece and cutting tool. The cutting tool wear condition has not been considered in the models.

3. The monitoring of the cutting tool wear condition also presents important researches using Artificial Intelligence techniques for indirect monitoring of cutting edge. It is necessary to improve models to estimate the cutting tool wear condition by considering new feature extraction from different process state signals and increasing the performance of models for recognizing different states of the cutting tool wear condition.

The general scope of this research is defined as: *Design and implement an intelligent monitoring and supervisory control system for peripheral milling process in high speed machining*. The system must compute the optimum cutting parameters as a function of a merit variable. Also, the system must allow the monitoring of the cutting tool wear condition and the surface roughness during the machining process. Figure 1.1 shows the proposal architecture with the blocks required to develop the different functions of the system.

The main objectives of this research are:

1. Design and implement an intelligent monitoring and process planning system in peripheral milling process for *HSM*. The proposal implies to use a multi-sensor system in the *CNC* machining center for recording several process state variables (i.e., forces, vibration, and acoustic emission) during the machining process. Statistical and artificial intelligence techniques must be applied to integrate an intelligent system and build new models for monitoring and diagnosing the surface quality and the cutting tool wear condition.

2. Implement new models to estimate the surface roughness (R_a) by considering several aluminium alloys, cutting parameters, geometries, and cutting tools. The most relevant factors that affect the R_a must be selected, and the Design of Experiments must be defined with the objective of building a model for covering a machine domain with the aforementioned considerations.

3. Predict the optimal cutting parameters *Pre* and *In-process* operating mode for maintaining the surface roughness quality. With the statistical models and using artificial intelligence techniques, the intelligent system

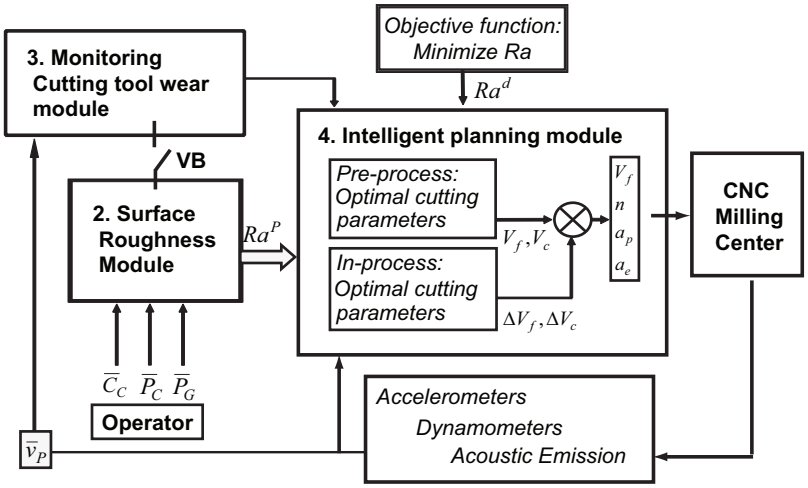

Figure 1.1: Diagram of the intelligent monitoring and supervision system used to control the milling parameters based on R_a and cutting tool wear condition. The process state signals are recorded and used for monitoring the cutting tool wear condition (module 3). The surface roughness module (module 2) estimates the R_a in Pre-process operating mode. The intelligent planning module (module 4) computes the optimal parameters in Pre-process and In-process operating mode. Finally, the optimal parameters are used in the cutting process.

must allow for computing the optimal cutting parameters and guarantee the same surface quality during the tool's lifetime.

4. Design and implement a monitoring and diagnostic system for the cutting tool wear condition during the machining process. New methodologies for computing feature vectors from the process signals and a new approach based on a speech recognition system will be applied to classify and recognize the cutting tool wear condition. This system must be reliable, robust, and high performance to identify the tool wear condition. Related with the *CNC* operation, the system must allow to change the worn tool in time and reduce the tool costs with a precise exploitation of the tool's lifetime.

5. Design and develop an intelligent process planning system that includes a merit variable to compute the optimum cutting parameters and a decision-making module to recommend some actions in agreement with the cutting tool wear condition. *HSM* systems demand advanced features such as intelligent control under uncertainty. The intelligent control must guide the actions of the operator in peripheral milling processes and yield several benefits in the operation of the *CNC* machining center (e.g., minimum production cost, maximum production rate, increase tool life). It is an important module that several authors have been proposed in the process level.

1.5 Outline

This research is organized as follows:

- Chapter 2 defines important concepts of the machining theory, surface roughness, cutting tool wear condition, and the state of the art in machining processes.
- In Chapter 3 a description of the intelligent monitoring and supervisory control system is included with a description of the main modules. Also, the complete data acquisition system module is presented.
- In Chapter 4, the design of experiments is defined with a complete analysis for computing the surface roughness models with *RSM*.
- Chapter 5 presents the modelling of the cutting tool wear and the implementation of the indirect monitoring system to predict the cutting tool condition.
- In Chapter 6 the intelligent monitoring and process planing system is developed as is the decision-making module to recommend actions at minimum cost.
- Chapter 7 presents contributions and conclusions of the research and some guidelines for future work are presented.
- References. This section presents the papers, proceedings, technical reports, international norms, and books, which were consulted and analyzed during the development of this research.
- Appendix A. A description of the concepts related with the mechanical cutting process is included.
- Appendix B. The behaviour of the accelerometers and acoustic emission signals is explained. Technical information of the sensors, amplifiers, and data acquisition boards is included.
- Appendix C. This appendix defines the specifications of the different aluminium alloys.
- Appendix D. The procedure for measuring the R_a, flank wear, and run-out is described.
- Appendix E. A complete description of the statistical analysis of the screening factorial design is presented.
- Appendix F. The *ANOVA* results of the modeling analysis with *RSM* for all cutting tool wear conditions is presented.
- Appendix G. This appendix presents the concepts, recommendations, and different tool-life parameters, which were computed during the experimentation in the *CNC* Kondia machining center.
- Appendix H. The theory of the Hidden Markov Models is presented.
- Appendix I. The appendix presents the machining costs for computing the optimal policy and minimizing the production costs.
- Appendix J. A list of publications is included in this appendix.

Chapter 2

State of the Art

2.1 Introduction

This chapter defines important basic concepts about the theory of the machining process, and includes a discussion of the most relevant research in the fields of surface roughness, cutting tool wear condition, and optimization systems in machining processes.

2.2 Basic concepts of machining processes

Milling is one of the most important metal cutting processes, and its application in the mold/die manufacturing processes is very important in the automotive and aeronautic industries. A complete description of milling machines, types of milling cutters, and milling operations can be found in [Boothroyd and Knight, 2006], [Childs *et al.*, 2000], [de Lacalle Marcaide *et al.*, 2004], and [Trent and Wright, 2000]. For this research work, a vertical milling machine was used. Figure 2.1 shows the milling machine with the main components and movements.

2.2.1 Cutting operation and parameters

In milling, the main cutting motion is the rotation of a multi-toothed cutter that machines a workpiece that performs translative feed motions. The geometry of milling operations considers two basic modes: (a) face milling, and (b) peripheral milling. The peripheral milling implies two cutting operations, depending on the relation between the direction of the rotation of the cutter and the direction of the feed: (a) up-milling, and (b) down-milling. Figure 2.2 shows the milling operations and the cutting operations. The down-milling operation was selected because it allows a high surface quality. In peripheral milling, the relative motion of the cutting edge with respect to the workpiece is a sum of the rotation of the cutter with speed n (rpm) and the translation with feed rate v_f (mm/min). The peripheral speed of the cutter is called the cutting speed v_c (m/min). The feed per tooth f_z is the distance that cutter advances across the workpiece during one revolution. The feed per tooth is also called the chip load, and it is

Figure 2.1: Main components and movements of the vertical milling machine

equal to

$$f_z = \frac{v_f}{n} \tag{2.1}$$

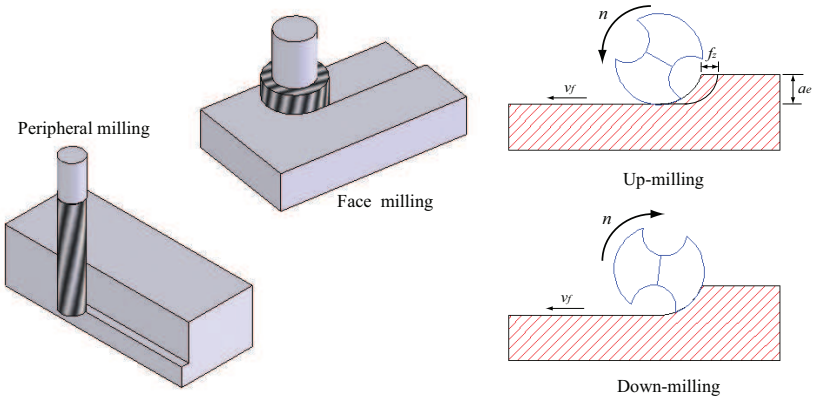

Figure 2.2: The face and peripheral milling are basic geometric modes of milling operations. Also, two important milling operations are up and down milling.

A type of peripheral milling is called *end milling*. An end mill is a cutter of a smaller diameter (usually between 5 mm and 30 mm diameter) clamped in overhang, and its length is several times its diameter. For the end milling, the thickness of the removed layer from the workpiece is the radial depth of cut ae and the width of the workpiece is the axial depth of cut ap. Before starting up the *CNC* machining center, it is very important to set up the milling operation, and this implies defining the following parameters:

1. The cutting speed:

$$v_c = \frac{\pi \times D_{tool} \times n}{1000}(m/min) \tag{2.2}$$

2. The number of revolutions of the spindle:

$$n = \frac{v_c \times 1000}{\pi \times D_{tool}}(rpm) \tag{2.3}$$

3. The feed per tooth:

$$f_z = \frac{v_f}{n \times z}(mm) \tag{2.4}$$

where D_{tool} is the cutting tool diameter, v_f is the feed rate, and z is the number of teeth. The operator must specify the f_z, n, and z.

2.2.2 Surface roughness

Surface roughness (R_a) is a widely used index of product quality and in most cases a technical requirement for mechanical products. R_a is of significant interest in the manufacturing process because it determines the friction between two surfaces, how the surface wears, how it retains lubricant, and how it holds a load. To illustrate the concept of the R_a, Figure 2.3 shows the surface finish imperfections during the machining process. These imperfections are defined in Appendix A.

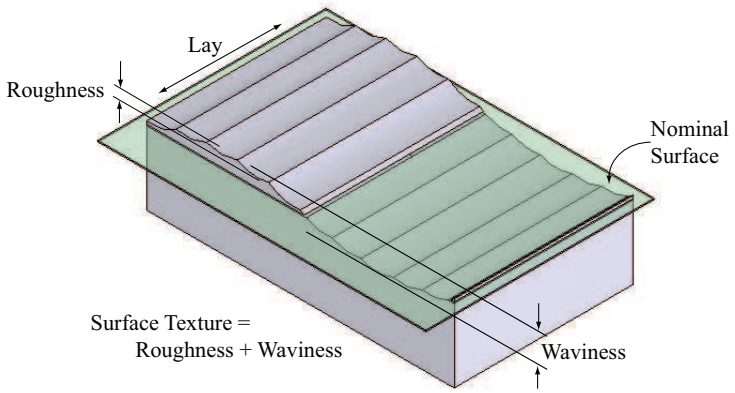

Figure 2.3: Surface shape after the machining process with different imperfections.

Currently, some geometric models allow for computing the surface roughness. In [Boothroyd and Knight, 2006], the final surface roughness during a practical machining operation is defined as the sum of two independent effects:

1. The ideal R_a, which is a result of the geometry of the tool and the feed speed.
2. The natural R_a, which is a result of the irregularities in the cutting operation.

Ideal surface roughness

The ideal surface roughness represents the best possible finish that may be obtained only if built-edge, chatter, inaccuracies in machine-tool movement, and so on, are eliminated. The idealized model is depicted in Figure 2.4. The Surface Roughness (R_a) can be evaluated by the sum of the areas above and below the mean line divided by the evaluation length (L). Analytically, R_a is given by:

$$R_a = \frac{1}{L}\int_0^L \mid z(x) \mid dx \tag{2.5}$$

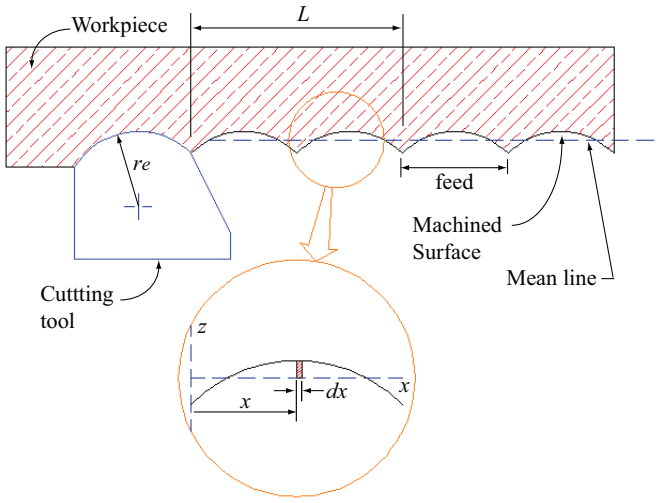

Figure 2.4: Idealized model of surface roughness for a cutting tool. The waviness is the result of the cutting tool through the machined surface.

Natural surface roughness

In practice, it is not usually possible to achieve only an ideal surface roughness, and normally the natural surface roughness forms a large proportion of the actual roughness. The factors that contribute to natural surface roughness are: a) built-up edge; b) chatter of the machine tool; c) inaccuracies in machine tool movements; d) irregularities in the feed mechanism; e) defects in the structure of the work material; d) discontinuous chip formation when brittle materials are machining. It is very important to control the previous factors to reduce the natural surface roughness during the machining process.

2.2.3 Cutting tool wear

Cutting tool life is one of the most important economic considerations in metal cutting. In roughing operations the various tool angles, cutting speeds, and feed rates are usually chosen to give an economical tool life. The life of a cutting tool can be defined by considering the following actions:

1. The gradual or progressive wearing away of certain regions of the face and flank of the cutting tool. Figure 2.5 shows the progressive wear in two distinct areas: (a) wear on the tool face characterized by the formation of a crater, and (b) wear on the flank.

2. Failures bringing the life of the tool to a premature end, which is called tool breakage.

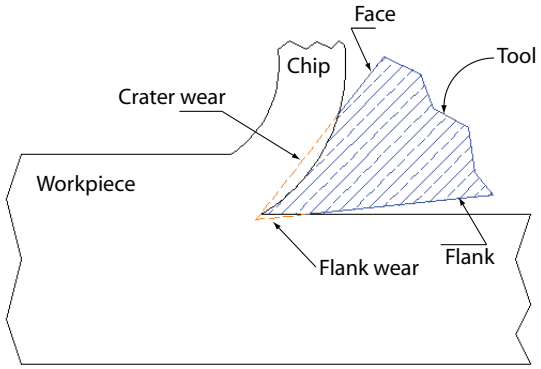

Figure 2.5: Several areas of the cutting tool that present wear during the metal cutting process.

A complete description of the crater wear and flank wear, and other concepts are including in Appendix A.

2.3 State of the art in surface roughness

Section 2.2.2 defines the R_a as the combination of the ideal and natural roughness. There are several factors affecting the R_a, and they are separated in different groups as depicted in the fish bone of Figure 2.6. Surface roughness has been investigated for many years. In [Benardos and Vosniakos, 2003] the authors divided the different research into four major categories: machining theory, experimental research, design of experiments, and artificial intelligence. With this classification, a summary of the most important ideas, and methodologies for Ra modelling will be discussed.

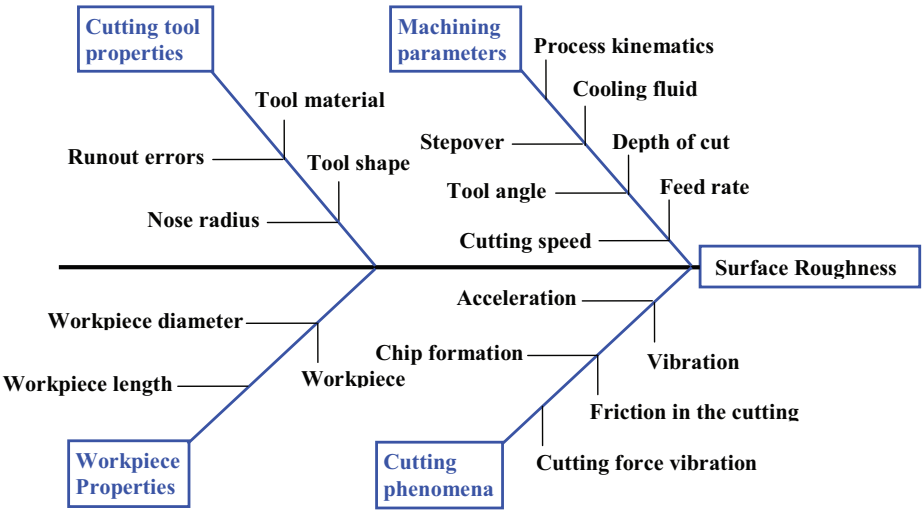

Figure 2.6: Classification of the factors that affect the R_a of a workpiece. Machining parameters and cutting phenomena groups present more damage than other groups over the R_a.

2.3.1 Machining theory approach

This approach follows the theory of machining that considers process kinematics, cutting tool properties, chip formation mechanism, and so on. Two modelling methods are considered: geometric and mechanistic. For the mechanistic model, enough knowledge of the physical mechanism is required to deduce the form of the functional relationship between the output and the input of a process. Geometric modeling is based on the motion geometry of a metal cutting process regardless of the cutting dynamics.

In [Kim and Chu, 1999] a texture superposition method to evaluate the surface asperity of milled surfaces is presented. The geometric roughness was expressed as a function of the feed per tooth, the path interval, the depth of cut, and the geometries of the tool and workpiece. The authors concluded that for flat and end-milling with a small fillet radius, the cutter marks are important factors to influence the surface quality of a precision machined surface. In [Lee *et al.*, 2001] a method for the simulation of the machined surface in high-speed end milling is presented. A geometric model was used for modeling the end mill offset and tilt angle. The end milling process was examined by discretizing it angle by angle and flute by flute, and after dividing the end mill into axial segments, slice by slice. An accelerometer is used to monitor the vibrational state, and the amplitude and frequency of the principal harmonics are obtained from the signal analysis. An algorithm and programming method are used to simulate the machined surface (Ra) by considering cutting parameters, cutter and workpiece geometry, run-out parameters, and the vibration signals. In [Jung *et al.*, 2004], the authors dealt with the geometrical surface roughness in ball-end milling. They applied a rigid method to predict the machined surface roughness. The equations of the ridges were given as function of the tool radius, the feed per tooth and the rotation angle of the cutting edges. The results were

compared with a simulation method. The method can be useful for evaluating the geometrical machining error of ball-end milling process. Other geometrical models based on different factors (i.e., speed, feed, and depth of cut) have been developed by [Boothroyd and Knight, 2006] for estimating the surface roughness. An example for estimating the surface roughness in turning process, is given by,

$$R_a = \frac{f^2}{32re} \tag{2.6}$$

where R_a is the ideal arithmetic average surface roughness, f is the feed, and r is the cutter nose radius. This model assumes a large nose radius and slow feed. For a zero nose radius and relatively large feed, the following model is recommended ([Boothroyd and Knight, 2006]):

$$R_a = \frac{f}{4(cot\alpha + cot\beta')} \tag{2.7}$$

where α and $\beta^{'}$ are the major and end cutting edge angles. In the case of multi-point cutting tools used in the milling process and under ideal conditions, the surface roughness can be obtained by assuming that the cutting tool has only one tooth. The equation proposed by [Boothroyd and Knight, 2006] is given by,

$$R_a = \frac{0.0642}{D_{tool}} \left(\frac{v_f}{n}\right)^2 \tag{2.8}$$

where v_f is the feed speed, D_{tool} is the cutting tool diameter, and n is the rotational frequency of the cutter.

2.3.2 Experimental approach

This approach implies to conduct experiments with the most important factors affecting the surface quality. Regression analysis is employed to build models. Important research is discussed in this section.

Research based on multiple regression analysis was presented by [Lou *et al.*, 1998] to predict the surface roughness as a function of the feed rate (four levels), spindle speed (seven levels), and the depth of cut (three levels). The multiple regression model was a three-way interaction type. The experiments were done in a vertical machining center, specifically for the end-milling process, and the workpiece material was 6061 aluminium. The model was trained with 84 specimens, and tested with 24 samples. The success of the model to predict R_a was 90%. In [Savage and Chen, 1999] was developed a multilevel recognition system was developed to evaluate surface roughness *In-process* and in real time. The workpiece material was 6061 aluminium and 1018 steel. The regression model considered seven variables: feed rate, depth of cut, spindle speed, vibration average per revolution, tool diameter, tool material, and workpiece material. Eight multiple-regression equations were developed from the training data collection. The system presented a performance of 82% by using a testing data set. Based on a regression model, [Barber *et al.*, 2001] found that Ra is a quadratic function of tool service time. The authors assumed an empirical model to fit the arithmetic surface roughness to a quadratic function of the tool service time. The experiments were made for the face milling process and the workpiece material was 4140 steel. When the tool life based on flank wear reaches $0.35\ mm$, it reaches its failure criterion. Three models were defined to compute the surface roughness with the quadratic function of the tool service time. In [Abouelatta and Madl, 2001], a correlation between Ra and

vibration signals in turning is presented. It was found that models with cutting parameters and tool vibrations are more accurate than those depending only on cutting parameters. The workpiece material was steel. Four regression math models were computed for certain selected surface roughness: R_a, R_t, and R_{sk}. The independent variables were: feed, speed, depth of cut, tool overhang, tool nose radius, approach angle, workpiece diameter, workpiece length, and tool vibration levels (maximum autocorrelation, maximum power spectrum density, and the frequencies at which they occur). An empirical model for surface roughness prediction in finish turning is presented in [Feng and Wang, 2003]. A nonlinear regression analysis was used to define the relationship between R_a and the following factors: workpiece hardness, feed, tool nose radius, depth of cut, and cutting speed. Two levels were defined for each factor, and a full factorial design was used to facilitate model construction. The workpiece material was 8620 Steel (86 HRB), and 6061 Aluminium (52 HRB). The mean absolute percent error between the measured and estimated R_a was 19.06%. A multiple regression analysis for modelling the Ra was proposed by [Ertekin *et al.*, 2003]. Three different materials (i.e., $6061 - T6$ Aluminium, $7075 - T6$ Aluminium, and ANSI-4140 Steel) were machined on a vertical *CNC* milling machine, and several process variables were acquired to find the best correlate with the surface roughness and dimensional accuracy (bore tolerance). Fresh tools were used for each material and the machining continued until tools wore out. Specific values of the spindle speed, cutting speed, feed rate, and radial and axial depths of cut were defined for each material. The most significant features were the *RMS* values of the vertical force and *AEDC* signal. Finally, multiple regression analysis was applied to compute a $3rd$ order model of the R_a as a function of the vertical force and *AEDC* features. The model provided a regression coefficient of 99%.

In [E D Kirby and Chen, 2004], the authors developed an *In-process* R_a surface roughness prediction system using an accelerometer and multiple regression techniques for a *CNC* lathe operations. The experiments involve a basic factorial design, with three factors (spindle speed, feed rate, and depth of cut) and four response variables (surface roughness, and the vibration signals in X,Y, and Z axes). The workpiece material was $6061 - T6511$ Aluminium alloy. The Pearson correlation was computed between the factors and surface roughness, and *ANOVA* was performed between the factors and vibration signals. The correlation coefficient of the regression model was 0.96. The mean absolute error between the measured and estimated R_a was 10.77%. In [Sai and Bouzid, 2005] regression models were developed to describe the roughness, and to compute the optimal cutting parameters. The workpiece material used in the face milling process was 1042 Steel (160 HV). The studied factors were cutting speed and feed per tooth, while the depth of cut and cutting tool diameter were constants. Two regression models were obtained for computing the surface roughness R_a and the maximum height of surface profile R_t. The authors validated that roughness increases with the feed due to increased cutting forces and strains. For small values of cutting speed, the roughness increases due to the formation of built-up edge, and for high values of cutting speed, the roughness increases due to vibrations.

2.3.3 Design of experiments approach

This approach constitutes a systematic method concerning the planning of experiments, collection, and analysis of data with near-optimum use of available resources. The optimization of the cutting parameters is very important

to maintain high surface quality and low production costs. Optimization process is required to be undertaken in two stages: (i) modelling input-output and *In-process* parameter relationship, and (ii) determination of optimal or near-optimal cutting conditions. The Response Surface Methodology (*RSM*) and Taguchi techniques for Design of Experiments (*DoE*) are the most wide-spread methodologies for the R_a prediction problem and optimization process.

In [Fuh and Chang, 1997], a dimensional-accuracy model in peripheral milling of aluminium is postulated as a second order equation and developed in terms of the workpiece hardness, the cutting speed, the feed, and radial and axial depths of cut. The *RSM* with an orthogonal rotatable central composite design is used to build a quadratic model and to minimize the number of experiments. The tests were performed on a vertical machining center, and five different aluminium alloys ($5052 - O$, $6061 - T4$, $6061 - T6$, $2024 - T3$, and $7075 - T3$) were selected in the experimentation. The mean absolute percent error was 8.13% with a standard deviation of 3.18%. The research in [Suresh *et al.*, 2002] deals with the study and development of a R_a prediction model for machining mild steel, using *RSM*. A second order mathematical model was developed for R_a prediction, and the selected factors were cutting speed, feed, depth of cut, and nose radius of the cutting tool. Full factorial design was applied for the experimentation, and some conclusions about the factor effects on the R_a were the following: (i) The R_a decreases with an increase in cutting speed and increases as feed increases; (ii) The R_a increases with an increase in depth of cut and nose radius.

A statistical model is presented in [Ozcelik and Bayramoglu, 2006], where the R_a is estimated in a high speed flat end milling process. A rotatable central composite design was considered with the *RSM* to compute a second order model. The most significant variables were the total machining time, depth of cut, step over, spindle speed, and feed rate. The experiments were carried out in wet conditions on a Deckel high speed *CNC* milling center, and the workpiece material was 1040 steel. The cutting tool was used until it reached a maximum flank wear of $V_Bmax \sim 0.1mm$. The standard error between experimental and estimated values was 13.4%, and the adjusted coefficient of multiple correlations was 87.9%. In [Öktem *et al.*, 2006] the Taguchi optimization method was applied to model the R_a in terms of process parameters when milling the mold surfaces of $7075 - T6$ Aluminium material. Milling experiments were carried out on a Deckel Maho *CNC* milling machine. Five factors (feed per tooth, cutting speed, radial and axial depths of cut, and machining tolerance) and three levels were defined for the experimentation, and by using the Taguchi optimization method and an L_{18} orthogonal array, only 18 milling experiments were done. *ANOVA* computed the significant effects of the factors on the R_a: machining tolerance of 96.035%, radial depth of cut of 2.152%, axial depth of cut of 1.537%, feed of 0.177%, and cutting speed of 0.092%.

2.3.4 Artificial intelligence approach

There have been a number of studies on the application of Artificial Intelligence (*AI*) techniques in Computer Numerical Control (*CNC*) machining for determining optimum or appropriate cutting parameters, and for modelling the surface roughness in the machining processes. These *AI* techniques have been used to minimize machining errors such as tool breakage, tool deflection, tool wear, surface roughness, and to automatically adapt and optimize the machining parameters based on sensor information, thus yielding a high surface quality, high productivity or minimum

cost. In [Park and Kim, 1998] a review is presented of *AI*-based techniques for providing a better understanding of the importance of these techniques in machining control.

In [Azouzi and Guillot, 1997a] the authors combined the *ANN* modeling, statistical tool, and sensor fusion technique to estimate on-line R_a and Dimensional Deviations (*DD*) during the turning process. The design of experiments considered cutting parameters (feed, speed, and depth of cut), process conditions (coolant, cutting tool wear, and material properties) and only one type of cutting tool and workpiece material ($AISI-1018$ steel). The Taguchi optimization method was applied with an L_{16} orthogonal array. During the machining processes several process variables were acquired (forces, vibration, acoustic emission, and tool deflections). The authors concluded that radial and feed forces present the highest correlation with the *DD* and R_a, and they can be used in the fusion model. Different *ANN* models were evaluated, and the best ANN model was built using the feed, depth of cut, and the radial and feed forces from sensors. The R_a was assessed with an error varying from 2 to 25% under different cutting conditions and parameters. In [Tsai *et al.*, 1999] the authors proposed an *In-process* surface recognition system for R_a prediction of the end milling process and $6061-T6$ aluminium alloy. The factors and levels were the following: 4 levels of spindle speed, 4 levels of feed rate, and 3 levels of depth of cut. The rotation and vibration were also collected simultaneously by the proximity sensor and the accelerometer, respectively. The vibration average per revolution (*VAPR*) was considered as the fourth independent variable in the model to predict the R_a. Different *ANN* structures were proposed to select the best model. The $4 \times 5 \times 1$ structure presented the lowest *RMS* among the structures with one hidden layer, and the $4 \times 7 \times 7 \times 1$ structure was better than other structures with two hidden layers. The accuracy of prediction was 92.07% and 96.07% for the $4 \times 5 \times 1$ *ANN* model and $4 \times 7 \times 7 \times 1$ *ANN* model, respectively. The average absolute percent error for the testing data set was 4.13% and 0.73% for each *ANN* model.

In [Benardos and Vosniakos, 2002], a neural network modelling approach is presented for the prediction of R_a in the *CNC* face milling process. The used factors were the following: depth of cut, the feed rate, the cutting speed, the engagement of the cutting tool, the cutting tool wear, and the cutting forces. The Taguchi optimization method with orthogonal arrays was used for planning the *DoE*. The experiments were conducted in a Deckel Maho *CNC* milling machine. The workpiece material was series 2 aluminium alloy. A L_{27} orthogonal array for the six factors was defined for the *DoE*. The Levenberg-Marquant algorithm was selected for training the *ANN* models. Owing to the nine factors considered as inputs to the *ANN* model, a L_{32} orthogonal array was selected to define the 32 different models to be tested. The Mean Squared Error (*MSE*) was used to select the best *ANN* model. The $5 \times 3 \times 1$ structure with an average $MSE = 1.86\%$ was selected, with the following factors: the feed per tooth, the F_x component of the cutting force, the depth of cut, the engagement of the cutting tool, and the cutting fluid. Also, [Lee and Chen, 2003] presented an online surface recognition system based on the *ANN* model, and the effect of vibration produced during the turning process. The factorial design was performed in the *DoE*, and the factors and levels considered were the following: spindle speed with 4 levels, feed rate with 7 levels, and depth of cut with 3 levels. During the experimentation, a triaxial accelerometer and a proximity sensor were used to acquire the vibration signals and the spindle rotation. A Pearson correlation was performed to compute the most significant correlation between the cutting parameters and the Vibration Average Per Revolution (*VAPR*). Finally, a statistical analysis was carried out to find the most significant vibration direction related to surface roughness. The transformed

radial (x) vibration was found the most relevant on R_a. With the cutting parameters and the radial vibration, different *ANN* models were defined to compute R_a. Based on the *RMS* error of the training and testing data sets, the best structure for prediction R_a was $4 \times 7 \times 7 \times 1$. The prediction accuracy of the *ANN* model was 96.3%, including testing and validation data sets. In [Özel and Karpat, 2005] an *ANN* model to predict R_a and tool flank wear over the machining time in finish hard turning is presented. The authors studied the effects of cutting edge geometry, workpiece hardness, feed rate and cutting speed on R_a and tool wear in the finish dry hard turning of AISIH13 steel. Full factorial design was applied to define the experiments with four factors, two levels, and 16 replications. A feed forward multilayer neural network was developed to predict the R_a, and the *Levenberg-Marquardt* method was used together with *Bayesian regularization* in training at the *ANN*. First, the R_a and tool wear are predicted by using direct cutting parameters, tool edge, hardness, cutting speed, feed rate, and cutting length as input parameters. The model structure was $5 \times 15 \times 2$ and the average *RMS* error was 7.98% on the test data. Secondly, the geometry of the cutting tool changes to chamfered and honed tool edge geometry, and the mean value of the cutting forces were included as inputs. The defined structures for these models were $7 \times 10 \times 1$ and $7 \times 13 \times 1$. The average *RMS* errors were 9.3% and 5.5% for R_a prediction with chamfered and honed tools, respectively. Even though previous works exhibit satisfactory results, more general and practical solutions are needed. Exploiting sensor fusion techniques could be a great opportunity. Sensor fusion modeling is a problem of signal estimation, interpolation, and prediction. Fusion techniques can be classified into three different groups: (1) fusion based on probabilistic models such as Bayesian reasoning; (2) fusion based on least-squares techniques such as Kalman filtering, optimal theory, and regularization; (3) intelligent fusion that includes fuzzy logic, artificial neural networks, etc.. The third group will be exploited in this research.

2.3.5 Comparison and limitations of the research on surface roughness

Tables 2.1, 2.2, 2.3, and 2.4 present a comparison of the different research by considering the main factors affecting the R_a, sensor signals, and the model implemented for each approach. Table 2.1 shows a comparison of the

Table 2.1: Machine theory approach. Comparison of the studied factors over R_a and the implemented models.

Process	Studied Factors over R_a	Sensor Signals (Processing Features)	Model Approach	References
Milling	feed per tooth, path interval, fillet radius, runout, and depth of cut		Geometric model	[Kim and Chu, 1999]
End milling	Cutting parameters, tool geometry, workpiece geometry, vibration	Accelerometer (frequencies amplitudes)	Geometric model	[Lee *et al.*, 2001]
End milling	Cutter radius, feed per tooth, rotation angle of cutter edges		Geometric model	[Jung *et al.*, 2004]

research related to the machining theory and milling processes. The computed models can estimate the ideal R_a

with excellent results. However, they can only be used for conventional *CNC* machining centers and only consider new cutting tools. A mechanistic model can be developed only if enough knowledge is know of the physical mechanism, [Azouzi and Guillot, 1997a]. The surface roughness depends of many factors (cutting parameters, cutting tool geometry, workpiece material, process uncertainty, etc.) and it is complicated to understand the physics of the cutting process in *HSM* for computing a mechanistic model. The mechanistic and geometric models did not consider the cutting tool wear condition, and they can be used to estimate the ideal R_a. Tables 2.2 and 2.3 present a comparison of the results in the experimental approach and design of experiments for estimating R_a. R_a models were computed to be used in the machining process with normal speeds (conventional *CNC*), and almost all of them did not consider the cutting tool wear condition. Additionally, the authors did not apply a screening factorial design to confirm the most significant factors over R_a. The evaluation of R_a was made by considering only one parameter in its assessment. Finally, table 2.4 shows a comparison of the results in the artificial intelligence approach. The R_a models were computed to be used in conventional *CNC* machining centers, and the experiments only considered one type of cutting tool and workpiece material. The majority of the models did not consider the cutting tool wear condition to predict the R_a. From the reported research works, nobody considered the effect on the geometric path (curvature) on the R_a.

2.4 State of the art in the cutting tool wear condition

The cutting tool wear condition is an important factor in all metal cutting processes. However, direct monitoring systems are not easily implemented because they require ingenious measuring methods. For this reason, indirect measurements are needed for estimation of the cutting tool wear. Different signals coming from sensors in machine tools are used for monitoring and diagnosis of the cutting tool wear condition. Several research works [Koren *et al.*, 1999; Erol *et al.*, 2000; Liang *et al.*, 2004] concluded that future manufacturing systems will have special characteristics such as intelligent functions, to enhance the manufacturing process; the ability to perform an effective, reliable, and superior manufacturing procedure, and new process level technology, mainly in the process monitoring and control field. One of the main goals in a Computer Numerically Controlled (*CNC*) machining center is to find an *appropriate trade-off* among the cutting tool condition, the surface quality, and productivity. In [Sick, 2002b] it is mentioned that any manufacturing process can be optimized significantly using a reliable and flexible tool monitoring system. There are important contributions for cutting tool monitoring systems based on Artificial Neural Networks (*ANN*), the Bayesian Network (*BN*), multiple regression approaches, and stochastic methods. A cutting tool monitoring approach was presented by [Owsley *et al.*, 1997]. A feature extraction from vibrations during the drilling is generated by a Self-Organizing Feature Map (*SOFM*). The pre-processing of the signals implies a spectral feature extraction to obtain time-frequency representation. The features are the inputs of a Hidden Markov Model (*HMM*) classifier. A methodology based on the frequency domain is presented by [Chen and Chen, 1999] for on-line detection when a cutting tool breaks. The frequency domain presents two important peaks at low frequencies, which are compared to compute a ratio that could be an indication for monitoring tool breakage. [Atlas *et al.*, 2000] also used *HMM* for evaluation of the tool wear in milling process. The feature extraction from vibration signals was the root mean squared, energy, and its derivative. The cutting tool conditions were worn and no-worn. The reported performance

Table 2.2: Experimental approach. Comparison of the studied factors over R_a and the implemented models. AC= Accelerometer, PS= Proximity Sensor, DY= Dynamometer, AE= Acoustic Emission, and RA= Regression Analysis.

Process	Studied Factors over R_a	Sensor Signals (Processing Features)	Model Approach	References
End milling	Spindle speed, feed rate, and depth of cut		Multiple RA	[Lou *et al.*, 1998]
Milling	Tool wear, depth of cut, feed rate, tool diameter, spindle speed vibration, workpiece material	AC, PS (Average vibration per revolution)	Multiple RA	[Savage and Chen, 1999]
Face milling	Tool service time, feed rate		Empirical model	[Barber *et al.*, 2001]
Turning	Rotational speed, feed rate, tool geometry, depth of cut, diameter, workpiece length, and vibration	AC (maximum auto-(correlation, power frequencies)	Geometric model	[Abouelatta and Madl, 2001]
Turning	Hardness, cutter nose radius, feed, spindle speed, depth of cut		Nonlinear RA, ANN	[Feng and Wang, 2003]
End milling	Spindle speed, cutting speed, axial and radial depths of cut	DY, AC, AE (frequency analysis, mean forces)	Multiple RA, ANN	[Ertekin *et al.*, 2003]
Turning	Spindle speed, feed rate, depth of cut	AC, (mean vibration amplitude)	Multiple RA	[E D Kirby and Chen, 2004]
Face milling	Cutting speed, feed rate, tool service time		Regression math model	[Sai and Bouzid, 2005]

was around $93\ \%$. In [Mesina and Langari, 2001] a proposal based on a Neuro-fuzzy system was used to predict the condition of the cutting tool in a milling process. The system was configured to diagnose sharp and worn cutting tools. Another work, based on *HMM*, is presented by [Wang *et al.*, 2002] in which the feature vectors were extracted from vibration signals by using wavelet analysis.

[Sick, 2002a] proposed a new hybrid technique for cutting tool wear monitoring in turning which fuses a physical process model with an *ANN* model. The physical model describes the influence of cutting conditions on measure force signals and it is used to normalize those force signals. The performance for the best model was 99.4% for the learning step and $70.0\ \%$ for testing step. Haber and Alique, [Haber and Alique, 2003] developed an intelligent supervisory system for cutting tool wear prediction using a model-based approach. The dynamic behaviour of the cutting force is associated with the cutting tool and process conditions. First, an *ANN* model is trained considering the cutting force, the feed rate, and the radial depth of the cut. Second, the residual error obtained from the measure and predicted force was compared with an adaptive threshold in order to estimate the cutting tool condition. This

Table 2.3: Design of experiments approach. Comparison of the studied factors over R_a and the implemented models.

Process	Studied Factors over R_a	Sensor Signals (Processing Features)	Model Approach	References
End milling	Hardness, cutting speed, feed rate, axial and radial depths of cut		*RSM* (statistical model)	[Fuh and Chang, 1997]
Turning milling	Cutting speed, depth of cut, feed and tool nose radius		*RSM*	[Suresh *et al.*, 2002]
Flat milling	Tool machining time, depth of cut, step over, spindle speed, feed rate		*RSM*	[Ozcelik and Bayramoglu, 2006]
Flat end milling	Feed per tooth, cutting speed, radial and axial depth of cut, and machining tolerance		Taguchi optimization method	[Öktem *et al.*, 2006]

Table 2.4: Artificial Intelligence approach. Comparison of the studied factors over R_a and the implemented models. AC= Accelerometer, DY= Dynamometer, AE= Acoustic Emission.

Process	Studied Factors over R_a	Sensor Signals (Processing Features)	Model Approach	References
Turning	Cutting speed, feed, depth of cut, cutting fluid flow, tool wear, workpiece diameter	DY, AC, AE (Average frequency value)	ANN	[Azouzi and Guillot, 1997a]
End milling	Spindle speed, feed, depth of cut, average vibration	AC (Average amplitude per rev.)	ANN	[Tsai *et al.*, 1999]
Face milling	Depth of cut, cutting speed, feed rate, wear of cutting tool cutting fluid, cutting forces	DY (mean, max, and min forces values)	ANN	[Benardos and Vosniakos, 2002]
Turning	Spindle speed, depth of cut, feed rate, and vibration	AC (Average vibration per rev.)	ANN	[Lee and Chen, 2003]
Turning	Hardness, edge radius, feed, cutting speed, and machining length	DY (mean force value)	ANN and regression models	[Özel and Karpat, 2005]

condition can be new, half-worn, and worn cutting tool. In [Saglam and Unuvar, 2003], the authors worked with a multilayered *ANN* for monitoring and diagnosis of the cutting tool condition and surface roughness. The obtained success rates were 77 % for tool wear and 80 % for surface roughness. In [Dey and Stori, 2004], a monitoring and diagnosis approach based on a Bayesian Network (*BN*) is presented. This approach integrates multiple process metrics from sensor sources in sequential machining operations to identify the causes of process variations. The *BN* was trained with a set of 16 experiments, and the obtained performance was evaluated with 18 new experiments. The *BN* diagnosed the correct state with 60 % confidence level in 16 of 18 cases. In [Haber *et al.*, 2004] an investigation of cutting tool wear monitoring in a High Speed Machining process is presented based on the analysis of different signals. They used sensorial information coming from dynamometers, accelerometers, and acoustic emission sensors in order to obtain the deviation of representative variables. The tests were designed at different cutting speeds and feed rates to determine the effects of a new and worn cutting tool. Data were transformed from time to frequency domain using the Fast Fourier Transform (*FFT*) algorithm. They concluded second harmonic of the tooth path excitation frequency in the vibration signal is the best indicator for cutting tool wear monitoring.

2.4.1 Limitations on the research works in the cutting tool wear condition

Table 2.5 summaries the discussed approaches in this section. Once again, the proposal models are limited to be used in *CNC* conventional, and almost all the models only used the vibration signals to estimate the flank wear of the cutting tool. It is important to include other process signals and new feature extraction from the acquired signals for improving the performance of intelligent monitoring system.

Table 2.5: Comparison of different research efforts in cutting tool condition monitoring. AC = Accelerometer, DY = Dynamometer, AE = Acoustic Emission, SP = Spindle Power.

Process	Monitoring States	Sensor Signals	Recognition Methods	References
Drilling	Tool wear	AC	HMM	[Owsley *et al.*, 1997]
End Milling	Tool Breakage (Normal,Broke)	AC	FFT	[Chen and Chen, 1999]
End Milling	Tool wear (worn, no-worn)	AC	HMM	[Atlas *et al.*, 2000]
Turning	Tool wear (Wear value)	Process parameters	ANN	[Sick, 2002a]
Face Milling	Tool wear, Surface Roughness	DY	ANN	[Saglam and Unuvar, 2003]
Milling	Tool wear (New,half worn, worn)	Process parameters	ANN	[Haber and Alique, 2003]
Milling	Tool wear (New, worn)	AE, DY,AC	FFT	[Haber *et al.*, 2004]
Face Milling	Tool wear (Low-high)	AE, SP	BN	[Dey and Stori, 2004]

2.5 State of the art in the optimization systems

This section presents important research works related with different optimization methods and modelling techniques to compute the optimal cutting parameters in the machining processes. In [Chua *et al.*, 1993] research is presented to study the effects of depth of cut, feed rate and cutting speed of the tool life, and cutting forces and power consumption during the turning of the medium carbon steel workpieces. Full factorial design was applied, and mathematical models for the prediction of the tool life and cutting forces were computed by using multiple regression analysis. From the *ANOVA* analysis, the model for the tool life was computed with a correlation coefficient of 0.9083. For the forces model, the correlation coefficient was 0.997. These mathematical models were required to compute the optimal cutting conditions by using a sequential quadratic programming technique. [Carpenter and Maropoulos, 2000] described a procedure to select tools for rough and finish milling operations in a *CNC* machining center. First, the cutting data are generated for each tool using an iterative method in the permissible depth/width/feed space for good chip control. Second, the cutting data are refined by a set of technological constraints, which include tool life, surface finish, machine power, and available spindle speeds and feeds. The optimization criterion is selected by the user and it could be minimum cost, maximum production rate or predefined tool life. In [Dereli *et al.*, 2001], the authors described an optimization system called *Cutting Parameters Optimization System* (*CPOS*). The system was developed by using a two-stage methodology. In the first stage, a tentative number of passes and depth of cuts to be removed are determined through a method called *volume sectioning*. In the second stage, the cutting speed and feed for each pass are optimized by using Genetic Algorithms (*GA*). The cutting tools are selected from respective tool libraries. The optimization strategy is based on minimum production time and minimum production cost and incorporates several technological constraints, such as power, surface finish, speed, feed limitations, etc.. The percentages of the cost and time-saving were found to be 33% and 39%, respectively.

In [Suresh *et al.*, 2002], a second order mathematical model was developed for R_a prediction. The *RSM* methodology was used for modelling the R_a as a function of the cutting speed, feed, depth of cut, and nose radius of the cutting tool in turning operations. The mathematical model was taken as an objective function and was optimized using a Genetic Algorithmic (*GA*) approach. With the *GA* approach, a combination of high cutting speed, low feed, and moderate depth of cut and nose radius were selected for a better R_a. In [Mursec and Cus, 2003], a general algorithm is implemented for the selection of optimal cutting conditions (feed rate, cutting speed, and depth of cut) and calculating the number of required cuts and time machining. The algorithm consists to follow several sequential steps. First, it uses various technological databases to select the cutting parameters. Secondly, specific working conditions are compared with the limitations of the machine tool, the cutting tool, the workpiece, the cutting conditions, and the necessity of minimization of the machining costs. In [Zuperl *et al.*, 2004] a new hybrid optimization technique is presented based on the maximum production rate criterion and ten technological constraints. A general algorithm, called *OPTIS*, is used in conjunction with the *ANN* model in order to solve the complex optimization problem. The *OPTIS* selects the optimum cutting conditions from commercial databases with respect to minimum machining costs. The optimal machining parameters (cutting speed, feed rate, and depth of cut) are selected in order to optimize an objective function for turning processes. [Tzeng and Chen, 2005] proposed a two-phase optimization strategy based on the Taguchi dynamic characteristic theory. Experimental results showed that the machining time

can be reduced with low process variance and increased robustness of the *CNC* milling processes. The Taguchi method coupled with Principal Component Analysis (*PCA*) in the process optimization of high speed *CNC* milling processes is presented in [Yih-fong, 2005]. Optimal process conditions are selected for producing the best dimensional precision, surface roughness, and tool wear. The select factors are milling type, cutting speed, feed per tooth, film material, tool material, number of teeth, rake angle, and helix angle, which are designed in a L_{18} orthogonal array and carried out in the experiments.

After *OPTIS*, [Zuperl *et al.*, 2006] proposed an adaptive neural controller for on-line optimal control of a milling process. The milling state was estimated by the measured cutting force, and the feed-rate was selected as the optimized variable. Tool wear and tool breakage were prevented by adjusting the feed rate. In [Tansel *et al.*, 2006], a Genetically Optimized Neural Network Systems (*GONNS*) was proposed for the selection of optimal cutting conditions from experimental data in milling processes, and it was was tested in two different conditions. First, optimal operating conditions were found to keep the cutting forces in the desired range, while the metal removal rate was maximized in micro-end milling. Second, optimal operating conditions were calculated to obtain the best possible compromise between the surface roughness of the machining time. A Deckel Maho with five axis was used, and the workpiece material was 6061 aluminum. The *ANN* models allow computing of the metal removal rate and feed direction cutting force for the first case and the surface roughness and machining time for the second case. In both cases, a Genetic Algorithm (*GA*) was used to maximize the metal removal rate and minimize the surface roughness. In [Palanisamy *et al.*, 2007] a mathematical model was developed based on both the material behavior and the machine dynamics to determine cutting force for end-milling operations. Furthermore, a genetic algorithm was introduced to optimize the cutting parameters for minimizing machining time and maximizing tool life for a constant material removal rate. The experiments were carried out on a *Star Mill-ATC* milling machine and the workpiece material was mild steel.

2.5.1 Limitations on the optimization systems

Table 2.6 shows a comparison of the research works in optimization of machining process. It is observed that several optimization criterions have been used for computing the optimal cutting parameters. However, these approaches have been implemented with the support of different databases and libraries for selecting the cutting tools and optimal cutting parameters for conventional *CNC* machining centers. Additionally, different *AI* techniques have been implemented in the optimization systems. One limitation is that they have not included a decision-making block to recommend optimal actions at the *CNCs* operator.

2.6 Analysis of the contributions

Even though there is enough research to predict R_a, more general and practical solutions are needed owing to new materials and cutting tools that are employed in *HSM*. Furthermore, exploiting sensor fusion techniques should be a great opportunity. Specifically, intelligent fusion that includes fuzzy logic, artificial neural networks, and genetic algorithms must be used to model the R_a. In this field, the contributions will be focused on the following items:

Table 2.6: Summary of the optimization research works in the machining process.

Reference	Machining	Optimization Process	Objective Function
[Chua *et al.*, 1993]	Turning	Sequential quadratic programming technique	Cutting speed, feed rate, and tool life.
[Carpenter and Maropoulos, 2000]	Milling	Iterative method	Minimum cost, predefined tool life, maximum production rate.
[Dereli *et al.*, 2001]	End, Face milling	Volume sectioning and *GA*	Minimum production time and cost.
[Suresh *et al.*, 2002]	Turning	Response Surface Methodology and *GA*	Minimum surface roughness.
[Mursec and Cus, 2003]	Turning, milling	Data from tool manufactures	Minimize the machining cost.
[Zuperl *et al.*, 2004]	Turning	*OPTIS* algorithm and *ANN*	Maximum production rate and minimize machining costs.
[Tzeng and Chen, 2005]	Milling	Taguchi dynamic characteristic theory	High machining efficiency and geometrical accuracy.
[Yih-fong, 2005]	Milling	Taguchi method and *PCA*	Process conditions (milling type, cutting speed, feed per tooth, etc.)
[Zuperl *et al.*, 2006]	Milling	Adaptive neural controller	Regulate the cutting force by adjusting the feed rate.
[Tansel *et al.*, 2006]	Milling	*GONNs* and *ANN*	Maximum metal removal rate and minimize surface roughness.
[Palanisamy *et al.*, 2007]	End milling	Mathematical model and *GA*	Minimum machining time and maximize tool life.

- Define important factors which directly affect the surface roughness and build statistical models by considering several materials and cutting tools in the peripheral end milling process.
- Include the concept of the geometric curvature during the cutting process. It could be an important factor affecting the R_a.
- Select important information of the process state variables and apply sensor fusion techniques to improve the estimated R_a of the models.
- The models must consider the cutting tool wear condition to predict the surface roughness.

In the field of indirect cutting tool wear monitoring, several suggestions of directions that should be exploited in future research are presented. At the feature extraction level, the most frequently used techniques are the computation of average values or trends, power values in different adjacent spectral bands or statistical features (variance or standard deviation). It is relevant to propose other techniques to compute the features from recorded signals that allow the characterization of the different cutting tool conditions during the tool life. The future of a Tool Condition Monitoring (*TCM*) system will have to be based on inexpensive, simple, and rugged sensors and methodologies. An important contribution could be the implementation of the *TCM* in the aeronautic and automotive industries.

It is very important to consider the integration of machine tool and cutting process dynamics with *TCM* systems. Also, the future of the *TCM* systems must include applications where prior knowledge or cutting data may not exist. Artificial Intelligence, *ANNs*, fuzzy logic systems, and *GAs* should be some options to solve this situation. With respect to the optimization methods in the metal cutting process, process planners continue to experience great difficulties owing to lack of performance data on the numerous new commercial cutting tools with different materials, geometry, resistance and effective chip breaking. Furthermore, specific data on relevant machining performance measures such as tool life, surface roughness, and chip form, etc. are hard to find owing to a lack of predictive models for these measures. The determination of optimal cutting conditions is regarded as the only way of ensuring maximum technical and economic efficiency of production. Additionally, a decision-making block is recommended to predict optimal actions for the operator and minimize the operation costs.

Chapter 3

Intelligent Monitoring and Supervisory Control System

3.1 Introduction

Milling processes have been improved with the introduction of new technologies such as High Speed Machining (*HSM*), new cutting tool materials, and high precision sensing devices. Nowadays, peripheral milling processes in *HSM* require to be operated with Optimum Cutting Data (*OCD*), which take into account both economic and technical limitations of the *CNC* machining center [Tönshoff *et al.*, 1988]. Also, technical information about the *OCD* in *HSM* is not available in handbooks or databases. Therefore, the cutting parameters are estimated with a direct impact on the metal cutting economics: high costs, low productivity, and poor quality of the product. Operation with *OCD* and the need of technical information for computing optimal cutting parameters are some reasons for modelling the behavior of the R_a as a function of the Cutting Conditions (C_C), Geometric Parameters (P_G), Cutting Parameters (P_C), and cutting tool wear condition. Additionally, the inexperience of the operator has a direct impact on the performance and reliability of the *CNC* machining center because the cutting tools are not used to their full tool-life capability, the poor quality of the R_a is not detected on time, and the training curve in the *CNC* operation has a huge impact in the effective machining time, among others.

Currently, there is a need to develop an Intelligent Monitoring and Process Planning System to determine the optimal cutting parameters in milling operations, especially in *HSM* and giving support to the operator of the *CNC*. A proposal to design and implement a Supervisory Control System for the Peripheral Milling Process in *HSM* is presented in this chapter.

3.2 Intelligent monitoring and process planning system

A cost-effective supervisory system implies the design and integration of an intelligent monitoring and process planning system, as shown in Figure 3.1. The system estimates the surface roughness and recommends the *OCD* before running the *CNC* machining center (*Pre-process*). During the machining process (*In-process*), the R_a is computed by using the process state signals, and the system should be adapted to the needed changes in the cutting parameters and maintain the R_a quality. The system integrates four main modules (see chapter 6), in which R_a and the cutting tool condition are key variables. The modules are:

- **Data acquisition system**. During the machining process, several process variables are measured with multiple-sensors (accelerometers, acoustic emissions, and dynamometer). The LabView program is used as *HMI* to monitor and record the process variables during the machining process.
- **Surface roughness**. The surface roughness is estimated (R_a^P) as a function of C_C, P_C, P_G, and the flank wear of the cutting tool. The parameters are defined by the operator to compute the desired value of R_a^d. The statistical models are described in Chapter 4.
- **Cutting tool wear monitoring**. This module predicts the cutting tool wear condition by using the process variables. It is very important to know when a tool ceases to produce workpieces with excellent surface quality before it damages workpieces. Chapter 5 develops the recognition system for the cutting tool wear condition.
- **Intelligent process planning system**. The system computes optimal cutting parameters by considering tool life, minimum surface roughness, and including a decision-making block to recommend operator's actions that minimize production cost. Chapter 6 presents a complete description of control of the R_a in *Pre-process* and *In-process* operating mode. The results of validation tests are also included.

3.3 Data Acquisition System

The data acquisition module was implemented in the machining center HS-1000 Kondia. Several sensors were installed to improve the reliability of the intelligent monitoring and diagnosis system. The sensors have reliable frequency bandwidth, good signal to noise ratio, and signals with reliable correlation to the process state.

3.3.1 Experimental set-up and sensors

The experiments were conducted in a *HSM* center HS-1000 Kondia with a 25 KW drive motor, three axis, a maximum spindle speed of $24,000$ rpm, and a Siemens open Sinumerik $840D$ controller. The *CNC* machining center is shown in Figure 3.2. During the experiments, several *HSS* end mill cutting tools (25^o helix angle, and 2-flute) from Sandvik Coromant were selected for the end milling process, and different workpiece materials (aluminium with hardness from 70 to 157 BHN) were used for the experimentation. The workpiece materials and cutting tools

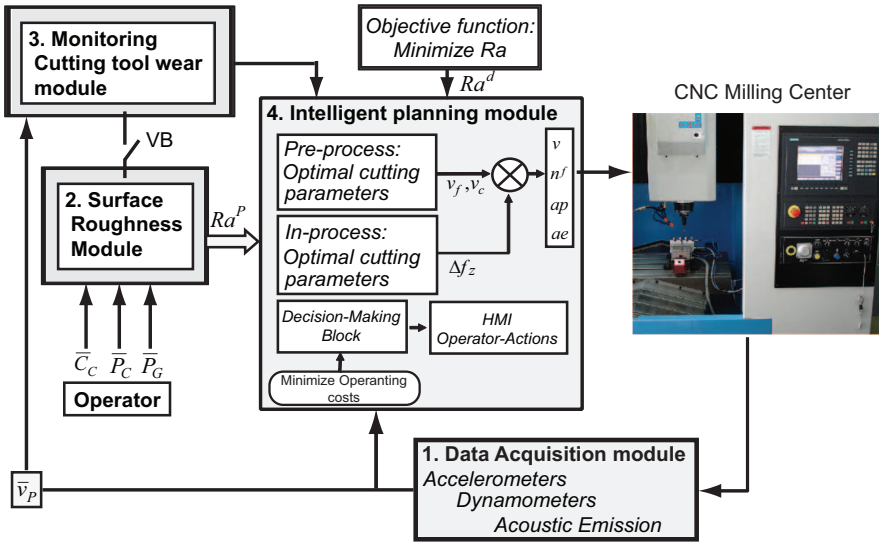

Figure 3.1: An intelligent monitoring and supervisory control system can provide cost effective control of milling parameters based on surface roughness and cutting tool condition. The process state signals are recorded (module 1) and used for monitoring the cutting tool wear condition (module 3). The R_a module (module 2) estimates the R_a in Pre-process operating mode. The intelligent planning module (module 4) computes the optimal parameters in Pre-process and In-process operating mode.

are defined in Table 3.1. These materials were selected because they have important applications in the mold/die manufacturing industry. Several cutting tool diameters (from 8 to 20 mm) were also used.

The Data Acquisition System consists of several sensors, amplifiers for conditioning, and filtering the signals, two data acquisition boards, and LabView software for controlling the data acquisition system. Figure 3.2 shows the complete experimental set-up. Figure 3.3 depicts all the sensors for monitoring the peripheral milling process.

3.3.2 Sensors, amplifiers, and data acquisition boards

Several research works have used multiple sensors to monitor and control different process parameters in the metal cutting process ([Dimla, 2000], [Azouzi and Guillot, 1997b], [Ghosh *et al.*, 2007]). Multiple sensors (accelerometer, acoustic emission, and dynamometer) installed in the *CNC* machining center will be described in this section. Table 3.2 shows a list of the sensors installed on the *CNC* machining center.

Accelerometer (vibration signals)

For measuring the vibration between the workpiece and cutting tools, two PCB Piezotronics accelerometers model 353B04 were fixed on the workpiece in X and Y axis directions (see Figure 3.4). These sensors record the vibration

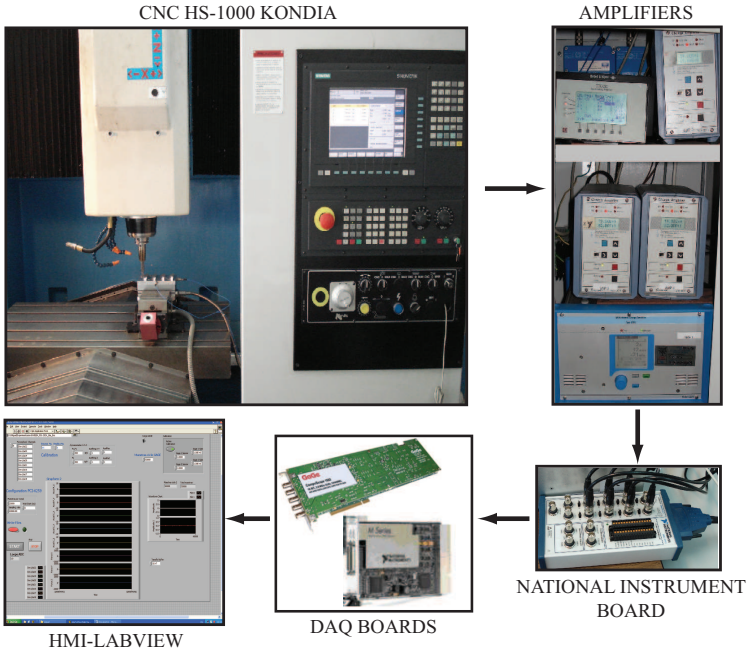

Figure 3.2: Experimental set-up: *CNC* machining center, amplifiers, DAQ boards, and LabView program.

Table 3.1: Workpiece materials and cutting tools

Workpiece Materials		Cutting Tools	
Aluminium alloy	Average hardness (BHN)	Sandvik code	Diameter (mm)
$AW5083-H111$	70	$R216.32-08025-AP12AH10F$	8
$AW6082-T6$	95	$R216.32-10025-AP14AH10F$	10
$AW2024-T3$	110	$R216.32-12025-AP16AH10F$	12
$AW7022-T6$	139	$R216.32-16025-AP20AH10F$	16
$AW7075-T6$	157	$R216.32-20025-AP20AH10F$	20

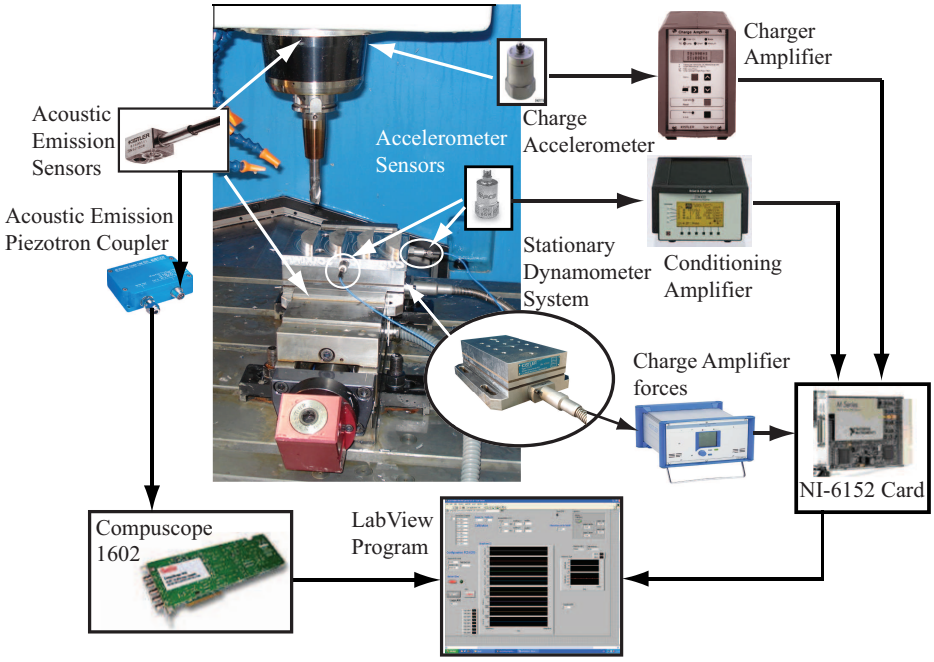

Figure 3.3: The Data acquisition system is shown with the different sensors (Accelerometers, Acoustic Emission, and Dynamometer), the charger amplifiers, and the acquisition boards. A LabView program was used to control and record the different process state signals during the experimentation.

signals during the cutting process. The accelerometers have a sensitivity of $10\ mV/g$ in a frequency range from 0.35 to $20,000\ Hz$, and the measurement range is $500g$. The technical information of the sensors is presented in [Acc-PCB, 2006]. Another three Brüel & Kjær piezoelectric accelerometers (one model 4370 in Z axis, and two model 4371 in X and Y axis) were installed on a ring fixed to the spindle of the *CNC* machining center, Figure 3.4. The sensors were fixed inside of the ring to protect them from chips and harsh environment. The characteristics of these sensors (see [Acc-Brüel & Kjær, 2006]) are: charge sensitivity of $98 \pm 2\%\ pC/g$ (model 4370), and $9.8 \pm 2\%$ pC/g (model 4371); resonance frequency of $16\ KHz$ for the model 4370 and $42\ KHz$ for the model 4371. The acquired signals from the *AC* sensors are conditioned by different amplifiers (charge or voltage). For the *AC* sensors fixed on the workpiece, a Nexus conditioning amplifier 2693 model from Brüel & Kjær was used. For each Brüel & Kjær piezoelectric accelerometer a Kistler charge amplifier type $5011B$ was used. The amplifier converts the electrical charge yielded by the piezoelectric sensor into a proportional voltage signal. The amplifier configuration is presented in Appendix B.

Table 3.2: Characteristics of the sensors installed on the *CNC* machining center

Qty	Sensor (Model)	Characteristics	Localization
2	PCB piezotronics accelerometers (353B04)	Sensitivity: $10mV/g$ Frequency range: $0.35 - 20000Hz$	$y\&x$ axis Workpiece
2	Kistler Piezotron Acoustic Emission (8152B1)	Sensitivity: $700V/(m/s)$ Frequency range: $50 - 400KHz$	One fixed on the spindle; another fixed on the hydraulic clamping
1	Kistler 3-Component force Dynamometer (9257B)	Force range: -7.5 pC/N in x, y axis, -3.5 pC/N in z axis Natural frequency: $3.5KHz$	Fixed on the hydraulic clamping
3	Brüel and Kjær piezotronics accelerometers (4370 and 4371)	Charge sensitivity: $98 \pm 2pC/g$ Resonant frequency: $16KHz$ (4370), $42KHz$ (4371)	All fixed on the ring in the *CNC* spindle

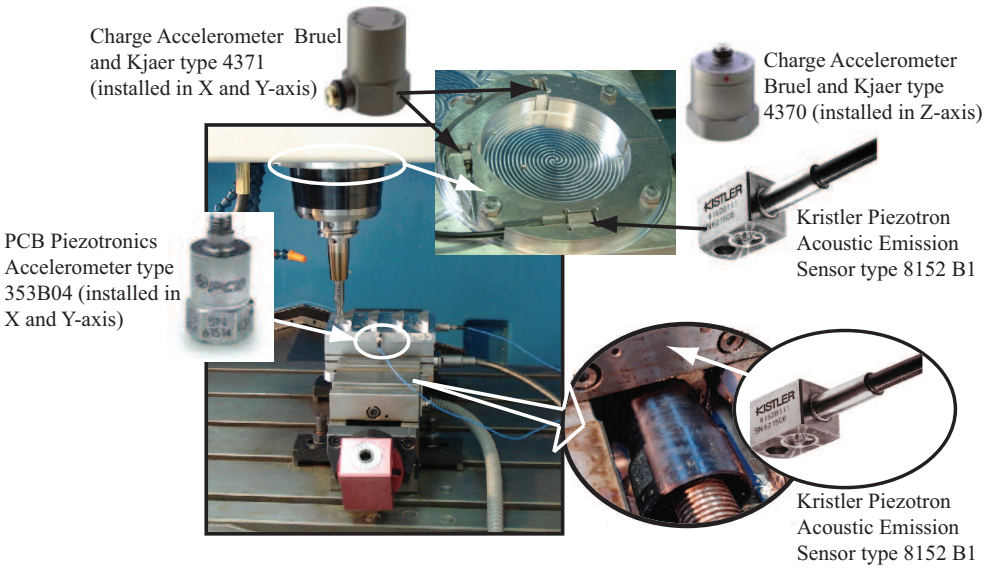

Figure 3.4: The accelerometers and acoustic emission sensors were fixed in a ring (up plot), and it was fixed on the *CNC's* spindle. Another acoustic emission sensor (see lower right plot) was attached to the back of the hydraulic clamp. Two accelerometers were directly attached to the workpiece material.

Acoustic emission

Several research works, [Li, 2002], [Kannatey-Asibu and Dornfeld, 1982], [Guo and Ammula, 2005], have shown that *AE* has been successfully used to detect tool wear, fracture in cutting tools, and quality of surface roughness. *AE* signals can be classified into two types ([Kannatey-Asibu and Dornfeld, 1982] and [Guo and Ammula, 2005]): continuous signals and burst-type signals. Burst-types are a result of slip-line formation and surface microcracks, while signals present high amplitude and low frequency. Continuous type are associated with internal mechanisms activity (such as tensile test of specimens) and with shearing on the wear of the tool flank. These signals present lower amplitude and high frequency. The *AE* signals were recorded with a Kistler Piezotron Acoustic Emission $8152B1$ model ([Kistler-AE, 2006]). It was installed on a ring in the *CNC's* spindle. The *AE* has a frequency range from 50 to 400 KHz and sensitivity of 700 $V/(m/s)$. Figure 3.4 shows the *AE* installed on the ring and on the *CNC* table. The high frequency output signals from the *AE*-Piezotron sensors must be processed with an *AE*-Piezotron coupler. The *AE*-Piezotron coupler with built-in *RMS* converter and limit switch has been designed for the processing of high-frequency sound emission signals from Kistler Piezotron *AE* sensors. The coupler output signals are the following analog signals: *AE-Out* (filter), *AE-Out*(RMS) and a digital output signal (limit switch). The coupler supplies power to the sensor and processes the sound emission signal. During the experimentation the *AE-out* (filter) signal was selected to be recorded. Technical information (see [Kistler-AE-Coupler, 2006]) of Piezotron coupler is given by:

- For the *AE-out* signal frequency range from 15 to 1000 KHz, 5% of accuracy, and output voltage of ± 5 V.
- For the *AE*-RMS signal frequency range from 10 to 1000 KHz, 3% of accuracy, and output voltage of 0 to 5 V.

Dynamometer

The cutting forces are important owing to the forces could be correlated to tool wear and surface roughness. The force becomes important in worn tool conditions as a result of the variations produced owing to friction between a tool flank and the workpiece. A Kistler 3-Component Dynamometer, $9257B$ model, was used to measure the cutting forces [Kistler-Dy, 2006]. The main technical characteristics are forces range ± 5 KN, sensitivity for the X and Y Forces at -7.5 pC/N, Z-Force at -3.5 pC/N, and natural frequency at 3.5 KHz. A multi-channel charge amplifier type, $5070A$ from Kistler, was used to amplify the force signals. The amplifier configuration is shown in Appendix B.

Data acquisition boards

The signals were acquired with two data acquisition boards. Two boards were used because the required sampling rate for the *AE* sensors was higher than the other signals. The data acquisition boards were the following:

1. A high speed multifunction DAQ NI-6152 card was used to record the signals from accelerometers and forces; it ensures a $16-$bit accuracy at a sampling rate of 1.25 MS/s.

2. A CompuScope 1602 card for a *PCI* bus with two analog input channels, 16bit resolution, and a sampling rate of 2.5 MS/s.

The data acquisition boards are depicted in Figure 3.3, and technical information can be found in [NI-DAQ, 2006] and [Gage-Compuscope, 2006].

3.3.3 Pre-processing of the signals

The process signals recorded during the machining process contain abundant information related to tool status and surface roughness. This information can be fundamental frequencies, frequency bandwidth, amplitude, energy, and sensitivity to detect chatter condition, cutting tool wear, and the surface finishing. On the other hand, for the estimation of the surface roughness and cutting tool condition, several research works have reported different processing methodologies to capture and pre-processing the signals. In [Azouzi and Guillot, 1997b], the authors used dynamometer, accelerometers and acoustic emission sensors. All the signals were acquired at a frequency of 880 Hz. The signals were required to estimate on-line surface roughness and dimensional deviations during the turning process. In [Ertekin *et al.*, 2003] the authors used different sensors to control the dimensional accuracy and surface roughness in the *CNC* milling process. The acceleration and force signals were acquired with a sampling rate of 10 KHz and 2048 samples points per signal. The *AE* signals were recorded with a sampling rate of 1 MHz.

Relevant information from the accelerometers and dynamometer signals

Several tests were done to determine the correct sampling rate and the required adjustments for the amplification system. The first test was defined to identify the tooth passing frequency for each process signal. The force and acceleration signals were recorded at a sampling rate of $40,000$ Hz with the amplification system described in section 3.3.2. In the time domain, the signals were transformed at the frequency domain by applying the Fast Fourier Transform (*FFT*), and the Power Spectral Density (*PSD*) was computed. Figure 3.5 shows the recorded signals during the cutting process with a new cutting tool (experiment number 02 and second replicate of the *DoE*, Chapter 4, Section 4.7). The cutting conditions for this experiment are defined in Table 3.3. Figure 3.6 shows the frequency domain of the process state variables and where the cutting frequency is shown of each signal. Also, additional information can be observed in the plots (energy, amplitude, frequency bandwidth, etc.) to characterize the process. The first test was validated with these results.

The second test was defined to compare the behavior of the signals with different flank wear of the cutting tool. Figure 3.7 depicts the frequency domains obtained from different sensors (accelerometers in the workpiece, and spindle, and Y axis force) and for different cutting tool conditions. The signals correspond to the cutting conditions defined in Table 3.3. The plots of frequency domain of other cutting tool conditions are shown in Appendix B.

The observed behavior during this experimentation, with different states of the cutting tool condition, is described as follows:

- The frequency domain for the Y axis workpiece accelerometers shows that second harmonic of the tooth passing frequency is dominant (1200 Hz) for low frequencies. The amplitude is almost constant for the

Table 3.3: Cutting conditions of the selected experiment (number 02 and second replicate, Chapter 4, Section 4.7).

Cutting Conditions	Value-Units
Feed per tooth (f_z)	0.1 mm/tooth
Cutting speed (v_c)	565 m/min
Spindle speed (n)	18000 rpm
Radial depth of cut (ae)	4 mm
Workpiece hardness (HB)	94 mm
Cutting tool diameter (D_{Tool})	16 mm
Geometry path	Concave

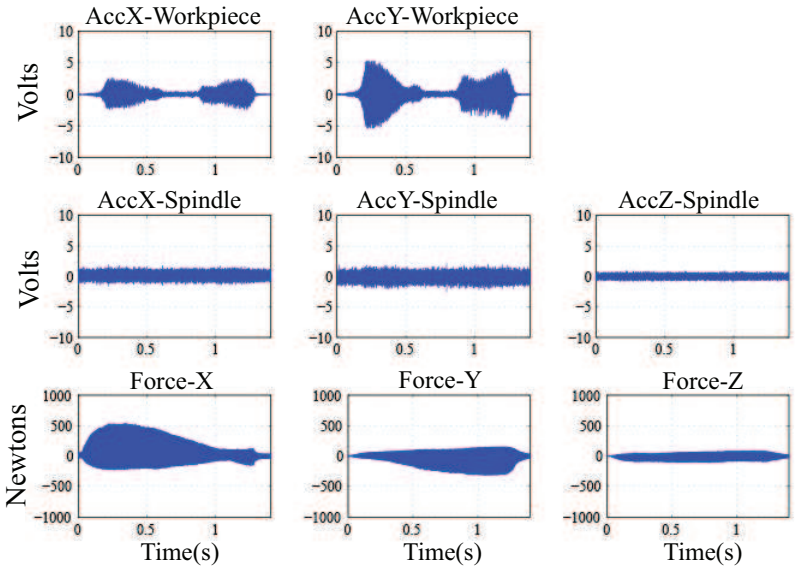

Figure 3.5: Process signals recorded during the cutting process with fresh cutting tool. The $AccX-Y$ Workpiece plots show the vibration recorded from the accelerometers installed on the workpiece. The $AccX-Y-Z$ Spindle plots depict the vibration signals from the accelerometers fixed to the spindle. The $ForceX-Y-X$ plots show the behaviour of the cutting forces during the cutting process.

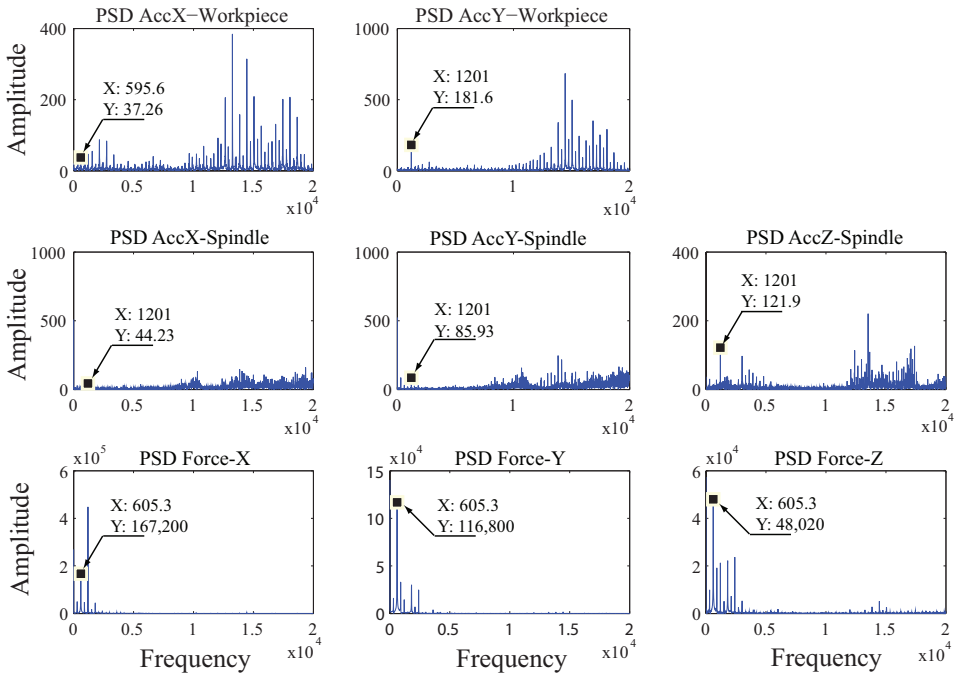

Figure 3.6: Power spectral density (PSD) plots in the frequency domain of the signals. The harmonics of the tooth passing frequency are shown for each signal. The first harmonic (600 Hz) is observed in the cutting force signals, and the second harmonic (1200 Hz) is dominant in the vibration signals.

new and half-new cutting tool condition, and it decreases for the half-worn condition. However, for the worn cutting tool condition, the amplitude presents a significant increase with respect to the new cutting tool condition. Also, it is observed that an important frequency bandwidth between 10 to 20 Khz can be used to characterize the different states of the cutting tool condition.

- The frequency domain for the Y axis accelerometer in the spindle shows a similar behavior for the sensors installed in the workpiece. However, the plots do not show all the signal spectrum owing to the limitations in the frequency range of the sensors. These signals could not be adequate to identify the cutting tool wear condition, and the correlation with the surface roughness could be unsatisfactory.

- The frequency domain of the Y Force signals depict a constant increase in the amplitude of the first harmonic (600 Hz) with the evolution of flank wear in the cutting tool. These signals are recommended to evaluate the surface roughness and cutting tool wear condition.

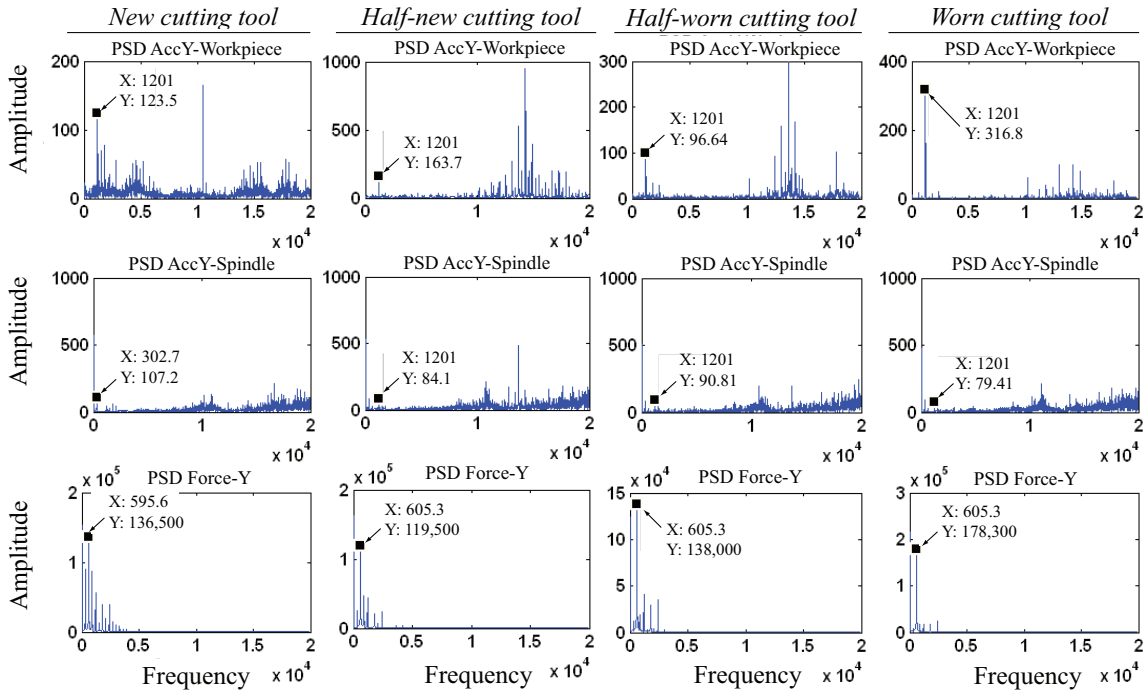

Figure 3.7: Power spectral density (PSD) plots in the frequency domain of specific signals for the experiment number 02 and different states of the cutting tool condition. For the acceleration $Acc-Y$-Workpiece and $Force-Y$ signals, a similar behaviour is observed in the amplitude of the second and first harmonics, respectively: The amplitude is high for new cutting tool condition, it decreases for half-new and half-worn condition, and finally presents a higher amplitude value for the worn cutting tool condition. The amplitude for the $Acc-Y$ Spindle signal always decreases from new until worn cutting tool condition.

Relevant information from the Acoustic Emission signals

Several tests were made to determine the correct sampling rate for the *AE* sensors. The signals were recorded with a sampling rate of 1 MHz and the output signal from the *AE*-Piezotron coupler was the *AE-out* signal, with a frequency range from 15 to 1000 KHz, 5% of accuracy, and an output voltage of ± 5 V. The first step was to determine the sampling rate for the *AE* signals. During the cutting process of a straight path, the *AE* signals were recorded with a different sampling rates. The cutting conditions were $v_f = 1200$ mm/min, $n = 18000$ rpm, $ae = 2$ mm, and $ap = 5$ mm. Figure 3.8 shows three plots of the same experiment, but with different sampling rates: 200 KHz, 500 KHz, and 1 MHz respectively. Figure 3.9 depicts the frequency domain of each experiment, and where it is observed, the third experiment allows for the capture of complete frequency bandwidth of signals. From results, the selected sampling rate was 1 MHz.

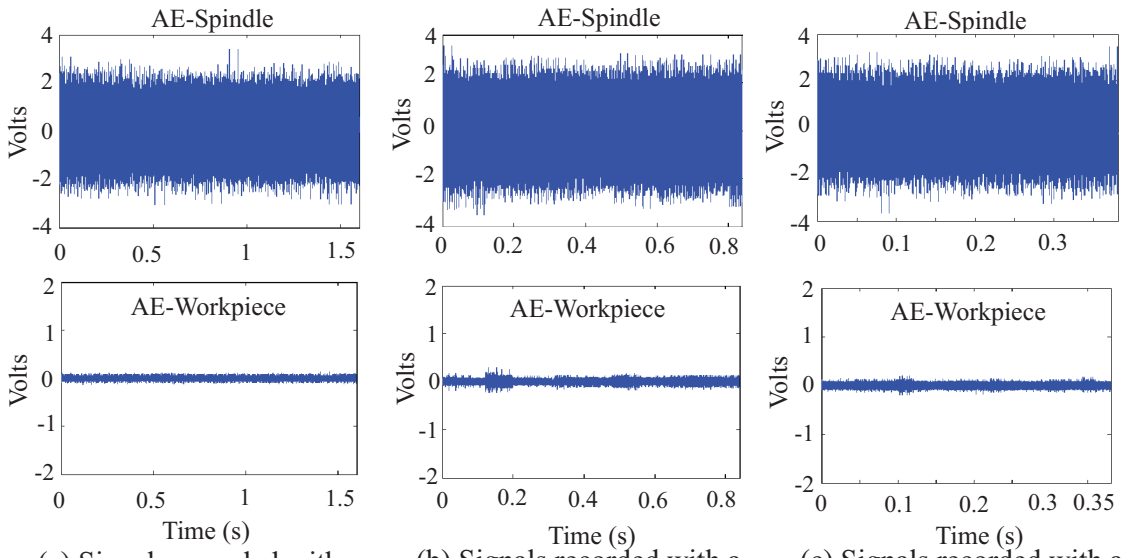

(a) Signals recorded with a sampling rate of 200 KHz

(b) Signals recorded with a sampling rate of 500 KHz

(c) Signals recorded with a sampling rate of 1 MHz

Figure 3.8: AE-signals recorded with different sampling rate during the machining process of a straight path.

The second test with the *AE* was defined to determine the correlation between two *AE* sensors (one installed in the spindle and the other attached to the back of the workpiece). By considering the signals obtained in experiment number 02 (see Chapter 4, Section 4.7), several frames were selected to compute the power spectral density of both signals. The cross-correlation between the two signals in the frequency domain was computed to demonstrate that both signals present similar behaviour for the frequency bandwidth during the machining process. Figure 3.10 defines the following observations: (a) At 0.1 seconds the frequency bandwidth is shown owing only to the *CNC* rotational speed (i.e., there is not cutting process); (b) At 0.2 seconds the bandwidth between 140 and 180 KHz appears, and it corresponds with the cutting process; (c) and (d) At 0.3 and 0.4 seconds, the plots show the decrease in frequency amplitude owing to the turn off of the *CNC*.

Finally, Figure 3.11 shows the power spectral density in the frequency domain of the *AE* signals at different cutting tool wear conditions. Other results are depicted in Appendix B with different cutting tool conditions.

3.3.4 Feature vectors extracted from vibration, forces, and acoustic emission signals

The process signals contain abundant information which can be used to recognize the cutting tool condition during the machining process. The signal features describe the power level of the signals in a given time interval and can be classified in the following domains:

Time domain. These are computed from the force and vibration signals. Some examples are: average values or

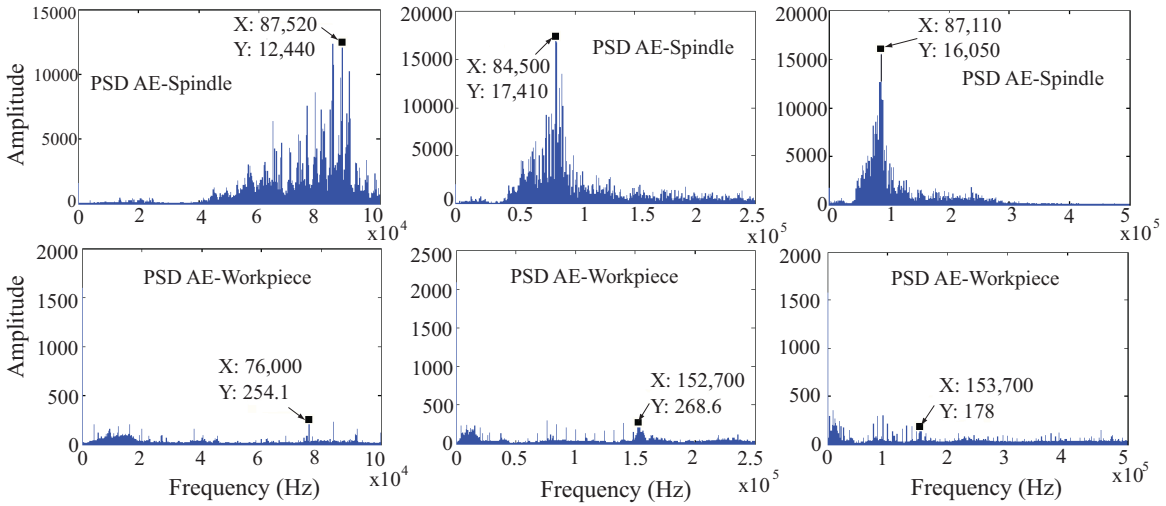

(a) PSD computed for the AE-signals with a sampling rate of 200 KHz

(b) PSD computed for the AE-signals with a sampling rate of 500 KHz

(c) PSD computed for the AE-signals with a sampling rate of 1 MHz

Figure 3.9: Power spectral density (PSD) of the *AE* signals. Three different tests were defined to compute the sampling rate for the *AE* signals.

Root Mean Square (*rms*) values in certain time intervals, changes in signal levels such as increments or decrements, crest factors, and polynomial approximations of force and vibration signals.

Frequency domain. The determination of spectral features is based on a discrete windowed Fourier Transform, which is the total power level of a signal with or without a static component and the power in different spectral bands.

Statistical domain. The signals are non-stationary, but they are assumed to be stationary during short time intervals, for which features are computed. Features that describe the probability distribution of random process are the mean, variance, standard deviation, skew, and kurtosis.

Time-frequency domain. These features are usually computed by applying the wavelet transforms. The use of wavelet coefficients as features allow the time resolution to be adapted for analysis of local frequency of the signal. The selected features represent the signal characteristics that could be sensitive to tool wear in a compact form.

The feature selection process is very important because it can reduce the cost of recognition by reducing the number of features that need to be collected and also improve the classification accuracy of the system. The selection process is not necessarily trivial. Using all possible features is not practical because irrelevant features add noise to the classifier, making the diagnostic task harder or computationally expensive. This section describe a new approach to compute important features of the process signals based on the Mel Frequency Cepstrum Coefficients (*MFCC)*. In speaker identification systems the *MFCCs* define the speaker characteristics (features) of a speech segment. In [Davis and Mermelstein, 1980], [Wong and Sridharan, 2001], and [Molla and Hirose, 2004] used the *MFCCs* in

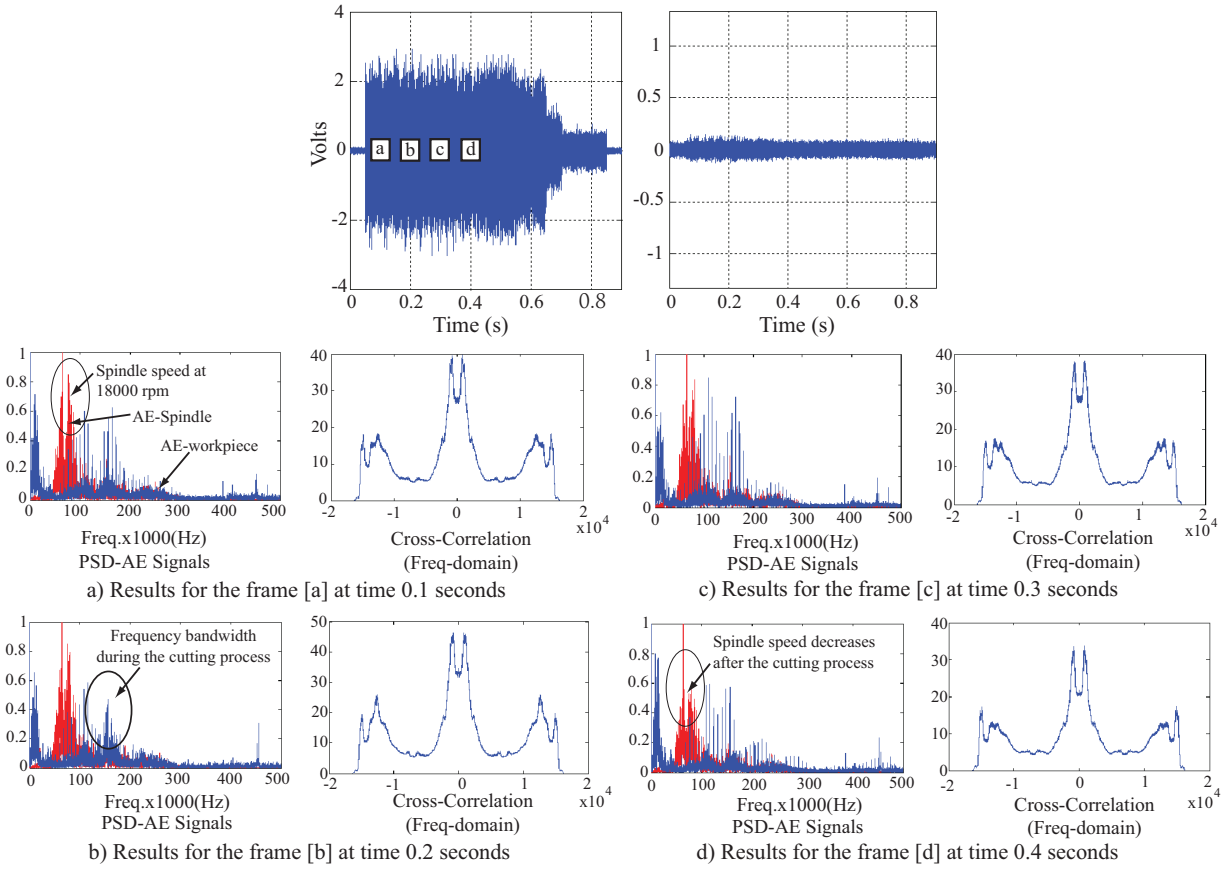

Figure 3.10: AE Signals in the time domain and Power spectral density of AE-signals. The plots show the correlation between the AE-Spindle and AE-Workpiece signals at different times. Figure (a) shows only the power spectral density of the spindle speed before starting the cutting processes. Figure (b) depicts the frequency bandwidth owing to the cutting process, and Figures (b) and (c) show only the power spectral density of the spindle speed after the cutting process.

different modeling techniques (*ANN*, *HMM*, etc.) to implement robust speech recognition systems. These features will be used to identify the cutting tool wear condition by using the *HMMs* and *ANN* models.

Mel frequency cepstrum coefficients

The cepstrum techniques are suited for the analysis of data contain echoes (wavelets) or reverberations of a fundamental wavelet whose shape need not be known *a priori*. The power cepstrum is usually used to determine the arrival times of the fundamental wavelet and its echoes and their relative amplitudes. In speech recognition systems

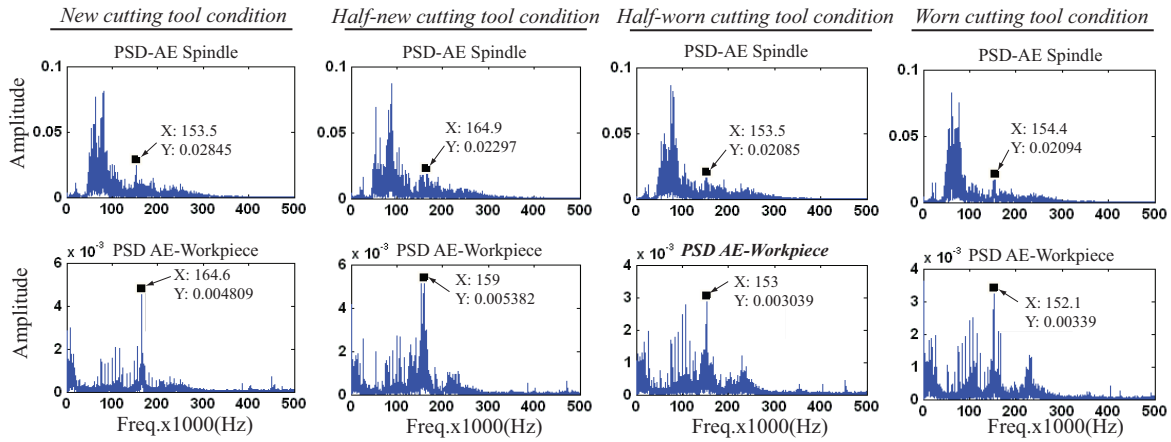

Figure 3.11: The plots depict the power spectral density for the *AE* signals at different cutting tool wear conditions of experiment number 02. The plots show the frequency bandwidth for the cutting process and the variation in the amplitude for the $153\ KHz$ harmonic at different cutting tool wear condition.

the cepstrum analysis has given better results that any other model. The main advantage of cepstrum analysis is its homomorphic properties, the ability to separate the transfer function of the vocal tract from the input signal. [Childers *et al.*, 1977] defined the ***cepstrum*** *of a function as the power spectrum of the logarithm of the power spectrum of a signal in a time domain*. Several authors ([Davis and Mermelstein, 1980], [Molla and Hirose, 2004], and [Zigelboim and Shallom, 2006]) have demonstrated that an important improvement in the speech recognition systems could be obtained if they use the so-called *mel-cepstrum*. A *mel* is a unit of measure of perceived pitch or frequency of a tone. The Mel Frequency Cepstrum Coefficients (*MFCC*) is based on the nonlinear human perception of sound. It utilizes a filter bank to perform a nonlinear frequency mapping of the spectrum of each speech frame. The procedure for computing the *MFCC* of a process signal consists of different steps (see Figure 3.12), and it can be summarized as follows:

1. A small segment of the signal is selected to compute the *MFCC*. The selected segment, of N samples is divided into short frames and windowing of N_f samples.

2. The Discrete Fourier Transform is applied for computing the energy spectrum.

$$X(k) = \sum_{n=1}^{N} x(n)\omega_N^{(n-1)(k-1)} \tag{3.1}$$

   where, $\omega_N = e^{(-2\pi i)/N}$.

3. The magnitude of the energy spectrum is transformed to a logarithm scale,

$$\chi(k) = log|X(k)| \tag{3.2}$$

4. The next step considers a mapping between the real frequency scale (f_{Hz}) and the perceived frequency scale (f_{Mel}). Psychophysical studies have shown that human perception of the frequency content of sounds does not follow a linear scale [Molla and Hirose, 2004]. The defined constants in the logarithmic transformation are computed by considering the relation, $100\ KHz$ to 3000 mel-frequency scale [Wong and Sridharan, 2001],

$$f_{Mel} = 2595 * log\left(1 + \frac{f_{Hz}}{700}\right) \tag{3.3}$$

5. A triangular bandpass filter bank is applied to smooth the scaled spectrum. The output of each filter is given by,

$$Y(i) = \sum_{k=0}^{N_f/2} \chi(k)\phi_i(k) \tag{3.4}$$

where $1 \leq i \leq Np$, with $Np =$ number of filters, and,

$$\Sigma_{k=0}^{N_f/2}\phi_i(k) = 1 \tag{3.5}$$

is a triangular weighted function associated with the i^{th} filter.

6. Finally, the *MFCC* are computed using the inverse discrete Fourier Transform:

$$MFCCc = \sum_{j=1}^{Np} Y(j)cos\left(\frac{\pi}{Np}(j - 0.5)c\right) \tag{3.6}$$

where c defines the cepstrum coefficient number ($c = 1, 2, \ldots, Nc$), and Nc defines the total number of cepstrum coefficients.

The result is a seven-dimension vector, where each dimension corresponds to one parameter. *MFCC* were computed by using the VOICEBOX: Speech Processing Toolbox for MatLab [Brokes, 2006]. The selected programs require the following configuration and parameters:

- The selected segment is divided into short frames and analyzed with a rectangular or hamming window in time domain.
- The filters bank is evaluated with triangular shaped filters in Mel domain. The number of filters could be 20 or 40. These values are recommended in research of speech recognition system ([Childers *et al.*, 1977], [Davis and Mermelstein, 1980], [Wong and Sridharan, 2001], and [Zigelboim and Shallom, 2006]).
- The Mel coefficients could include the 0'th order cepstral coefficient or the log energy.
- The number of coefficients could be 12, 10 or 6. These coefficients could also include the delta coefficients and the delta-delta coefficients.

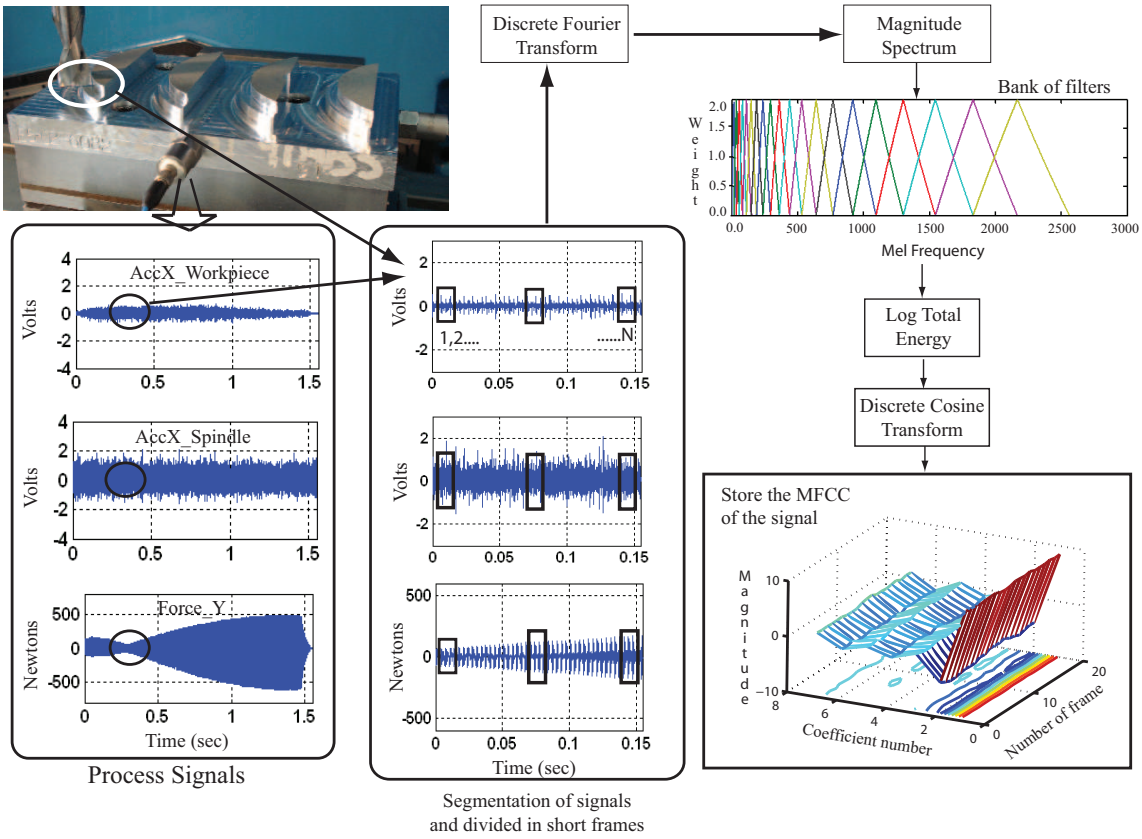

Figure 3.12: Feature extraction process. The process state variables (signals) are segmented and divided in short frames. A Discrete Fourier Transform and a mapping between the real frequency and the Mel frequency are computed. Then a bandpass filters bank is applied for smoothing the scaled spectrum. Finally, the *MFCC* are computed by using the inverse discrete cosine transform.

Figure 3.13 shows the *MFCC* computed from the Acc_y signal (Y-axis acceleration in the workpiece) . Different parameters were used to compute and compare the *MFCC* of the signal. The cutting tool condition was new, and the cutting conditions and geometric parameters were: $f_z = 0.025$, $ae = 3$, $D_{tool} = 12$, $HB = 110$, $Curv = 0.0$, and 2024 Aluminium Alloy. The observed behaviour in the *MFCC*(Figure 3.13) can be summarized as follows:

1. There is a different behaviour of *MFCC* if the rectangular or Hamming window in time domain is used.
2. The variation in magnitude of *MFCC* after of the coefficient number 7 is almost null. Only the first 7 coefficients will be considered to characterize the signals.
3. The number of filters affects the behaviour of the signal. Both configurations (i.e. 20 and 40) will be evaluated

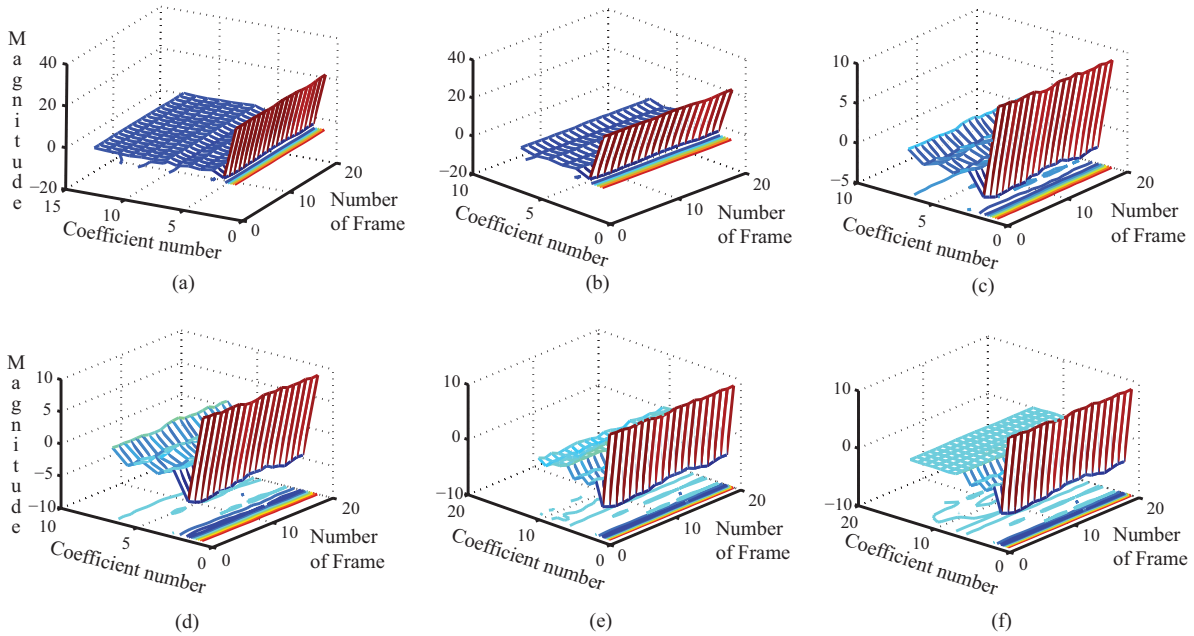

Figure 3.13: *MFCC* computed from the acceleration (Acc_y) process signal, with different parameters and configuration: (a) Rectangular window, 13 coefficients, 0'th order cepstral coefficient, and 20 filters; (b) Rectangular window, 6 coefficients, 0'th order cepstral coefficient, and 20 filters; (c) Hamming window, 6 coefficients, log energy, and 20 filters; (d) Hamming window, 6 coefficients, log energy, and 40 filters; (e) Hamming window, 10 coefficients, log energy, and 40 filters; (f) Hamming window, 6 coefficients, log energy, delta coefficients, and 40 filters.

to determine which is better in the pattern classification.

4. The delta coefficients present a flat behavior, and they will not be considered for characterization of the signals.

MFCC for vibrations and force signals

Specifically for vibrations and force signals, the process signals were recorded with a sampling rate of $40\ KHz$, and the *MFCC* were computed with the following two configurations:

1. A rectangular window in time domain and a triangular shaped bandpass filter with 20 filters. The feature vector considers the first element as the 0'th order cepstral coefficient and 6 Mel-cepstrum coefficients.

2. Hamming window in time domain and a triangular shaped bandpass filter with 40 filters. The feature vector considers the first element as the log energy and 6 Mel-cepstrum coefficients.

Figure 3.14 depicts the *MFCC* computed for the different cutting tool conditions (new, half-new, half-worn, and worn), the process state signal as the acceleration in Y-axis, and experiment number 17 ($f_z = 0.025$, $ae = 3$, $D_{tool} = 12$, $HB = 110$, $Curv = 0.0$, and 2024 aluminium Alloy). Two different plots are used to evaluate the behaviour of *MFCC* for different cutting tool conditions. It is observed that log energy is high for new cutting tool condition, and it is almost constant for other cutting tool conditions. The first coefficient decreases with flank wear. The second coefficient is $\simeq 0$ for new cutting tool condition and changes among 0 and 5 for other cutting tool conditions. This behavior allows for characterization of the evolution of flank wear.

Appendix B depicts the *MFCC* as computed for other cutting tool conditions.

***MFCC* for acoustic emission signals**

The acoustic emission signals were pre-processing to compute the *MFCC* by considering two configurations:

1. A rectangular window in time domain and a triangular shaped bandpass filter with 20 filters. The feature vector considers the first element as the 0'th order cepstral coefficient and 6 cepstrum coefficients.

2. A hamming window in time domain and a triangular shaped bandpass filter with 40 filters. The feature vector considers the first element as the log energy and 6 Mel cepstrum coefficients.

Figure 3.15 depicts the *MFCC* computed for different cutting tool conditions (new, half-new, half-worn, and worn), the process state signal as the acoustic emission signal (fixed on the spindle), and experiment number 08 ($f_z = 0.1$, $ae = 4$, $D_{tool} = 16$, $HB = 94$, $Curv = -0.025$, and 6082 aluminium alloy). Two different plots are shown to evaluate the behaviour of the *MFCC* with the evolution of flank wear in the cutting tool.

3.3.5 *PCA* Theory

Principal Components Analysis (*PCA*) is a technique of multivariate linear data analysis. The objective of *PCA* is to reduce the dimensionality of a data set while retaining as much as possible of variation in the data set. *PCA* has been applied in data compression, image analysis, visualization, pattern recognition, regression, process monitoring, and fault detection ([Yue and Tomoyasu, 2004], [Tien *et al.*, 2004],[Detroja *et al.*, 2006]), and is a common technique for finding patterns in data of high dimension.

The basic approach in *PCA* is simple. First, the n-dimensional mean vector (μ) and the $n \times n$ covariance matrix (Σ) are computed for the full data set. Next, the eigenvectors and eigenvalues are computed and sorted according to decreasing eigenvalue. It is e_1 $(eigenvector)$ with eigenvalue λ_1, e_2 with λ_2 until the last eigenvector e_n with λ_n. If the original variables are correlated, it is possible to summarize most of the variability present in the n variable space in terms of a lower p dimensional subspace ($p << n$). Here p defines the number of principal components, and it also represents subspace governing the signal. The other dimensions are only noise. Finally, the last step is pre-process data according to the selected *PCA*, and the linear combinations of the original variables are $TP = TP^{'} + \varepsilon$, where the columns of $P(n \times p)$ are the principal component loadings; $T(m \times n)$ representing the original data set, and the columns of $TP(m \times p)$ are the scores for each observation, with ε as the residual error. An application of

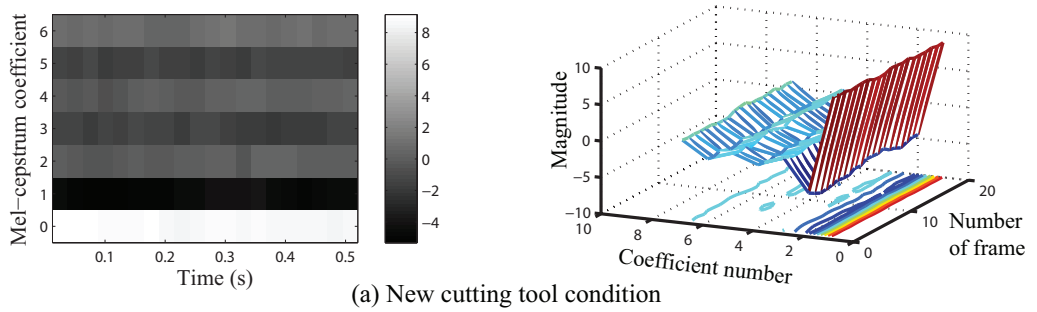

(a) New cutting tool condition

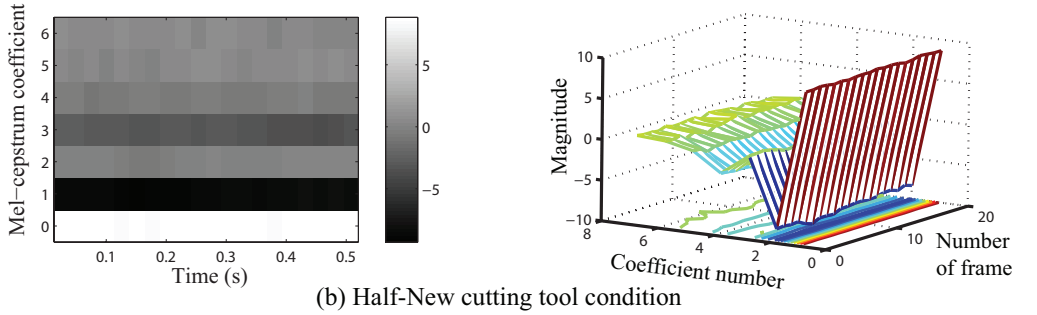

(b) Half-New cutting tool condition

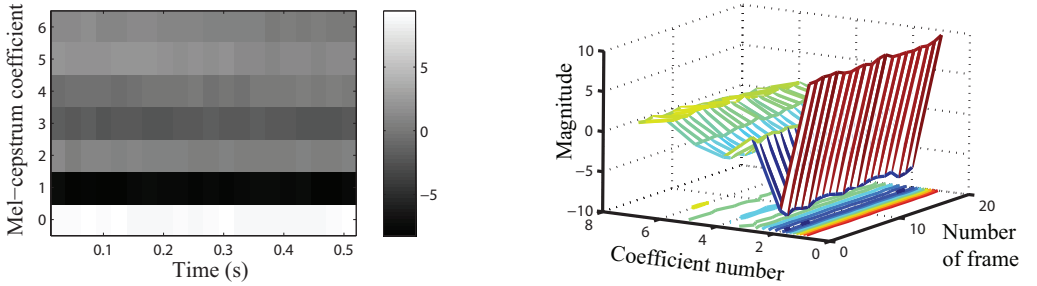

(c) Half-Worn cutting tool condition

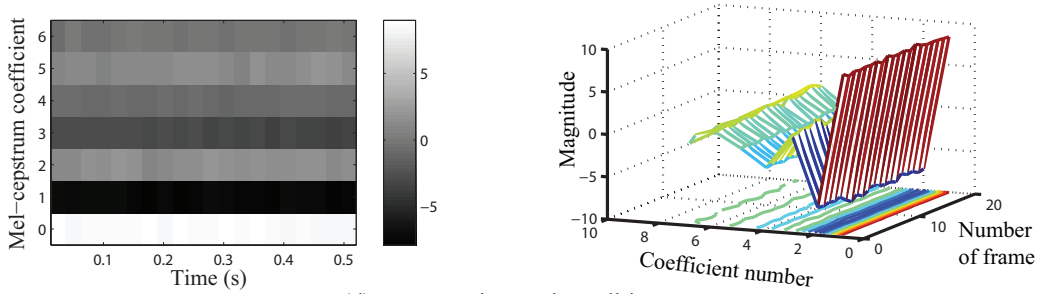

(d) Worn cutting tool condition

Figure 3.14: The *MFCC* computed from the acceleration (Acc_y) process signal and the cutting conditions correspond to the experiment number 17. The parameters and configuration were a Hamming window, 6 coefficients, log energy, and 40 filters.

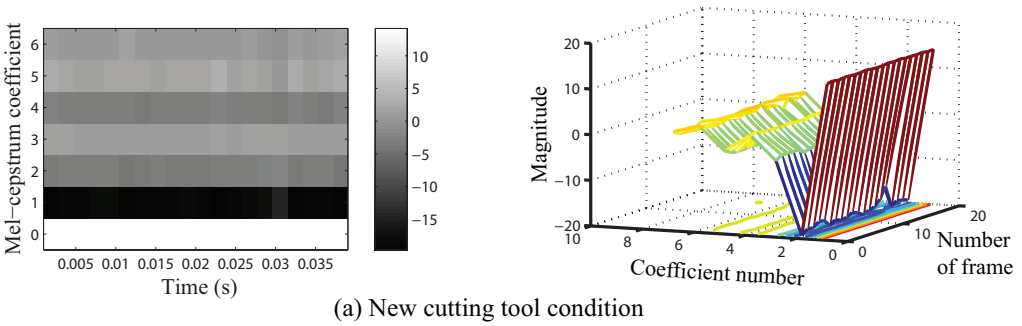

(a) New cutting tool condition

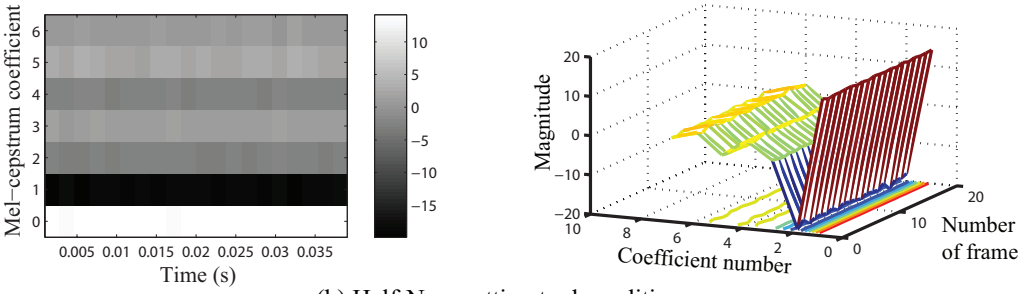

(b) Half-New cutting tool condition

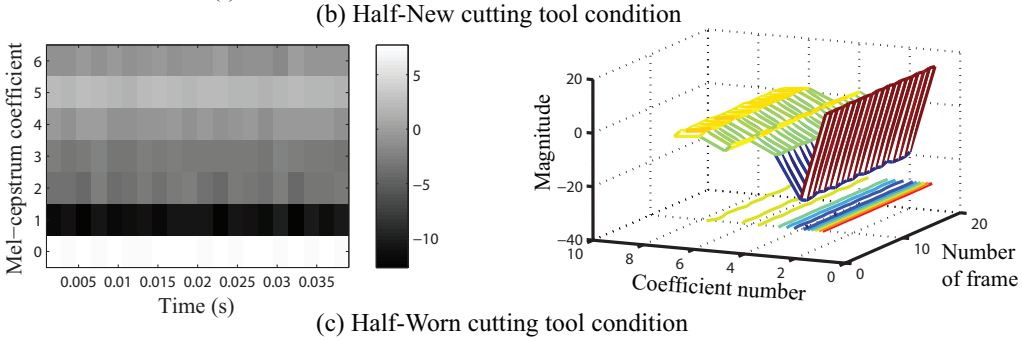

(c) Half-Worn cutting tool condition

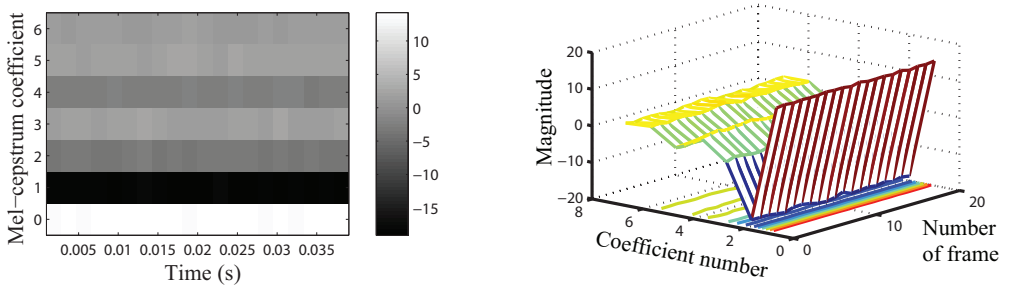

(d) Worn cutting tool condition

Figure 3.15: The *MFCC* computed from the acoustic emission (AE spindle) process signal and the cutting conditions correspond to the experiment number 08. The parameters and configuration were a Hamming window, 6 coefficients, log energy, and 40 filters.

the *PCA* will be described by using the original data set obtained for all the experiments with half-worn cutting tool. The data set is defined by:

1. The matrix $T(110, 12)$ with all values that correspond with cutting conditions, cutting parameters, geometric parameters (f_z,ae,D_{tool},HB, $Curv$), and seven *MFCC*, for each sensor.
2. The matrix $TR(110, 4)$ with the different parameters computed for characterizing the surface roughness for each experiment.

Consider the TR matrix that uses four different parameters to characterize the surface roughness (R_a, RSm, R_q, and R_z). Table 3.4 shows some samples of these parameters. Previously, data set was normalized.

Table 3.4: Parameters to characterize the surface roughness of the test pieces machined with a half worn cutting tool.

$Exp.$	R_a	RSm	R_q	R_z
1	-0.1701	-0.6175	-0.1737	-0.2107
2	-0.0659	-0.6130	-0.0778	-0.0218
3	-0.1701	-0.6175	-0.1737	-0.2107
4	-0.1400	-0.6806	-0.1430	-0.1521
$\vdots$	$\vdots$	$\vdots$	$\vdots$	$\vdots$
107	-0.2449	-0.1752	-0.2417	-0.3116
108	-0.2947	0.0005	-0.2949	-0.3776
109	-0.3385	-0.0340	-0.3377	-0.4406
110	-0.2419	-0.0299	-0.2537	-0.3735

The *PCA* were computed by using the following MatLab functions *princomp* and *prepca*. The first output of the *princomp* function contains the coefficients for the four principal components, and are the eigenvectors of the covariance matrix. The E matrices are:

$$\mathbf{E} = \begin{pmatrix} 0.4617 & 0.2539 & -0.5282 & 0.6659 \\ 0.4843 & -0.8748 & 0.0143 & 0.0092 \\ 0.4724 & 0.2471 & -0.4048 & -0.7429 \\ 0.5737 & 0.3306 & 0.7463 & 0.0682 \end{pmatrix} \tag{3.7}$$

The third output defines the variance explained by the corresponding principal components. This variance is represented by the eigenvalues and they are sorted according to their decreasing value. They are:

$$\lambda = \begin{pmatrix} 0.33895 & 0 & 0 & 0 \\ 0 & 0.12712 & 0 & 0 \\ 0 & 0 & 0.00528 & 0 \\ 0 & 0 & 0 & 0.000089 \end{pmatrix} \tag{3.8}$$

By considering the variance, the percent of total variability explained by each principal component can be computed as 71.89, 26.96, 1.12, 0.019. With this information, it was observed that using only the first and second principal component, the variability of the data set can be explained as 98.85%, and the last two principal components are not required. The second output of the *princomp* function contains the scores of the original data mapped into the new coordinate system defined by the principal components. This output is the same size as the input data matrix. Figure 3.16a shows both the principal component coefficients for each variable and the principal component scores for each observation. The plot shows the scores as a function of the two principal components. Each of the four variables is represented in this plot by a vector, and the direction and length of the vector indicates how each variable contributes to the two principal components in the plot. The *prepca* MatLab function also performs a principal component analysis and retains only those components that contribute with a specific percent to the variance in the data set. Figure 3.16b shows the results computed with *prepca* function and retained the 98% of the variability. It was observed that both figures show the same behaviour.

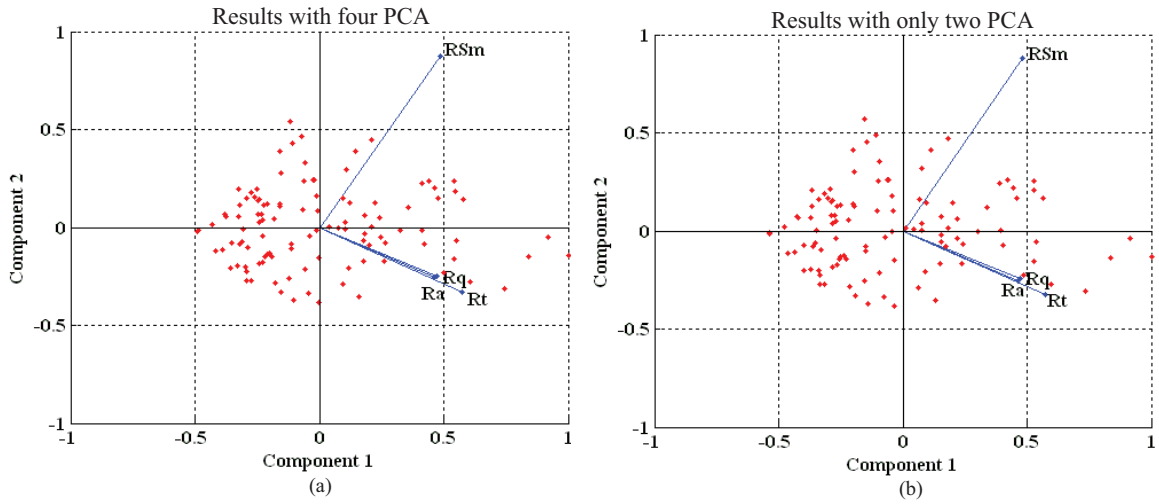

Figure 3.16: The plots show the scores of the original data (surface roughness parameters) mapped into the new coordinate system defined by the principal components. Similar behaviour is observed in the scores which were computed with four *PCA* (left-plot) and only two *PCA* (right-plot).

3.4 Analysis of the results

With respect to the data acquisition system, the following results are considered relevant:

1. Installed accelerometers (*AC*) in the workpiece present excellent mechanical and electrical characteristics to acquire vibration signals during the cutting process.

2. Acquired forces with the dynamometric platform correspond with the tendency of the flank wear. The forces will increase with the dulling of the cutting tool. The mechanical and electrical characteristics of the dynamometric platform allow to capture the cutting forces in the *HSM* process.

3. Installed *AC* sensors in the ring (fixed to the spindle) do not have a satisfactory frequency bandwidth. Figure 3.6 depicts that the frequency domain is not totally shown in the *PSD* graph. It is necessary to increase the sampling rate to capture all the frequency bandwidth and to confirm that sensors are not limited by their resonance frequency.

4. The tendency shown in the signals owing to the evolution of the cutting tool wear condition is satisfactory, and the features obtained from the signals allow the characterization of four states of the cutting tool wear condition.

5. Obtained features from signals allow for their characterization by using only seven *MFCCs*. It was not necessary to compute the delta and delta-delta coefficients.

6. The *PCA* technique was applied to reduce the dimensionality of data set by using only the components that retain maximum variability of the data set.

Chapter 4

Surface Roughness Monitoring Module

4.1 Introduction

Currently, experimentation in the majority of research on Surface Roughness (R_a) only considers a specific combination of cutting tool and workpiece material. Several authors ([van Luttervelt and Peng, 1999], [Mursec and Cus, 2003], [Zuperl *et al.*, 2004], and [Jawahir and Wang, 2007]) have pointed out the importance of building databases with information about different materials and cutting tools and the computing models by considering a wider domain in the machining process. Different methodologies were analyzed and evaluated to estimate R_a, and a methodology for computing robust R_a models is proposed, which can be used off and on-line during the machining process. The models will be used to estimate the R_a value as a function of several factors and process variables. [Tönshoff *et al.*, 1988] pointed out that more generic use of process models is possible when the model constants are adapted to different machine tools, material batches, and environment conditions. In agreement with proposal of this research, a Design of Experiments (*DoE*) will be defined for covering a machining domain for several cutting tools and workpiece materials in High Speed Machining (*HSM*).

4.2 Selection of the materials and test pieces for the experimentation

In the mold/die industry the peripheral milling process is an important cutting process, where the geometric path can be defined as as simple straight line, concave or convex curvature. In the aeronautic and automotive industry it is necessary to consider a wider domain in hardness and mechanical properties owing to the multiple requirements and applications of the workpieces. Therefore, five different aluminium alloys were selected for the experimentation. Table 4.1 presents the selected aluminium alloys and Appendix C describes their characteristics, properties and chemical compositions.

Table 4.1: Aluminium Alloys selected for the experimentation.

Alloy	Hardness	Applications
$5083 - H111$	70 BHN	Extrusion processes: Flat bar, bulb angle, and tee sections.
$6082 - T6$	90 BHN	Extrusion process (Flat bar, and tee sections)
$2024 - T3$	120 BHN	Aircraft fittings, gears and shafts, bolts, computer parts, missile parts, etc.
CERTAL	140 BHN	Industrial tools, molds, and mechanical structures.
$7075 - T6$	150 BHN	Gears, shafts, regulating valve parts, keys, aerospace and defense applications.

4.3 Test pieces for the experimentation

The workpiece material was acquired in test pieces with the dimensions $170 \times 100 \times 25$ mm, and the designed geometries were the following:

1. For the concave path for the peripheral milling process, the geometry was specified with two radii: (a) a small box with a radius equal to 20 mm, and (b) a big box with a radius equal to 40 mm. Figures 4.1a, and 4.1b show these geometries.

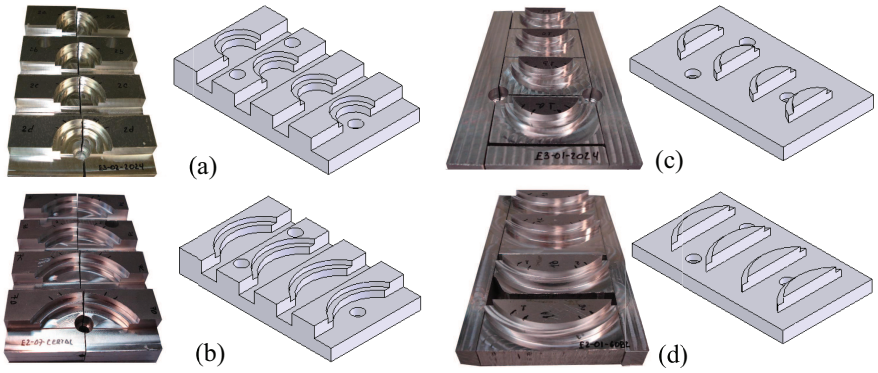

Figure 4.1: Test pieces designed for the experimentation with concave and convex paths. (a) small box with radius equal to 20 mm; (b) big box with 40 mm radius; (c) small island with 20 mm of curvature radius; (d) big island with a curvature radius of 40 mm.

2. For the convex path, the geometry was also specified with two radii: (a) a small island with a radius equal to 20 mm, and (b) a big island with a radius equal to 40 mm. Figures 4.1c, and 4.1d depict these geometries.

3. The straight path geometry was defined to consider an infinite radius. Figure 4.2 shows the test pieces with the straight path and different cutting tool diameters.

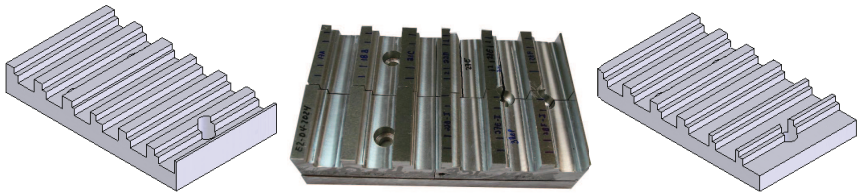

Figure 4.2: Test pieces used for the experimentation with the straight path.

4.4 Measurement of the surface roughness

The profile parameters that allow the characterization of the R_a are defined in this section, and the recommended methodology for measuring these parameters is described in Appendix D. The measurement of the R_a is supported by the norms [ISO 4287:1997(E/F), 1997] and [ISO 4288:1996(E), 1996]. Figure 4.3 shows the variables required to compute the profile parameters. These parameters are:

1. R_z is the sum of the height of the largest profile peak height Z_p and the largest profile valley depth Z_v within a sampling length.
2. R_t is the sum of the height of the largest profile peak height Z_p and the largest profile valley depth Z_v within the evaluation length.
3. R_a is the arithmetical mean of the absolute ordinate values $Z(x)$ within a sampling length.
4. R_q is the root mean square value of the ordinate values $Z(x)$ within a sampling length.
5. RSm is the mean value of the profile element widths Xs within a sampling length.

The equipment for measuring the R_a was a portable Surfcom type $130A$. The selected sampling length and evaluation length for the R_a assessment were 0.8 and $4\ mm$, respectively. Also, the λ_c profile filter which defines the intersection between the roughness and waviness components must be equal to the sampling length (0.8). Appendix D describes the procedure to compute these values. Roughness is a dominant surface feature. In manufacturing, roughness is caused by the material's microstructure and the action of the cutting tool. From the different parameters previously defined, the most common parameter is R_a. It reflects the average height of roughness component irregularities from a mean line. R_a provides a simple value for accept/reject decisions.

4.5 Screening factorial design

In many manufacturing applications the number of potential input variables (called factors) is large and sometimes unknown, therefore, a process characterization (screening) is used to reduce the input variables by identifying the

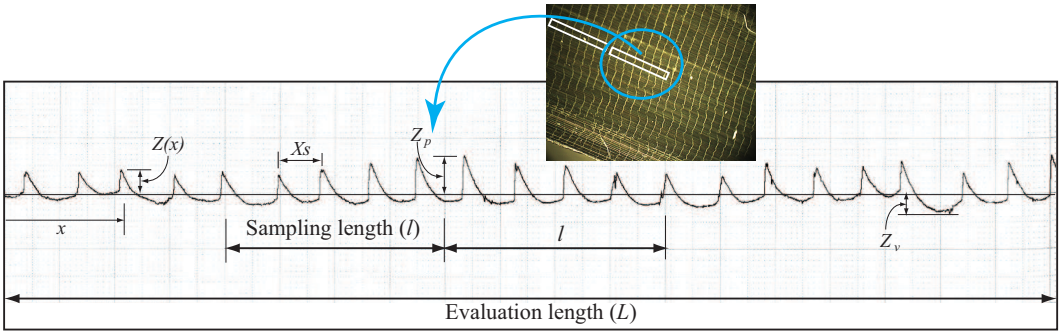

Figure 4.3: Example of the obtained profile from the R_a measurements with the Surfcom type $130A$. The profile shows the following variables: $Z(x)$ absolute ordinate value at specific x value, Z_p height of the largest profile peak, Z_v height of the largest profile valley, X_s distance between peak to peak.

main independent variables that affect product quality. This reduction allows to focus process improvement efforts on the really key variables. Screening may also suggest the best or optimal settings for these factors and indicate if the response can be computed with a lineal or quadratic model. Optimization experiments can be done to compute the best settings and define the nature of the curvature. Chapter 2 identified R_a as dependent in several factors in any machining process. Owing to the large number of factors in the process, a screening design is required in a first experimental stage to compute the critical variables of R_a. In agreement with important research by [Fuh and Chang, 1997], [Savage and Chen, 1999], [Ertekin *et al.*, 2003], [Öktem *et al.*, 2006] and the defined domain for the peripheral milling process, eight factors were selected for the screening design. Those factors were the following: f_z, v_c, D_{tool}, ap, ae, HB, R, and convex (I) and concave (C) path (I/C). Two levels and a fractional factorial design were used to screen for the really important factors that influence R_a. The factors and levels are shown in Table 4.2.

Table 4.2: Factors and levels defined for the screening design.

Factors	Low Level	High Level	Units
f_z	0.04	0.13	$mm/rev/tooth$
v_c	500	850	m/min
ap	5	10	mm
D_{tool}	12	16	mm
ae	1	5	mm
HB	65	145	HB
R	20	40	mm
I/C	Convex	Concave	undimensional

If full factorial design is defined, responses are measured at all combinations of the factor levels. However, this may result in a prohibitive number of experiments (e.g., a two-level full factorial design with eight factors requires 256 experiments). To minimize time and cost, it is necessary to exclude some of the factor level combinations if these have no effect on the fitting of the response. Fractional factorial designs are useful in factor screening because they reduce down the number of experiments to a manageable size. Choosing the best fraction often requires specialized knowledge of the process under study. The *DoE* was computed by considering eight factors, two levels, $1/8$ fraction, 32 runs, and zero center points. The obtained *DoE* is depicted in Table 4.3. Four replicates were considered for each experiment, and during the machining process, the following process signals were recorded: accelerations, acoustic emission, and forces. The R_a was measured with the procedure described in the Appendix D.

4.5.1 Statistical analysis

Standard screening using fractional factorials provides an inexpensive way to determine which factors from a long list significantly affect system performance. The fractional factorials are based on experimental plans because they are computed by only a fraction of the prototypes that would constitute all combinations of levels for all factors of interest (full factorial). The selected fractional factorial must be proposed by an expert in the process, because he can reasonably assume that certain high-order interactions are negligible, and the information on the main effects and low-order interactions may be obtained by running only a fraction of the complete factorial experiment (see [Montgomery, 2001], [Allen, 2006]). With the experimental results, the next step is to apply an Analysis Of Variance (*ANOVA*), which offers a standard approach for analyzing significance of factors and/or model terms that addresses the multiplicity of the tests. Therefore, with the *DoE* and the observed R_a for each condition, the procedure to select the most relevant factors is defined in Figure 4.4. A complete description of the above steps is explained as follows:

1. The *ANOVA* will be computed by considering the main effects, two and three way interactions. The *ANOVA* implies to compute the following variables:

   - The Degrees of Freedom (DF). The DF for the levels (a) of each factor is $a-1$. The DF for the experimental error is $n-1$, where n is the number of replicates. The DF for the total sum of squares is $N-1$, where N is the total number of observations (na).
   - The explained variation or regression sum of squares (SS_R) is given by

   $$SS_R = \sum_{j=1}^{n} (R_a^{'} - R_{a,avg})_j^2 \tag{4.1}$$

   where $(R_a^{'} - R_{a,avg})$ is defined as the difference between the predicted of the j^{th} data value and the average value.

   - The unexplained variation or the error sum of squares (SS_E) is given by

   $$SS_E = \sum_{j=1}^{n} (R_{a,measured} - R_a^{'})_j^2 \tag{4.2}$$

Table 4.3: Design of experiments for the screening design stage, and the measurement of R_a (μm) for each replicate. The cutting tool wear condition was fresh.

Number	f_z	v_c	ap	D_{tool}	ae	HB	R	I/C	$R_a, 1$	$R_a, 2$	$R_a, 3$	$R_a, 4$
1	0.04	500	5	12	1	65	20	Convex	0.4115	0.4053	0.4081	0.4270
2	0.13	500	5	12	1	145	40	Convex	0.3512	0.3632	0.3507	0.3415
3	0.04	850	5	12	1	145	40	Concave	0.2219	0.1778	0.1338	0.1567
4	0.13	850	5	12	1	65	20	Concave	0.3091	0.3177	0.3153	0.2921
5	0.04	500	10	12	1	145	20	Concave	0.1192	0.1132	0.1238	0.1146
6	0.13	500	10	12	1	65	40	Concave	0.3934	0.4061	0.3707	0.3918
7	0.04	850	10	12	1	65	40	Convex	0.1796	0.1812	0.1712	0.1705
8	0.13	850	10	12	1	145	20	Convex	0.4186	0.4378	0.4143	0.3685
9	0.04	500	5	16	1	65	40	Concave	0.1077	0.1191	0.1174	0.1243
10	0.13	500	5	16	1	145	20	Concave	0.2077	0.1935	0.1793	0.1654
11	0.04	850	5	16	1	145	20	Convex	0.1703	0.1684	0.1546	0.1653
12	0.13	850	5	16	1	65	40	Convex	0.4232	0.4354	0.4432	0.4432
13	0.04	500	10	16	1	145	40	Convex	0.1468	0.1546	0.1331	0.1321
14	0.13	500	10	16	1	65	20	Convex	0.8703	0.8397	0.8762	0.8637
15	0.04	850	10	16	1	65	20	Concave	0.1266	0.1464	0.1584	0.1410
16	0.13	850	10	16	1	145	40	Concave	0.2550	0.2404	0.2469	0.2213
17	0.04	500	5	12	5	65	20	Concave	0.1765	0.1570	0.1458	0.1682
18	0.13	500	5	12	5	145	40	Concave	0.3571	0.3312	0.3181	0.3071
19	0.04	850	5	12	5	145	40	Convex	0.1734	0.1589	0.1649	0.1787
20	0.13	850	5	12	5	65	20	Convex	0.3537	0.3312	0.3181	0.3071
21	0.04	500	10	12	5	145	20	Convex	0.3861	0.3639	0.3793	0.3670
22	0.13	500	10	12	5	65	40	Convex	0.2516	0.3477	0.6998	0.7142
23	0.04	850	10	12	5	65	40	Concave	0.1789	0.1743	0.1796	0.1925
24	0.13	850	10	12	5	145	20	Concave	0.4300	0.5171	0.4760	0.4769
25	0.04	500	5	16	5	65	40	Convex	0.2559	0.2026	0.2359	0.1832
26	0.13	500	5	16	5	145	20	Convex	0.3865	0.4259	0.4103	0.3939
27	0.04	850	5	16	5	145	20	Concave	0.1148	0.1066	0.1131	0.1131
28	0.13	850	5	16	5	65	40	Concave	0.4173	0.4065	0.4397	0.4074
29	0.04	500	10	16	5	145	40	Concave	0.1664	0.1940	0.1202	0.1202
30	0.13	500	10	16	5	65	20	Concave	0.3804	0.3655	0.3662	0.3662
31	0.04	850	10	16	5	65	20	Convex	0.2956	0.3247	0.3031	0.2994
32	0.13	850	10	16	5	145	40	Convex	0.3886	0.3714	0.3899	0.3433

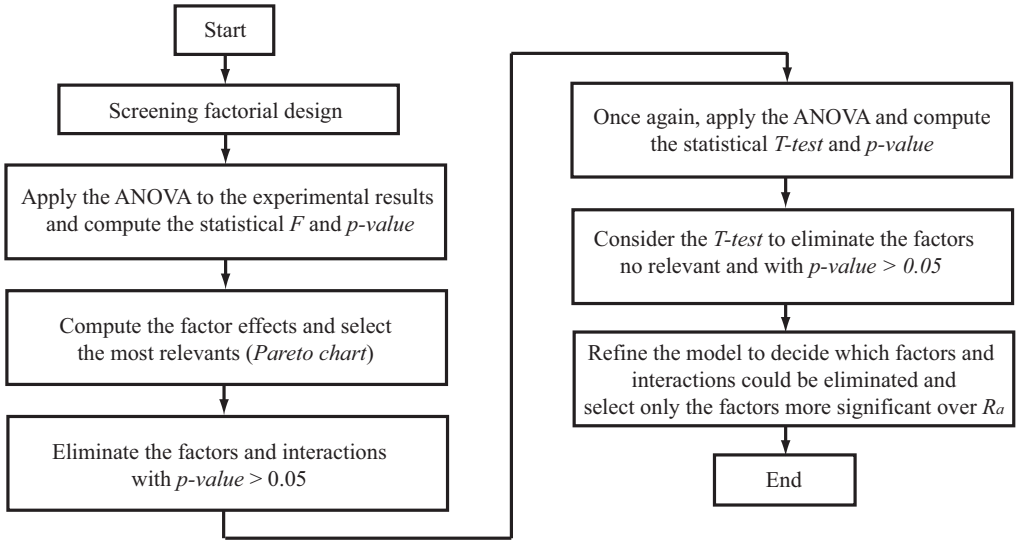

Figure 4.4: Flow diagram to select the most relevant factors over R_a in the screening analysis.

where $(R_{a,measured} - R_a^{'})$ is the difference between the measured and predicted response.

- The total sum of squares (SS_T) is given by

$$SS_T = SS_R + SS_E \tag{4.3}$$

- The mean square (MS) is given by

$$MS = \frac{SS}{DF} \tag{4.4}$$

- The statistical test is made by computing the F distribution,

$$F_o = \frac{MS_{levels}}{MS_E} \tag{4.5}$$

- $p - value$ represents the probability of rejecting the null hypothesis when it is true. The smaller the $p - value$, the smaller is the probability that you would be making a mistake by rejecting the null hypothesis. A cutoff value often used is 0.05, that is, reject the null hypothesis when the $p - value$ is less than 0.05.

The results of the *ANOVA* are shown in Table 4.4.

2. From the Pareto chart must be selected the factors and interactions more significant. This implies to eliminate the factors with small effect (small F value) and $P - value > 0.05$. From Figure 4.5, the factors and interactions with a $P - value > 0.05$ were eliminated. Only the D_{tool} and ae factors were not canceled owing to their influence with other important factors.

Table 4.4: Analysis of Variance for R_a (coded units).

Source	Degrees of Freedom (DF)	Sum of Squares (SS)	Mean Squares MS	Statistical F	$p-value$
Main Effects	8	2.18338	0.272922	130.64	0.000
2-Way Interactions	20	0.91351	0.045676	21.86	0.000
3-Way Interactions	3	0.04079	0.013596	6.51	0.000
Residual Error	96	0.20055	0.002089		
Pure Error	96	0.20055	0.002089		
Total	127	3.33823			

3. Once again, compute the *ANOVA* for R_a, including the main effects and interactions charts. The following variables are required to estimate the effects and coefficients for computing R_a:

   (a) The effect of a factor is defined as the change in response produced by a change in the level of that factor averaged over the levels of the other factor.

   (b) The coefficients ($Coef$) are computed for the linear multiple regression that will be used to compute the estimated response.

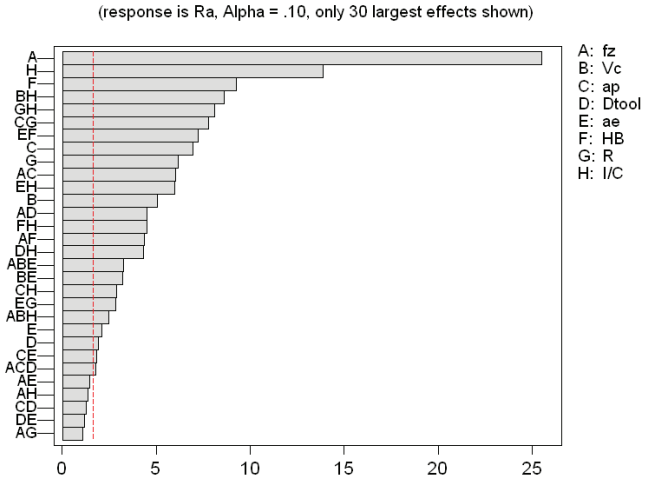

Figure 4.5: Pareto chart of the standardized effects. The vertical red line on the chart divides the factors most relevant in agreement with the $p-value$. The most significant factors are to the right of the red line.

(c) The estimated standard error (SE) of the coefficients is given by

$$SE = \frac{2\sigma}{\sqrt{n2^k}} \tag{4.6}$$

where σ is the standard deviation of the predicted response, n the number of replicates, and k the number of factors.

(d) The $T - test$ is the most commonly used method to evaluate the difference in means by considering each coefficient of the linear multiple regression. If $T_i > T_{\alpha,DoF}$, then the coefficient in the regression model is significant for the alpha level and the other coefficient.

From these charts it is important to make an analysis to select the main factors and its correlations with the other factors. The new *ANOVA* results are shown in Table 4.5 and 4.6, and Figure 4.6.

From the upper plot in Figure 4.6 the following can be defined:

- The f_z factor shows the highest impact over R_a, when it changes from minimum to maximum value.
- The I/C factor shows that R_a increases from concave to convex peripheral milling.
- The HB and R factors show a negative effect over R_a behavior.
- The axial depth (ap) shows a small effect over R_a.
- The v_c factor shows a negative effect over R_a
- The D_{tool} and ae factors show a minimum affect over R_a

The lower plot in Figure 4.6 shows the effects over R_a owing to factor interactions. Important conclusions can be defined.

- The cutting speed (v_c) does not show a correlation with ap, D_{tool}, and ae factors for low or high values. For v_c high values there is no correlation with HB, R, and I/C factors, therefore, these factors and their interactions can be eliminated. It is not relevant for R_a prediction.
- The f_z factor shows a correlation with HB, ae, R, and I/C factors; these interactions must be included.
- The ap factor does not show correlation with D_{tool}, ae, and HB; this factor and its interactions must be eliminated.
- The ae factor shows an excellent correlation with HB, f_z, and I/C; this factor must be considered.
- The HB factor has excellent correlation with f_z, I/C, and R.

The next step is to refine the model. This implies to evaluate which other factors and interactions should be eliminated (see Appendix E) by computing once again the *ANOVA*. The final factors that were selected from this analysis are the following: f_z, D_{tool}, ae, HB, R, and I/C. The last two factors were fused into a new factor called curvature ($Curv$). Curvature is computed as the inverse of the radius of the workpiece geometry, and its sign defines the curvature type: positive for the convex path, negative for the concave path. The $Curv$ is considered a new factor because it has not been used in other research.

Table 4.5: Estimated effects and coefficients for R_a (coded units). The estimated standard error (SE) is equal to 0.002177.

Term	Effect	Coefficient $Coef$	T-test	$p-value$
Constant		0.29529	135.64	0.000
f_z	0.20073	0.10037	46.10	0.000
v_c	-0.03532	-0.01766	-8.11	0.000
ap	0.05066	0.02533	11.63	0.000
D_{tool}	-0.01001	-0.00501	-2.30	0.024
ae	0.01159	0.00579	2.66	0.009
HB	-0.06917	-0.03458	-15.88	0.000
R	-0.05501	-0.02751	-12.63	0.000
I/C	0.10648	0.05324	24.45	0.000
$f_z * ap$	0.04317	0.02158	9.91	0.000
$f_z * D_{tool}$	0.04141	0.02070	9.51	0.000
$f_z * HB$	-0.02974	-0.01487	-6.83	0.000
$v_* ae$	0.03082	0.01541	7.08	0.000
$v_c * I/C$	-0.06397	-0.03199	-14.69	0.000
$ap * R$	-0.06810	-0.03405	-15.64	0.000
$ap * I/C$	0.01769	0.00885	4.06	0.000
$D_{tool} * I/C$	0.03985	0.01992	9.15	0.000
$ae * HB$	0.06349	0.03174	14.58	0.000
$ae * R$	0.01742	0.00871	4.00	0.000
$ae * I/C$	-0.05330	-0.02665	-12.24	0.000
$HB * I/C$	-0.03083	-0.01542	-7.08	0.000
$R * I/C$	-0.07058	-0.03529	-16.21	0.000
$f_z * v_c * ae$	0.03134	0.01567	7.20	0.000
$f_z * v_c * I/C$	-0.01458	-0.00729	-3.35	0.001

4.6 Design of Experiments (*DoE*)

4.6.1 Factors and levels for the *DoE*

Chapter 2 defined that several groups of factors affect R_a. The first group is represented by the cutting conditions (cutting speed, feed rate, axial depth of cut, etc); the second group is defined by the geometry of the cutting tool (tool, diameter, helix angle, edge radius, number of flutes, etc.); the third group considers the workpiece material

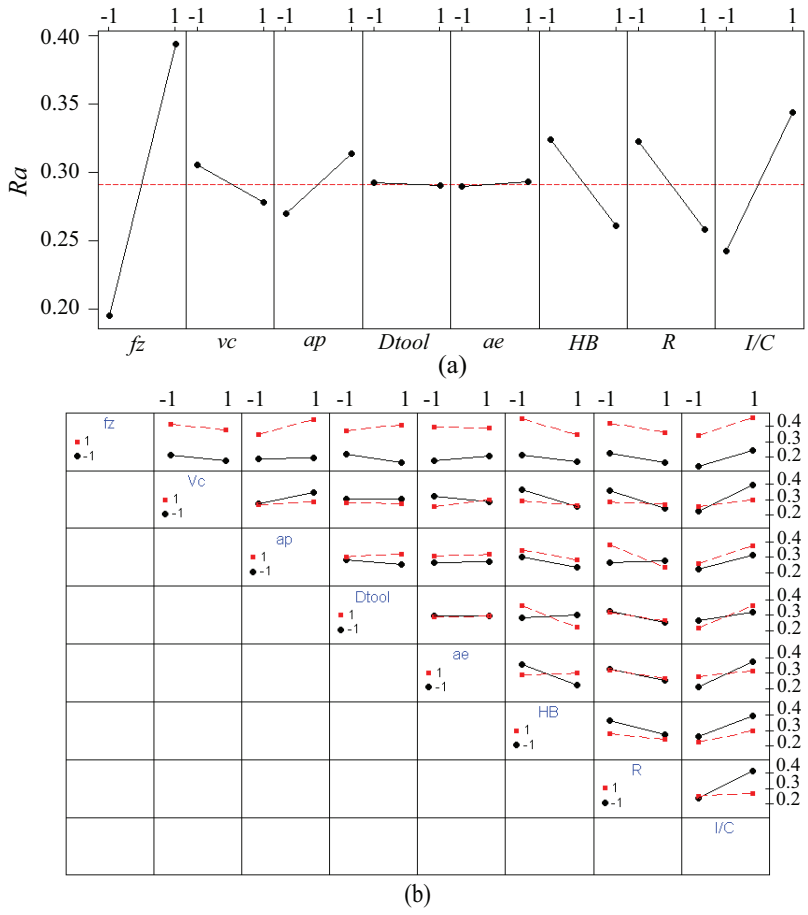

Figure 4.6: The eight factors are shown with the main effects plot for R_a in the upper plot. The effect of each factor is defined as a change in response for applying the low and high level values.The lower plot defines the interactions of the factors over the response R_a. The red line defines the tendency of the response with a high level value of the factor and the other factors changing from low to high level value. The black line corresponds to the low level value of the factors.

(hardness, ductility, etc) and path of the peripheral milling process (concave, convex or straight path); the last group is represented by the uncertainty of the process owing to the variations in machine vibrations and repeatability, work-holding devices, and other factors. Other variables also must be considered, but they are less important or they can be controlled (coolant, thermal conditions, humidity, and so on). It is important to define which factors represent the main effects over the R_a. This was made with the application of a screening factorial design. The significant factors were: feed per tooth (f_z), cutting tool diameter (D_{tool}), radial depth of cut (ae), hardness of the workpiece material (HB), and the machining geometry curvature $(Curv)$. The next steps must be made for the

Table 4.6: Analysis of Variance for R_a (coded units)

Source	Degrees of Freedom (DF)	Sum of Squares (SS)	Adjusted Sum of Squares ($AdjSS$)	Adjusted Mean Squares ($AdjMS$)	Statistical (F)	$p-value$
Main Effects	8	2.01424	1.66366	0.207957	385.63	0.000
2-Way Interactions	13	0.88788	0.89146	0.068574	127.16	0.000
3-Way Interactions	2	0.03733	0.03733	0.018665	34.61	0.000
Residual Error	100	0.05393	0.05393	0.000539		
Lack of Fit	7	0.02403	0.02403	0.003433	10.68	0.000
Pure Error	93	0.02990	0.02990	0.000321		
Total	123	2.99337				

experimentation:

1. Run experiments with a sharp cutting tool. Record the following process variables:
   - Acceleration signals in x and $y-axis$ directly on the workpiece ($Acc_{x,wp}$, $Acc_{y,wp}$).
   - Acceleration signals in x, y, and $z-axis$ directly on the *CNCs* spindle ($Acc_{x,sp}$, $Acc_{y,sp}$, $Acc_{z,sp}$).
   - Force signals.
   - Acoustic emission signals in the table and spindle of the *CNC*.
   - At the end of each test, the R_a was measured.
2. Machine harder aluminium alloys until the cutting tool reaches a specific flank wear.
3. Run another set of experiments with the cutting tool worn.
4. Repeat the steps 2 and 3 until R_a presents considerable damage or the cutting tool reaches the maximum tool-life criterion, [ISO 8688-2:1989(E), 1989].

4.7 Modeling of the R_a using Response Surface Methodology

Response Surface Methodology (*RSM*) will be applied to define the runs of the experiments with the five factors. *RSM* is an excellent statistical and mathematical technique for the modeling and analysis of models with several factors that have a great influence in a response. Also, *RSM* can be used to optimize the process by including a merit function (for example, to minimize the R_a). Eventually, the objective of *RSM* is to determine the optimum operating conditions for the system or to determine a region of the factor space in which operating requirements are satisfied. The proposal method is the *standard response surface method*, and it is based on the Central Composite

Design (*CCD*) for the design of experiments matrices ([Allen, 2006], [Montgomery, 2001]). The *CCD* consists of a 2^{k-1} fractional factorial of resolution with n_F runs, and n_c center runs. Figure 4.7 shows the representation of the *CCD* for $k = 2$ and $k = 3$ factors.

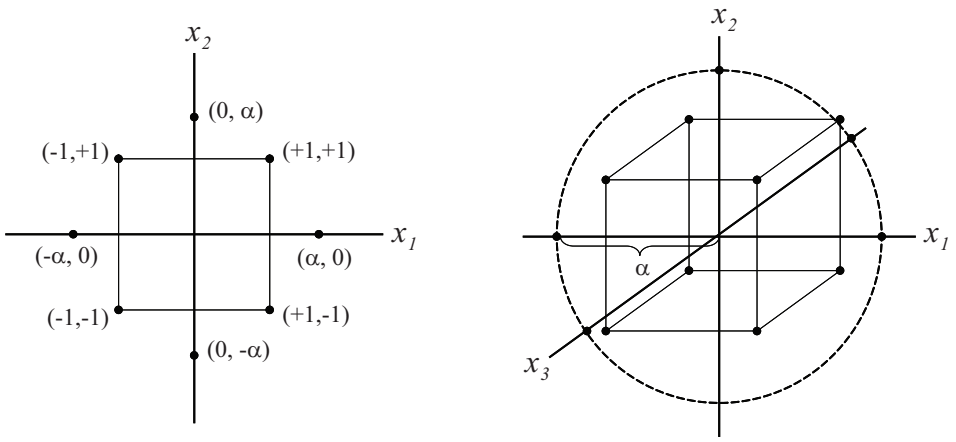

Figure 4.7: Representation of the central composite designs for $k = 2$ and $k = 3$ factors. The figure shows the cube points and levels of each factor. The distance α defines the rotatability of the *DoE* and it depends from the cube points.

The *CCD* is a very efficient design for fitting the second-order model. There are two parameters in the design that must be specified, the distance α of the axial running from the design center and the number of center points. Also, for this method it is very important the rotatability for the second-order model provide good predictions throughout the region of interest. This means that the model must have a reasonably consistent and stable variance of the predicted response at points of interest. In [Montgomery, 2001], it is suggested that a second-order response surface design should be rotatable. This implies that the variance will be the same at all points that are the same distance from the design center. A *CCD* is made rotatable by the choice of α. The selection of α for rotatability depends on the number of cube points in the design (n_F). [Allen, 2006] recommends the following value for $\alpha = (n_F)^{1/4}$. Rotatability is a spherical property, that is, it makes the most sense as a design criterion when the region of interest is a sphere. However, it is not important to have exact rotatability to have a good design. The choice of α in the *CCD* is dictated by the region of interest. When this region is a sphere, the design must include center runs to provide reasonably stable variance of predicted response. Normally, three to six center runs are recommended. From among theses considerations and recommendations, the α value was computed as $n_F = 2^{k-1} = 16$, and $\alpha = (16)^{1/4} = 2$. From this value, five levels for the *CCD* were selected, and these are shown in Table 4.7.

Finally, the following parameters were defined to apply *RSM*: rotatable central composite design, with 16 points $(2^{k-1} = 16)$ on cube (k =number of factors), 10 points outside of cube, six central points, $\alpha = 2$ as the radius of the sphere, and four replicates. Table 4.8 defines the 32 runs that must be programmed during the experimentation. Appendix F presents the four parameters that were measured to characterize the R_a for each test piece.

Table 4.7: Factors and levels of the experimentation.

Levels	f_z mm/rev	D_{tool} mm	ae mm	HB HBN	$Curv$ mm^{-1}
-2	0.025	8	1	71	-0.05
-1	0.05	10	2	93	-0.025
0	0.075	12	3	110	0
1	0.1	16	4	136	0.025
2	0.13	20	5	157	0.05

Table 4.8: The experiments for the central composite design (half fraction)

Run Order	f_z	D_{tool}	ae	HB	$Curv$	Run Order	f_z	D_{tool}	ae	HB	$Curv$
1	-1	-1	-1	-1	1	17	-2	0	0	0	0
2	1	-1	-1	-1	-1	18	2	0	0	0	0
3	-1	1	-1	-1	-1	19	0	-2	0	0	0
4	1	1	-1	-1	1	20	0	2	0	0	0
5	-1	-1	1	-1	-1	21	0	0	-2	0	0
6	1	-1	1	-1	1	22	0	0	2	0	0
7	-1	1	1	-1	1	23	0	0	0	-2	0
8	1	1	1	-1	-1	24	0	0	0	2	0
9	-1	-1	-1	1	-1	25	0	0	0	0	-2
10	1	-1	-1	1	1	26	0	0	0	0	2
11	-1	1	-1	1	1	27	0	0	0	0	0
12	1	1	-1	1	1	28	0	0	0	0	0
13	-1	-1	1	1	1	29	0	0	0	0	0
14	1	-1	1	1	-1	30	0	0	0	0	0
15	-1	1	1	1	-1	31	0	0	0	0	0
16	1	1	1	1	1	32	0	0	0	0	0

4.7.1 *RSM* for the new cutting tool condition

Applying the results of the experimentation with the new cutting tool condition, the next step was to apply an *ANOVA* by considering the four replicates. The following considerations were evaluated:

- The effects owing to the several factor combinations.
- The percent contribution of each factor, denoted by a statistical ”F” factor. This factor reflects the portion of

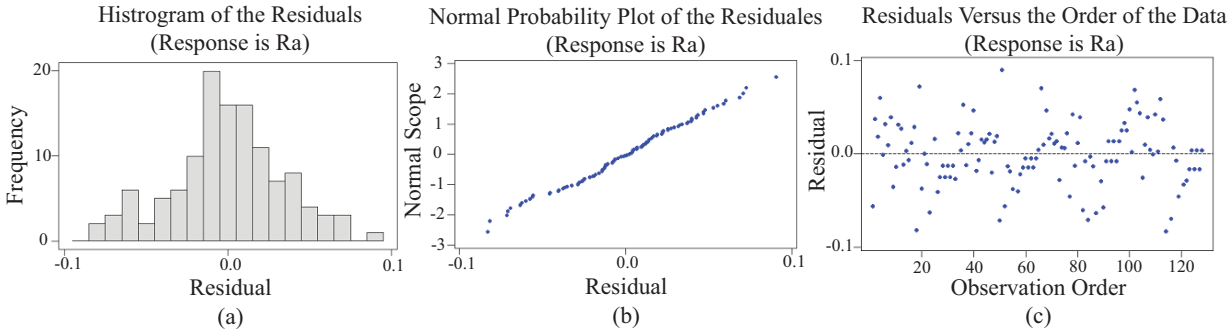

Figure 4.8: Validation of the used information to build the Statistical Model with new cutting tool: (a) Normal distribution of the residuals; (b) Normal probability plot; (c) Spread of points.

the total variation observed in an experiment attributed to each factor.

- The factors and their combinations with the $p - value$ less to 0.05 (when the hypothesis is true and the effect of the factor is representative).

The *ANOVA* results are described in Appendix E. Before applying an *ANOVA*, all the data set must be normalized by considering ± 1 level values (see Table 4.7) in the equation,

$$\bar{\xi} = \frac{\xi - \left(\frac{\xi_{(level+1)} + \xi_{(level-1)}}{2}\right)}{\left(\frac{\xi_{(level+1)} - \xi_{(level-1)}}{2}\right)} \tag{4.7}$$

The analysis of variance was applied to confirm the squared error $R^2 = 0.8858$ and the adjusted squared error $R^2_{adj} = 0.876$. The final fitted model is given by

$$\begin{aligned} R_a \quad = \quad & 0.1139 + 0.06513 \times f_z + 0.01913 \times f_z^2 - 0.0808 \times D_{tool} + 0.04961 \times D_{tool}^2 + 0.00896 \times HB^2 - \\ & - 0.0437 \times f_z \times D_{tool} - 0.0138 \times f_z \times HB + 0.01647 \times D_{tool} \times HB + \\ & + 0.01185 \times ae \times Curv + 0.00937 \times Curv^2 \end{aligned} \tag{4.8}$$

The range of the levels defines the domain where the model can be applied to predict the R_a. The model was validated in agreement with the results shown in Figure 4.8. Figure 4.8a. depicts the normal distribution of the residuals and it is observed that enough data was used to fit the model. Figure 4.8b. defines the normal probability plot, and the tendency (straight line) shows the normality of the error distribution. Also, Figure 4.8c. shows an excellent spread of points on either side of zero (No patterns are observed).

4.7.2 *RSM* for the half-new cutting tool condition

The *DoE* was reproduced with the half-new cutting tool condition, and the measurements of R_a were made in agreement with the procedure described in Section 4.4. The *RSM* was applied to build the model for the half-new

cutting tool condition. The *ANOVA* results are presented in Appendix F. The Ra is explained by the model with $R^2 = 90.0\%$ and the estimated parameters of model are significant in $R^2_{adj} = 88.7\%$. The fitted model is given by

$$\begin{aligned} R_a &= 0.13829 + 0.0573 \times f_z + 0.01273 \times f_z^2 - 0.08581 \times D_{tool} + 0.03293 \times D_{tool}^2 - 0.0435 \times HB + \\ &+ 0.07571 \times HB^2 - 0.0096 Curv + 0.00935 \times ae - 0.02156 \times f_z \times D_{tool} + \\ &+ 0.01401 \times f_z \times Curv - 0.02427 \times D_{tool} \times ae + 0.01059 \times D_{tool} \times HB + \\ &+ 0.01281 \times D_{tool} \times Curv + 0.01775 \times HB \times Curv \end{aligned} \tag{4.9}$$

4.7.3 *RSM* for the half-worn cutting tool condition

By using half-worn cutting tool condition, the *DoE* was reproduced and the measurements of R_a were made for each test piece. The *RSM* was required to build the model for this cutting tool condition. The *ANOVA* results are presented in Appendix F. The Ra is explained by the model with $R^2 = 92.7\%$. The estimated parameters of the model are significant in $R^2_{adj} = 91.60\%$. The fitted model is given by

$$\begin{aligned} R_a &= 0.18102 + 0.07536 \times f_z + 0.0284 \times f_z^2 - 0.0836 \times D_{tool} + 0.03139 \times D_{tool}^2 - 0.0068 \times HB + \\ &+ 0.04364 \times HB^2 + 0.00893 ae - 0.03986 \times f_z \times D_{tool} + 0.03416 \times f_z \times HB - \\ &- 0.03216 \times D_{tool} \times ae - 0.02981 \times D_{tool} \times HB + 0.01686 \times D_{tool} \times Curv + \\ &+ 0.0079 \times ae \times HB - 0.03216 \times ae \times Curv + 0.0087 \times Curv^2 \end{aligned} \tag{4.10}$$

4.7.4 *RSM* for the worn cutting tool condition

Finally, the *DoE* was reproduced with the worn cutting tool condition and the measured R_a was computed for each test piece. Applying *RSM*, the model was built for this cutting tool condition. The *ANOVA* results are presented in Appendix F. The Ra is explained by the model with $R^2 = 93.4\%$ and the estimated parameters of the model are significant in $R^2_{adj} = 92.50\%$. The final fitted model is given by

$$\begin{aligned} R_a &= 0.21686 + 0.06362 \times f_z + 0.02246 \times f_z^2 - 0.05339 \times D_{tool} + 0.02217 \times D_{tool}^2 - 0.02236 \times HB + \\ &+ 0.02962 \times HB^2 + 0.01674 Curv - 0.02925 \times f_z \times D_{tool} + 0.01303 \times f_z \times HB + \\ &+ 0.0208 \times f_z \times Curv - 0.00942 \times D_{tool} \times HB + 0.01582 \times D_{tool} \times Curv - 0.01047 \times ae \times HB - \\ &- 0.01047 \times ae \times Curv + 0.0175 \times HB \times Curv \end{aligned} \tag{4.11}$$

4.7.5 Analysis of results with the *RSM* models

The objective of the *RSM* is to determine the optimum operating conditions for the system, which guarantee a minimum R_a, or to define a region of the factor space in which the operating conditions are satisfied, and the R_a is inside the defined threshold value. Figure 4.9 shows the quadratic behaviour of the response R_a as a function of the defined factors. Therefore, an analysis may be performed to identify the path of improvement toward the vicinity of the *optimum*.

Figure 4.10A shows the effects of f_z and D_{tool} on R_a. Now, it is observed that R_a increases with the f_z owing to increased cutting forces and strains. R_a decreases with an increase in cutting tool diameter (or cutting speed) until it reaches minimum value. Then R_a increases with high cutting tool diameters (or high cutting speed) owing to vibration increase forces and strains. Similar behaviour is observed in the results shown in [Barber *et al.*, 2001], [Suresh *et al.*, 2002], and [Sai and Bouzid, 2005]. For a new cutting tool (Figure 4.10a), it was observed that R_a always increases for cutting tool diameters from 16 to 8 mm. R_a increases an average of 60% for small f_z values and 300% for big f_z values among the 16 and 8 diameters. Figure 4.10d shows the behaviour of the R_a for the worn cutting tool condition, and the tendency is similar at the fresh cutting tool condition. R_a increases an average of 12% for small f_z values and 89% for big f_z values. For all cutting tool worn conditions and 20 mm of diameter, the R_a lightly decreases when f_z increases, and finally increases for high f_z values. Figure 4.10B shows that R_a decreases as the workpiece hardness increases until reaching a minimum value, and then R_a increases with the hardness. High values of hardness induce greater cutting forces and the possibility of tool deformation, and higher R_a values are observed. It is important to evaluate this behaviour for computing minimum or maximum R_a values with different combinations of the cutting parameters. Also, it is observed that cutting conditions for minimum R_a changes with the evolution of the flank wear in the cutting tool. Figure 4.10h presents the behaviour of the R_a for the worn cutting tool condition, where the minimum R_a is located between 110 and 136 BHN, and low values of

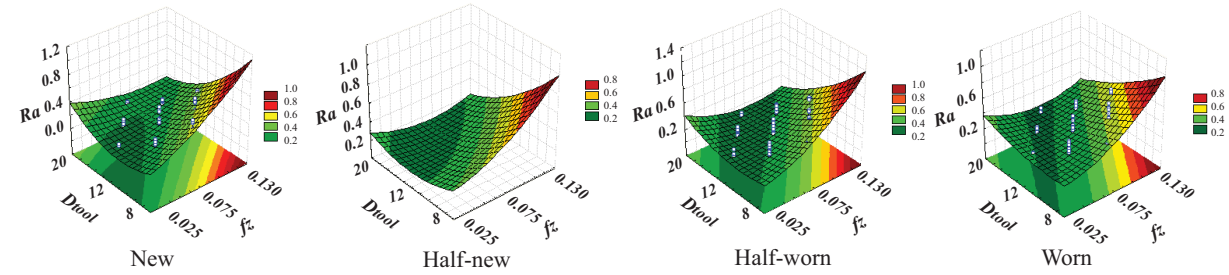

A) Effects fz and Dtool on Ra.

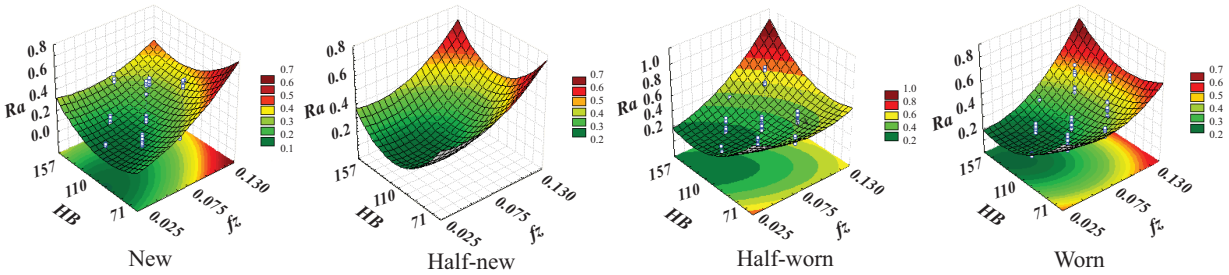

B) Effects *fz* and *HB* on *Ra*.

Figure 4.9: The plots depict the quadratic behaviour of the response R_a as a function of the defined factors: f_z, HB and D_{tool}. Also, it is shown how the optimal conditions for minimum R_a value are changed with the evolution of the cutting tool wear condition.

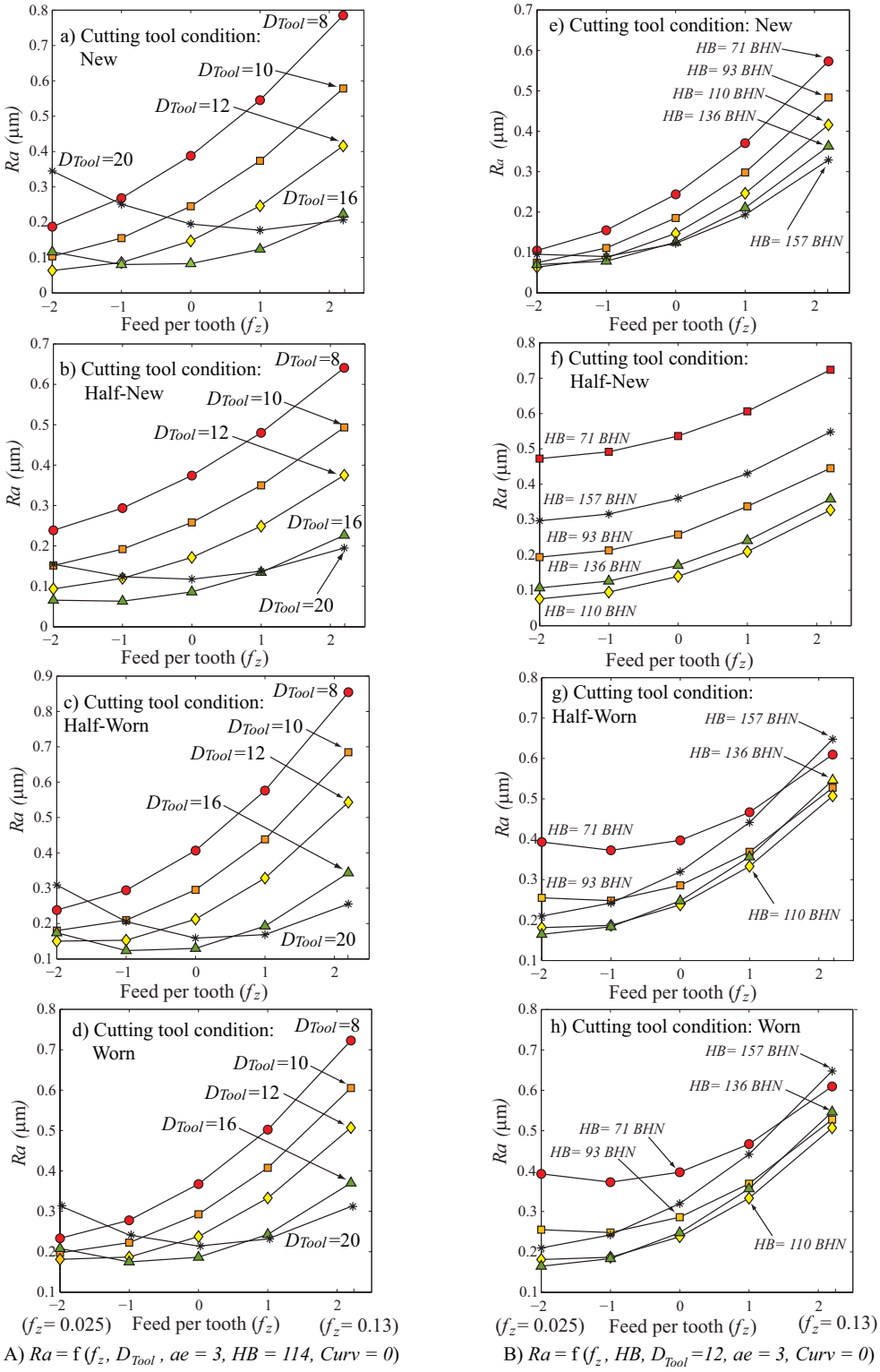

Figure 4.10: (A) These plots show the effects of f_z and D_tool on R_a, and it is observed that R_a increases when f_z also increases and R_a decreases when the cutting tool diameter increases. Also, it is observed that R_a increases with the evolution of the flank wear. B) Effects of f_z and HB on R_a. These plots show that R_a decreases if the hardness increases for new and half-new cutting tool wear condition. High values of R_a are observed if the hardness increases for half-worn and worn cutting tool wear condition.

f_z. The R_a increases for high values of hardness. Also, for all cutting tool conditions, the minimum R_a is defined for 110 BHN. Finally, Figure 4.11 depicts the quadratic behavior of the *RSM* and the regions where the minimum R_a is located as a function of the main factors. These observations justify the selection of the *RSM* as the objective function in the optimization process.

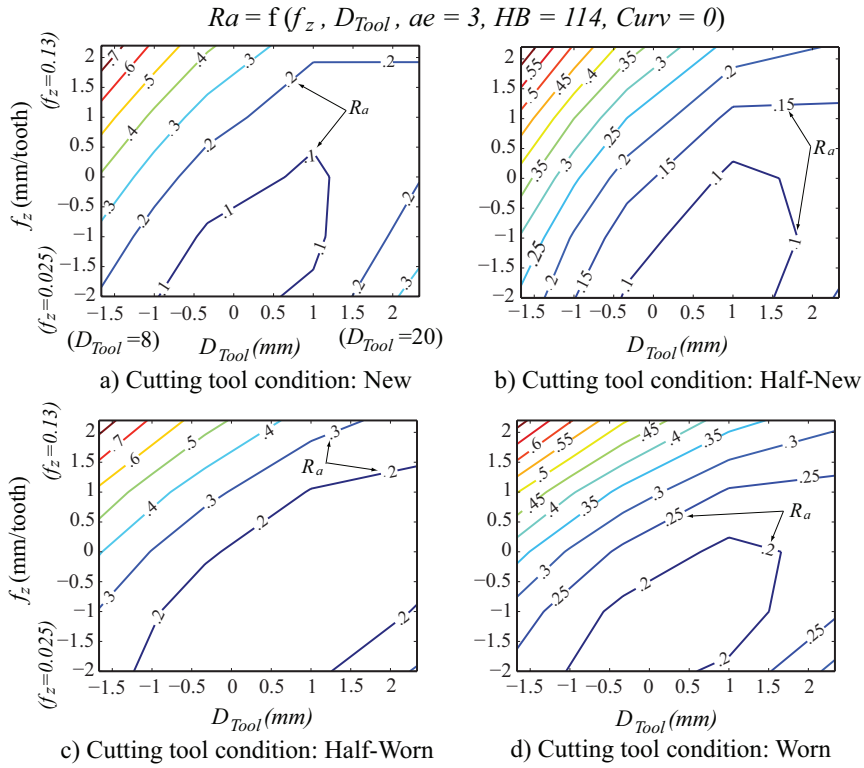

Figure 4.11: Contour plot to show the effects of f_z and D_{Tool} on R_a for all cutting tool conditions: a) New, (b) Half-New, (c) Half-Worn, and (d) Worn.

Two theoretical models will be used to compare the performance of *RSM* models. One mathematical model is given by [Boothroyd and Knight, 2006],

$$R_a = \frac{0.0642(f_z z)^2}{D_{tool}} \tag{4.12}$$

[Dereli *et al.*, 2001] and [Palanisamy *et al.*, 2007] present another theoretical model to compute the arithmetic value of the R_a in end milling process, and it is given by

$$R_a = \frac{318(f_z^2)}{4D_{tool}} \tag{4.13}$$

Figure 4.12 depicts the measured R_a versus the estimated R_a values computed with the *RSM* and the mechanistic

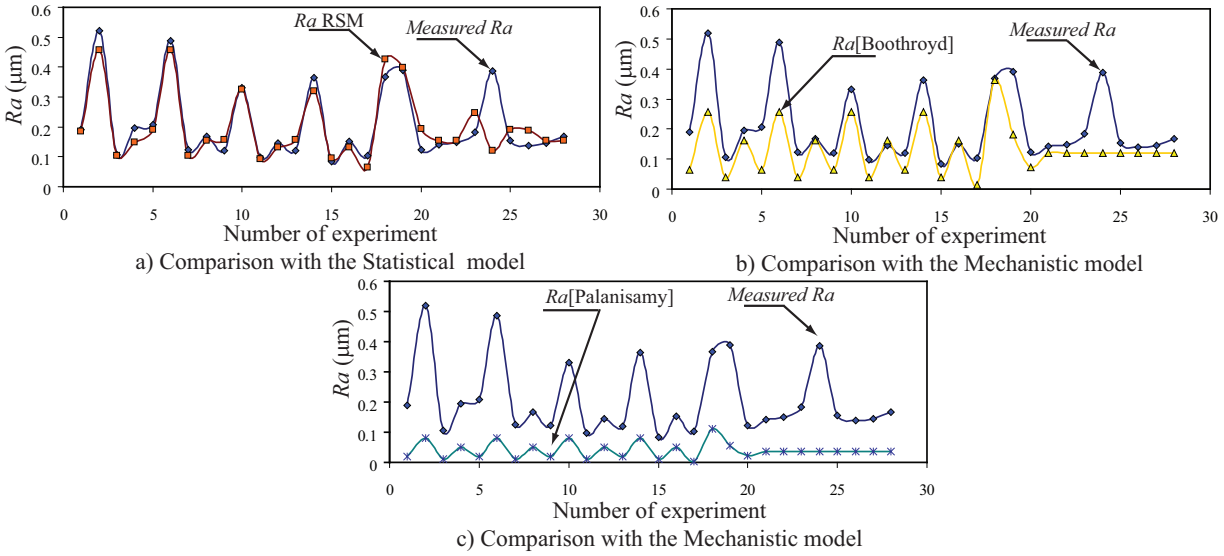

Figure 4.12: Comparison of the results of the *RSM* model with two mechanistic models. The results correspond to the new cutting tool condition, and a considerable error was observed between the measured and estimated R_a for the mechanistic models.

models. The average percentage error was computed with the following equations

$$E = \frac{ABS(R_{a,meas} - R_{a,pred})}{R_{a,meas}} \times 100 \tag{4.14}$$

$$ME = \sum_{i=1}^{n} \frac{E_i}{n} \tag{4.15}$$

where E is the absolute error and ME is the average percentage error. It is shown that the tendencies between the $R_{a,meas}$ and R_aRSM are very similar with an average percentage error of 16.37%. The average percentage error between the $R_{a,meas}$ and Eqs. 4.12, and 4.13 is 35.9% and 79.83% respectively. It is obvious that Eqs. 4.12 and 4.13 do not consider many factors that can really affect the R_a. In addition to the feed per tooth and cutting tool diameter, the statistical model (*RSM*) includes relevant factors such as depth of cut, hardness, and curvature of the machined path. Figure 4.13 shows the measured R_a versus the estimated R_a computed with the *RSM* and the mathematical models for different cutting tool conditions. Once again, an excellent similitude is observed between the $R_{a,meas}$ and R_aRSM. Furthermore, it is shown how the average percentage error increases with the evolution of the flank wear in the cutting tool (Table 4.9). Here, the importance of the flank wear is demonstrated in the prediction of R_a, and empirical models cannot be used for the R_a estimation owing to the high error computed in the R_a. Additionally, the *RSM* models were validated with new experiments. Table 4.10 shows the cutting conditions and the results for the measured and estimated R_a values. The last column defines the absolute percentage error between

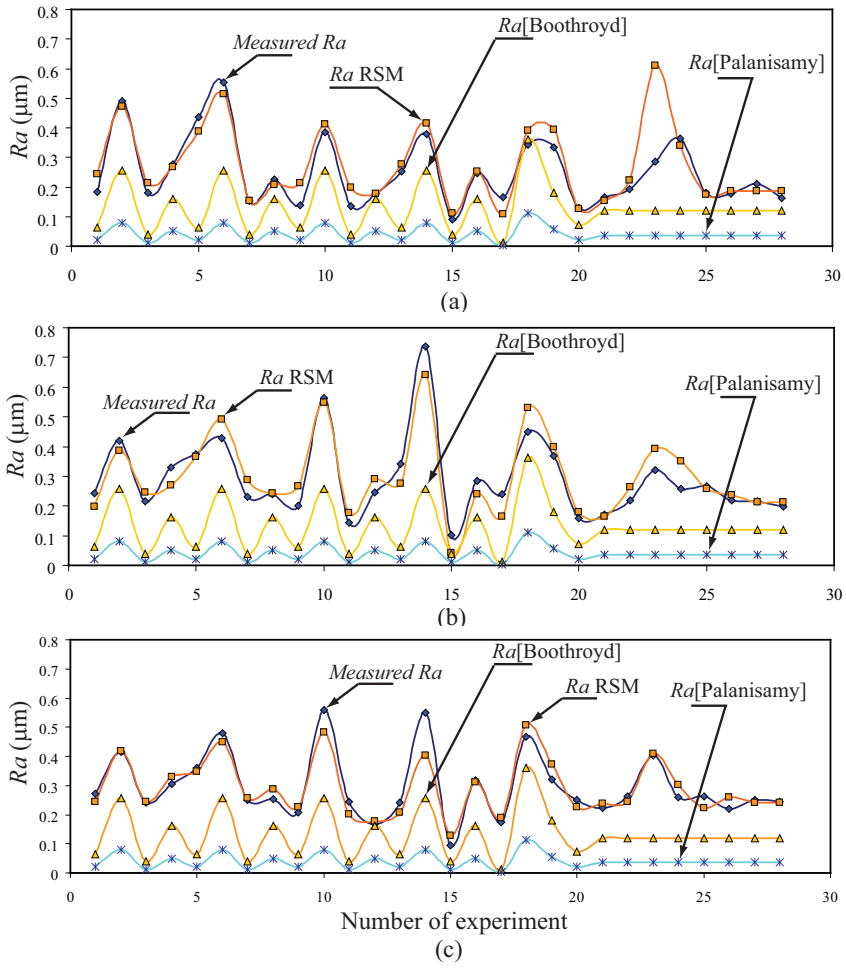

Figure 4.13: Comparison of the measured R_a versus estimated R_a value. The results correspond to the following cutting tool conditions: (a) Half-new; (b) Half-worn; and (c) Worn condition.

the measured and estimated R_a values. The geometric and cutting parameters were selected to define two evaluation ranges: inside the cube of the *DoE* domain ($0 - 50\%$) and outside the cube ($> 50\%$). Each percentage of factors is considered from the central value. Table 4.10 shows an excellent performance of the model, with an average percentage error of 12.87% when the cutting conditions correspond with central points of the *DoE* (inside of the cube). The test pieces with these conditions are $P01 - 2024$, $P03 - 2024$, $P04 - 2024$, and $P05 - 2024$. If the cutting conditions are defined outside the cube, the deviation between the measured and estimated R_a values increases. Also, Table 4.10 shows an increase of the average percentage error (71.37%) in the experiments outside the cube. When the feed per tooth and hardness present a deviation greater than 50%, the average percentage error

Table 4.9: Average percentage error between the measured and estimated R_a values with different models.

Cutting Tool Condition	R_a *RSM*	R_a Boothroyd	R_a Palanisamy, Dereli
New	16.37%	35.90%	79.83%
Half-New	16.87%	46.48%	83.32%
Half-Worn	14.92%	53.78%	85.69%
Worn	8.98%	56.31%	86.47%

increases from 12.87% to 95%. For this reason, these factors have a huge impact in the response (R_a). Also, the HB and D_{tool} factors have an important impact on response R_a because the average percentage error increases from 12.87% to 87.8% for a deviation greater than 50%.

4.8 Modeling of the R_a by using *ANN*

The statistical model computes the R_a by considering the cutting parameters, cutting tool geometry, and material properties. This model predicts the R_a with minimum error when the factors are inside the *RSM* domain. Therefore, these computed models can be used to predict the R_a before starting the metal cutting process. It is necessary to include the process variables that allow prediction of R_a value during machining. A multi-sensor system and data fusion techniques will be used to build the Artificial Neural Network (*ANN*) model. An estimator based on multi-sensor and data fusion provides an improved and robust estimation. There are different frameworks for fusing signal features such as mathematical functions, black-box models, rule-based fuzzy sets, *ANN*, etc. The *ANN* framework was selected because it has several attractive properties such as universal function approximation capability, insensitivity to noisy or missing data, and the ability to accommodate multiple non-linear variables for unknown interactions. Among the various *ANN* models, feed-forward architecture is a classic model, and back-propagation algorithm is an excellent training method for this architecture. The *ANN* model was built with the cutting parameters and process variables monitored from sensors. Figure 4.14 depicts the proposed architecture for the *ANN* model. A brief description of the normalized process of the input variables is discussed.

4.8.1 Input and Output variables selection

The input variables defined for the *ANN* model were the following: $x_1 = f_z$, $x_2 = D_{tool}$, $x_3 = ae$, $x_4 = HB$, $x_5 = Curv$, and Seven Mel Frequency Cepstrum Coefficients (*MFCC*) computed from the different process variables. Three different options were selected for the output layer: the first with only the R_a value, the second with R_a and RSm values, and the third by considering the R_a, RS_m, R_q, and R_z values. Figure 4.15 shows two experiments with different cutting and geometric parameters, but with similar R_a value. For this reason, it is necessary to include the other parameters (RS_m, R_q, and R_z) in the output layer. These parameters allow a better characterization of the

Table 4.10: Cutting parameters and conditions for the new experiments. Also, it is included the results of the R_a.

Test piece	Cutting Tool Condition	f_z %	D_{tool} %	ae %	HB %	$Curv$ %	$R_{a,meas}$ μm	$R_{a,pred}$ μm	Error %
P01-2024-Line	New	0	0	0	2	0	0.1612	0.1546	4.21
P01-2024-Island	New	0	0	0	2	74	0.1752	0.1756	0.25
P01-2024-Box	New	0	0	0	2	38	0.1436	0.1599	11.35
P03-2024-Line	Half-New	0	0	0	0	0	0.1582	0.1837	16.12
P03-2024-Island	Half-New	0	0	0	0	167	0.1598	0.189	18.27
P03-2024-Box	Half-New	0	0	0	0	111	0.145	0.1801	24.21
P04-2024-Island	New	0	0	0	0	50	0.1955	0.1624	16.93
P05-2024-Box	New	0	0	0	2	50	0.1504	0.164	9.04
P01-5083-Island	Half-New	53	67	53	91	154	0.2384	0.4732	98.49
P01-7075-Line	Half-New	76	133	76	112	0	0.2109	0.3621	71.69
P01-7075-Island	Half-New	76	133	76	112	78	0.2685	0.5156	92.03
P01-6082-Island	Half-Worn	67	0	67	49	77	0.1965	0.231	17.56
P01-6082-Box	Half-Worn	67	0	67	49	37	0.1361	0.30133	121.40
P02-6082-Line	Half-Worn	67	0	67	37	0	0.2591	0.2383	8.03
P02-6082-Island	Half-Worn	67	0	67	37	77	0.3218	0.2008	37.60
P02-7075-Box	Worn	10	67	100	93	57	0.1559	0.1363	12.57
P02-7075-Line	Worn	10	67	100	93	0	0.1624	0.1874	15.39
P03-7075-Box	Half-Worn	10	67	100	95	57	0.1277	0.2582	102.2
P03-7075-Island	Half-Worn	10	67	100	95	44	0.1262	0.1573	24.64
P03-7075-Line	Half-Worn	10	67	100	89	0	0.1091	0.1925	76.44
P01-CERTAL-Box	Worn	67	67	50	79	37	0.1692	0.1377	18.60
P09-2024-Box	Worn	48	133	50	0	63	0.1742	0.1975	13.38
P09-2024-Island	Worn	48	133	50	0	42	0.25	0.2802	12.07

surface roughness pattern.

4.8.2 Preprocessing of the input variables

All the experimental data set were normalized to avoid numerical instability. The data was normalized with a mean zero and a standard deviation equal to one (see Appendix F). Additionally, another method for normalizing the data set was used. The *Bipolar sigmoidal* normalization was employed because the minimum and maximum values are unknown in real-time, and it is given by

$$\bar{z_i} = \frac{1 - e^{-y_i}}{1 + e^{-y_i}} \tag{4.16}$$

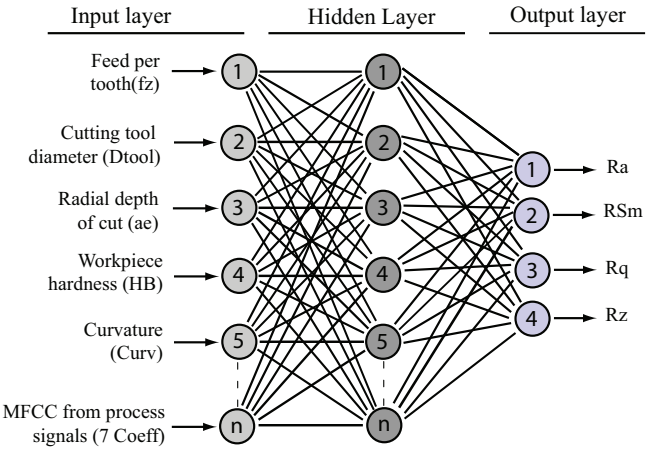

Figure 4.14: Proposal architecture for the *ANN* model with the inputs and outputs variables. The Multi-sensor and data fusion are used to build the *ANN* model for estimation of the surface roughness during machining process.

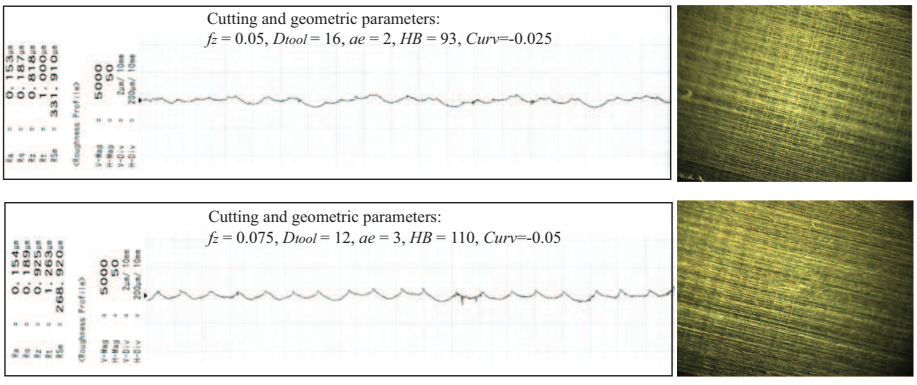

Figure 4.15: The plot depicts two experiments with different cutting and geometric parameters. However, both experiments present the same R_a value, but different R_z, and RS_m values.

where $\bar{z}_i$ defines the new normalized input variable, and $i = 1, 2..., n$, is the number of the input variable. The non-linear transformation prevents most values from being compressed into essentially the same values, and it also compresses the large outer values.

4.8.3 Training *ANN* Model

Several tests were defined to select the best *ANN* model to estimate the R_a as a function of the cutting parameters and some process variables represented by the *MFCC*. The considered *MFCC* were the $0'th$ order cepstral coefficient, and six cepstrum coefficients. The selected process variables were the acceleration signals from the workpiece and the cutting force signals. After an intensive searching procedure, four different *ANN* models were selected, as depicted in Table 4.11. Neural networks learn from input data. These systems analyze new pattern data according to previously-stored information and react to new data based on past input. Several learning methods have been developed for *ANN*. Among the various models training neural networks models, backpropagation was selected because it is one of the best general purpose models ([Tsai *et al.*, 1999], [Lee and Chen, 2003], and [Benardos and Vosniakos, 2002]). It is a supervised learning scheme by which a layered feed-forward network is trained to become a pattern-matching engine. When the networks are given input, the updating of value activation propagates forward from the input layer of the network, through each internal layer, to the output layer of the network. The output then provides the *ANN's* response. Neural networks can correct their internal parameters. The correction mechanism starts with the output units and backpropagates through each internal layer to the input. This process repeats until the weights of the network steps reach the final state, where the root mean square error approaches and converges on the acceptable minimum value. The *ANN* models were training with the data set taken of the experimentation of each cutting tool wear condition, and by using each process variable (accelerometers in X and Y axis in the spindle and workpiece, and the forces in X and Y axis). It was made only for the $B(12, 12, 1)$, $C(12, 12, 2)$, and $D(12, 12, 4)$ models. The information was randomly divided into two data set: 70% for the data training and 30% for the data testing. Four combinations of data set were selected to compute an average performance and to evaluate the generalization capacity of the *ANN* models. Table 4.12 presents the average computed performance for all *ANN* models with the training data set.

Table 4.11: Architecture of the *ANN* models used to compute the R_a.

ANN model	Variables of Input Layer	Number Hidden Layer and Neurons	Variables of Output Layer
$A(5, 5, 1)$	f_z, D_{tool}, ae, HB, $Curv$	$1 - 5$	R_a
$B(12, 12, 1)$	f_z, D_{tool}, ae, HB, $Curv$, and 7 *MFCC*	$1 - 12$	R_a
$C(12, 12, 2)$	f_z, D_{tool}, ae, HB, $Curv$, and 7 *MFCC*	$1 - 12$	R_a, RS_m
$D(12, 12, 4)$	f_z, D_{tool}, ae, HB, $Curv$, and 7 *MFCC*	$1 - 12$	R_a, RS_m, R_q, R_z

For the $D(12, 12, 4)$ model, the *PCA* technique was applied to the input and output data vectors. This technique was described in Chapter 4.

4.8.4 Testing *ANN* Model

Furthermore, the proposal models were validated with the testing data set. Table 4.13 shows the average performance of the *ANN* models for the testing data set. It is shown that applying the *PCA* over the input and output data vectors, the $D(12, 12, 4)$ model increases its performance with respect to the other models. The highest average performance was obtained when the *MFCC* are computed with the Fy force. For the four cutting tool wear conditions the average performance was 85.31%.

Table 4.12: Performance of the *ANN* models for the training data set. The performance was computed by considering the different combination of data set.

Cutting Tool Wear Condition	Model	Cutting Parameters %	Cutting Parameters and *MCFF*			
			$Acc_{x,workpiece}$ %	$Acc_{y,workpiece}$ %	$F_{x,force}$ %	$F_{y,force}$ %
New	$A(5, 5, 1)$	96.185				
	$B(12, 12, 1)$		100	100	100	100
	$C(12, 12, 2)$		96.12	96.82	97.41	97.99
	$D(12, 12, 4)$		97.93	98.34	98.09	97.89
Half-New	$A(5, 5, 1)$	97.78				
	$B(12, 12, 1)$		100	100	100	100
	$C(12, 12, 2)$		97.86	97.02	97.61	95.90
	$D(12, 12, 4)$		99.44	99.16	98.06	98.51
Half-worn	$A(5, 5, 1)$	83.13				
	$B(12, 12, 1)$		100	100	100	100
	$C(12, 12, 2)$		97.34	94.54	93.28	92.58
	$D(12, 12, 4)$		97.22	97.38	96.02	98.24
Worn	$A(5, 5, 1)$	98.2				
	$B(12, 12, 1)$		100	100	100	100
	$C(12, 12, 2)$		98.67	96.46	96.98	98.47
	$D(12, 12, 4)$		99.09	97.81	98.92	99.09

Table 4.13: Performance of the *ANN* models for the testing data set. The cutting parameters are f_z, ae, D_{tool}, HB, and $Curv$. The third column presents the results of the *ANN* model using only cutting parameters. The last four columns present the average performance of the *ANN* models using both cutting parameters and *MFCC* from the process signals.

Cutting Tool Wear Condition	Model	Cutting Parameters %	Cutting Parameters and 7 *MCFF*			
			$Acc_{x,workpiece}$ %	$Acc_{y,workpiece}$ %	$F_{x,force}$ %	$F_{y,force}$ %
New	$A(5,5,1)$	88.118				
	$B(12,12,1)$		73.49	70.42	80.31	88.18
	$C(12,12,2)$		82	85.30	73.80	87.54
	$D(12,12,4)$		85.12	84.43	83.30	90.87
Half-New	$A(5,5,1)$	91.54				
	$B(12,12,1)$		74.09	76.99	73.47	76.02
	$C(12,12,2)$		75.67	80.76	76.78	79.81
	$D(12,12,4)$		78.91	78.33	77.29	80.40
Half-worn	$A(5,5,1)$	91.93				
	$B(12,12,1)$		79.11	44.50	55.81	50.03
	$C(12,12,2)$		74.63	74.86	75.52	77.74
	$D(12,12,4)$		78.58	82.20	85.19	85.16
Worn	$A(5,5,1)$	67.55				
	$B(12,12,1)$		79.97	77.10	68.49	71.48
	$C(12,12,2)$		74.82	84.38	78.47	81.93
	$D(12,12,4)$		67.10	83.87	85.56	84.81

4.8.5 Validation tests for the *ANN* models

First, the validation of the *ANN* models were determined by considering original data set from the *DoE*. Second, new experiments with different cutting conditions were defined for validation. Table 4.14 shows four ($R_1, ..., R_4$) replicates of the selected *DoE* for each cutting tool wear condition. The cutting conditions, and the geometric parameters are $f_z = 0.05$, $ae = 2$, $D_{tool} = 16$, $HB = 90, 91, 93$, $Curv = -0.025$, and 6082 aluminium alloy. These values correspond to the central and extreme conditions of the *DoE*. From table 4.14 some observations can be summarized:

- The measured R_a changes for each experiment, even though the cutting conditions and workpiece material are the same. The maximum difference among the measured R_a for the same cutting conditions is 14%. This behavior of the R_a is only reproduced when the models consider the process variables.

Table 4.14: Selected experiments with measured and estimated R_a values computed with models $A(5,5,1)$ and $D(12,12,4)$ for two different process variables: $Acc_{x,workpiece}$ and $F_{y,force}$. The absolute percent error is shown in the table.

		Cutting	Estimated R_a with *ANN* Models					
	Measured	Tool	$A(5,5,1)$		$D(12,12,4)$ Acc_x		$D(12,12,4)$ F_y	
Exp03	R_a	Condition	R_a	$E(\%)$	R_a	$E(\%)$	R_a	$E(\%)$
E2-R1	0.127	New	0.129	1.57	0.126	0.78	0.112	11.81
E2-R2	0.113	New	0.129	14.16	0.110	2.65	0.114	0.88
E2-R3	0.108	New	0.129	19.44	0.113	4.63	0.110	1.85
E2-R4	0.122	New	0.129	5.73	0.104	14.75	0.112	8.19
E3-R1	0.167	H-New	0.155	7.18	0.172	2.99	0.171	2.39
E3-R2	0.191	H-New	0.155	18.84	0.079	58.63	0.172	9.95
E3-R3	0.179	H-New	0.155	13.40	0.175	2.23	0.146	18.43
E3-R4	0.179	H-New	0.155	13.40	0.126	29.61	0.160	10.62
E4-R1	0.234	H-Worn	0.165	29.48	0.214	8.54	0.241	2.99
E4-R2	0.235	H-Worn	0.165	29.78	0.188	20.00	0.310	31.92
E4-R3	0.241	H-Worn	0.165	31.53	0.221	8.29	0.230	4.56
E4-R4	0.227	H-Worn	0.165	27.31	0.213	6.16	0.254	11.89
E5-R1	0.266	Worn	0.223	16.16	0.285	7.14	0.272	2.25
E5-R2	0.272	Worn	0.223	18.01	0.255	6.25	0.284	4.14
E5-R3	0.267	Worn	0.223	16.47	0.269	0.74	0.284	6.36
E5-R4	0.272	Worn	0.223	18.01	0.249	8.45	0.290	6.62

- The estimated R_a with *ANN* models are better than the statistical models. The mean absolute percent errors of each model with respect to the measured R_a are 17.6% for $A(5,5,1)$ model (only cutting parameters), 11.36% for $D(12,12,4)$ model (cutting parameters + Ac_x), and 8.48% for $D(12,12,4)$ model (cutting parameters + F_y).
- Figure 4.16 depicts the comparison between the measured and estimated R_a. Here, it is observed that the $D(12,12,4)$ model with F_y process state variable follows a similar behaviour with the measured R_a.

New experiments with different cutting conditions were defined to validate the performance of the *ANN* models. Table 4.15 presents the C_C, P_G, and P_C for these experiments. Table 4.16 shows the results of the estimated R_a with the *ANN* models.

The shown results in Table 4.16 are plotted in Figure 4.17. Some observations of these results are the following:

- The computed models with *ANN* and sensor fusion present a better performance than statistical models.

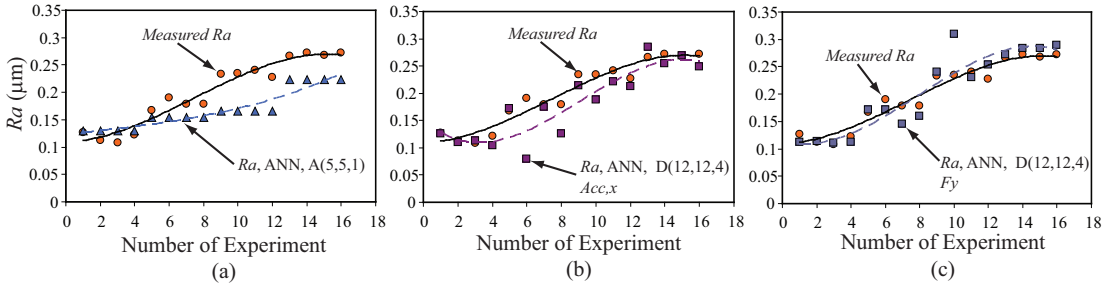

Figure 4.16: Comparison of the R_a values obtained from the *DoE* with: (a) *ANN* model by using only cutting parameters ($A(5,5,1)$), (b) *ANN* model with cutting parameters and Acc_x ($D(12,12,4)$), and (c) *ANN* model with cutting parameters and F_y ($D(12,12,4)$).

Table 4.15: Cutting conditions and geometric parameters defined for the new experiments. These experiments were used to validate the *ANN* models.

Experiment	Tool Condition	f_z	ae	D_{tool}	HB	$Curv$
P1-2024-line/Island/Box	New	.075	3	12	109	0 /0.037 /−0.019
P3-2024-line/Island/Box	Half-New	.075	3	12	110	0 /0.083 /−0.0556
P4-2024-Island	New	.075	3	12	110	.025
P5-2024-Box	New	.075	3	12	109	−.025
P1-5083-line/Island/Box	Half-New	.047	2	8	71	0 /0.077 /−0.0588
P1-7075-line/Island/Box	Half-New	.115	4.5	20	158	0 /0.039 /−0.0183
P1-6082-line/Island/Box	Half-Worn	.04	4	12	89	0 /0.038 /−0.0185

- Even though the mean absolute percent errors are higher than results presented in Table 4.14, the models show an excellent tendency in agreement with the measured R_a. The *ANN* model ($D(12,12,4)$) with the $F_{y,force}$ signal presents a better behaviour than other models.
- The results of the experiments from 9 to 14 in Table 4.16 present a bigger absolute percentage error than other experiments because the cutting conditions correspond with extreme values, and they are within the limits of the domain defined in the *DoE*.

4.9 Results and contributions

In relation to the R_a modeling, important contributions and results can be deduced from this chapter. Important results are the following:

Table 4.16: Results of the estimated R_a with the *ANN* models. The absolute percent error between the measured and estimated R_a is shown.

		Estimated R_a with *ANN* models					
	Measured	$A(5,5,1)$		$D(12,12,4)$ Acc_x		$D(12,12,4)$ F_y	
Experiment	R_a	R_a	$E(\%)$	R_a	$E(\%)$	R_a	$E(\%)$
1)P1-2024Line	0.161	0.147	8.69	0.139	13.66	0.083	48.44
2)P1-2024Island	0.176	0.160	9.09	0.220	25.00	0.154	12.5
3)P1-2024Box	0.144	0.148	2.77	0.136	5.55	0.104	27.77
4)P3-2024Line	0.158	0.190	20.25	0.220	39.24	0.132	16.45
5)P3-2024Island	0.160	0.174	8.75	0.283	76.87	0.123	23.12
6)P3-2024Box	0.145	0.200	37.93	0.300	106.89	0.166	14.48
7)P4-2024Island	0.196	0.156	20.40	0.099	49.48	0.164	16.32
8)P5-2024Box	0.150	0.150	0.00	0.197	31.33	0.025	83.33
9)P1-5083Line	0.238	0.614	157.98	0.302	26.89	0.416	74.79
10)P1-5083Island	0.238	0.532	123.52	0.263	10.50	0.365	53.36
11)P1-5083Box	0.202	0.461	128.21	0.359	77.72	0.357	76.73
12)P1-7075Line	0.211	0.331	56.87	0.132	37.44	0.298	41.23
13)P1-7075Island	0.268	0.268	0.00	0.110	58.95	0.186	30.59
14)P1-7075Box	0.147	0.160	8.84	0.072	51.02	0.339	130.61
15)P1-6082Line	0.163	0.297	82.20	0.139	14.72	0.337	106.74
16)P1-6082Island	0.196	0.323	64.79	0.117	40.30	0.170	13.26
17)P1-6082Box	0.136	0.134	1.47	0.177	30.14	0.107	21.32

- Response surface methodology was applied with excellent results for modeling the R_a. A rotatable central composite design with 32 runs and four replicates was defined for the *DoE*, and after the *ANOVA*, a quadratic model with the main interaction of factors was computed. For the new cutting tool condition, the R_a is explained by the model with a performance of $R^2 = 90.0\%$. For the other three models, the R_a is computed with the following performance: 90.0% for half-new cutting tool, 92.7% for half-worn cutting tool, and 93.4% for worn cutting tool condition.

- The behaviour of the R_a with the variation of factors was compared with others research, with excellent results. R_a increases with f_z and decreases with an increase of the cutting tool diameter until it reaches a minimum value. The R_a decreases as the workpiece hardness increases until it reaches a minimum value, and then R_a increases with the hardness. Also, the R_a increases with the evolution of flank wear, and the models can estimate the R_a with excellent results. The performance was compared with the mechanistic models of other authors, and the average percentage error can be reduced from 86.47% to 8.98% by using proposed

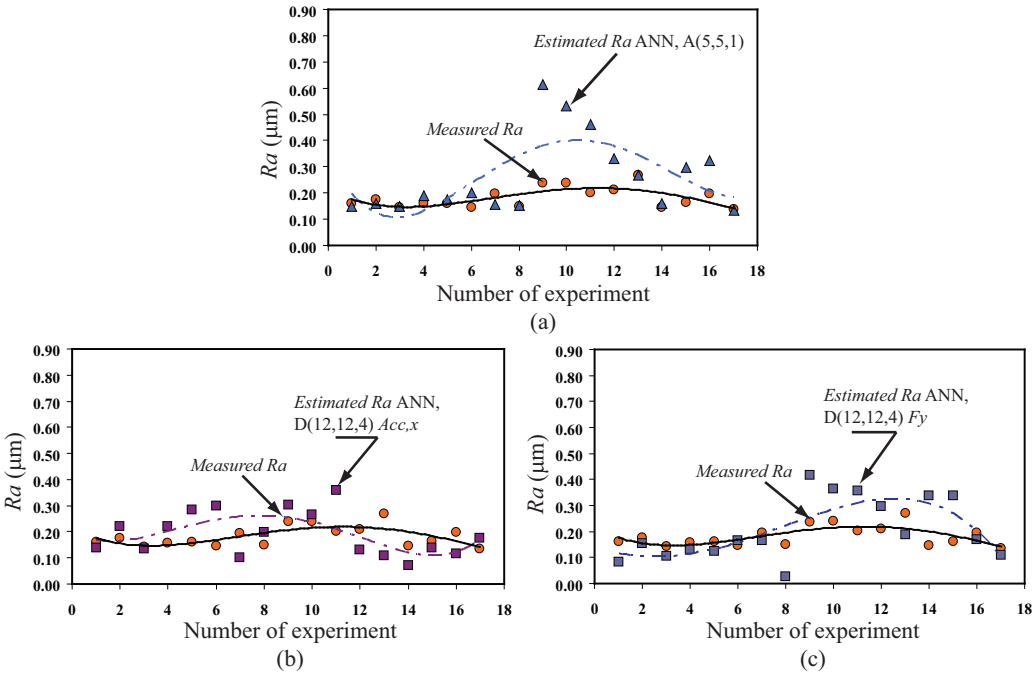

Figure 4.17: Comparison of the R_a values which were observed from new experiments, with (a) *ANN* model by using only factors ($A(5,5,1)$), (b) *ANN* model with factors and Acc_x ($D(12,12,4)$), and (c) *ANN* model with factors and F_y ($D(12,12,4)$).

models.

- Multi-sensor and data fusion were used to build *ANN* models with excellent results. By applying Principal Component Analysis and the process signals, *ANN* models were computed with high performance, and they can be used in *In-process* operating mode.

The contributions in the modeling of R_a are the following:

- The most important factors affecting the R_a were deduced by applying the screening factorial design. These factors are f_z, D_{tool}, ae, HB and $Curv$. The $Curv$ factor is considered a new factor because it has never been used in other research related to R_a. This factor allows the identification of path geometry from concave, straight, and convex path.

- It was observed that R_a value increases with the evolution the flank wear. Four models were computed to consider tool life, which allows the R_a to be estimated as a function of flank wear.

- An *ANN* model was developed based on cutting parameters and process state variables for monitoring the R_a

in *In-process* operating mode. The relevant features of the process state variables were identified through the computation of the *MFCC*.

- The consideration of four parameters to characterize the surface roughness allowed for the increase of performance of *ANN* models. Similar R_a values can be computed by the *ANN* models, even though the cutting and geometric parameters in the machining process are totally different. Therefore, it is relevant to characterize the surface roughness with these parameters.

In addition to the contributions, it is important to include some limitations for the *RSM* and *ANN* models; they are as follows:

- The estimation of the R_a with the *RSM* model is an excellent result only if the cutting and geometric parameters are inside the defined cubic points in the *DoE*.
- It is important to mention that cutting conditions for the finishing operation were defined for the experiments. This implies that models cannot be used in the roughing operation, where high material removal rates are required during the cutting process.
- *ANN* models can be used only in *In-process* operating mode because they require the process state variables to estimate the R_a.
- The *RSM* and *ANN* models cannot be used for the estimation of R_a in the machining of other materials (e.g., steel, copper, brass) because the cutting tools are different and the cutting parameters cannot be equals. It is, therefore, necessary to define new conditions in the *DoE*, and with the obtained information, to build new models.

Chapter 5

Cutting tool wear monitoring module

5.1 Introduction

This section focuses on the determination of wear, the most difficult of the tasks in a cutting tool wear condition monitoring system. The importance of tool wear monitoring is implied by exchanging worn tools in time, and tool costs can be reduced with a precise exploitation of the tool's lifetime. However, cutting tool monitoring is not an easy task for several reasons. Firstly, the machining processes are non-linear, time-variant systems, which makes them difficult to model, and secondly, the signals obtained from sensors are dependent on a number of other factors, such as machining conditions. Additional to the complexity of the process and the large number of machining conditions (i.e. cutting conditions), signals from sensors in machine tools are disturbed for many reasons: outbreaks at cutting edges, chatter, variances of tool geometry, properties of workpiece material, sensor non-linearity, noise of digitizers, crosstalk effects between sensor channels, etc. Sensor-based approaches can be divided into direct and indirect methods. Direct methods measure the actual values of certain wear parameters, whereas indirect methods measure suitable process parameters, which are correlated with tool wear (e.g. cutting forces or vibrations). Another important classification criterion for sensor-based methods depends on the monitoring period. In continuous or on-line methods, significant parameters are measured throughout a cutting process, whereas in intermittent or off-line methods the parameters are measured during intervals in the cutting process. An indirect and intermittent method is proposed for cutting tool monitoring and diagnosis with intelligent features.

5.2 Cutting tool wear condition

Important concepts and recommendations about the cutting tool wear condition are described in the international standard *ISO-8688-2*, "Tool life testing in milling. Part 2: End milling". Appendix G presents the main concepts from the *ISO-8688-2* norm and the methodology and process used to wear the cutting tool during experimentation. It is necessary to identify and classify the cutting tool deterioration phenomena and where it occurs at the cutting

edges. Figure 5.1 defines the terms related to the tool deterioration phenomena on end milling cutters.

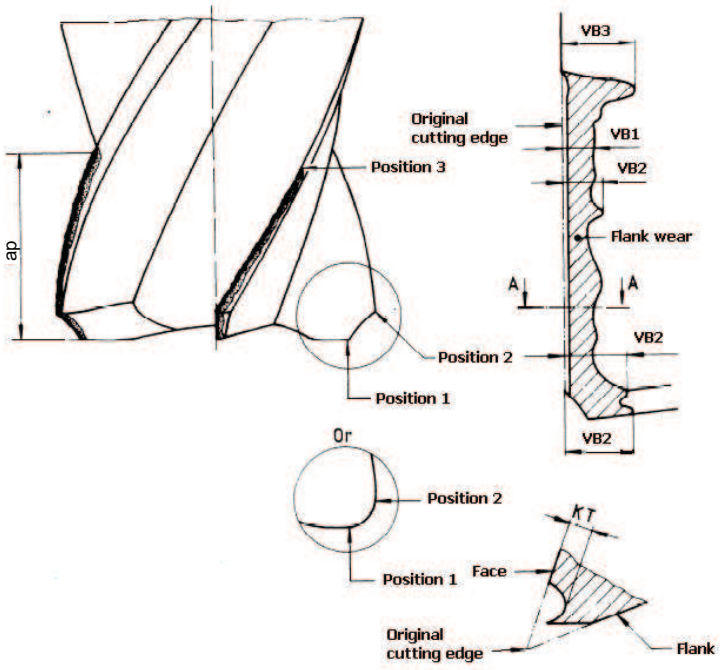

Figure 5.1: The figure shows the area, where the flank wear is located, and the terms used to define the wear on the end milling cutter (Figure taken from ISO 8688-2:1989(E)).

- Flank wear (VB): Loss of tool material from the tool flanks results in the progressive development of flank wear land.
- Uniform flank wear $(VB1)$: Wear land, which is normally of constant width and extends over the tool flanks of the active cutting edge.
- Non-uniform wear $(VB2)$: Wear land, which has an irregular width, and the original flank varies at each position of measurement.
- Localized flank wear $(VB3)$: Exaggerated form of flank wear which develops at a specific part of the flank.

The tool-life criterion can be a predetermined numerical value of any type of tool deterioration that can be measured. If there are different forms of deterioration, they should be recorded, and when any of the deterioration phenomena limits have been attained, the end of the tool life has been reached. Predetermined numerical values of specific types of tool wear are recommended. These numerical values are:

- For a width of the flank wear land (VB) the following tool life end points are recommended: a) uniform wear: 0.3 mm averaged over all teeth; and b) localized wear: 0.5 mm maximum on any individual tooth.
- When chipping occurs, it must be treated as $VB3$ and equal to 0.5 mm (tool-life end point).

Finally, flank wear measurement is carried out parallel to the surface of the wear land and in a direction perpendicular to the original cutting edge. Appendix D shows the procedure to measure the flank wear on the cutting tool edges. Although the flank wear land on a significant portion of the flank may be of uniform size, there will be variations in its value at others portions of the flanks depending on the tool profile and edge chipping. Values of flank wear measurements shall be related to the area or position along the cutting edges at which the measurement is made.

5.3 Methodology to wear the cutting tool

The design of experiments implies the use of new cutting tools, and the repetition of experiments with different cutting tool wear conditions. Four different cutting tool wear conditions were defined to consider the total tool life: new, half-new, half-worn, and worn. Therefore, it was necessary to define a methodology and process to wear the cutting tool and to use the total tool life during the experimentation. The assessment of the flank wear was taken as tool life criterion. The process to wear the cutting tool considers two working conditions: (a) the wear of the cutting tool during the Design of Experiments (*DoE*) and (b) the wear of the cutting tool during the machining of the straight path until the flank wear reaches a specific value. The process implies the following steps:

1. New cutting tools are specified and the *DoE* with four replicates is executed, as was defined in Chapter 4.
2. After running the *DoE*, the flank wear is measured and registered.
3. The cutting tools were worn by using several workpiece materials, and in the process flank wear was measured. The cutting tools are worn until a specific flank wear value is reached.
4. The *DoE* is repeated with a new stage of cutting tool.
5. Steps 2, 3, and 4 are repeated twice. The flank wear is measured and registered at the end of each stage.

Several equations and parameters were defined to assess the flank wear during the experimentation, and they are included in Appendix G.

5.4 Results of the tool life tests

During the machining process of the *DoE*, the machining time, the volume of the removed metal, and the number of cycles of the cutting tools were computed. The results are presented in Appendix G. Also, the flank wear evolution is shown in Appendix G. The uniform flank wear (VB_{avg}) represents the average value of the two cutting tool

edges, and the maximum flank wear (VB_{max}) corresponds to the higher value found in the cutting edges. With these results, the range of flank wear to classify the four cutting tool conditions is defined in Table 5.1.

Table 5.1: Cutting tool wear condition and the flank wear observed during the experimentation.

Cutting Tool Wear Condition	Uniform Flank Wear (mm)
New	$0 \leq VB < 0.07$
Half-new	$0.07 \leq VB < 0.1$
Half-worn	$0.1 \leq VB < 0.18$
Worn	$0.18 \leq VB < 0.45$

Figure 5.2 depicts the evolution of flank wear during the experimentation. The clustering of the data for each cutting tool wear condition is observed. The top plot in Figure 5.2 shows the evolution of the VB versus the machining length and the bottom plot in Figure 5.2 depicts the VB versus the volume of removed metal. Figure 5.3 shows the same plots as Figure 5.2, however instead of plotting average VB, maximum flank wear is shown. The observed behaviour in Figures 5.2 and 5.3 justifies the selection of the four cutting tool wear conditions during experimentation. The half-new condition represents the ending of the fast evolution of flank wear for the new cutting edge, and the half-worn condition defines the beginning of the fast evolution of the worn cutting tool condition.

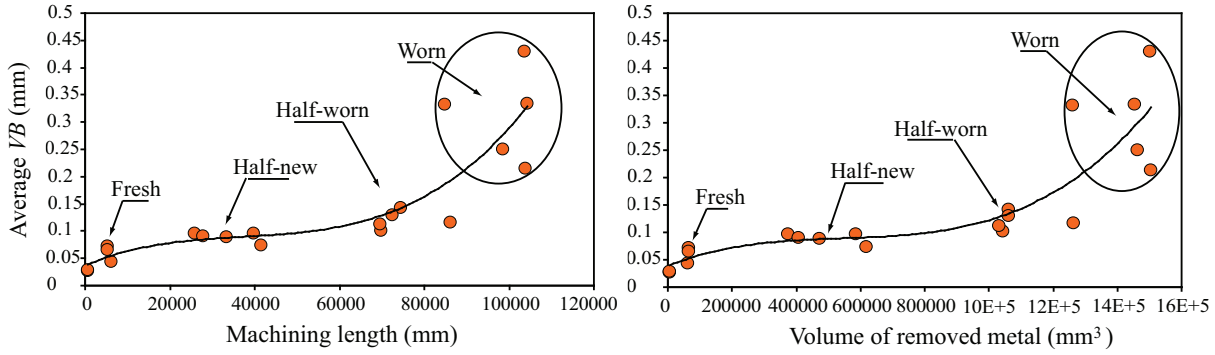

Figure 5.2: Evolution of flank wear on the cutting edges. Right plot shows average flank wear versus the machining length. The left plot shows average flank wear versus the volume of removed metal.

5.5 Hidden Markov Model approach

In this section one type of stochastic signal model, Hidden Markov Model (*HMM*) is described. This approach will be used for modelling the gradual loss of tool material at contact zones with the workpiece. The assessment of flank

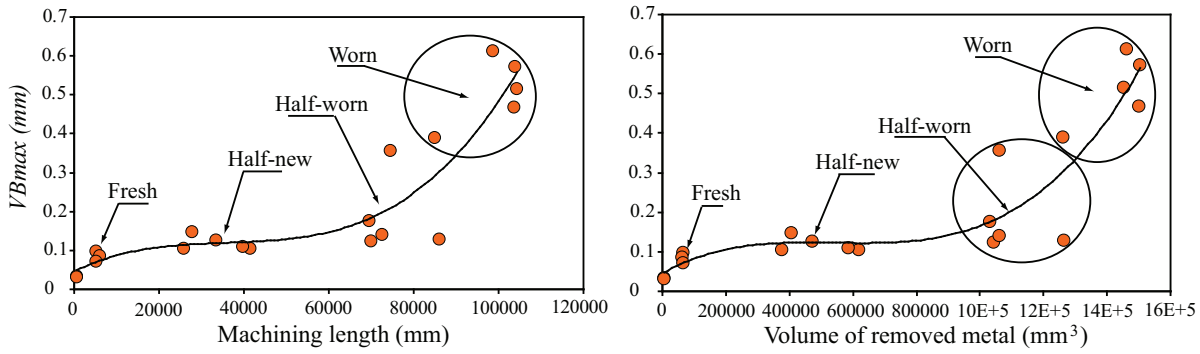

Figure 5.3: Evolution of the maximum value of flank wear on the cutting edges. Right plots shows the maximum VB versus the machining length. Left plot shows the maximum VB versus the volume of removed metal.

wear during the machining process is not an easy task because several factors are involved and there is not a direct method for measuring cutting tool wear. A *HMM* framework is developed in order to identify VB based on the process variable measurements. A complete description of the *HMM* can be found in Appendix H [Rabiner, 1989] and [Mohamed and Garder, 2000]. A *HMM* is characterized by the following parameters:

- N_s is the number of states in the model. The states could be interconnected in such a way that any state can be reached from any other state (Ergodic model). The individual states are $S = S_1, S_2, \cdots, S_N$, and the state at time t as q_t.
- M is the number of distinct observation symbols per state. The individual symbols are $V = v_1, v_2, \cdots, v_M$.
- $A = a_{ij}$ is the state transition probability distribution. Where

$$a_{ij} = P[q_t = S_j | q_{t-1} = S_i], 1 \leq i, j \leq N \tag{5.1}$$

- $B = b_j(k)$ is the observation symbol probability distribution in state j. Where

$$b_j(k) = P[v_k \; at \; t | q_t = S_j], 1 \leq j \leq N, 1 \leq k \leq M \tag{5.2}$$

- $\pi = \pi_i$ is the initial state distribution. Where

$$\pi_i = P[q_1 = S_i], 1 \leq i \leq N \tag{5.3}$$

A *HMM* requires the following parameters: N_s, M, specification of observation symbols, and the three probability measures, A, B, and π. For convenience the compact notation $\lambda = (A, B, \pi)$ is used. These parameters are learned by using the Baum-Welch algorithm.

5.5.1 Baum-Welch Algorithm

The Baum-Welch algorithm is an iterative process that uses the forward and backward probabilities to solve the problem. The goal is to obtain a new model, $\overline{\lambda} = (\overline{A}, \overline{B}, \overline{\pi})$ to maximize the function,

$$Q(\lambda, \overline{\lambda}) = \sum_{Q} \frac{P(O, Q \mid \lambda)}{P(O|\lambda)} log\left[P(O, Q|\overline{\lambda})\right] \tag{5.4}$$

First, a current model is defined as $\lambda = (A, B, \pi)$ and used to estimate a new model as $\overline{\lambda} = (\overline{A}, \overline{B}, \overline{\pi})$. Based on this procedure, if $\overline{\lambda}$ is iteratively used in place of λ and repeats the calculus, then we can improve the probability of O being observed from the model until some limiting point is reached. The result of the recalculation procedure is called a maximum likelihood estimate of the *HMM*. At the end, the new set of parameters (means, variance, and transitions) is obtained for each *HMM*. With the computed parameters for the *HMM* models, next step implies the pattern recognition by using the observation sequences from sensors. A decoded algorithm is required to compute the best state sequence that allows the identification of the cutting tool wear condition.

5.5.2 Viterbi Algorithm

In pattern recognition applications it is useful to associate an optimal sequence of states with a sequence of observations, given the parameters of the model. A reasonable optimal criterion consists of choosing the state sequence (or path) that brings a maximum likelihood with respect to a given model. This sequence can be determined recursively via the *Viterbi* algorithm. This algorithm allows to find the single best state sequence, $Q = \{q_1\ q_2\ \cdots\ q_T\}$ for the given observation sequence $O = \{O_1\ O_2\ \cdots\ O_T\}$, and it makes use of two variables:

1. The highest likelihood $\delta_t(i)$ along a single path among all the paths ending in state i at time t:

$$\delta_t(i) = \max_{q_1, q_2, \cdots, q_{t-1}} P[q_1\ q_2\ \cdots q_t = i, O_1\ O_2 \cdots O_t|\lambda]$$

2. A variable $\psi_t(i)$ that allows keeping track of the best path ending in state j at time t.

Using these two variables, the algorithm implies the following steps:

1. Initialization

$$\delta_1(i) = \pi_i b_i(O_1)\ \ 1 \leq i \leq N$$

$$\psi_i = 0$$

2. Recursion

$$\delta_t(j) = \max_{1 \leq i \leq N} [\delta_{t-1}(i) a_{ij}] b_j(O_t),\ 2 \leq t \leq T,\ \ 1 \leq j \leq N$$

$$\psi_t(j) = arg \max_{1 \leq i \leq N} [\delta_{t-1}(i) a_{ij}],\ 2 \leq t \leq T,\ \ 1 \leq j \leq N$$

3. Termination

$$P^* = \max_{1 \leq i \leq N} [\delta_T(i)]$$

$$q_T^* = arg \max_{1 \leq i \leq N} [\delta_T(i)]$$

4. Path (state sequence) backtracking

$$q_t^* = \psi_{t+1}(q_{t+1}^*), \ \ t = T-1, T-2, \cdots, 1$$

The *Viterbi* algorithm delivers the best states path, which corresponds to the observations sequence. This algorithm also computes a likelihood along the best path.

5.6 Monitoring and diagnosis of cutting tool wear condition

This section presents the obtained results with the Hidden Markov Models for monitoring and diagnosis of cutting tool wear condition during peripheral end milling process in *HSM*. Additionally, the Artificial Neural Network approach was used to monitor and diagnose cutting tool wear condition. However, the results with *HMM* were better than those obtained with the *ANN* approach shown in Appendix H. In agreement with the experiments, a database was built with 441 experiments: 110 experiments with a new cutting tool, 112 with a half-new cutting tool, 110 with a half-worn cutting tool, and 109 with a worn cutting tool. A Monte Carlo simulation for the training/testing steps was implemented owing to stochasticity of the approach. The results correspond to an average of 10 runs. Different training data sets (Tr) and testing data sets (Ts) were generated in agreement with Figure 5.4.

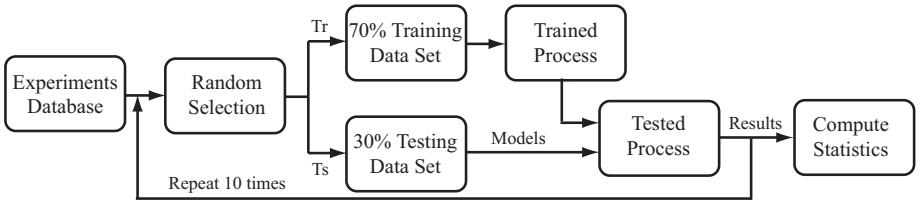

Figure 5.4: Procedure for computing the approach performance. A random simulation for splitting the experimental data set in training/testing sets was implemented owing to the stochastic nature of the process.

5.6.1 Classification of the cutting tool wear condition by using *HMM*

The implemented flow diagram for monitoring and diagnosis of the cutting tool wear condition in *In-process* operating mode is shown in Figure 5.5. First, the signals are processed and split into two branches training and testing. Second, the training branch produces the *HMM* parameters by using the Baum-Welch algorithm. Third, the testing

branch uses the preprocessed signals and the *HMMs* to compute the $P(O/\lambda)$ using the Viterbi algorithm for each model. The model with higher probability is selected as the result.

Four continuous *HMM* (first order) were defined in agreement with different cutting tool wear conditions. Computed parameters for each *HMM* were the initial state distribution, the transition model, and the observation model. Hence, each *HMM* can be written as $HMM(\pi, A, B)$. The transition model is usually characterized by a conditional multinomial distribution $A\{a_{ij}\}$. The computed transition matrices with the Baum-Welch algorithm, considering four states, is as follows:

- For the new cutting tool condition

$$\mathbf{A}(\mathbf{4},\mathbf{4}) = \begin{pmatrix} 0.0459 & 0.4135 & 0.2788 & 0.2617 \\ 0.0061 & 0.9939 & 0.0 & 0.0 \\ 0.0118 & 0.9939 & 0.0 & 0.0 \\ 0.0056 & 0.0 & 0.0 & 0.9944 \end{pmatrix} \tag{5.5}$$

- For the half-new cutting tool condition

$$\mathbf{A}(\mathbf{4},\mathbf{4}) = \begin{pmatrix} 0.8553 & 0.0854 & 0.0403 & 0.019 \\ 0.0 & 1.0 & 0.0 & 0.0 \\ 0.0 & 0.0 & 0.9967 & 0.0033 \\ 0.0177 & 0.0 & 0.0089 & 0.9933 \end{pmatrix} \tag{5.6}$$

- For the half-worn cutting tool condition

$$\mathbf{A}(\mathbf{4},\mathbf{4}) = \begin{pmatrix} 0.0001 & 0.282 & 0.4795 & 0.2384 \\ 0.0 & 1.0 & 0.0 & 0.0 \\ 0.0 & 0.0 & 0.9978 & 0.0022 \\ 0.0 & 0.0 & 0.0066 & 0.9934 \end{pmatrix} \tag{5.7}$$

- For the worn cutting tool condition

$$\mathbf{A}(\mathbf{4},\mathbf{4}) = \begin{pmatrix} 0.8584 & 0.0554 & 0.0535 & 0.0327 \\ 0.0 & 0.9826 & 0.0174 & 0.0 \\ 0.0 & 0.0176 & 0.9824 & 0.0 \\ 0.0 & 0.0 & 0.0 & 1.0 \end{pmatrix} \tag{5.8}$$

The observation distributions were selected to be continuous, and they were specified using a parametric model family. It is common to represent $P(O_t|q_t)$ as a Gaussian for observation vectors

$$P(O_t = o|q_t = S_i) = \aleph(o; \mu_i, \Sigma_i) \tag{5.9}$$

where $\aleph(o; \mu_i, \Sigma_i)$ is the Gaussian density with mean μ and covariance Σ. Also, it is common to use weighted mixture of Gaussian functions

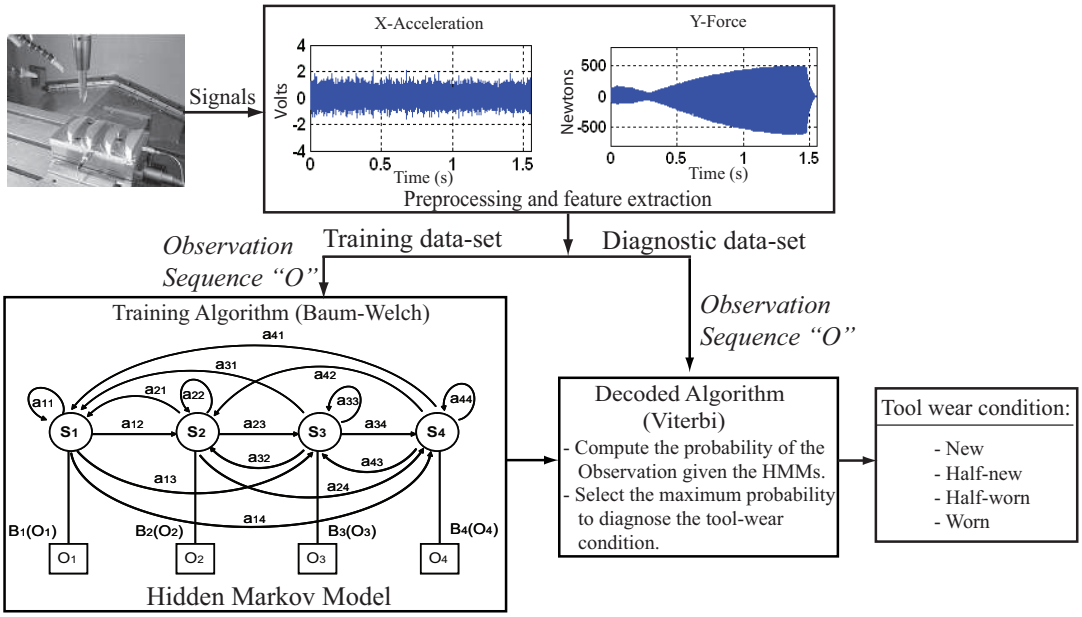

Figure 5.5: Flow diagram for monitoring and diagnosis of the cutting tool wear condition with continuous *HMM*. The features from signals are separated into 2 branches. The training branch leads to *HMM* and the diagnosis branch uses new observations and *HMMs* to recognize cutting tool condition.

$$b_j(o) = \sum_{k=1}^{M} c_{jk} \aleph(o, \mu_{jk}, \Sigma_{jk}) = \sum_{k=1}^{M} c_{jk} b_{jk}(o, \mu_{jk}, \Sigma_{jk}) \tag{5.10}$$

where c_{jk} is the weight of the Gaussian k. It allows for a better representation of the behaviour of the process signals. Therefore, the model can be described in terms of μ_{jk}, Σ_{jk}, and c_{jk}, and the observation model is defined as

$$b_{jk}(o_t, \mu_{jk}, \Sigma_{jk}) = \frac{1}{\prod_{i=1}^{d} \sqrt{2\pi\Sigma_{jki}}} e^{-\frac{1}{2}\sum_{i=1}^{d}(\frac{o_{ti}-\mu_{jki}}{\Sigma_{jki}})^2} \tag{5.11}$$

The *HMM* framework was evaluated for different states and Gaussians in order to find the optimum performance results. Three different configurations were defined for the *HMM*, in agreement with Section 5.5. The configuration with acceptable performance was selected to be used in the monitoring and diagnosis system. The proposal configurations were the following: 1) Three states, 2 Gaussians, and 7 *MFCC* of $AE-$Spindle; 2) Four states, 2 Gaussians, and 7 *MFCC* of $AE-$spindle, and 3) Four States, 4 Gaussians, and 7 *MFCC* of $AE-$spindle.

First, the maximum likelihood estimation implies an iterative process to compute the set of parameters which define each *HMM*. It was made by using the Baum-Welch algorithm. Figure 5.6 shows the iterative process for three

different configurations of *HMM*. It is observed that the number of iterations increases if the number of states (Q) and Gaussians (M) also increase. However, the three configurations can be used for monitoring and diagnosis of the cutting tool wear condition. The selected configuration must be chosen by considering the following: (a) The selected number of Q and M must allow an acceptable performance in the pattern recognition; (b) High values of Q and M must be avoided because it implies the consumption of enough processing time during the classification process with the Viterbi algorithm.

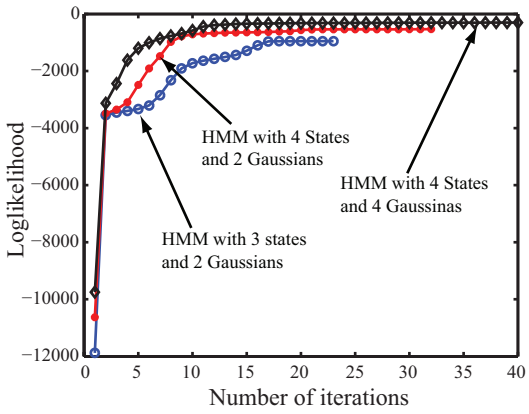

Figure 5.6: Number of iterations required to compute the *HMM* parameters as a function of the number of states and Gaussians.

Figure 5.7 shows how the average performance increases if the number of states and Gaussians are also increasing in the *HMM* approach. Figures 5.6, and 5.7 show that the *HMM* with four states and two Gaussians present an excellent performance, and they were selected for the monitoring and diagnosis system of cutting tool wear condition.

5.6.2 Performance of the *HMM* approach

With configuration defined for the *HMM*, the next step will be to select the process signal that allows a high performance in the classification of cutting tool wear condition. First, the *HMMs* were built and evaluated for each of eight process state signals and the *MFCC* were computed with the following configuration: Rectangular window in time domain, triangular shape bandpass filter with 20 filters, the 0'th order cepstral coefficient, and six cepstrum coefficients. Figure 5.8 shows the performance of the *HMMs* for each one of the process signals. In this test the acoustic emission (*AE*) signal was the best process state variable, which allowed a high performance of the *HMM* approach. For the *AE*-Spindle signal the average performance was 98.72% for training data set and 95.83% for testing data set. Second, the *HMM* performance was computed with the process described in Section 5.6 owing to the stochasticity of the approach.

The *HMM* performance with the testing data set and different configurations was evaluated. The observations

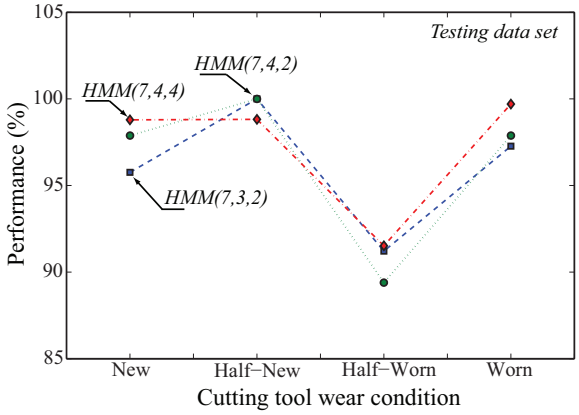

Figure 5.7: Evaluation of the *HMM* performance with the testing data set and different configurations. The observations were computed with the *MFCC* from the acoustic emission signals in the *CNC's* spindle. The figure shows the results for each cutting tool wear conditions and similar performance is observed for different configurations. The total average performance was 96.06% for $HMM(7,3,2)$, 96.29% for $HMM(7,4,2)$, and 97.21% for $HMM(7,4,4)$.

were computed with the *MFCC* from the acoustic emission signals in the *CNC's* spindle. The figure shows the results for each cutting tool wear condition, and similar performance is observed similar for different configurations. The tests were defined to evaluate the success of the *HMMs* with the following signals: Acoustic Emission in the spindle

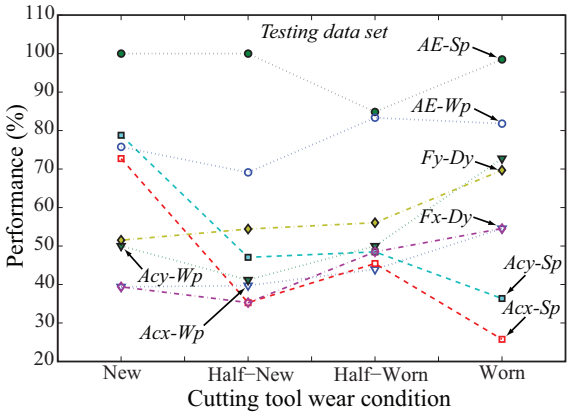

Figure 5.8: Evaluation of the *HMM* performance using different process state variables: vibrations, forces, and acoustic emission signals. The results are shown for each cutting tool wear condition and a specific signal. It is observed that acoustic emission signals represent the best option for monitoring the cutting tool wear condition.

($AE - Sp$), cutting force in $Yaxis$ of the dynamometric platform ($Fy - Dy$), and acceleration in $Yaxis$ in the workpiece ($Acy - Wp$). Figure 5.9 shows the box and whisker plot for comparison of the obtained success of the *HMMs* with training data set. The boxes have lines at lower quartile, median, and upper quartile values. The whiskers are lines extending from each end of a box to show the extent of the rest of the data. The boxes are notched to represent a robust estimate of the uncertainty about the medians for box-to-box comparison. It is observed that the $AE - Sp$ signal presents the highest performance for all cutting tool wear conditions. Also, figure 5.9 shows the box and whisker plot for comparison of the obtained success of the *HMMs* with testing data set. Once again, the best results were computed with the AE-Sp signal. For the AE-p signal the average performance was 98.15% for training data set and 96.29% for testing data set. Third, the *HMMs* were built and evaluated with only the AE-Sp, Fy-Dy, and Acy-Wp process signals, and the *MFCC* were computed with different configurations: hamming window in time domain, triangular shaped bandpass filter with 40 filters, Log energy coefficient, and six *MFCC*. Figure 5.10a shows the performance of *HMMs* for the training data set. This figure shows the box and whisker plot for comparison of the obtained success of the *HMMs* with training data set. Figure 5.10b shows the box and whisker plot for the testing data set. Once again the best results were computed for the $AE - Sp$ process signal. Average performance was 98.78% for training data set and 98.18% for testing data set. Results with the new *MFCC* configuration are better than those computed with the first configuration of the *MFCC*. The performance increases 0.64% for training data set and 1.96% for testing data set specifically for the *AE*-Spindle signal.

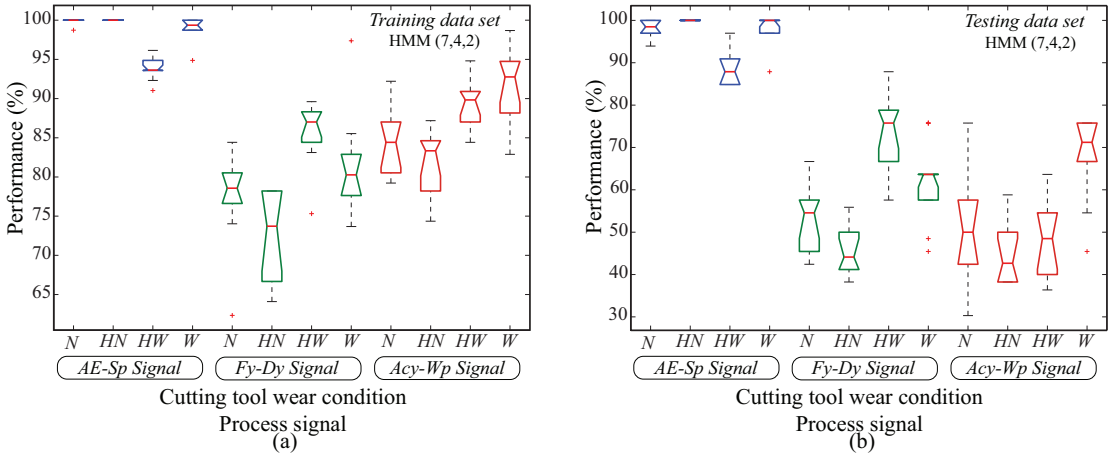

Figure 5.9: Performance of the *HMMs* with 10 runs and different process signals. These results correspond with (a) the training data set, and (b) testing data set and all cutting tool wear conditions (N = new, HN = Half-New, HW = Half-Worn, and W = Worn).

Finally, a classical test in a diagnosis system is to identify two alarms owing to a false classification of the cutting tool condition. These alarms are False Alarm Rate (*FAR*) and False Fault Rate (*FFR*). *FAR* condition represents a damage tool, but it is not true. *FFR* condition corresponds to a good state of the tool, but it is really damaged.

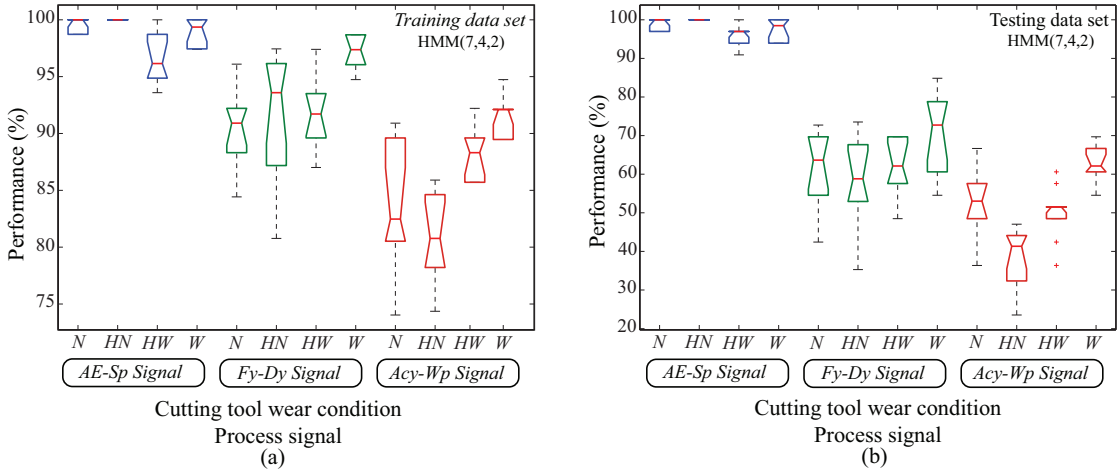

Figure 5.10: Performance of the *HMM* with the *MFCC* computed with Hamming window, 40 filters, and Log energy coefficient. The results correspond with (a) the training data set, and (b) the testing data set for all cutting tool wear conditions (N = new, HN = Half-New, HW = Half-Worn, and W = Worn).

The *FAR* condition is not a problem in diagnosis, but it reduces productivity. However, the *FFR* condition might represent a critical problem when the rate is high because the tool can break before it is replaced. Therefore, it is recommended to have a low rate of *FFR* condition. Figure 5.11 shows the misclassification percentage owing to the *FFR* condition. The classifier with the lowest percentage of *FFR* was with the *AE* sensors. The *AE*-Spindle shows the lowest percentage of *FFR* condition (only 1.52% for the worn condition).

5.7 Analysis of the results and contributions

New ideas based in the Hidden Markov Models (*HMM*) and the Mel Frequency Cepstrum Coefficients (*MFCC*), usually applied in speaker identification systems, were developed for monitoring and diagnosis of the cutting tool wear condition for peripheral milling process in a *HSM* with excellent results. The system was implemented for recognizing four cutting tool wear conditions: new, half-new, half-worn, and worn condition. The monitoring and diagnosis system was designed and implemented to recognize the cutting tool wear condition on-line, using only process state variables recorded during the machining process. Best results were obtained with signals coming from AE-Spindle, with an average performance of 98.15% for training data set and 96.29% for testing data set. The *MFCC* were computed by considering two configurations in the preprocessing stage. Basically, the number of filters changed from 20 to 40, and they allowed for the capture of more information about the characterization of cutting tool wear condition. With a bank of 40 filters, the performance of the *HMM*, increases to 98.18% for testing data set.

The main contributions in the Tool Condition Monitoring (*TCM*) are the following:

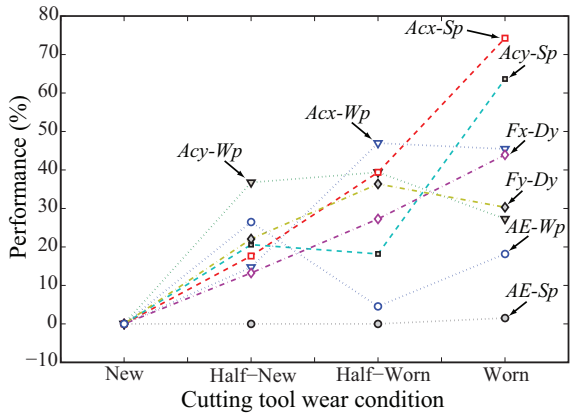

Figure 5.11: Evaluation of the misclassification percentage in *FFR* conditions. For specific signals, the *FFR* condition was computed. The lowest percentage of the *FFR* condition was obtained for the *HMM* using the *AE* signal.

1. The *HMMs* can be used to recognize the worn condition of five different cutting tool diameters in *HSM* with five different hardnesses in the workpiece materials.

2. The characterization of *AE* signals with the *MFCC* allowed for a high performance of the *HMM* with only one process signal. The *MFCC*, have not been used in previous research to recognize cutting tool wear condition.

3. The (*TCM*) system with the *HMM* approach and *MFCC* features can be utilized in the aeronautic and automotive industry to maximize tool life and decrease operation cost.

Chapter 6

Intelligent monitoring and process planning system

6.1 Introduction

Competitive business demands production systems based on intelligent machines because the aerospace and automotive industry must be able to manufacture accurate components and get it right the first time [Nacsa, 2001]. In [Balic, 2006] the main features of an intelligent *CNC* machine are defined by: prediction of operations, reduction of set up time, detection of cutting tool condition, acquisition of knowledge, and inference from incomplete information.

This chapter presents the design and implementation of an Intelligent Monitoring and Process Planning System (*IMPPS*) in *HSM*, which represents the main contribution of the Intelligent Monitoring and Supervisory Control System. Figure 3.1 in Chapter 3 depicts the implemented supervisory control system. The system predicts the R_a and suggests optimal cutting conditions before running the *CNC* machining center (*Pre-process*). Then, during the machining process (*In-process*), the system adapts needed changes in cutting parameters and maintains the R_a quality. The quality is considered an objective function. Furthermore, the planning system recommends an optimal policy for minimum operation cost. Robust models based on statistical methods and Artificial Intelligence (*AI*) techniques were computed to predict the surface roughness *Pre* and *In-process* operating mode (see Chapter 4). Also, a pattern recognition system based on the *HMM* approach was implemented to monitor and diagnose the cutting tool wear condition as described in Chapter 4. Furthermore, the decision-making block for computing the optimal actions for the operator is described.

6.2 Intelligent monitoring and process planning system

[Monostori, 2000] classifies the possible intelligent parts of a *CNC* in cutting tool monitoring, operation/machine tool modelling, and adaptive control. The *IMPPS* considers these intelligent parts, and their main tasks are the following:

1. In *Pre-Process* operating mode, the module estimates Ra^p with the statistical model and some factors defined by the operator. The optimal cutting parameters are computed with a Genetic Algorithm (*GA*), which guarantees a minimum R_a value.

2. For the *In-Process* condition, the module is based on the knowledge of cutting tool wear condition (VB), and process state variables. Ra^p is estimated by using an *ANN* model.

3. Simultaneously, the module predicts the optimal policy that minimizes production cost. Based on this policy, this module guides the operator. The policy is constrained at different aluminium alloys, cutting tool diameters, and cutting tool wear condition.

Figure 6.1 depicts the flow diagram implemented for steps 1, 2, and 3, where the cutting parameters are estimated in agreement with the requirements of the operator and the cutting tool wear condition.

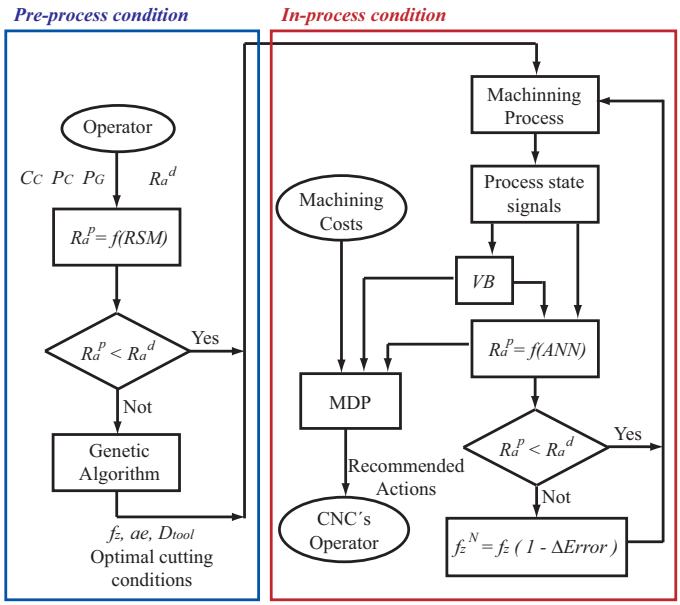

Figure 6.1: Flow diagram of the *IMPPS*. This diagram shows the procedure to compute the optimal cutting conditions in *Pre-process* and *In-process* operating modes. Also, the *MDP* is included in the flow diagram.

6.2.1 Optimization process in *Pre-process* operating mode

The optimization process is mainly applied in *Pre-process* operating mode for computing the optimal cutting parameters. It is based on the statistical model for R_a and the Genetic Algorithm *GA*. The *GA* is probably the most general approach of evolutionary computation methods. It is a population-based search optimization technique and has been used as a powerful tool for optimizing cutting parameters in end milling process ([Suresh *et al.*, 2002], [Brezocnik *et al.*, 2004], and [Palanisamy *et al.*, 2007]).

The data processed by *GA* includes a set of strings (or chromosomes) with an infinite length in which each bit is called a gene. A selected number of strings is called a population and the population at a given time is a generation. The generation of the initial population of strings is done randomly. A binary encoding scheme is used to represent the chromosomes with zeros or ones. The fitness value (objective function) of each member is computed. The population is then operated by reproduction, crossover, and mutation to create a new population. One iteration of these operators is known as a generation in the *GA*. The implementation of *GA* implies the following steps:

1. *Coding*. In order to use the *GA* to solve a problem, the variables f_z, D_{Tool}, and ae are coded in string structures. Binary-coded strings having zeros and ones are used. The length of the string is determined by the desired solution accuracy. In the calculation, 8 bits are recommended for the strings, with excellent accuracy for the selected variables.

2. *Fitness function*. *GAs* mimic the *survival of the fittest* principle. A fitness function $F(x)$ is derived from the objective function and is used in successive genetic operations. The independent variables for optimal cutting parameters are: f_z, D_{Tool}, and ae. The R_a is the response, and it allows for minimization of the fitness function represented by the *RSM* model.

3. Apply the basic operation of *GA*:

   - Reproduction. In this process individual strings are copied into a separate string, called the *mating pool*, according to their fitness values, i.e., strings with a higher value have a higher probability of contributing to the next generation.
   - Crossover. After reproduction, the population is enriched with good strings from the previous generation but does not have any new string. A crossover operator is applied to the population to hopefully create better strings. The total number of participatory strings in crossover is defined by crossover probability, which is the ratio of total strings selected for mating and population size.
   - Mutation. It represents the occasional random alteration of the value of a string position. This means changing 0 to 1 or vice versa on a bit by bit basis and with a small mutation probability. The need for mutation is to keep diversity in the population.

   After applying the *GA* operators, a new set of population is decoded and objective function values are calculated. It represents one generation of *GA*. Such iterations are continued until termination criterion is achieved.

The *GA* was simulated with a computer program in *MatLab* and configured with the following parameters: 100 generations, population of 20, 0.8 crossover probability, and 0.2 mutation probability. The applied constraints at independent variables were $0.025 \leq f_z \leq 0.13$, $1 \leq ae \leq 5$, and $8 \leq D_{tool} \leq 20$.

6.2.2 Optimization process in the *In-process* operating mode

In the *In-process* operating mode the optimization process computes only an absolute percent error between the estimated R_a^p and the desired R_a^d

$$\Delta Error = \frac{(R_a^p - R_a^d)}{R_a^d} \tag{6.1}$$

with this deviation, a new value of f_z^N is computed with the equation

$$f_z^N = f_z * (1 - \Delta Error) \tag{6.2}$$

Finally, the R_a is computed with the new f_z value and the *ANN* model. During the *In-process* operating mode, it is not recommended to change the values of the D_{tool}, HB, ae, and $Curv$ parameters because they directly affect the design of the machined part. For this reason, the f_z parameter is the only one that can be modified. Also, Chapter 4 was demonstrated that by decreasing the f_z, the R_a decreases for all cutting tool wear conditions. Additionally, Chapter 4 defined the limits of f_z value. With these considerations, the f_z is a parameter that can be controlled *on-line* and allows the minimization of the R_a.

6.3 Markov Decision Process

The Markov Decision Process (*MDP*) provides a framework for sequential decision-making in a stochastic environment. The goal of the decision maker is to choose a sequence of actions to optimize a predetermined criterion. Markov chains provide a useful tool for determining expected profits or cost associated with certain types of systems. The key characteristic of a Markov model is a probability law in which future behaviour of the system is independent of past behaviour, given the present condition of the system. Therefore, the *MDP* is a controlled stochastic process satisfying the Markov property with cost assigned to state transitions. A solution of the *MDP* is a policy that mapping states to actions, and that determines the state transitions to minimize the cost according to the performance criterion. A formal description of the *MDP* is as follows:

- S is a finite set of states of the machining process.
- A is a finite set of actions that the operator can do.
- $P : S \times A$ is the state transition probability distribution function. For each action and state of the machining process, there is a probability distribution over the states of cutting process that can be reached after the actions. The function $P(s \mid s', a)$ is defined as the probability of reaching state s starting in state s' and given action a.

- f is the instantaneous cost function, and it is defined for each action.
- $R : S \times A$ is a reward function. For each action in each state of the world, it assigns a real number. The function is defined as the reward of executing action a in the state s.
- β is an action function, and it defines a vector that maps the state space into the action space, that is, an action function assigns an action to each state.
- A stationary policy (π) is a policy that can be defined by an action function. The stationary policy is define by the function β takeing action $a(i)$ at time n, if $S_n = i$, independent of previous state, and previous action and time n. The set of all (decisions) policies is denoted by ϑ.
- Non-stationary policy is a sequence of situation-action mappings indexed by time, i.e., the optimal sequence of action may change when time advances.

The *Expected Discount Cumulative Cost* will be used to compute the optimal minimum cost. This option is equivalent to using a present worth calculation for the basis of decision making. Let α be a discount factor such that one dollar, for example, obtained at time $n = 1$ has a present value of α at time $n = 0$. If r is a rate of return (interest rate), then α can be computed by $\alpha = 1/(1 + r)$. Let $\chi = x_n; n = 0, 1, 2...$, be a Markov Chain with Markov Matrix P. Let f be cost function and let α be a discount factor. In [Feldman and Valdez-Flores, 2004] and [Rajabi-Ghahnavie and Fotuhi-Firuzabad, 2006], the authors describe an algorithm to compute the optimal cost function and the optimal policy that minimize the cost function. The expected total discounted cost is given by

$$E\left[\sum_{n=0}^{\infty} \alpha^n f(x_n) \mid x_0 = i\right] = \left[(I - \alpha P)^{-1} f\right](i) \tag{6.3}$$

Therefore, the total expected discounted cost under the probability law specified by the policy (π), is given by

$$\nu_{\pi}^{\alpha} = \left[(I - \alpha P_{\pi})^{-1} f_{\pi}\right](i) \tag{6.4}$$

Thus, the discount cost optimization problem can be stated as follows: Find $\pi^{\alpha} \in \vartheta$ such that $\nu_{\pi^{\alpha}}^{\alpha}(i) = \nu^{\alpha}(i)$ where the vector $\mathbf{v}_{\alpha}$ is defined by

$$\nu^{\alpha}(i) = \min_{\pi \epsilon \vartheta} \nu_{\pi}^{\alpha}(i) \tag{6.5}$$

The optimum discounted cost value and the optimal policy are computed with the following procedure:

- The expected discounted cumulative cost with respect to a state **i** for a particular policy π and fixed discount factor α is defined by (for all $i \in S$)

$$\nu_{\pi}^{\alpha}(i) = f_i^{\pi(i)} + \alpha \sum_{j \epsilon S} P_{ij}^{\pi(i)} \nu_{\pi}\left(\Sigma_{\alpha} \mid j\right) \tag{6.6}$$

- The optimal total cost function is defined as

$$\nu^*\big(\Sigma_\alpha \mid i\big) = \min_{\pi} \nu_\pi\big(\Sigma_\alpha \mid j\big) \tag{6.7}$$

- The last equation satisfies the following optimal equations (for all $i \in S$)

$$\nu^*(i) = \min_{k \epsilon A} \Big[f_i^k + \alpha \sum_{j \epsilon S} P_{ij}^k \nu^*\big(\Sigma_\alpha \mid j\big) \Big] \tag{6.8}$$

- The optimal policy can be found from the total cost function as follows (for all $i \in S$)

$$\pi^*(i) = arg \min_{k \epsilon A} \Big[f_i^k + \alpha \sum_{j \epsilon S} P_{ij}^k \nu^*\big(\Sigma_\alpha \mid j\big) \Big] \tag{6.9}$$

There are different algorithms to solve the *MDP* and analyze their running times. These algorithms are: Linear programming, policy iteration, and value iteration. Only the last two algorithms will be presented in this section and their results will be compared to decide which algorithm requires less iteration to solve the *MDP*.

6.3.1 Police iteration

The police iteration alternates between a value determination phase, in which the current policy is evaluated, and a policy improvement phase, in which an attempt is made to improve the current policy. The algorithm applies the following steps:

1. Let π' be a deterministic stationary policy.
2. Create a loop with the following operations:
   (a) Set π to be π'.
   (b) Determine for all $i \in S$, $\nu(\Sigma_\alpha|i)$ by solving the set of N (number of states) equations in N unknowns described by Equation 6.6.
   (c) For each $i \in S$ if there exist some $k \in A$ such that

$$\left[f_i^k + \alpha \sum_{j \in S} P_{ij}^k \nu(\Sigma_\alpha|j) \right] < \nu(\Sigma_\alpha|i) \tag{6.10}$$

   then set $\pi'(i)$ to be k otherwise set $\pi'(i)$ to be $\pi(i)$.
   (d) Repeat loop if $\pi \neq \pi'$.
3. Return π.

Step $2b$ is the value determination phase and step $2c$ is the policy improvement phase.

6.3.2 Value iteration

Value iteration algorithm works by computing the optimal total-cost function assuming first a non-stage finite horizon, then a two-stage finite horizon, and so on. The computed total cost functions are guaranteed to perform at optimal minimum cost. In addition, the policy associated with successive total cost functions will perform optimally with a finite number of iterations. This algorithm is described as follows:

1. For each $i \in S$, initialize $\nu^o(\Sigma_\alpha|i)$.
2. Set n to be 1.
3. While $n <$ maximum number of iterations.
   (a) For each $i \in S$ and $k \in A$, let
   $$\nu^n(\Sigma_\alpha|i,k) = \left[f_i^k + \alpha \sum_{j \in S} P_{ij}^k \nu^{n-1}(\Sigma_\alpha|j) \right] \tag{6.11}$$
   $$\nu^n(\Sigma_\alpha|i) = \min_{k \in A} \nu^n(\Sigma_\alpha|i,k) \tag{6.12}$$
   (b) Set n to $n+1$.
4. For each $i \in S$,
   $$\pi(i) = \arg\min_{k \in A} \nu^n(\Sigma_\alpha|i,k) \tag{6.13}$$
5. Return π.

The maximum number of iterations is either set in advance or determined automatically using an appropriate stopping rule. The *Bellman residual* at step n is defined to be

$$\max_{i \in S} \mid \nu^n(\Sigma_\alpha|i) - \nu^{n-1}(\Sigma_\alpha|i) \mid \tag{6.14}$$

By examining the Bellman residual during value iteration and stopping, when it gets below some threshold $\epsilon' = \epsilon(1-\alpha)/(2\alpha)$, it is guaranteed that the resulting policy will be $\epsilon-$optimal. The optimal total cost function and the optimal policy were computed using the *MDP* Toolbox $V2.0$ for MatLab. The toolbox includes both algorithms.

6.4 Implementation of the *IMPPS*

Figure 6.2 depicts the flow diagram of the *IMPPS*. The flow diagram defines the two conditions: *Pre-process* and *In-process*. First, the operator defines C_C, P_C, and P_G for machining the workpiece, and R_a^d is defined. The cutting tool condition is considered as a new tool. Second, the module computes the R_a^p with the statistical module. If $R_a^p \geq R_a^d$, the *GA* is executed to compute new values of f_z, ae or D_{tool} to minimize the R_a value. Third, during the machining the process state variables are recorded, and the cutting tool monitoring module is executed to recognize

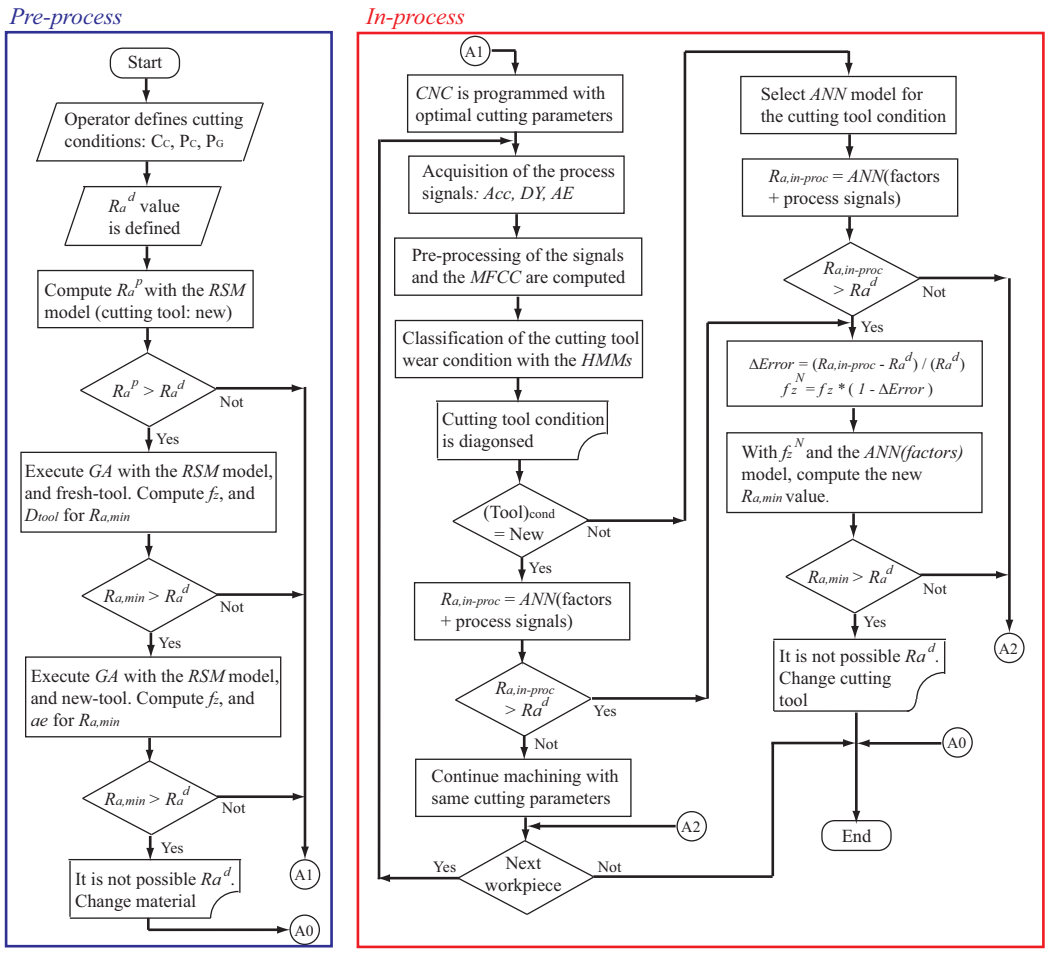

Figure 6.2: Flow diagram for the intelligent monitoring, diagnostic of cutting tool condition and evaluation of the optimal cutting parameters. In *Pre-process* operating mode the steps for computing the optimum cutting parameters are defined. The *In-process* operating mode defines the steps for recognizing the cutting tool condition, computing the R_a, and controlling the f_z value to maintain the desired R_a.

the cutting tool wear condition. Fourth, in *In-process* condition, the *AI* models are used to compute the new value of the R_a^p by considering the cutting tool wear condition. Once again, if $R_a^p \geq R_a^d$ an error is computed, the f_z value must be changed. With the *ANN* model, the R_a value is obtained with the new f_z. The module makes recommendations to continue with the same or new optimal cutting parameters for the next workpiece.

6.5 Results

Several experiments were used to validate the *IMPPS*. First, the experiments include all the replicates obtained during the full life of the cutting tool. Second, new experiments were implemented to validate different modules.

6.5.1 Validation with original experiments

Exploiting the data set used for modeling the R_a, the complete system was tested. The cutting conditions corresponded with experiment number 3, and the four replicates (R_1, R_2, R_3, R_4) were used. For this experiment, the cutting conditions and the geometric parameters are the following: $f_z = 0.05$, $ae = 2$, $D_{tool} = 16$, $HB = 90, 91, 93$, $Curv = -0.025$, and 6082 aluminium alloy. The experiments are classified according to cutting tool wear condition: $E2$ for new, $E3$ for half-new, $E4$ for half-worn, and $E5$ for worn condition. Table 6.1 shows the selected experiments and the results computed with intelligent monitoring and the process planning module. Results can be summarized as follows:

- The cutting tool monitoring module recognized the cutting tool wear condition with a performance of 100%.
- Even though the cutting conditions are the same for all experiments, the measured R_a changes owing to flank wear and other factors (vibration, chatter, run-out, etc). This behaviour is reproduced with excellent results only if process state variables are included in the *ANN* models.
- The mean absolute percent error of each R_a model with respect to the estimated R_a is 11.81% for the ***RSM*** model, 17.48% for the the *ANN* with only factors, 11.25% for the *ANN* with factors and Acc_x, and 8.59 for the *ANN* with factors and F_y. The best assessment of R_a was observed with the last *ANN* model, therefore, it will be used to compute the estimated R_a *In-process* condition.

6.5.2 Validation tests with new experiments

New experiments with different cutting conditions were defined in order to evaluate the system performance. Table 6.2 presents the new cutting conditions, and the test pieces are shown in Figure 6.3. The test pieces were designed to consider three geometries for machining. Furthermore, the cutting conditions were defined to include central points, limit points, and external points in agreement with the domain defined in the *DoE*. Table 6.3 shows the computed results with the *IMPPS*.

Results are plotted in Figure 6.4, and they can be summarized as follows:

- The success of the cutting tool monitoring module was 88% for recognizing the cutting tool condition. Only three experiments were badly classified. These are experiment numbers 16, 19, and 23.
- The mean absolute percent error of each R_a model with respect to the measured R_a is 59.82% for the ***RSM*** model, 42.22% for the *ANN* with only factors (CP), and 39.37 for the *ANN* with $CP + F_y$. In Figure 6.4 it is observed that the *ANN*$(CP + F_y)$ model shows an excellent tendency with respect to the measured R_a.

Table 6.1: Experiments selected with the measured and estimated R_a values in *Pre* and *In-process* operating modes, and the results of the monitoring cutting tool wear condition. $CP =$ Cutting parameters.

				In-process R_a *ANN*			Absolute percent error			
Exp.	$R_{a,meas}$ μm	*Pre-process* R_a*RSM* μm	Cutting Tool Condition	Only CP μm	CP $+Acc_x$ μm	CP $+F_y$ μm	*RSM*	Only CP	CP $+Acc_x$	CP $+F_y$
$E2-R_1$	0.127	0.105	New	0.129	0.126	0.112	17.42	1.73	0.80	11.72
$E2-R_2$	0.113	0.105	New	0.129	0.110	0.142	7.09	14.45	2.31	0.92
$E2-R_3$	0.108	0.105	New	0.129	0.113	0.110	2.96	19.54	4.48	2.14
$E2-R_4$	0.122	0.105	New	0.129	0.104	0.112	14.24	5.65	14.69	8.55
$E3-R_1$	0.167	0.215	Half-New	0.155	0.172	0.171	28.41	7.42	3.18	2.49
$E3-R_2$	0.191	0.215	Half-New	0.155	0.079	0.172	12.53	18.87	58.60	9.94
$E3-R_3$	0.179	0.215	Half-New	0.155	0.175	0.146	19.81	13.62	2.46	18.65
$E3-R_4$	0.179	0.215	Half-New	0.155	0.126	0.159	19.74	13.66	29.85	10.79
$E4-R_1$	0.234	0.251	Half-Worn	0.165	0.214	0.241	7.22	29.37	8.63	2.842
$E4-R_2$	0.235	0.251	Half-Worn	0.165	0.188	0.311	6.77	29.67	19.85	32.37
$E4-R_3$	0.241	0.251	Half-Worn	0.165	0.221	0.232	4.11	31.42	8.12	3.54
$E4-R_4$	0.227	0.251	Half-Worn	0.165	0.213	0.213	12.66	25.79	4.40	14.03
$E5-R_1$	0.266	0.245	Worn	0.223	0.285	0.272	7.88	16.12	7.26	2.22
$E5-R_2$	0.272	0.245	Worn	0.223	0.255	0.283	9.91	17.97	6.33	4.24
$E5-R_3$	0.267	0.245	Worn	0.223	0.269	0.284	8.24	16.43	0.82	6.46
$E5-R_4$	0.272	0.245	Worn	0.223	0.249	0.289	9.93	17.97	8.24	6.57

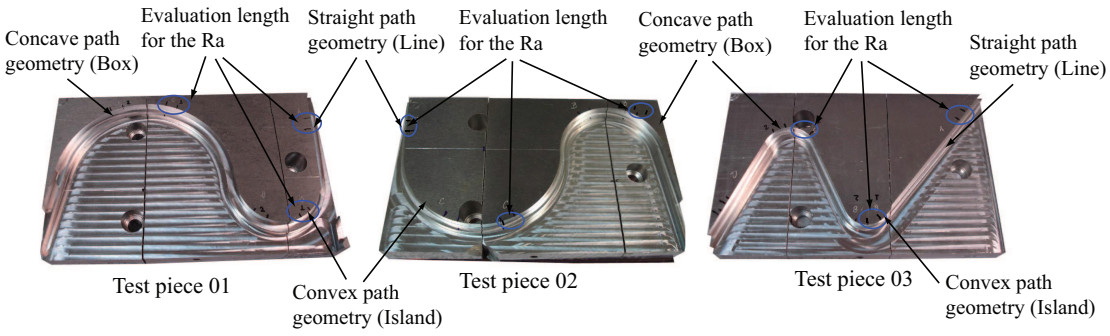

Figure 6.3: Test pieces 01, 02, and 03 with machining geometries, straight, concave and convex paths.

Table 6.2: Test pieces with the cutting conditions, and geometric parameters defined for the new experiments.

Number	Experiments	Cutting tool Condition	f_z	ae	D_{tool}	HB	$Curv$
1, 2, 3	P1-2024-Line,Island,Box	New	0.075	3	12	109	$0, 0.037, -0.019$
4, 5, 6	P3-2024-Line,Island,Box	Half-New	0.075	3	12	110	$0, 0.083, -0.556$
7	P4-2024-Island	New	0.075	3	12	110	0.025
8	P5-2024-Box	New	0.075	3	12	109	-0.025
9	P1-5083-Island	Half-New	0.047	2	8	71	0.077
10, 11	P1-7075-Line,Island	Half-New	0.115	4.5	20	158	$0, 0.039$
12, 13	P1-6082-Island,Box	Half-Worn	0.04	4	12	89	$0.038, -0.0185$
14, 15	P2-6082-Line,Island	Half-Worn	0.04	4	12	94	$0, 0.0385$
16, 17	P2-7075-Box,Line	Worn	0.08	5	16	150	$-0.0286, 0$
18, 19, 20	P3-7075-Box,Island,Line	Half-Worn	0.08	5	16	151	$-0.0286, 0.022, 0$
21	P1-CERTAL-Box	Worn	0.04	4	16	144	-0.0185
22, 23	P9-2024-Box,Island	Worn	0.05	2	20	110	$-0.0313, 0.0208$
24, 25, 26	P3-5083-Line,Island,Box	Half-Worn	0.05	2	16	67	$0, 0.0357, -0.0192$

- The results of experiment numbers 9, 10, 11, 24, 25, and 26 show a higher absolute percent error. It is owing to cutting conditions corresponding to extreme values (limit points) of the machining domain defined in *DoE*. However, it is observed that the *ANN* model can predict the R_a with less error for the same experiments.

6.5.3 Optimization in *Pre-process* operating mode

The optimization process in *Pre-process* operating mode was validated with several tests. In the first test the operator defines cutting conditions, cutting parameters, geometric parameters, and the desired R_a^d value. Table 6.4 presents information and data for the test. The R_a^p is computed and compared with R_a^d. With $R_a^p > R_a^d$ the *GA* computes the new value of f_z to minimize R_a (see Figure 6.5a). With the new f_z value, the R_a is computed, but it continues high. The *GA* computes the new values of f_z and D_{tool} that minimizes R_a, as depicted in Figure 6.5b. The new R_a value continues high, and the *GA* executes another iteration to find new cutting conditions for f_z, and ae, Figure 6.5c. The final values of f_z, D_{tool}, and ae allow minimizing the R_a. Results are shown in Table 6.4. In the second test the operator knows the cutting conditions, cutting parameters, and geometric parameters, which guarantee $R_a^p < R_a^d$ (see Table 6.5). The operator requires the increase of the f_z value from 0.075 to 0.1 and verifies that R_a is less than R_a^d. The result is a high value of R_a and the *GA* computes the new f_z to minimize R_a (see Figure 6.6). The final results show that it is not possible to increase the f_z value (see Table 6.5).

In the third test, the operator defines the cutting conditions, cutting parameters, geometric parameters, and the

Table 6.3: Results of the estimated R_a in *Pre* and *In-process* operating mode for new experiments. $CP =$ Cutting parameters.

Number of Experiment	$R_{a,meas}$ μm	*Pre-process* R_a*RSM* μm	Cutting Tool Condition	*In-process*, R_a*ANN* Only CP μm	*In-process*, R_a*ANN* $CP + F_y$ μm	Absolute percent error *RSM*	Absolute percent error Only CP	Absolute percent error CP $+F_y$
1) P1-2024-Line	0.161	0.155	New	0.147	0.083	4.21	8.71	48.73
2) P1-2024-Island	0.176	0.175	New	0.160	0.154	0.23	8.74	12.39
3) P1-2024-Box	0.144	0.156	New	0.148	0.104	11.35	3.29	27.72
4) P3-2024-Line	0.158	0.184	Half-New	0.190	0.132	16.12	20.37	16.54
5) P3-2024-Island	0.160	0.189	Half-New	0.174	0.125	18.27	8.84	21.80
6) P3-2024-Box	0.145	0.180	Half-New	0.200	0.166	24.21	38.04	14.76
7) P4-2024-Island	0.196	0.162	New	0.156	0.164	16.93	20.00	16.14
8) P5-2024-Box	0.150	0.164	New	0.150	0.026	9.04	0.17	82.87
9) P1-5083-Island	0.238	0.473	Half-New	0.533	0.365	98.49	123.5	53.07
10)P1-7075-Line	0.211	0.362	Half-New	0.331	0.298	71.69	57.04	41.29
11)P1-7075-Island	0.268	0.515	Half-New	0.268	0.186	92.03	0.01	30.77
12)P1-6082-Island	0.196	0.231	Half-Worn	0.323	0.169	17.56	64.43	13.88
13)P1-6082-Box	0.136	0.301	Half-Worn	0.264	0.252	121.4	93.85	85.05
14)P2-6082-Line	0.259	0.238	Half-Worn	0.296	0.239	8.03	14.43	7.64
15)P2-6082-Island	0.322	0.200	Half-Worn	0.322	0.238	37.60	0.19	25.87
16)P2-7075-Box	0.156	0.136	Half-Worn	0.289	0.292	12.57	85.38	87.62
17)P2-7075-Line	0.128	0.187	Worn	0.081	0.266	15.39	49.63	63.92
18)P3-7075-Box	0.136	0.258	Half-Worn	0.289	0.233	102.2	126.3	82.46
19)P3-7075-Island	0.126	0.157	New	0.227	0.219	24.64	80.03	74.17
20)P3-7075-Line	0.110	0.192	Half-Worn	0.287	0.148	76.44	163.4	35.47
21)P1-CERTAL-Box	0.169	0.137	Worn	0.175	0.274	18.60	3.51	62.07
22)P9-2024-Box	0.174	0.197	Worn	0.094	0.217	13.38	45.91	24.51
23)P9-2024-Island	0.250	0.280	Half-Worn	0.167	0.319	12.07	33.20	27.60
24)P3-5082-Line	0.150	0.532	Half-Worn	0.157	0.232	254.7	5.00	55.04
25)P3-5082-Island	0.195	0.619	Half-Worn	0.144	0.217	217.3	26.19	11.33
26)P3-5082-Box	0.138	0.500	Half-Worn	0.163	0.137	260.7	17.53	0.87

required R_a^d value (see Table 6.6).

The R_a^p is computed and compared with R_a^d. Owing to the $R_a^p > R_a^d$, the *GA* computes the new value of f_z to minimize R_a (see Figure 6.7a). With the new f_z value the R_a is computed, but it continues high. The *GA* computes the new values of f_z and D_{tool} that minimizes R_a, as depicted in Figure 6.7b. The new R_a value is less to the R_a^d,

Table 6.4: Optimal cutting conditions to minimize the R_a in *Pre-process* condition (7075 Aluminium alloy).

Cutting conditions defined by Operator	Results of the first running *GA*	Results of the second running *GA*	Final optimal cutting conditions with *GA*
$f_z = 0.115$	$f_z = 0.06814$	$f_z = 0.0425$	$f_z = 0.04078$
$ae = 4.5$	$ae = 4.5$	$ae = 4.5$	$ae = 4.98$
$D_{tool} = 20$	$D_{tool} = 20$	$D_{tool} = 16$	$D_{tool} = 16$
$Curv = 0$	$Curv = 0$	$Curv = 0$	$Curv = 0$
$R_a^d = 0.28$	$R_a^d = 0.28$	$R_a^d = 0.28$	$R_a^d = 0.28$
$HB = 158$	$HB = 158$	$HB = 158$	$HB = 158$
Tool Cond. = Half-New	Tool Cond. = Half-New	Tool Cond. = Half-New	Tool Cond. = Half-New
$R_a^p = 0.3622$	$R_a^p = 0.3174$	$R_a^p = 0.2815$	$R_a^p = 0.2741$

Table 6.5: Evaluation of R_a with new cutting conditions to demonstrate if it is possible to increase f_z value with $R_a^p < R_a^d$. Workpiece material 2024 aluminium alloy.

Initial Cutting Conditions	New Cutting Conditions Defined by the Operator	Results of the First Running *GA*
$f_z = 0.075$	$f_z = 0.1$	$f_z = 0.025$
$ae = 3$	$ae = 3$	$ae = 3$
$D_{tool} = 12$	$D_{tool} = 12$	$D_{tool} = 12$
$Curv = 0.037$	$Curv = 0.037$	$Curv = 0.037$
$R_a^d = 0.2$	$R_a^d = 0.2$	$R_a^d = 0.2$
$HB = 109$	$HB = 109$	$HB = 109$
Tool Cond. = Fresh	Tool Cond. = Fresh	Tool Cond. = Fresh
$R_a^p = 0.1756$	$R_a^p = 0.2775$	$R_a^p = 0.085$

and the final results are shown in Table 6.6. These results define an increase in D_{tool}, which implies an increase in cutting speed. This condition allows an increase in the f_z value, and thus the production rate.

6.5.4 Optimization in the *In-process* operating mode

During the *In-process* operating mode, the optimization process implies the modification of the f_z parameter only if $R_a^p > R_a^d$ is satisfied. During *on-line* condition it is not recommended to change other parameters because these affect directly the machining part design. This optimization process was validated by considering some experiments, where the R_a^p computed in *Pre-process* operating mode was less than R_a^d. However, during the *In-process* operating mode the intelligent system computed a high R_a value because the process state variables were considering in the *ANN* model. Table 6.7 shows proposal experiments with cutting parameters, the R_a values computed in *Pre-process* and *In-process* operating mode, and the new f_z parameter computed to decrease the R_a value. The increase in R_a could be owing to several reasons: changes in the workpiece hardness, worn edge of the cutting tool, chatter condition, etc. In all these conditions it is recommended to decrease the f_z parameter. Table 6.7 shows the R_a value is acceptable when the f_z is decreasing.

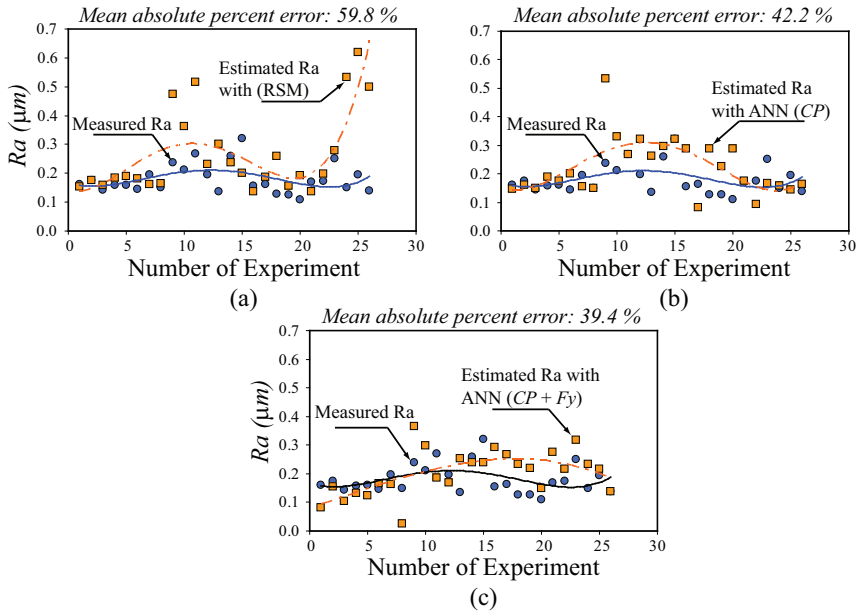

Figure 6.4: Comparison between the measured and estimated R_a values by using (a) *RSM*, (b) *ANN* with only Cutting Parameters (CP), and (c) *ANN* with $CP + F_y$.

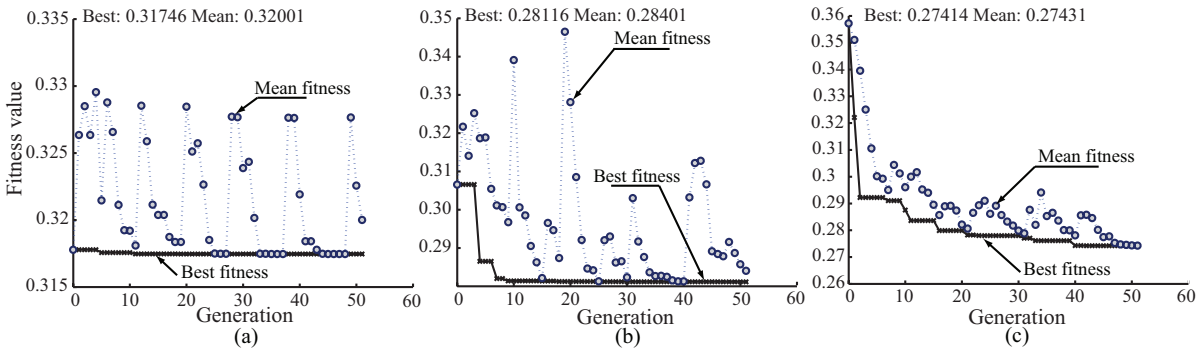

Figure 6.5: Evaluation of optimum cutting parameters with *GA* in *Pre-process* operating mode: (a) Optimization with f_z, (b) Optimization with f_z and D_{tool}, and (c) Optimization with f_z and ae.

6.5.5 Optimal machining policy

An important task of the intelligent planning module must be to propose an optimal policy (actions) for operating the *CNC* machining center. In this case, a methodology based on the Markov Decision Process (*MDP*) approach was implemented to compute the expected total discount cost and the optimal policy. *MDP* was validated with the experiments done in the Kondia machining center. The application of the *MDP* for computing the optimal policy during the peripheral milling process is described as follows:

1. Identification of the stochastic process is represented by the state of cutting tool wear condition defined as

$$S = \{s_1, s_2, s_3, s_4, s_5\} \tag{6.15}$$

   where the state of the cutting tool is: s_1 for new tool condition, s_2 for half-new tool condition, s_3 for half-worn condition, s_4 is worn condition, or s_5 defining tool breakage condition.

2. Definition of the action space with all possible decisions. Note that decisions are equal to actions. The action space is defined with three possible actions

$$A = \{a_1, a_2, a_3\} \tag{6.16}$$

   The actions represent the following:

   - a_1 means no action when the $R_a < R_a^d$. This action represents an aggressive condition because the operator uses the cutting tool until it reaches maximum VB.
   - a_2 represents a conservative condition and the operator needs to change the cutting tool when the intelligent monitoring system recognizes the worn cutting tool condition. Also, it is necessary to confirm that $R_a < R_a^d$.

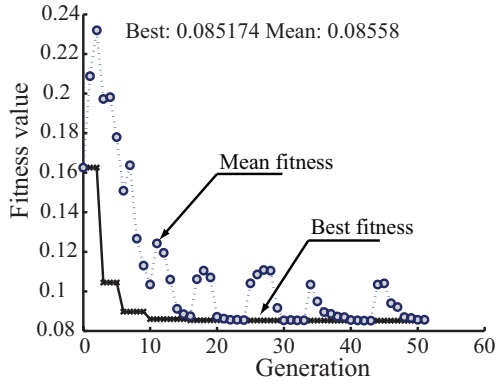

Figure 6.6: Evaluation of the optimum cutting parameters with *GA* in *Pre-process* operating mode. Optimization with f_z.

Table 6.6: Optimal cutting conditions to minimize the R_a in *Pre-process* condition (6082 Aluminium alloy).

Cutting Conditions Defined by Operator	Results of the First Running *GA*	Results of the Second Running *GA*
$f_z = 0.04$ $ae = 4$ $D_{tool} = 12$ $Curv = -0.0185$ $R_a^d = 0.25$ $HB = 94$ Tool Cond.=Half-Worn	$f_z = 0.05032$ $ae = 4$ $D_{tool} = 12$ $Curv = -0.0185$ $R_a^d = 0.25$ $HB = 94$ Tool Cond.=Half-Worn	$f_z = 0.0921$ $ae = 4$ $D_{tool} = 20$ $Curv = -0.0185$ $R_a^d = 0.25$ $HB = 94$ Tool Cond. = Fresh
$R_a^p = 0.2710$	$R_a^p = 0.2662$	$R_a^p = 0.174$

- a_3 means to always stop the machine and inspect the cutting tool, which is an intermediate condition between a_1 and a_2 actions.

3. Evaluation of the cost function for each action, which is computed by considering three concepts:

   (a) The Decision theory implies computing a decision cost based on a right or wrong action [Poole *et al.*, 1998].

   (b) The operation cost involves operator cost, depreciation, energy cost, and the operator's labor [Childs *et al.*, 2000] and [Boothroyd and Knight, 2006].

   (c) Cost of the cutting tool.

   The cost function must be defined for all cutting tool wear conditions and actions. For this application the parameters, cost and procedure for computing cost functions are defined in Appendix I. Cost function depends on selected cutting tool diameter and workpiece material, therefore, cost was computed for the $6082 - T6$ aluminium alloy and a cutting tool diameter of 16 mm. Experiments with these conditions were used to determine the optimal policy by applying the *MDP*. These experiments are defined in Table 6.1.

   - Cost function for the a_1 action with $6082 - T6$ aluminium alloy and $16mm$ of tool diameter, is given by

   $$f_{a_1} = \{44.15, 46.89, 49.28, 87.84, 320.52\} \tag{6.17}$$

   The function defines the following:

   (a) If a new cutting tool condition is recognized and a_1 action is done by the operator, the cost is \$44.15.

   (b) If a half-new cutting tool condition is recognized, the operation cost is \$46.89 for the a_1 action.

   (c) If a half-worn condition is detected, the operation cost is \$49.28.

   (d) If a worn condition is detected, the operation cost is \$87.84.

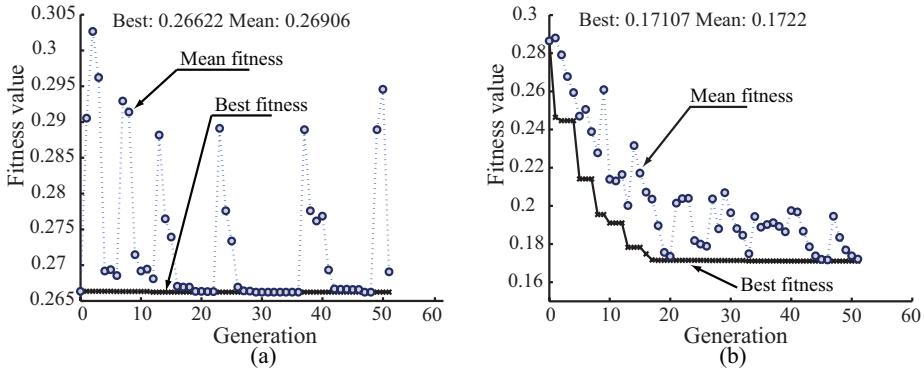

Figure 6.7: Evaluation of the optimum cutting parameters with *GA* in *Pre-process* operating mode: (a) The f_z value is computed to decrease the R_a, (b) New f_z and D_{tool} values are computed to minimize the R_a.

Table 6.7: Experiments used to validate the optimization process during the *In-process* operating mode.

Experiment (C_c, P_c, P_G)	$R_{a,obs}$	*Pre-process* R_aRSM	*In-process* R_aANN	R_a^d	New Value f_z	New Value R_a^p
P2-2024-Island ($f_z = 0.075$, $ae = 3$, $D_{tool} = 12$ $HB = 111$, $Curv = 0.0213$)	0.1432	0.1822	0.2552	0.25	0.0734	0.1816
P1-7075-Box ($f_z = 0.115$, $ae = 4.5$, $D_{tool} = 20$ $HB = 158$, $Curv = -0.0183$)	0.1467	0.2906	0.3386	0.3	0.099	0.1116
P1-6082-Line ($f_z = 0.04$, $ae = 4$, $D_{tool} = 12$, $HB = 89$, $Curv = 0.0$)	0.1629	0.2686	0.3376	0.3	0.0349	0.294
P9-2024-Box ($f_z = 0.05$, $ae = 2$, $D_{tool} = 20$, $HB = 110$, $Curv = -0.0313$)	0.1742	0.1975	0.2169	0.2	0.0457	0.15
E4-P5-6082-Box R2 ($f_z = 0.05$, $ae = 2$, $D_{tool} = 16$, $HB = 90$, $Curv = -0.025$)	0.235	0.2509	0.31107	0.26	0.04	0.1657
E5-P5-6082-Box R1 ($f_z = 0.05$, $ae = 2$, $D_{tool} = 16$ $HB = 90$, $Curv = -0.025$)	0.266	0.245	0.2719	0.26	0.047	0.2434
E5-P5-6082-Box R3 ($f_z = 0.05$, $ae = 2$, $D_{tool} = 16$, $HB = 90$, $Curv = -0.025$)	0.267	0.245	0.2842	0.26	0.045	0.2443

(e) Finally, for a broken cutting tool condition, the operation cost is $320.52.

- Cost function for the second action is

$$f_{a_2} = \{44.15, 46.89, 49.28, 300.37, 320.52\} \tag{6.18}$$

- The last cost function for the a_3 action is

$$f_{a_3} = \{49.2, 51.94, 54.32, 52.60, 320.52\} \tag{6.19}$$

4. Evaluation of the transition matrices by considering the three actions during the machining process. $P : S \times A$ is the state transition probability distribution function. For each action and state of the system there is a probability distribution over the states that can be reached after the actions. These transition matrices were

defined to reach the tool breakage condition from any state of the cutting tool. Tool breakage was included to simulate random failure of the cutting tool, which can occur at any time during the machining process. Function $P(s|s', a)$ is defined as the probability of reaching state s, given the state s' and action a.

- The transition matrix for the first action was computed in agreement with evolution of cutting tool life during the experimentation. It was estimated by considering the number of machined workpieces for each cutting tool wear condition. The information was taken from Figure 5.2. The transition matrix is given by

$$\mathbf{P_{a1}} = \begin{pmatrix} 0.951 & 0.048 & 0 & 0 & 0.001 \\ 0.026 & 0.932 & 0.041 & 0 & 0.001 \\ 0.001 & 0.02 & 0.921 & 0.055 & 0.003 \\ 0 & 0.001 & 0.05 & 0.944 & 0.005 \\ 0 & 0 & 0 & 0 & 1 \end{pmatrix} \tag{6.20}$$

- The transition matrix for the second action was computed to allow that system always gets back at the first state (new tool) if cutting tool is changing to the worn condition. The transition matrix is

$$\mathbf{P_{a2}} = \begin{pmatrix} 0.951 & 0.048 & 0 & 0 & 0.001 \\ 0.026 & 0.933 & 0.04 & 0 & 0.001 \\ 0.001 & 0.02 & 0.921 & 0.055 & 0.003 \\ 0.849 & 0.02 & 0.01 & 0.12 & 0.001 \\ 0 & 0 & 0 & 0 & 1 \end{pmatrix} \tag{6.21}$$

- The transition matrix for the third action was computed by considering the system has a similar behavior to the first action.

$$\mathbf{P_{a3}} = \begin{pmatrix} 0.951 & 0.048 & 0 & 0 & 0.001 \\ 0.026 & 0.932 & 0.041 & 0 & 0.001 \\ 0.001 & 0.02 & 0.921 & 0.055 & 0.003 \\ 0 & 0.001 & 0.05 & 0.944 & 0.005 \\ 0 & 0 & 0 & 0 & 1 \end{pmatrix} \tag{6.22}$$

5. Reward function ($R = S \times A$) is computed as a function of the defined states and cost functions. It is given by

$$\mathbf{R} = \begin{pmatrix} 44.15 & 44.15 & 49.20 \\ 46.89 & 46.89 & 51.94 \\ 49.28 & 49.28 & 54.32 \\ 87.84 & 300.37 & 52.59 \\ 320.52 & 320.52 & 320.52 \end{pmatrix} \tag{6.23}$$

6. The discount factor (α) is a function of the interest rate considered for a period of production. The required time for producing several machining parts is very short and a rate of return of 8% could be used. Therefore, a typical value of the discount factor is given by

$$\alpha = 1/(1 + 0.08) = 0.925$$

The next step was to use the Markov Decision Process Toolbox $v2.0$ for *MatLab*. By using the transitions matrices, the cost functions, and the Policy and Value Iteration algorithms, a test was done to determine which algorithm is more efficient to solve the *MDP* and compute the optimal total-cost function, and the optimal policy. The test considered two typical values of the discount factor and the results are shown in Table 6.8, and 6.9. From these results, it is observed that both algorithms compute the same results for $\alpha = 0.9$, and $\alpha = 0.925$. However, the Policy Iteration algorithm is more efficient, because the solution can be found with only 2 iterations.

Table 6.8: Results computed with the Policy Iteration algorithm.

α Value	Optimal Value Function ($)	Number of Iterations	Optimal Policy actions
0.9	$\{479, 509, 574, 620, 3205\}$	2	$\{1, 2, 1, 3, 1\}$
0.925	$\{659, 704, 803, 868, 4273\}$	2	$\{1, 2, 1, 3, 1\}$

Table 6.9: Results computed with the Value Iteration algorithm.

α Value	Optimal Value Function ($)	Number of Iterations	Optimal Policy actions
0.9	$\{479, 509, 574, 620, 3205\}$	117	$\{1, 2, 1, 3, 1\}$
0.925	$\{659, 704, 803, 868, 4273\}$	160	$\{1, 2, 1, 3, 1\}$

In summary, the optimal total cost function was computed with the Policy Iteration algorithm and the function is given by

$$\nu^* = \{659, 704, 803, 868, 4273\} \tag{6.24}$$

Also, the optimal policy was computed with the Policy Iteration algorithm and it is given by

$$\pi = \{a_1, a_2, a_1, a_3, a_1\} \tag{6.25}$$

The optimal policy defines the following recommendations to the operator:

- If a new cutting tool condition is detected, the action a_1 should be applied.

- For a half-new cutting tool condition, the action a_2 should be applied.
- For a half-worn cutting tool condition, the action a_1 should be applied.
- For a worn cutting tool condition, the action a_3 should be applied.
- For a tool breakage condition, the action a_1 should be applied.

Given that *MDP* is a stochastic model defined by a Markov system, the transition matrices and an initial distribution of the states (i.e.,$s_1, 0, 0, 0, 0$) were simulated several times to compute the variability of the results. Figure 6.8a shows the simulation of the Markov chain by using the transition matrix of Eq.(6.20), which corresponds with the aggressive condition. Figure 6.8a shows different states of cutting tool during the machining cycles and this behaviour represents a normal evolution of flank wear (VB) in the cutting tool, while the operator does not take any action and only waits for a possible tool breakage. It can happen when the cutting tool reaches the maximum worn condition. Figure 6.8b depicts a situation where the tool breakage is detected during the simulation of the Markov system.

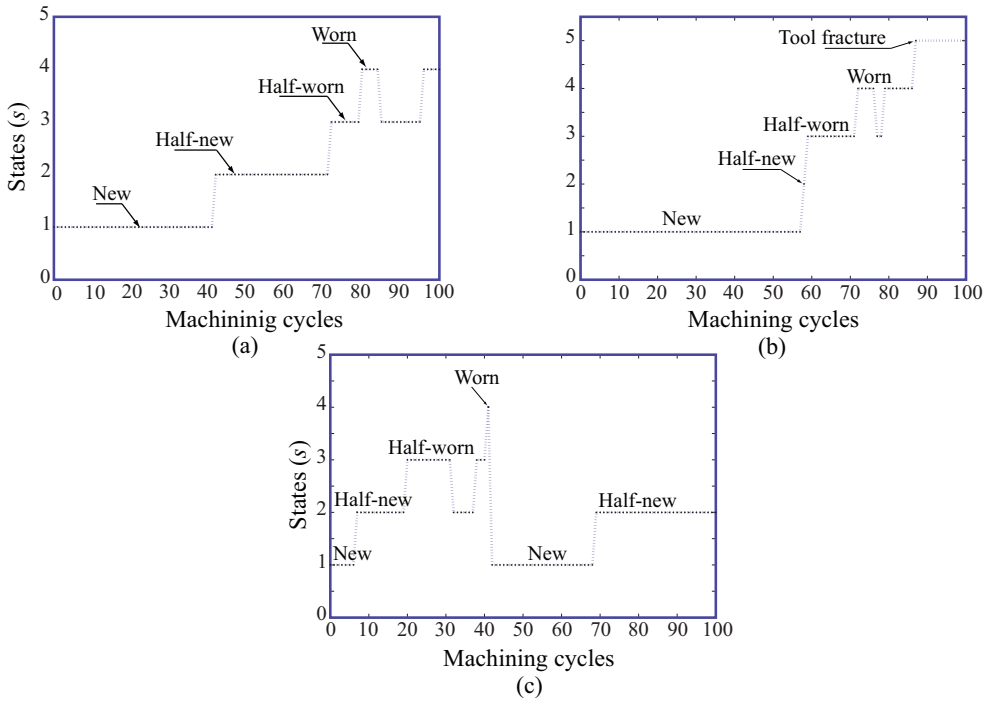

Figure 6.8: Simulation of the Markov system. (a) For an aggressive condition (P_{a1}). (b) For an aggressive condition with the tool breakage condition. (c) For a conservative condition (P_{a2}).

Figure 6.8c shows the simulation of the Markov chain by using the transition matrix of Eq.(6.21), which corresponds with the conservative condition. Figure 6.8c depicts different states of the cutting tool during the machining cycles. If a worn condition is recognized, the operator immediately changes the cutting tool, and the state of cutting tool returns to a new condition. Figure 6.9 illustrates the results of the variability of the Markov system with 30 evaluations. The "box and whisker" plot shows the comparative cost between the different actions and the optimal policy determined by the *MDP*. The boxes are notched to represent a robust estimate of the uncertainty about the medians for box-to-box comparison. These results demonstrate that the optimal policy presents the lower costs when they are compared with the aggressive, intermediate, and conservative actions. In Figure 6.9 (right plot), the average accumulative cost for the 100 machining cycles are USD \$4973.79, \$4755.87, and \$4385.18 for actions a_1, a_3, and optimal policy, respectively. Therefore, the potential savings are USD \$588.6, and \$370.7 for the a_1-optimal policy, and a_3-optimal policy, respectively. To demonstrate that optimal policy allows to minimize the operation

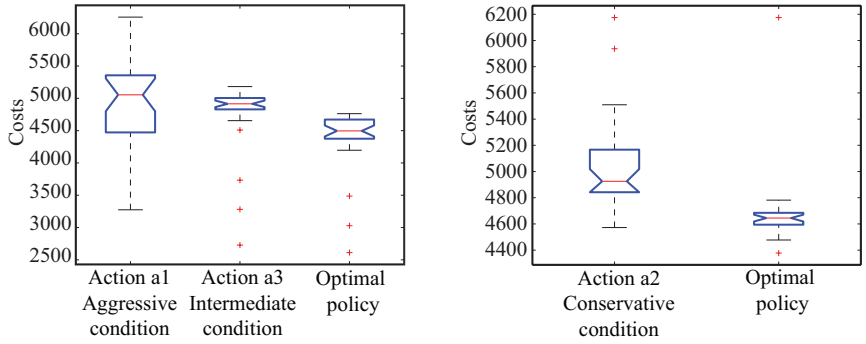

Figure 6.9: Comparison of costs for the different actions versus the optimal policy. Right plot depicts the variability of the costs for actions a_1, a_3 and optimal policy. Left plot shows the variability of the costs for action a_2, and optimal policy.

cost, several experiments with the $6082-T6$ workpiece material and 16 mm cutting tool diameter were selected in random form of the design of experiments. The Intelligent Planning Module always identified a R_a value less to the recommended value ($R_a^d \leq 0.25$ mm) for the selected experiments. Table 6.10 shows the results of one example for a specific operation. The cutting conditions were $f_z = 0.05$ mm/tooth, $n = 18000$ rpm, $V_f = 1800$ mm/min, $ae = 2$ mm, and $HB = 90-94$ HBN. The first column in Table 6.10 presents the cutting tool condition recognized by the intelligent monitoring Module. The second column defines the operation cost of the actions recommended by the optimal policy. The following three columns define the operation costs for the aggressive, conservative and intermediate actions.

From these results, it can be observed that optimal policy minimizes the production cost. During the machining process of $6082-T6$ aluminium alloy, the optimal policy saves the following amounts: \$106 dollars with respect to the first action; \$743 dollars with respect to the second; and \$65 dollars with respect to the third action. The cutting tool life is approximately 40 minutes (machining time), and it can be used to produce 100 similar pieces. It means

Table 6.10: Comparison of the applied cost for $6082-T6$ workpiece material and 16 mm cutting tool diameter. The first first column defines the cutting tool wear condition, and the following columns correspond with the operation cost of the optimal policy and the defined actions.

Cutting Tool Condition	Optimal Policy	a_1 based Policy	a_2 based Policy	a_3 based Policy
Worn	\$52.60	\$87.84	\$300.37	\$52.60
New	\$44.15	\$44.15	\$44.15	\$49.20
Half worn	\$49.28	\$49.28	\$49.28	\$54.33
Half new	\$46.89	\$46.89	\$46.89	\$51.94
Worn	\$52.60	\$87.84	\$300.37	\$52.60
Half worn	\$49.28	\$49.28	\$49.28	\$54.33
New	\$44.15	\$44.15	\$44.15	\$49.20
Worn	\$52.60	\$87.84	\$300.37	\$52.60
Half new	\$46.89	\$46.89	\$46.89	\$51.94
New	\$44.15	\$44.15	\$44.15	\$49.20
Total	\$482.61	\$588.35	\$1225.93	\$517.93

that it is possible to save ten times the aforementioned amounts. Therefore, if the optimal policy is applied, it is possible to save 18% when it is compared with doing nothing (risky option); and 60% with respect to change the cutting tool as soon as possible (conservative option).

6.6 Results and contributions

The design and implementation of the *IMPPS* represents the main module of the intelligent monitoring and supervisory control system. The important tasks and results of the *IMPPS* are the following:

1. In *Pre-process* operating mode the module estimates R_a^p with the *RSM* model and computes the optimal cutting parameters for minimizing R_a value by applying a Genetic Algorithm (*GA*).

2. In the *In-process* operating mode, the module uses the *HMM* to identify the cutting tool wear condition and estimates the R_a^p by using the process state variables and the *ANN* model.

3. The Markov Decision Process was implemented and used to predict the optimal policy for minimizing the production cost.

4. During the validation tests with *DoE*, the *HMM* with the AE-signal of spindle allows an identification of the cutting tool wear of 100% of success. It is important to select the correct *RMS* model for estimation of R_a.

5. During the validation tests with new experiments the *HMM* showed a performance of 88% for recognizing cutting tool wear condition. It was acceptable because only extreme conditions were badly classified.

From the analysis of the results, important contributions can be summarized, and they are the following:

- The multi-sensor and data fusion applied in *ANN* models improve the estimation of R_a *In-process* operating mode. The consideration of the four R_a parameters in the output layer of the *ANN* model improved the estimation of R_a. The behaviour of the R_a is reproduced with excellent results, and the mean absolute percent error between the measured and estimated R_a was reduced from 11.81% with *RSM* model to 8.5% with *ANN* model.

- The implementation of a *GA* with *RSM* models was another important contribution because it allows for computing the optimal cutting parameters in *Pre-process* operating mode with excellent results. This information is relevant in the machining process to guarantee a minimum R_a.

- Another relevant contribution was the implementation of the Markov Decision Process (*MDP*) in the optimization process. The *MDP* allows modeling decision-making under uncertainty where the actions of the operator are partly under control. This algorithm recommends optimal actions for minimizing the operation cost during the production of specific workpieces. Next step implies to evaluate the implementation of the *MDP* in the automotive or aeronautic industry.

Chapter 7

Discussion and future work

This research was leading to solve a real problem in High Speed Machining (*HSM*) processes, specifically in the peripheral milling process. Currently, the aeronautic and automotive industry demand machining of long aluminium parts and high metal removal rates to produce components. The *HSM* is an excellent option owing to high dimensional precision and high surface quality, which can be reached with this technology.

7.1 General contributions

The general scope of this research was to design and implement an intelligent monitoring and supervisory control system for the peripheral milling process in high speed machining. The system must compute the optimum cutting parameters as a function of a merit variable (surface roughness). Also, the system must allow for the monitoring of cutting tool wear condition and surface roughness during the machining process. The main contributions of this research were to:

1. Design and implement an intelligent monitoring and process planning system in the peripheral milling process for *HSM*.
2. Implement a general model to predict surface roughness by considering several aluminium alloys, cutting parameters, geometries, and cutting tools.
3. Design and implement a monitoring and diagnostic system for cutting tool wear condition during the machining process.
4. Design and develop an intelligent process planning system that includes a merit variable to compute the optimum cutting parameters and a decision-making module to recommend some actions in agreement with the cutting tool wear condition.

7.2 Specific results and contributions

Specifically, for each module of the intelligent monitoring and supervisory control system, important results and contributions are discussed in this section.

7.2.1 Important research results

From analysis done at the end of each chapter, the following list of results is defined for each module.

Data acquisition module

A complete data acquisition system was implemented in a *CNC* machining center $HS-1000$ Kondia. Important results are described as follows:

- Installed accelerometers (*AC*) in the workpiece presented excellent mechanical and electrical characteristics to acquire the vibration signals during the cutting process. The signals allowed for the characterization of the R_a in agreement with the cutting tool wear condition.
- Forces acquired with a dynamometric platform corresponds with the tendency of flank wear. The mechanical and electrical characteristics of the dynamometric platform allowed capture of the cutting forces, with excellent results, even thought the process is for high speed machining.
- The *AC* sensors installed in the ring (fixed to the spindle) did not have a satisfactory frequency bandwidth. It is necessary to change the sensors for others with different mechanical and electrical characteristics.
- A new proposal to characterize process signals was implemented with excellent results. Mel Frequency Cepstrum Coefficients computed from process signals were used to model the R_a with *ANN* models and with the *HMM* approach to classify cutting tool wear condition.

Surface roughness monitoring module

Related with R_a modelling, important results were obtained. They are as follows:

- Response surface methodology was applied with excellent results for modeling the R_a. A rotatable central composite design with 32 runs and four replicates was defined for the *DoE*, and after the *ANOVA*, a quadratic model with the main interactions of factors was computed. For the new cutting tool condition, the R_a was explained by the model with a performance of $R^2 = 90.0\%$. For the other three models, the R_a was computed with performances of 90.0% for half-new cutting tool, 92.7% for half-worn cutting tool, and 93.4% for worn cutting tool condition.
- The behaviour of R_a with variation of the factors was compared with other research, with excellent results. R_a increases with f_z, and decreases with an increase of the cutting tool diameter until to reach a minimum value.

R_a decreases as the workpiece hardness increases until it reaches a minimum value, and then R_a increases with the hardness. Also, the R_a increases with the evolution of flank wear, and the models estimated the R_a, with excellent results. The performance was compared with the mechanistic models of other researchers, and the average percentage error can be reduced from 86.47% to 8.98% by using proposal models.

- Multi-sensor and data fusion were used to build *ANN* models, with excellent results. By applying Principal Component Analysis and process signals, *ANN* models were computed with high performance and they can be used in *In-process* operating mode.

Cutting tool wear monitoring module

New ideas based on the Hidden Markov Models (*HMM*) and the Mel Frequency Cepstrum Coefficients (*MFCC*) were developed for monitoring and diagnosis of cutting toll wear condition in *HSM*.

- The *HMM* approach was configured with four states and two Gaussians, and the *HMM* models were computed with each process state signal. The best results were obtained with the signals coming from AE installed in the spindle. By using the AE-Spindle signal, average performance was 98.15% for training data set and 96.29% for testing data set.

- The *MFCC* were computing by considering two configurations in the preprocessing stage. Basically, the number of filters changed from 20 to 40, and it allowed for capture of more information about the characterization of cutting tool wear condition. The proposal values of the number of filters are typically used in speaker identification systems. By using 40 filters, performance of the *HMM* was 98.18% for testing data set.

- Finally, *HMM* models with the lowest percentage of False Fault Rate (*FFR*) were computed with AE sensors. The AE-Spindle shows the lowest percentage for *FFR* condition, with only 1.52% for worn condition.

Intelligent monitoring and process planning module

The design and implementation of the *IMPPS* represent the main module of intelligent monitoring and the supervisory control system, resulting as follows:

- In *Pre-process* operating mode, the module estimates R_a^p with the *RSM* model and computes the optimal cutting parameters for minimizing R_a value by applying a Genetic Algorithm (*GA*).

- In the *In-process* operating mode, the module uses the *HMM* to identify the cutting tool wear condition and estimates the R_a^p by using process state variables and the *ANN* model.

- The Markov Decision Process was implemented and used to predict the optimal policy for minimizing production cost.

- During validation tests with *DoE*, the *HMM*, with the AE-signal of spindle, allowed for identification of cutting tool wear at 100% success. It is important to select the correct *RMS* model for estimation of R_a.

- During validation tests with new experiments, the *HMM* showed a performance of 88% for recognizing cutting tool wear condition. It was acceptable because only extreme conditions were badly classified.

7.2.2 Specific contributions of the research

Important contributions related to R_a modelling were realized during development of this research:

1. The most important factors affecting R_a were deduced by applying the screening factorial design. These factors were f_z, D_{tool}, ae, HB, and $Curv$. A new concept to consider a different geometric pattern was defined with the $Curv$ factor. This factor had never been used in other research related to R_a, and it had an important effect on the estimated R_a.

2. Multi-sensor and data fusion were used to build *ANN* models, with excellent results. By applying the Principal Component Analysis and process signals, *ANN* models were computed, resulting in high performance, and they can be used in *In-process* operating mode.

3. An *ANN* model was developed based on cutting parameters and process state variables for monitoring R_a in *In-process* operating mode. Relevant features of process state variables were identified through computation of *MFCC*. Also, consideration of the R_a, RS_m, R_q, and R_z parameters to characterize surface roughness allowed for an increase of performance of *ANN* models. Similar R_a values can be computed by *ANN* models, even though cutting and geometric parameters in the machining process are totally different. Therefore, it is relevant to characterize surface roughness with these parameters.

With respect to the design and implementation of the cutting tool wear monitoring system, contributions were as follows:

1. The designed *HMMs* can be used to recognize the worn condition of five different cutting tool diameters in *HSM* with five different harnesses in workpiece materials.

2. Characterization of *AE* signals with *MFCC* allowed for a high performance of *HMM* with only one process signal. The *MFCC* have not been used in previous research to recognize cutting tool wear condition.

3. The implemented methodology in the Tool Condition Monitoring (*TCM*) system, with the *HMM* approach and *MFCC* features, can be exploited to be used in the aeronautic and automotive industry for maximizing the tool life and decreasing operation cost.

Contributions of the *IMPPS* are as follows:

1. Multi-sensor and data fusion applied in *ANN* models improved the estimation of R_a in *In-process* operating mode. Consideration of the four R_a parameters in the output layer of the *ANN* model improved the estimation of R_a. The behaviour of the R_a was reproduced, with excellent results, and the mean absolute percent error between the measured and estimated R_a was reduced from 11.81% with a *RSM* model to 8.5% with an *ANN* model.

2. Implementation of a *GA* with *RSM* models was another important contribution because it allowed for computation of optimal cutting parameters in *Pre-process* operating mode, with excellent results. This information is relevant in the machining process to guarantee a minimum R_a. Estimation of these optimal cutting parameters is important to satisfy quality assurance the first time during the machining process.

3. Another relevant contribution was the implementation of the Markov Decision Process (*MDP*) in the optimization process. The *MDP* allows modeling decision-making following uncertainty, where the actions of the operator are partly under control. This algorithm recommends optimal actions for minimizing operation cost during production of specific workpieces. The next step implies evaluating implementation of the *MDP* in the automotive or aeronautic industry.

7.3 Future work

Research presented in this thesis is the result of great effort to design and implement an intelligent machine in *HSM*. This research represents a base from which implementation of the intelligent monitoring and supervisory control system in different industry sectors (aeronautic, automotive, and mold/die). Therefore, the challenges and new research fields will be mentioned for each module of the system, with the objective to improve and continue this research in intelligent machines.

1. Data acquisition system module.

   - With respect to installed sensors, it is necessary to change the accelerometer sensors fixed in the spindle. It is recommended to increase the sampling rate and the resonance frequency range of sensors to obtain a satisfactory frequency bandwidth. Signals recorded from these sensors should be adequate to characterize cutting process. Therefore, performance of the *ANN* models must be better, and it could represent an excellent option to eliminate fixed sensors at the workpiece.
   - Recorded forces signals also represent a great option to exploit more features. First, the recorded forces must be separated in the static and dynamic component, by applying some filters, and with those the static components, compute the tangential and radial components of cutting forces. It should represent a better correlation between R_a and cutting force and increase performance of *ANN* models. Second, the same procedure must be applied to dynamic forces.
   - Recorded signals must be processed with other techniques to compute new features that allow the finding of new correlations between R_a and process state variables. An excellent option could be to apply wavelet transformation, and evaluate if the wavelet coefficients are more sensitive to cutting tool wear and R_a.

2. Surface roughness module. With respect to the statistical model (*RSM*), results were very satisfactory when they were applied to the *Pre-process* operating mode. On the other hand, *ANN* models applied in the *In-process* operating mode represent a great opportunity to experiment with other paradigms in dynamic neural

networks. These new paradigms could be based on non-recurrent mechanisms like delay elements in feedforward directions (i.e. Time Delay Neural Networks, Adaptive time-delay neural networks). Other *ANN* models are recurrent mechanisms based on a combination of delay elements in feedforward direction and feedback connections, like the *NARX* networks (Non-linear autoregressive model with exogenous inputs).

3. Cutting tool wear monitoring module. The implemented Hidden Markov Models (*HMM*) approach to recognizing the cutting tool wear condition presented an excellent performance (almost 100%) by using only the AE-signals in the spindle. However, some observations and recommendations will be mentioned for future work.

    - For the AE-signals it is recommended to apply a bandpass filter for separating frequency bandwidth that corresponds only with cutting process. If this option increases performance, it is necessary to compute pre-processing time of the signal, and it must be compared with actual time.
    - Currently, an ergodic *HMM* model is applied for cutting tool wear monitoring. For future work, other types of the *HMM* model must be evaluated with more than two process signals. Other types are Factorial *HMM*, Auto-regressive *HMM*, and hidden filter *HMM*. It is important to evaluate if these options could increase performance for new experiments defined in the Chapter 6.

4. Intelligent monitoring and process planning module (*IMPPS*).

    - The Genetic Algorithm (*GA*) was applied with excellent results, to compute the optimal cutting parameters with the *RSM* model. To compute the optimal cutting parameters, the *GA* requires between 50 and 60 generations. It is necessary to make additional tests with parameters of the *GA*: number of generations, population size, crossover probability, and mutation probability. The objective will be to decrease the number of generations to find optimal cutting parameters.
    - An important function of the *IMPPS* is to compute optimal cutting parameters before the *CNC* starts running. Therefore, it is relevant to integrate the *IMPPS* as one CAD/CAM system, which will allow production of a G-Code and optimal cutting parameters at the same time for machining of a specific workpiece.
    - The Markov Decision Process (*MDP*) represents an important contribution in the optimization process. It is necessary to find a real application in the industry, where different operator actions must be defined. The cost function and transition matrixes must also be computed. With this information, the *MDP* will compute the optimal policy that minimizes the operation cost. It will represent an important test to validate application of the *MDP*.
    - In general, it is important to validate the complete system in other machining centers. Machine tools have multiple degrees of freedom and are mainly related with vibrations and dynamic loading of mechanical structures. Therefore, it is important to compute performance of the proposal models (*RSM*, *ANN*, and *HMM*) in different machine tools and estimate deviations with respect to the original *HSM* machining center. It is important to evaluate the robustness of designed models.

7.4 Concluding discussion

The presented research of the intelligent monitoring and supervision control system was the result of several research works, which support final proposal models. A short description of these works is presented in this section.

1. The idea of indirect monitoring of the cutting tool wear condition was taken from a speech recognition systems that uses *HMMs* to recognize voice patterns. Several experiments were made with aluminium 6061 and steel 1045, and two databases were obtained and used to build the models. Vibration signals among workpiece materials and cutting tools were recorded and preprocessing to compute feature vectors (*MFCC*). The diagnostic system with continuous *HMM* was validated with two recommended techniques Learning Vector Quantization (*LVQ*) and *ANN*. The best results were obtained with continuous *HMM*.

2. With respect to the surface roughness (R_a) model, the idea was born with the concept to cover a complete domain of the machining process in *HSM* for the finishing operation of components for the automotive and aeronautic industry. The proposal considered the building of models for estimation of R_a off-line. The multiple sensors installed in the *CNC* were used to apply sensor and data fusion techniques. Several statistical features were computed from the process signals and used to build the *ANN* models. Results were not satisfactory, and the *MFCC* features were used to build the models, which were used the In-process operating mode.

3. All the models were integrated into a complete intelligent monitoring and supervision control system. The Markov Decision Process was selected to define a decision-making block in the intelligent monitoring and process planning module. The main function of the *MDP* was to define an optimal policy during the peripheral milling process. The objective of the optimal policy was to minimize production cost.

References

[Abouelatta and Madl, 2001] O B Abouelatta and J Madl. Surface roughness prediction based on cutting parameters and tool vibrations in turning operations. *Journal of Materials Processing Technology*, (118):269–277, 2001.

[Acc-Brüel & Kjær, 2006] Acc-Brüel & Kjær. Specifications-charger accelerometer type 4370, 4371. Technical report, Brüel & Kjær, 2006.

[Acc-PCB, 2006] Acc-PCB. Technical information of the *PCB* piezotronic accelerometer model 353b04. Technical report, PCB Piezotronics, 2006.

[Allen, 2006] T T Allen. *Introduction to Engineering Statistics and Six Sigma*. Springer-Verlag, Springer-Verlag London, first edition, 2006.

[Atlas *et al.*, 2000] L Atlas, M Ostendorf, and G D Bernard. Hidden markov models for monitoring machining tool-wear. *IEEE*, pages 3887–3890, 2000.

[Azouzi and Guillot, 1997a] R Azouzi and M Guillot. On-Line Prediction of Surface Finish and Dimensional Deviation in Turning Using Neural Network Based Sensor Fusion. *Int. J. Mach. Tools Manufact.*, 37(9):1201–1217, 1997.

[Azouzi and Guillot, 1997b] R Azouzi and M Guillot. On-line prediction of surface finish and dimensional deviation in turning using neural network based sensor fusion. *Mach. Tools Manufacture*, 37(9):1201–1217, 1997.

[Balic, 2006] J. Balic. Intelligent CAD/CAM systems for CNC Programming - An Overview. *Advances in Production Eng & Management*, (1):13–22, 2006.

[Barber *et al.*, 2001] G C Barber, R Gu, Q Jiang, and Simon Tung. Surface roughness model for worn inserts of face milling: Part II - an empirical model. *Tribology Transactions*, 44(1):142–146, 2001.

[Benardos and Vosniakos, 2002] P G Benardos and G C Vosniakos. Prediction of surface roughness in cnc face milling using neural networks and taguchi's design experiments. *Robotics and Computer Integrated Manufacturing*, (18):343–354, 2002.

[Benardos and Vosniakos, 2003] P G Benardos and G C Vosniakos. Predicting surface roughness in machining: a review. *International Journal of Machine Tools and Manufacture*, pages 833–844, 2003.

[Boothroyd and Knight, 2006] G Boothroyd and W A Knight. *Fundamentals of Machining and Machine Tools*. Taylor and Francis Group, 6000 Broken Sound Parkway NW, Suite 300 Boca Raton, FL 33487-2742, 3rd edition, 2006.

[Brezocnik *et al.*, 2004] M Brezocnik, M Kovacic, and M Ficko. Prediction of Surface Roughness with Genetic Programming. *Journal of Materials Processing Technology*, 158(157):28–36, 2004.

[Brokes, 2006] M Brokes. Voicebox: Speech processing toolbox for matlab. Technical report, http://www.ee.ic.ac.uk/hp/staff/dmb/voicebox/voicebox.html, Exhibition Road, London SW7 2BT, UK, 2006.

[Carpenter and Maropoulos, 2000] I D Carpenter and P G Maropoulos. Automatic Tool Selection for Milling Operations. Part 1: Cutting Data Generation. *Proc Instn Mech Engrs*, 214:271–282, 2000.

[Chen and Chen, 1999] J C Chen and Wei-Liang Chen. A tool breakage detection system using an accelerometer sensor. *J. of Intelligent Manufacturing*, 10(2):187–197, 1999.

[Childers *et al.*, 1977] D G Childers, D P Skinner, and R C Kemerait. The Cepstrum: A Guide to Processing. *Proceedings of the IEEE*, 65(10):1428–1443, 1977.

[Childs *et al.*, 2000] T Childs, K Maekawa, T Obikawa, and Y Yamane. *Metal Machining, Theory and Applications*. Arnold, 338 Euston Road, London NW1, first edition, 2000.

[Chua *et al.*, 1993] M S Chua, Y S Wong, and H T Loh. Determination of Optimal Cutting Conditions using Design of Experiments and Optimization Techniques. *Int J Mach. Tools Manufact.*, 33(2):297–305, 1993.

[Cus *et al.*, 2007] F Cus, U Zuperl, and V Gecevska. High-speed Milling of Light Metals. *Journal of Achievements in Materials and Manufacturing Engineering*, 24(1):357–364, 2007.

[Davis and Mermelstein, 1980] S B Davis and P Mermelstein. Comparison of Parametric Representations for Monosyllabic Word Recognition in Continuously Spoken Sentences. *IEEE Transactions on Acoustics, Speech, and Signal Processing*, 4:357–366, 1980.

[de Lacalle Marcaide *et al.*, 2004] L N López de Lacalle Marcaide, J A Sánchez Galíndez, and A L Menchaca. *Mecanizado de Alto Rendimiento Procesos de Arranque*. Ediciones Tecnicas Izaro, Mazustegui 21, 3a planta, primera edition, 2004.

[Dereli *et al.*, 2001] T Dereli, I H Filiz, and A Baykasoglu. Optimizing Cutting Parameters in Process Planning of Prismatic Parts by using Genetic Algorithms. *Int. J. Prod. Research*, 39(15):3303–3328, 2001.

[Detroja *et al.*, 2006] K P Detroja, R D Gudi, S C Patwardhan, and K Roy. Fault Detection and Isolation Using Correspondence Analysis. *Ind. Eng. Chem. Res.*, 45(1):223–235, 2006.

[Dey and Stori, 2004] S Dey and J A Stori. A Bayesian network approach to root cause diagnosis of process variations. *International Journal of Machine Tools & Manufacture*, (45):75–91, 2004.

[Dimla, 2000] D E Dimla. Sensor Signals for Tool-Wear Monitoring in Metal Cutting Operations-A Review of Methods. *Int. J of Machine Tools & Manufacture*, (40):1073–1098, 2000.

[E D Kirby and Chen, 2004] Z Zhang E D Kirby and J C Chen. Development of an Accelerometer-Based Surface Roughness Prediction System in Turning Operations Using Multiple Regression Techniques. *Journal of Industrial Technology*, 20(4):1–8, 2004.

[Erol *et al.*, 2000] N A Erol, Y Altintas, and M R Ito. Open System Architecture Modular Tool Kit for Motion and Machining Process Control. *IEEE/ASME Transactions on Mechatronics*, 5(3):281–291, 2000.

[Ertekin *et al.*, 2003] Y M Ertekin, Y Kwon, and T Tseng. Identification of Common Sensory Features for the Control of CNC Milling Operations under Varying Cutting Conditions. *International Journal of Machine Tools and Manufacture*, 43:897–904, 2003.

[Feldman and Valdez-Flores, 2004] R M Feldman and C Valdez-Flores. *Applied Probability and Stochastic Processes*. Thomson Brooks/Cole, 511 Forest Lodge Road, Pacific Grove, CA 93950, first edition, 2004.

[Feng and Wang, 2003] C X Feng and X F Wang. Surface Roughness Predictive Modeling: Neural Networks versus Regression. *IIE Transactions on Design and Manufacturing*, (35):11–27, 2003.

[Fuh and Chang, 1997] K H Fuh and K Y Chang. An Accuracy Model for the Peripheral Milling of Aluminium Alloys Using Response Surface Design. *Journal of Materials Processing Technology*, (72):42–47, 1997.

[Gage-Compuscope, 2006] Gage-Compuscope. Compuscope 1602 card specifications. Technical report, GaGe, 2006.

[Ghosh *et al.*, 2007] N Ghosh, Y B Ravi, A Patra, S Mukhopadhyay, S Paul, A R Mohanty, and A B Chattopadhyay. Estimation of tool wear during *CNC* milling using neural network-based sensor fusion. *Mechanical Systems and Signal Processing*, (21):466–479, 2007.

[Guo and Ammula, 2005] Y B Guo and S C Ammula. Real-Time Acoustic Emission Monitoring for Surface Damage in Hard Machining. *International Journal of Machine Tools & Manufacture*, 45:1622–1627, 2005.

[Haber and Alique, 2003] R E Haber and A Alique. Intelligent process supervision for predicting tool wear in machining processes. *Mechatronics*, (13):825–849, 2003.

[Haber *et al.*, 1998] R E Haber, C R Peres, A Alique, S Ros, C González, and J R Alique. Toward Intelligent Machining: Hierarchical Fuzzy Control for the End Milling Process. *IEEE Transactions on control systems technology*, 6(2):188–199, 1998.

[Haber *et al.*, 2004] R E Haber, J E Jiménez, C R Peres, and J R Alique. An investigation of tool-wear monitoring in a high-speed machining process. *Sensors and Actuators A*, (116):539–545, 2004.

[ISO 4287:1997(E/F), 1997] ISO 4287:1997(E/F). Geometrical Product Specifications (GPS) - Surface texture: Profile method-Terms, definitions, and surface texture parameters. Technical Report First edition, International Standard, ISO, 1997.

[ISO 4288:1996(E), 1996] ISO 4288:1996(E). Geometrical Product Specifications (GPS) - Surface texture: Profile method-Rules and procedures for the assessement of surface texture. Technical Report Second edition, International Standard, ISO, 1996.

[ISO 8688-2:1989(E), 1989] ISO 8688-2:1989(E). Tool life testing in milling - part 2: End milling. Technical Report First edition, International Standard, ISO, 1989.

[Jawahir and Wang, 2007] I S Jawahir and X Wang. Development of Hybrid Predictive Models and Optimization Techniques for Machining Operations. *Journal of Materials Processing Technology*, (185):46–59, 2007.

[Jung *et al.*, 2004] Tae-Sung Jung, Min-Yang Yang, and Kang-Jae Lee. A New Approach to Analysing Machined Surfaces by Ball-End Milling, Part I: Formulation of Characteristic Lines of Cut Remainder. *Advanced Manufacturing Technology*, pages 1–8, 2004.

[Kannatey-Asibu and Dornfeld, 1982] E Kannatey-Asibu and D A Dornfeld. A Study of Tool Wear using Statistical Analysis of Metal-Cutting Acoustic Emission. *Wear*, 76:247–261, 1982.

[Kim and Chu, 1999] B H Kim and C N Chu. Texture Prediction of Milled Surfaces Using Texture Superposition Method. *Computer-Aided Design*, 31:485–494, 1999.

[Kistler-AE-Coupler, 2006] Kistler-AE-Coupler. Technical information of the Kistler AE Coupler type 5152B. Technical report, Kistler, 2006.

[Kistler-AE, 2006] Kistler-AE. Technical information of the Kistler Acosutic Emission 8152B model. Technical report, Kistler, 2006.

[Kistler-Amplifier, 2006] Kistler-Amplifier. Technical information of the kistler charge amplifier. Technical report, Kistler, 2006.

[Kistler-Charge-amplifier, 2006] Kistler-Charge-amplifier. Technical information of the Kistler multi-channel charge amplifier, type 5050A. Technical report, Kistler, 2006.

[Kistler-Dy, 2006] Kistler-Dy. Technical information of the Kistler 3 component Dynamometer 9257B model. Technical report, Kistler, 2006.

[Koren *et al.*, 1999] Y Koren, U Heisel, F Jovane, T Moriwaki, G Pritschow, G Ulsoy, and H Van Brussel. Reconfigurable manufacturing systems. *Annals of the CIRP*, 48(2):527–540, 1999.

[Lee and Chen, 2003] S S Lee and J C Chen. On-line surface roughness recognition system using artificial neural networks system in turning operations. *International Journal of Advanced Manufacturing Technology*, 22:498–509, 2003.

[Lee *et al.*, 2001] K Y Lee, M C Kang, Y H Jeong, D W Lee, and J S Kim. Simulation of surface roughness and profile in high-speed and milling. *Materials Processing Technology*, (113):410–415, 2001.

[Li, 2002] X Li. A Brief Review: Acoustic Emisison Method for Tool Wear Monitoring during Turning. *International Journal of Machine Tools & Manufacture*, 42:157–165, 2002.

[Liang *et al.*, 2004] S Y Liang, R L Hecker, and R G Landers. Machining process monitoring and control: The state-of-the-art. *Manufacturing Science and Engineering*, 126:297–310, 2004.

[Lou *et al.*, 1998] M S Lou, J C Chen, and C-M Li. Surface roughness prediction technique for CNC end-milling. *Industrial Technology*, 15(1):1–6, 1998.

[Mesina and Langari, 2001] O S Mesina and R Langari. A Neuro-Fuzzy System for Tool Condition Monitoring in Metal Cutting. *Journal of Manufacturing Science and Engineering*, 123:312–318, 2001.

[Mohamed and Garder, 2000] M A Mohamed and P Garder. Generalized Hidden Markov Models - Part I: Theoretical frameworks. *IEEE Transactions on fuzzy systems*, 8(1):67–87, 2000.

[Molina *et al.*, 2005] A Molina, C A Rodriguez, H Ahuett, J A Cortéz, M Ramírez, G Jiménez, and S Martinez. Next-generation manufacturing systems: key research issues in developing and integrating reconfigurable and intelligent machines. *International Journal of Computer Integrated Manufacturing*, 18(7):525–536, 2005.

[Molla and Hirose, 2004] K I Molla and K Hirose. On the Effectiveness of MFCCs and their Statistical Distribution Properties in Speaker Identification. *IEEE International Conference on Virtual Environments, Human-Computer Interfaces, and Measurement Systems*, pages 136–141, 2004.

[Monostori, 2000] L Monostori. Intelligent Machines. In *Proc.* 2^{nd} *Conf on Mechanical Eng*, pages 24–36, Hungary, 2000.

[Montgomery, 2001] D C Montgomery. *Design and Analysis of Experiments*. John Wiley and sons, Inc., Clearence center, 222 Rosewood Drive, Danvers, MA 01923, fifth edition, 2001.

[Mukherjee and Ray, 2006] I Mukherjee and P K Ray. A review of Optimization Techniques in Metal Cutting Processes. *Computers and Industrial Engineering*, (50):15–34, 2006.

[Mursec and Cus, 2003] B Mursec and F Cus. Integral Model of Selection of Optimal Cutting Conditions from Different Databases of Tool Makers. *Journal of Materials Processing Technology*, (133):158–165, 2003.

[Nacsa, 2001] J Nacsa. Intelligent Open CNC System Based on the Knowledge Server Concept. In *Digital Enterprise Challenges - IFIP Prolamat*, pages 7–10, 2001.

[Narita *et al.*, 2004] H Narita, K Shirase, E Arai, K Nakamoto, L Chen, and H Fujimoto. Proposal of a Concept of Future Oriented Machine Tools for Advanced Manufcaturing Systems. *International journal of production research*, 42(17):3657–3673, 2004.

[Nexus-Amplifier, 2006] Nexus-Amplifier. Specifications-charger accelerometer model 2693. Technical report, Nexus, 2006.

[NI-DAQ, 2006] NI-DAQ. Technical information of the high speed multifunction card, daq ni-6153. Technical report, National Instrument, 2006.

[Öktem *et al.*, 2006] H Öktem, T Erzurumlu, and M Çöl. A Study of the Taguchi Optimization Method for Surface Roughness in Finish Milling of Mold Surfaces. *Int J Adv Manuf Technol*, (28):694–700, 2006.

[Owsley *et al.*, 1997] L M D Owsley, L E Atlas, and G D Bernard. Self-organizing feature maps and hidden markov models for machine-tool monitoring. *IEEE Transactions on Signal Processing*, 45(11):2787–2798, 1997.

[Ozcelik and Bayramoglu, 2006] B Ozcelik and M Bayramoglu. The Statistical Modeling of Surface Roughness in High-Speed Flat End Milling. *International Journal of Machine Tools and Manufacture*, 46:1395–1402, 2006.

[Özel and Karpat, 2005] T Özel and Y Karpat. Predictive modeling of surface roughness and tool wear in hard turning using regression and neural networks. *Machine Tools and Manufacture*, (45):467–479, 2005.

[Palanisamy *et al.*, 2007] P Palanisamy, I Rajendran, and S Shanmugasundaram. Optimization of Machining Parameters Using Genetic Glgorithm and Experimental Validation for End-Milling Operations. *Int. J Adv Manuf Technol*, (32):644–655, 2007.

[Park and Kim, 1998] K S Park and S H Kim. Artificial Intelligence Approaches to Determination of CNC Machining Parameters in Manufcaturing: A Review. *Artificial Intelligence in Engeneering*, (12):127–134, 1998.

[Poole *et al.*, 1998] D Poole, A Mackworth, and R Goebel. *Computational Intelligence A Logical Approach*. Oxford University Press, 198 Madison avenue, New York, New York, 10016, 1998.

[Rabiner, 1989] L R Rabiner. A tutorial on hidden markov models and selected applications in speech recognition. *Proceedings of the IEEE*, 77(2):257–286, 1989.

[Rajabi-Ghahnavie and Fotuhi-Firuzabad, 2006] A Rajabi-Ghahnavie and M Fotuhi-Firuzabad. Application of Markov Decision Process in Generating Units Maintanence Scheduling. *9th Intenational Conference on Probabilistic Methods Applied to Power Systems*, pages 1–6, 2006.

[Rangwala and Dornfeld, 1991] S Rangwala and D Dornfeld. A Study of Acoustic Emission Generated during Orthogonal Metal Cutting-1:Energy analysis. *Int. J. Mech. Sci.*, 33(6):471–487, 1991.

[Rehorn *et al.*, 2005] A G Rehorn, J Jiang, and P E Orban. State-of-the-Art Methods and Results in Tool Condition Monitoring: a Rreview. *Int. J. Adv. Manuf. Technol.*, (26):693–710, 2005.

[Saglam and Unuvar, 2003] H Saglam and A Unuvar. Tool condition monitoring in milling based on cutting forces by a neural network. *International Journal of Production Research*, 41(7):1519–1532, 2003.

[Sai and Bouzid, 2005] K Sai and W Bouzid. Roughness modelling in up-face milling. *Int. J. Adv. Manuf. Technol.*, (26):324–329, 2005.

[Savage and Chen, 1999] M D Savage and J C Chen. Multiple Regression-Based Multilevel In-Process Surface Roughness Recognition System in Milling Operations. *The Journal of Technology Studies*, pages 28–34, 1999.

[Sick, 2002a] Bernhard Sick. Fusion of hard and soft computing techniques in indirect, online tool wear monitoring. *IEEE Transactions on Systems, Man, and Cybernetics*, 32(2):80–91, 2002.

[Sick, 2002b] Bernhard Sick. On-Line and Indirect Tool Wear Monitoring in Turning with Artificial Neural Networks: A Review of more than a Decade of Research. *Mechanical Systems and Signal Processing*, 16(4):487–546, 2002.

[Suresh *et al.*, 2002] P V S Suresh, P Venkateswara, and S G Deshmukh. A Genetic Algorithm Approach for Optimization of Surface Roughness Prediction Model. *Int. J of Machine Tools and Manufacture*, (42):675–680, 2002.

[Tansel *et al.*, 2006] I N Tansel, B Ozcelik, W Y Bao, P Chen, D Rincon, S Y Yang, and A Yenilmez. Selection of Optimal Cutting Conditions by Using GONNS. *Int. J of Machine Tools and Manufacture*, (46):26–35, 2006.

[Tien *et al.*, 2004] D X Tien, K W Lim, and L Jun. Comparative Study of PCA Approaches in Process Monitoring and Fault Detection. *The 30th Annual Conference of the IEEE Industrial Electronics Society*, pages 2594–2599, 2004.

[Tönshoff *et al.*, 1988] H K Tönshoff, J P Wulfsberg, H J J Kals, W König, and C A van Luttervelt. Developments and Trends in Monitoring and Control of Machining Processes. *Annals of the CIRP*, 37(2):611–622, 1988.

[Trent and Wright, 2000] E M Trent and P K Wright. *Metal Cutting*. Butterworth-Heinemann, 225 Wildwood Avenue Woburn, MA 01801-2041, fourth edition, 2000.

[Tsai *et al.*, 1999] Y H Tsai, J C Chen, and S J Lou. An in-process surface recognition system based on neural networks in end milling cutting operations. *Machine Tools and Manufacture*, (39):583–605, 1999.

[Tzeng and Chen, 2005] Y-F Tzeng and F-Ch Chen. Optimization of High Speed CNC Milling Process Using Two-Phase Parameter Design Strategy by the Taguchi Methods. *JSME Int Journal, Series C*, 48(4):775–783, 2005.

[van Luttervelt and Peng, 1999] C A van Luttervelt and J Peng. Symbiosis of Modelling and Sensing to Improve the Accuracy of Workpieces in Small Batch Machining Operations. *Int. J Adv. Manuf Technol*, 15:699–710, 1999.

[Wang *et al.*, 2002] L Wang, M G Mehrabi, and E Kannatey-Asibu. Hidden Markov Model-Based Tool Wear Monitoring in Turning. *Journal of Manufacturing Science and Engineering*, 124:651–658, 2002.

[Wong and Sridharan, 2001] E Wong and S Sridharan. Comparison of Linear Prediction Cepstrum Coefficients and Mel-Frequency Cepstrum Coefficients for Language Identification. *Proceedings of 2001 International Symposium on Intelligent Multimedia, Video and Speech Processing*, pages 95–98, 2001.

[Yih-fong, 2005] T Yih-fong. A Hybrid Approach to Optimize Multiple Performance Chracteristics of High-Speed Computerised Numerical Control Milling Tool Steels. *Materials and design*, pages 1–10, 2005.

[Yue and Tomoyasu, 2004] H H Yue and M Tomoyasu. Weighted Principal Component Analysis and its Applications to Improve FDC Performance. *43rd IEEE Conference on Decision and Control*, pages 4262–4267, 2004.

[Zigelboim and Shallom, 2006] G Zigelboim and I D Shallom. A Comparison Study of Cepstral Analysis with Applictaions to Speech Recognition. *IEEE International Conference on Information Technology: Research and Education*, pages 30–33, 2006.

[Zuperl *et al.*, 2004] U Zuperl, F Cus, B Mursec, and T Ploj. A Hybrid Analytical-Neural Network Approach to the Determination of Optimal Conditions. *Journal of Materials Processing Technology*, 158(157):82–90, 2004.

[Zuperl *et al.*, 2006] U Zuperl, F $\check{C}us$, and E Kiker. Intelligent Adaptive Cutting Force Control in End-Milling. *Technical Gazette*, 13(1,2):15–22, 2006.

Appendix A

Machining Process Concepts

This appendix describes important basic concepts in machining processes. The concepts are necessary to understand and define the technical information related with the mechanical cutting process.

A.1 Important variables in machining processes

It is very important to set-up the milling operation before starting the *CNC* machining center. Therefore, some concepts must be established in the set-up procedure, and they define the dynamic of the rotating milling tool, with a diameter (D_{tool}) moving against the workpiece. The concepts are the following,

- Spindle speed $(n = rpm)$ is the number of revolutions per minute of the milling cutter.
- Cutting speed $(v_c = m/min)$ indicates the surface speed at which the cutting edge machines the workpiece.
- Feed per minute or feed speed $(v_f = mm/min)$ is the feed of the tool against the workpiece. It is also called the table-feed and machine feed. These variables are correlated by the following equations:

$$v_c = \frac{\pi \times D_{tool} \times n}{1000}(m/min) \tag{A.1}$$

$$n = \frac{v_c \times 1000}{\pi \times D_{tool}}(rpm) \tag{A.2}$$

- Feed per revolution (f) is a value used especially for feed calculations and determining the finishing capability of the milling process. It is an auxiliary value indicating how far the tool moves during the rotation.
- Feed per tooth (f_z) is an important key value in milling, because the milling cutter is a multi-toothed tool, and a correct value is needed to ensure that each edge machines under satisfactory conditions. The capability

of each tooth sets the limits for the tool. It defines the linear distance moved by the tool while one particular tooth is engaged in cut. It is given by

$$f_z = \frac{v_f}{n \times z}(mm) \tag{A.3}$$

It is a vital factor in milling, because it is very decisive for metal removal per edge, load per edge, tool life, and surface texture.

- The radial depth of cut (ae), and the axial depth of cut (ap), are defined for the peripheral milling.
- The volume of metal removed per time (V) unit can be established using some of these definitions. The volume is the depth of cut times the width of cut times the distance the tool moves along during the unit in question $[z_w]$. It is given by

$$V = ae \times ap \times v_f(mm^3/min) \tag{A.4}$$

A.2 Surface Roughness

Every machining operation leaves characteristic evidence on the machined surface. This evidence represents the form of finely spaced micro irregularities left by the cutting tool. Each cutting tool leaves its own individual pattern which can be identified. This pattern is known as surface roughness. Important definitions related with the surface finish imperfections are the following:

- *Nominal surface* is the intended surface. The nominal surface is usually shown and dimensioned on a drawing. It does not include intended surface roughness.
- *Surface texture* is the combination of fairly short wavelength deviations of a surface from the nominal surface. Texture includes roughness, waviness, and lay, that is, all the deviations that are shorter in wavelength than form error deviations.
- *Roughness* includes the fines (short wavelength) irregularities of a surface. Roughness results from a particular production process or material condition.
- *Waviness* defines the more widely space (longer wavelength) deviations of a surface from its nominal shape.
- *Lay* refers to the predominant direction of the surface texture. Ordinarily lay is determined by the particular production method and geometry used.

A.3 Tool wear in metal cutting

Tool wear is defined as a gradual loss of tool material at workpiece material and tool contact zones. The progressive wear of a tool can be evaluated in distinct ways:

1. *Crater wear occurs at the tool-chip contact area where the tool is influenced by a friction force of the moving chip under heavy loads and high temperatures*. At higher speeds ($v_c = 250\ m/min$ to machine steel workpiece) the temperature on the rake face of a carbide tool may reach over $1,000^oC$. At these temperatures, the atoms in the tool continuously diffuse to the moving chip. The temperature is greatest near the midpoint of the tool-chip contact length, where the greatest amount of crater wear occurs due to intensive diffusion. Crater wear can be minimized by selecting a tool material that has the least affinity to the workpiece material in terms of diffusion. The use of lubricants also reduces the wear. Under very high speed cutting conditions, crater wear is often the factor that determines the life of the cutting tool.

2. *Flank wear is caused by friction between the flank face of the tool and the machined workpiece surface*. At the tool flank-workpiece surface contact area, tool particles adhere to the workpiece surface, and are periodically sheared off. Adhesion of the tool and workpiece materials increase at higher temperatures. Abrasive wear occurs when hard inclusions of work material or escaped tool particles scratch the flank and workpiece surface as they move across the contact area.

3. *Tool fracture is defined as the loss of a major portion of the tool wedge, which terminates the total cutting ability of the tool*. Chipping of the tool (i.e., the loss of small particles from the cutting edge of the tool) is undesirable but does not prevent cutting totally. Chipping does, however, increases the friction on both the rake and flank faces of the chipping tool. If it remains undetected, chipping eventually leads to total breakage of the tool.

A.4 Mechanisms and causes in tool damage

Tool damage is due to several wear mechanism that may occur simultaneously. They can be listed as *abrasion*, *adhesion*, *diffusion*, *fatigue*, and *chemical wear*. The importance and occurrence of the mechanisms can be classified as a function of the cutting temperature, as shown in Figure A.1.

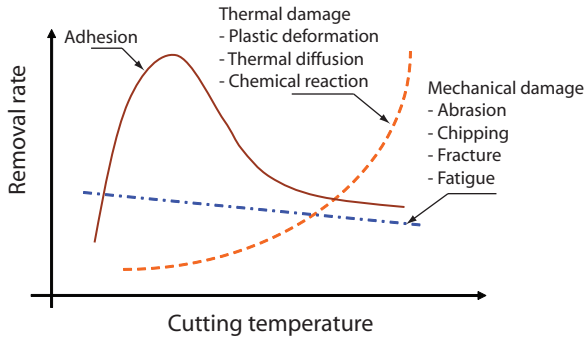

Figure A.1: Behavior of the tool damage mechanisms as a function of the cutting temperature and removal rate.

The most important mechanisms in tool damage are discussed in this section.

1. *Abrasion wear*. Abrasion occurs when a harder material (e.g., the tool) shears away small particles from the softer work material. However, softer work material also removes small particles from the tool material although at a smaller rate. The hard tool particles are caught between the hard tool and soft work material, and this causes additional abrasion wear.

2. *Adhesion wear*. When there is a relative motion between the two bodies that are the normal load, fragments of softer work material adhere to the harder tool. The typical example in metal cutting is a built-up edge, which usually occurs at low cutting speeds when part of the chip material welds to the cutting edge.

3. *Diffusion wear*. Solid-state diffusion occurs when atoms in a metallic crystal lattice move from a region of high atomic concentration to one of low concentration. This process is dependent on the existing temperature, and the rate of diffusion increases exponentially with increases in temperature. In metal cutting, where intimate contact between the work and tool materials occurs and high temperature exist, diffusion can occur where atoms move from the tool material to the work material.

4. *Mechanical damage*. It is classified as wear or fracture depends on its scale. The mechanical damage is due to the abrasion, adhesion, and diffusion wear. Now, we will explain the mechanical damage due to chipping and fracture on the cutting tool. Chipping (sometimes called micro-chipping) is caused by mechanical shock loading on a scale that leads to large fluctuations in cutting force. Fracture is classified into three types: *early stage, unpredictable and final stage*. The *early stage* occurs immediately after beginning a cut if the tool shape or cutting condition is improper. *Unpredictable* fracture can occur at any time if the stress on the cutting edge changes suddenly, for example caused by chattering or an irregularity in the workpiece hardness. *Final stage* fracture can be observed frequently at the end of a tool's life in milling: then fatigue due to mechanical or thermal stresses on the cutting edge is the main cause of damage.

A.5 Machining optimization

Analysis of production costs and production rates can be a complicated subject, and in many cases the analysis will apply only to the particular operation in question. Empirical rules or guideline principles for choosing the optimum cutting conditions for a given machining operation are discussed. The *production time* is defined as the average time taken to produce one component, and the *production cost* is defined as the total average cost of performing the machining operation on a component using one machine tool. In general, the production of a component will involve several machining operations using a variety of machine tools (often called *setups*). The total cost will be the sum of production costs for each machine setup.

Assuming the appropriate tool and cutting fluid were chosen for the machining of a batch of components, the only cutting conditions to be determined are the cutting speed and feed. Considering these two cutting conditions, at very low speeds and feeds will result in a high production time because of the long machining time. Alternatively, very high speeds and feeds will result in a high production time because of the frequent need to change cutting tools.

Clearly, an optimum condition will exist giving minimum production time. Similarly, an optimum condition will arise for minimum production cost. At low speeds and feeds costs will be high because of the cost of using the machine and operator for the longer machining times. At high speeds and feeds costs will be high because of the cost of frequent tool replacement.

A.5.1 Choice of feed

When a finishing cut is to be taken, the appropriate feed will be that which gives an acceptable surface finish. In this case the choice of feed is defined by the designer. In the case of roughing operation, from practical experience, the recommendations are: if an increased production rate is required in rough machining, it will always be preferable to increase the feed rather than increase speed. Of course, it is necessary to consider that an increase of feed increase the tool forces, whereas an increase in cutting speed will not.

A.5.2 Choice of cutting speed

Two distinct criteria can be used in choosing the cutting speed for a machining operation: *minimum production cost and minimum production time*. The optimum cutting speed implies to compute some mathematical expressions by considering the following: 1) The nonproductive time which considers the time taken to load and unload each component and to return the tool to the beginning of the cut; 2) The total machining time which defines the machining time for the component; and 3) The total time involved in changing worn tools.

The effect of cutting speed on the cost of production can more clearly be shown in the form of a graph as depicted in Figure A.2. This figure shows three important costs, and how an optimum cutting speed arises for a given set of conditions.

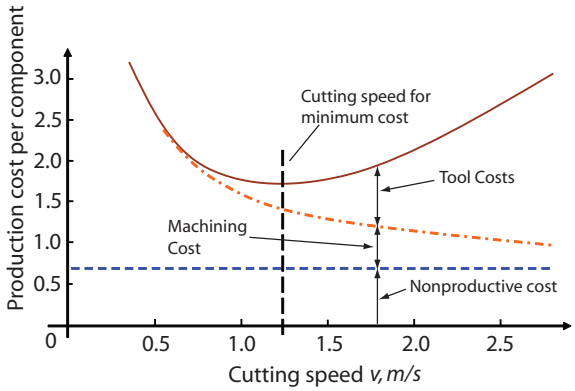

Figure A.2: Different costs for a typical machining operation

Appendix B

Sensors, amplifiers, and data acquisition boards

B.1 Introduction

Important concepts and behaviour of the process signals are described for the accelerometers, acoustic emission sensors, and configuration of amplifiers.

B.2 Accelerometers

Vibrations are produced by cyclic variations in the dynamic components of the cutting forces. Mechanical vibrations generally result from periodic wave motions. The nature of the vibration signal arising from the metal cutting process is such that it incorporates facets of free, forced, periodic and random types of vibration. Direct measurement of vibration is difficult to achieve because its determining characteristic, the vibration mode, is frequency dependent. Hence, related parameters such as the rate at which dynamic forces change per unit time (acceleration) are measured and the characteristics of the vibration derived from the patterns obtained. Nowadays, the piezoelectric accelerometer is universally used for vibration measurements. It has very wide frequency and dynamic ranges with good linearity throughout the ranges. It is relatively robust and reliable so that its characteristics remain stable over a long period of time. Piezoelectric measuring systems are active electrical systems. That is, the crystals produce an electrical output only when they perceive a change in load. For this reason, they are suitable for dynamic measurements. The main characteristics of these accelerometers are:

- Sensitivity. It is the first characteristic considered. High sensitivity normally entails a relatively big piezoelectric assembly and consequently a heavy unit. In normal circumstances the sensitivity is not critical problem due to the preamplifiers can be designed to accept these low level signals.

- Frequency range. Mechanical systems tend to have much of their vibration energy contained in the relatively narrow frequency between $10\ Hz$ to $1000\ Hz$ but measurements are often made up of $10\ KHz$ because these are often interesting vibration components at these higher frequencies. Then, the frequency range of the accelerometer must be selected to cover the range of interest. The upper limit of the frequency range is determined by the resonant frequency of the mass-spring system of the accelerometer itself. With small accelerometers the resonant frequency can be as high as $180\ KHz$, but for general purpose accelerometers, resonant frequencies of 20 to 30 KHz are typical.

B.3 Acoustic Emission

During metal cutting, the workpiece undergoes considerable plastic deformation as the tool pushes through it. Within the deformation zones (dislocations movements), strain energy is released as the bonds between the metal atoms are disturbed. This released energy is commonly referred to as acoustic emission. [Rangwala and Dornfeld, 1991], [Li, 2002] and define the following possible sources of *AE* during metal cutting processes: a) Plastic deformation during the cutting process; b) Plastic deformation of the chip; c) Frictional contact between the tool flank face and the workpiece; d) Frictional contact between the tool rank face and the chip; e) Collisions between chip and tool; f) Chip breakage; and g) Tool fracture.

B.4 Amplifiers configuration

For the *AC* sensors fixed on the workpiece, a Nexus conditioning amplifier 2693 model was used. The Amplifier can be reconfigurable at any time, to consider different input types (charge or voltage) in each of the available four channels, [Nexus-Amplifier, 2006]. The human interface of the Nexus Amplifier allows to set up the following parameters:

- Amplifier set-up: For setting up filters and gain for each individual channel.
- Transducer set-up: For selecting transducer type and entering calibrated sensitivity.
- Transducer supply: For setting up current supply, preamplifier/polarization voltages and cable length.
- Floating/correction: For selecting floating input/output and for entering application corrections.
- Store/Recall set-up: For storage/retrieval of five user-defined set-ups.
- Display set-up: For switching back-lighting on/off and adjusting the display contrast.
- Self-test: For testing the digital hardware.

For PCB Piezotronics accelerometers, $353B04$ model, the Nexus amplifier must present the configuration shows in Table B.1.

Table B.1: Nexus amplifier configuration for the two DeltaTron channels (△)

Amplifier Setup: ch1 △ 0.1 KHz 22.4 KHz 1 V/g ch2 △ 0.1 KHz 22.4 KHz 1 V/g	Transducer Setup: ch1 △ 10.04 mV/g ch2 △ 9.910 mV/g
Transducer Supply: ch1 △ 4 mA cable length 4 m ch2 △ 4 mA cable length 4 m	Floating correction: ch1 △ 50.0 ch2 △ 50.0

For each Brüel & Kjær piezoelectric accelerometers was used a Kistler charge amplifier ([Kistler-Amplifier, 2006]) type $5011B$, and it implies to setup the following parameters: transducer sensitivity, scale, low pass filter activation, and time constant for the high pass filter. Table B.2 defines the required parameters for each accelerometer. The sensors were fixed on the ring installed in the spindle. For the Kistler 3-Component Dynamometer, a multi-channel

Table B.2: Parameters defined to configure the Kistler charge amplifier type 5011 (M.U.=Mechanical units).

	$AC-X$axis	$AC-Y$axis	$AC-Z$axis
Transducer sensitivity ($pC/M.U.$)	9.8	9.8	98
Scale ($M.U./V$)	20	20	9.0
Low pass filter	OFF	OFF	OFF
Time constant for HP filter (s)	1	1	1

charge amplifier type $5070A$, from Kistler, was used to amplify the forces ([Kistler-Charge-amplifier, 2006]). The Piezoelectric force sensors produce an electric charge which varies in direct proportion with the load acting on the sensor. The charge amplifier converts the electric charge into a proportional voltage. To record the forces into an acceptable range, the multi-channel amplifier was configuring with the parameters shown in Table B.3.

B.5 Behaviour of the process state variables in the frequency domain

B.5.1 Accelerometers and dynamometers signals

Several tests were done to determine the correct sampling rate and the required adjustments for the amplification system. An excellent behavior in frequency domain and different cutting tool wear conditions was observed. A similar behavior was observed for the experiments with different cutting parameters and geometry paths. Table B.4 presents the cutting conditions for different experiments, and Figures B.1, B.2, and B.3, B.4 show the frequencies domain of the signals.

Table B.3: Configuration parameters for the multi-channel amplifier type 5070.

	$X-Force$ Channel 1	$Y-Force$ Channel 2	$Z-Force$ Channel 3
Sensitivity (pC/N)	-7.4	-7.5	-3.7
High Pass Filter	DC(Long)	DC(Long)	DC(Long)
Low pass filter	OFF	OFF	OFF
Range (N)	3000	3000	3000
Scale (N/V)	300	300	300

Table B.4: Cutting conditions for the experiments 07, 10, 25 and 17 (second replicate).

	Cutting Conditions			
Variable	Exp-07	Exp-10	Exp-25	Exp-17
f_z mm/tooth	0.05	0.1	0.075	0.025
V_c m/min	905	565.5	678.8	678.6
n rpm	18000	18000	18000	18000
a_e mm	4	2	3	3
HB HBN	$94, 90, 89, 90$	$138, 132, 144, 140$	$110, 111, 111, 110$	$111, 110, 110, 110$
D_{Tool} mm	16	10	12	12
Geometry path	Convex	Convex	Concave	Straight

B.5.2 Acoustic Emission signals

Several tests were done to determine the correct sampling rate for the acoustic emission (*AE*). Figures B.5, B.6, B.7, and B.8 show the power spectral density in the frequency domain of the *AEs* signals at different cutting tool wear conditions.

B.5.3 MFCC computed for the process state variables

Figure B.9 shows the *MFCC* computed for different cutting tool conditions and the process state variable: cutting force in Fy direction. Figure B.10 depicts the *MFCC* computed for the different cutting tool conditions (New, half-new, half-worn, and worn), the process state signal is the acoustic emission signal (fixed under the workpiece), and the experiment number 08.

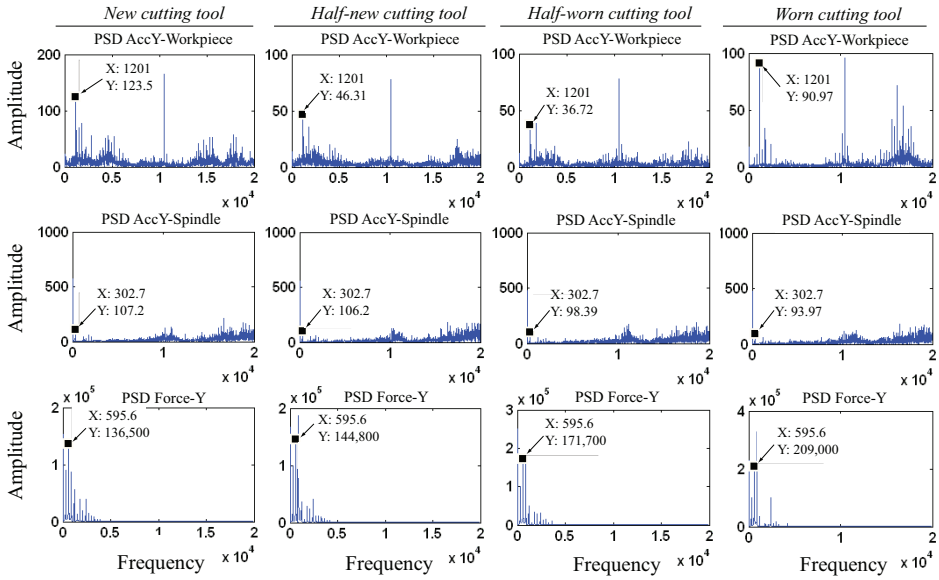

Figure B.1: Frequency domain of specific signals for the experiment number 07, with convex geometry and the four states of the cutting tool condition.

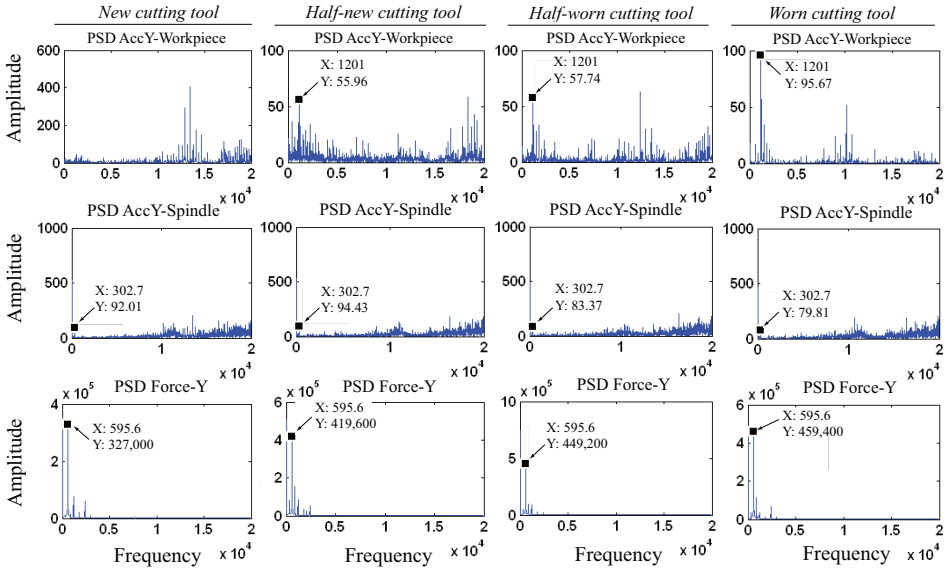

Figure B.2: Frequency domain of specific signals for the experiment number 10, with convex geometry and the four states of the cutting tool condition.

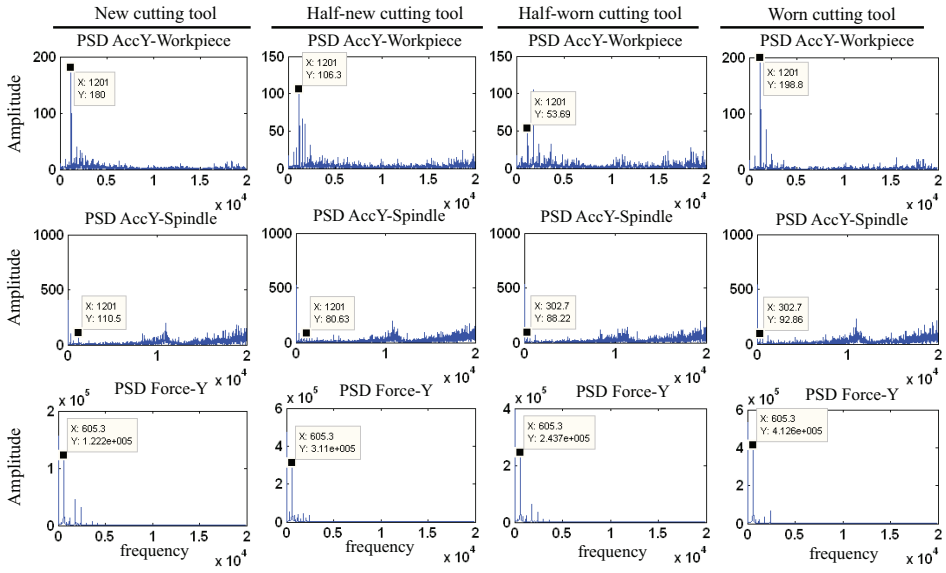

Figure B.3: Frequency domain of specific signals for the experiment number 25, with concave geometry and the four states of the cutting tool condition.

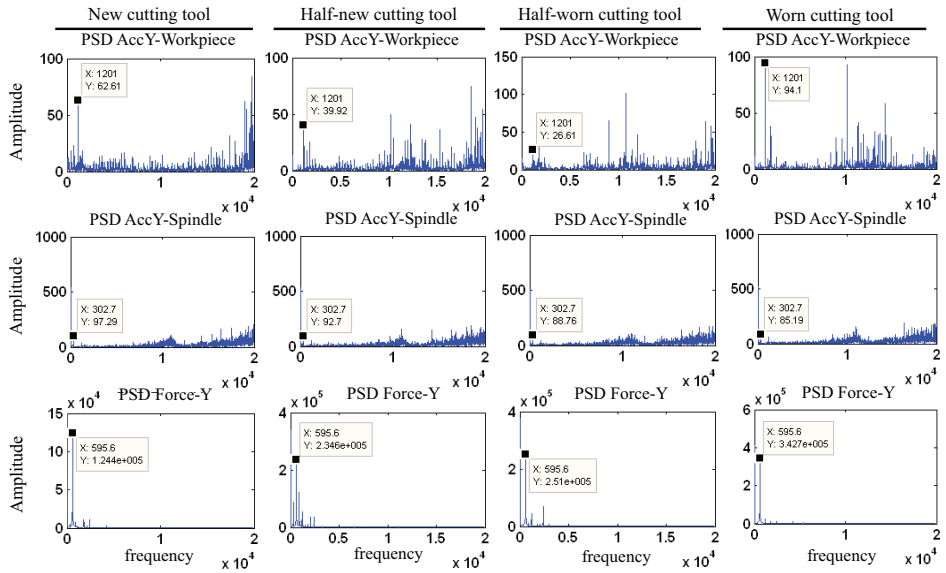

Figure B.4: Frequency domain of specific signals for the experiment number 17, with straight geometry and the four states of the cutting tool condition.

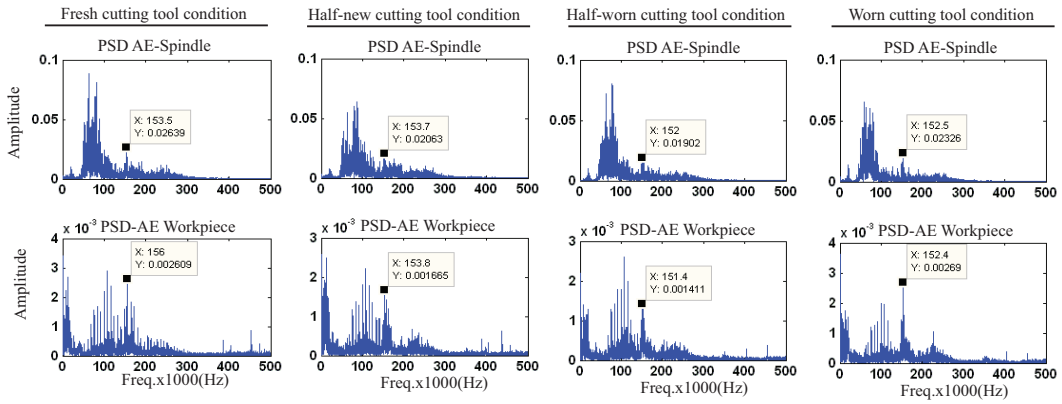

Figure B.5: Experiment number 07. Power spectral density for the *AE* signals and different cutting tool conditions.

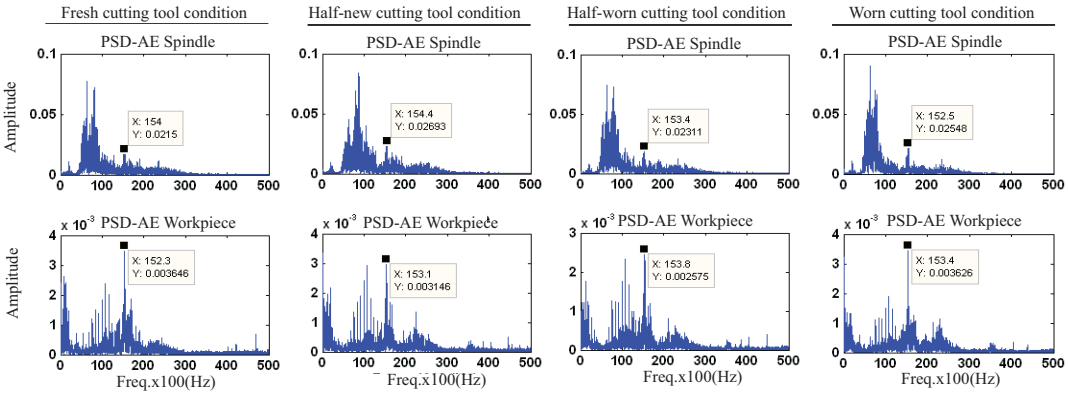

Figure B.6: Experiment number 10. Power spectral density for the *AE* signals and different cutting tool conditions.

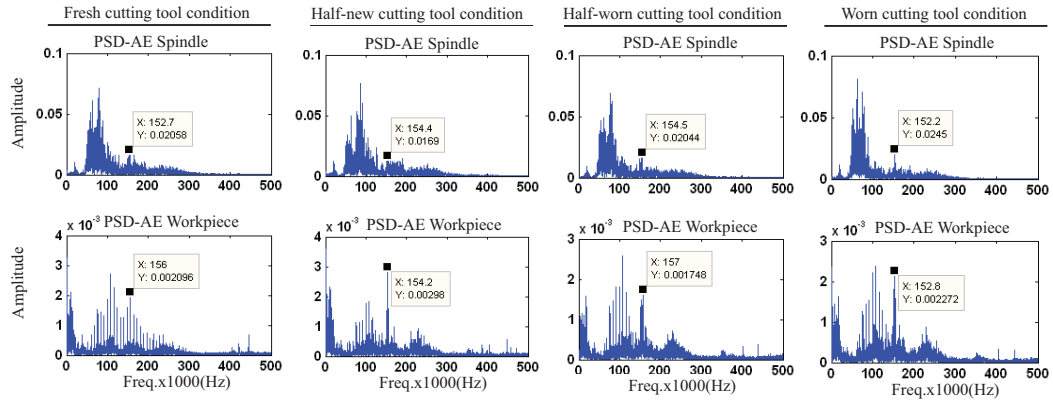

Figure B.7: Experiment number 25. Power spectral density for the *AE* signals and different cutting tool conditions.

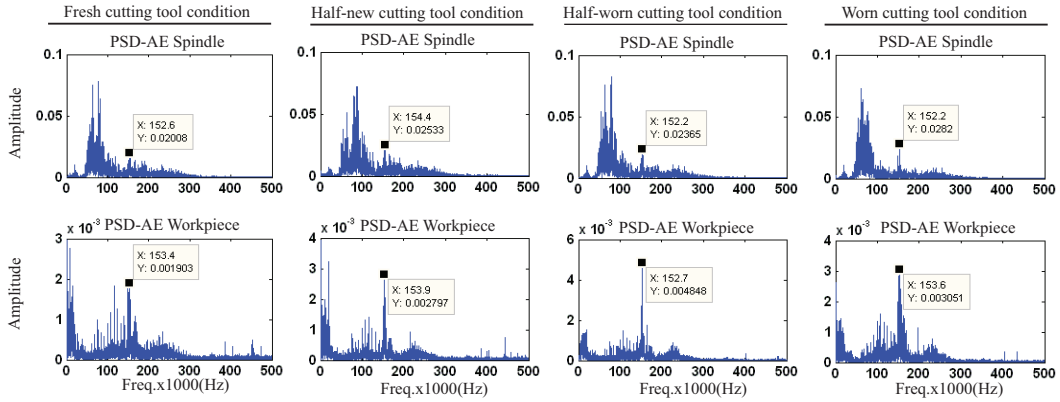

Figure B.8: Experiment number 17. Power spectral density for the *AE* signals and different cutting tool conditions.

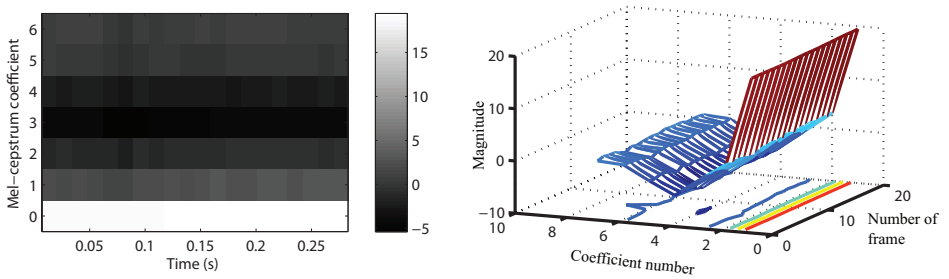

(a) New cutting tool condition

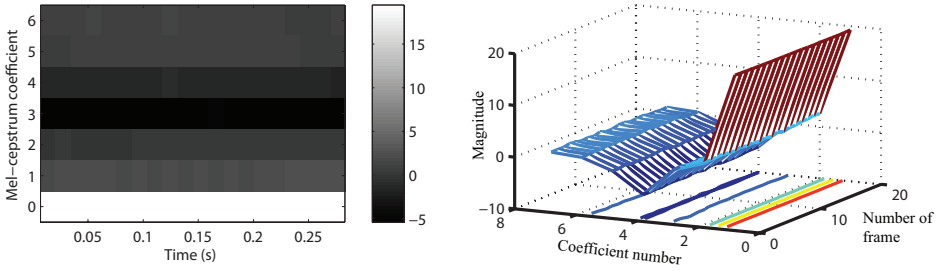

(b) Half-New cutting tool condition

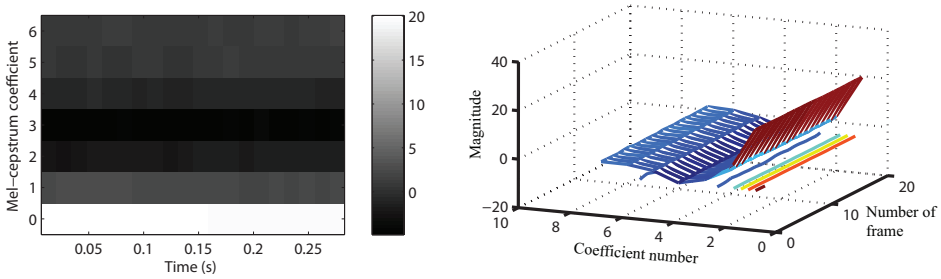

(c) Half-Worn cutting tool condition

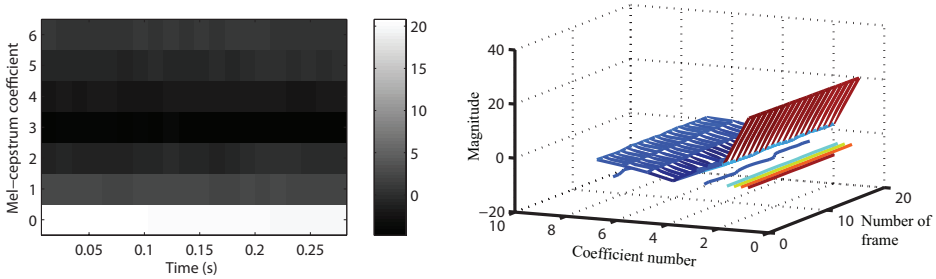

(d) Worn cutting tool condition

Figure B.9: *MFCC* computed from the cutting force (F_y) process signal and the cutting conditions correspond to the experiment number 01. The parameters and configuration were: Hamming window, 6 coefficients, log energy, and 40 filters.

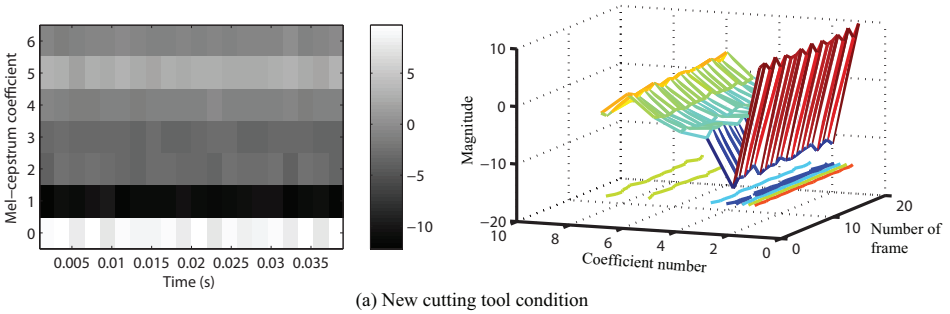

(a) New cutting tool condition

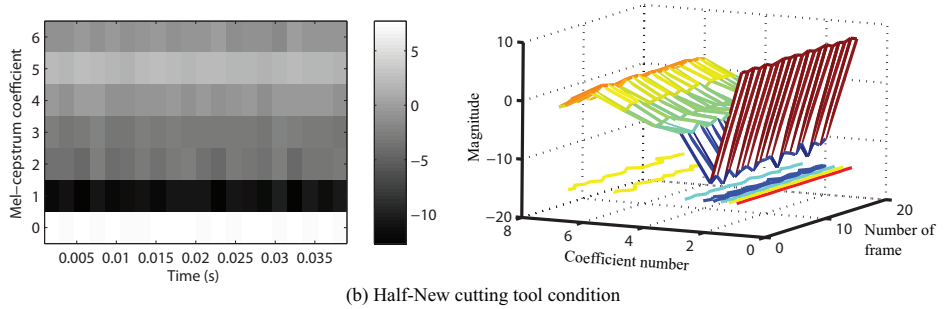

(b) Half-New cutting tool condition

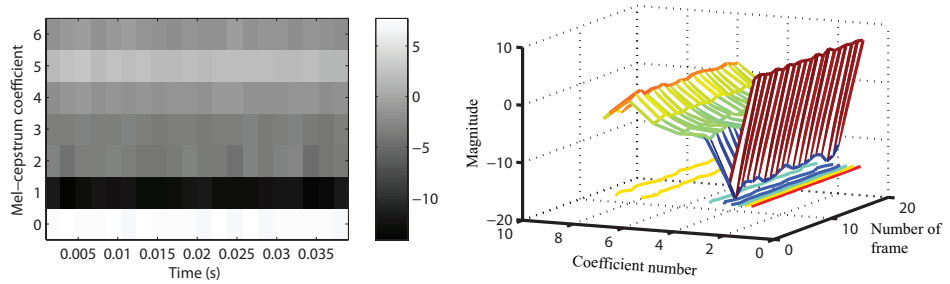

(c) Half-Worn cutting tool condition

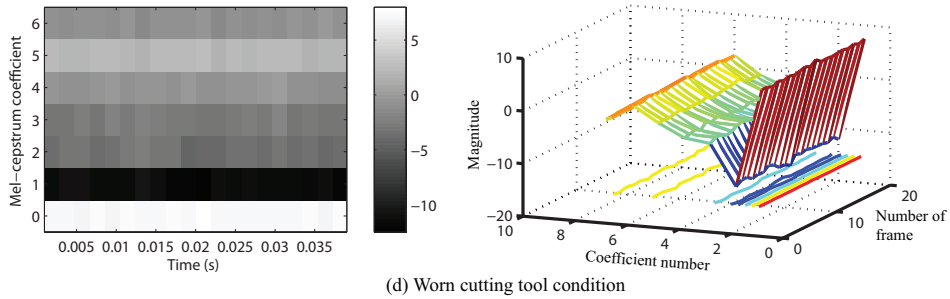

(d) Worn cutting tool condition

Figure B.10: *MFCC* computed from the acoustic emission (AE workpiece) process signal and the cutting conditions correspond to the experiment number 08. The parameters and configuration were: Hamming window, 6 coefficients, log energy, and 40 filters.

Appendix C

Aluminium Alloys

This appendix presents the characteristics, applications, and the chemical composition of the different aluminium alloys that were used in the design of experiments.

Aluminium 5083-H111	
Key words:	EN-AW-$5083-H111$; Aluminium $5083-H111$
Main characteristics:	Good machinability, and excellent for extrusion processes. Compared with other aluminium alloys its weight is low.
Applications:	Extrusions are produced in the conventional flat bar, bulb angle, angle, and tee sections.
Chemical composition:	$Al = 92.4 - 95.6\%$, $Cr = 0.103\%$, $Cu = 0.018\%$, $Fe \leq 0.3\%$, $Mg = 4.549\%$, $Mn = 0.578\%$, $Si = 0.106\%$, $Ti = 0.025\%$, $Zn = 0.004\%$, $Ni = 0.004\%$
Mechanical properties:	Important mechanical properties are: 70 BHN, ultimate tensile strength 275 MPa, tensile yield strength 165 MPa, and elastic module 71×10^3 MPa
Thermal properties:	The thermal conductivity is 117 $W/m-K$

Aluminium 6082-T6	
Key words:	EN-AW-6082, AlSi1MgMn; Aluminium $6082-T6$; SS-EN-AW-6082.
Main characteristics:	Effectively prevents the corrosion of acid, alkali and salt. Suitable for multi-purpose applications.
Applications:	Extrusions are produced in flat bar, bulb angle, angle, and tee sections.
Chemical composition:	$Al = 95.2 - 98.3\%$, $Cr \leq 0.25\%$, $Cu =\leq 0.1\%$, $Fe \leq 0.5\%$, $Mg = 0.4 - 1.2\%$, $Mn = 1.\%$, $Si = 0.7 - 1.3\%$, max $Ti = 0.1\%$, max $Zn = 0.2\%$
Mechanical properties:	Important mechanical properties are: 90 BHN, ultimate tensile strength $290 - 310$ MPa, and tensile yield strength $250 - 260$ MPa.
Thermal properties:	The thermal conductivity is 170 $W/m - K$.

Aluminium 2024-T3	
Key words:	Aluminium $2024 - T3$; UNS $A92024$; ISO AlCu4Mg1; DIN ALCuMg2; ASME $SB211$.
Main characteristics:	Good machinability, surface finish capabilities, a high strength material of adequate workability.
Applications:	Aircraft fittings, gears and shafts, bolts, clock parts, computers parts, couplings, fuse parts, hydraulic valve bodies, missile parts, munitions, nuts, pistons, rectifier parts, worm gears, fastening devices, orthopedic equipment, and structures.
Chemical composition:	$Al = 90.7 - 94.7\%$, $Cr \leq 0.1\%$, $Cu = 3.8 - 4.9\%$, $Fe \leq 0.5\%$, $Mg = 1.2 - 1.8\%$, $Mn = 0.3 - 0.9\%$, $Si \leq 0.5\%$, $Ti \leq 0.15\%$, $Zn = 2.5\%$
Mechanical properties:	Important mechanical properties are: 120 Brinell Hardness Number, ultimate tensile strength 483 MPa, tensile yield strength 345 MPa, module of elasticity 73.1 GPa, and 70% of machinability.
Thermal properties:	The thermal conductivity is 121 $W/m - K$, and melting point $502 - 638^oC$.

CERTAL Aluminium	
Key words:	CERTAL, Aluminium 7022; EN AW-7022; ISO AlZn5Mg3Cu.
Main characteristics:	Excellent machinability, stability in the form, and high strength.
Applications:	Industrial tools, molds for producing injection molded plastic parts, and some mechanical structures.
Chemical composition:	$Al = 88 - 92.4\%$, $Cr = 0.1 - 0.3\%$, $Cu = 0.5 - 1.0\%$, $Fe \leq 0.5\%$, $Mg = 2.6 - 3.7\%$, $Mn = 0.1 - 0.4\%$, $Si \leq 0.5\%$, $Ti + Zr \leq 0.2\%$, $Zn \leq 2.0\%$
Mechanical properties:	Important mechanical properties are: 140 BHN, ultimate tensile strength 460 MPa, and tensile yield strength 340 MPa.
Thermal properties:	The thermal conductivity is $120 - 150$ $W/m - K$.

Aluminium 7075-T6	
Key words:	Aluminium $7075-T6$; UNS $A97075$; ISO AlZn5.5MgCu; AA7075-T6.
Main characteristics:	High strength material used for highly stressed structural parts.
Applications:	Aircraft fittings, gears and shafts, fuse parts, meter shafts and gears, missile parts, regulating valve parts, worm gears, keys, aircraft, aerospace and defense applications, bike frames, and all terrain vehicle sprockets.
Chemical composition:	$Al = 87.1-91.4\%$, $Cr = 0.18-0.28\%$, $Cu = 1.2-2.0\%$, $Fe \leq 0.5\%$, $Mg = 2.1-2.9\%$, $Mn \leq 0.3\%$, $Si \leq 0.4\%$, $Ti \leq 0.2\%$, $Zn = 5.1-6.1\%$
Mechanical properties:	Important mechanical properties are: 150 BHN, ultimate tensile strength 572 MPa, tensile yield strength 503 MPa, modulus of elasticity 71.7 GPa, and 70% of machinability.
Thermal properties:	The thermal conductivity is 130 W/m-K, and melting point $477-635^{o}C$.

Appendix D

Measurement of R_a, flank wear and run-out

D.1 Procedure to measure R_a

The quality of machined surface is characterized by the accuracy of its manufacture with respect to the dimensions specified by the designer. Every machining operation leaves characteristic evidence on the machined surface, and it is in the form of finely spaced micro irregularities left by the cutting tool. Therefore, measuring surface roughness is vital to quality control of machining workpiece. The concept of R_a was defined in chapter 2 with the different factors affecting its value. This section defines the parameters which allow to characterize the R_a, and the recommended methodology for measuring these parameters. The measurement of the R_a is supported by the norms [ISO 4287:1997(E/F), 1997], and [ISO 4288:1996(E), 1996].

D.2 Surface profile parameters definitions

The surface roughness can be measured in different ways, and they are classified into three basic categories:

- *Statistical descriptors* that give average behavior of the surface height. For example, average roughness R_a; the root mean square roughness R_q; the skewness S_k and the kurtosis K.
- *Extreme value descriptors* that depend on isolated events. Examples are the maximum peak height R_p, the maximum valley height R_v, and the maximum peak to valley height R_{max}.
- *Texture descriptors* that describe variations of the surface based on multiple events. An example for this descriptor is the correlation length.

The profile parameters that allow the characterization of the R_a are the following:

1. R_z is the sum of height of the largest profile peak height Z_p and the largest profile valley depth Z_v within a sampling length.

2. R_t is the sum of the height of the largest profile peak height Z_p and the largest profile valley depth Z_v within the evaluation length. Since R_t is defined over the evaluation length, the following will always be true: $R_t \geq R_z$.

3. R_a is the arithmetical mean of the absolute ordinate values $Z(x)$ within a sampling length,

$$R_a = \frac{1}{l} \int_0^l |Z(x)| dx \tag{D.1}$$

4. R_q is the root mean square value of the ordinate values $Z(x)$ within a sampling length,

$$R_q = \sqrt{\frac{1}{l} \int_0^l Z^2(x) dx} \tag{D.2}$$

5. RSm is the mean value of the profile element widths Xs within a sampling length,

$$RSm = \frac{1}{m} \sum_{i=1}^{m} Xs_i \tag{D.3}$$

D.3 Methodology for assessment the surface texture

Surface texture parameters are not useful for the description of surface defects. Therefore, surface defects, e.g. scratches and pores, shall not be considered during inspection of surface texture. To decide whether or not a workpiece surface is in accordance with specification, a set of single values of the surface texture parameter, each determined from an evaluation length, shall be used. The assessment of the surface roughness of machined workpieces can be carried out by means of different measurement techniques. In this work, a direct method will be used by means of stylus type device. The equipment used for measuring the surface roughness was a portable Surfcom type $130A$, and it is depicted in Figure D.1. The methodology for the assessment of the surface texture is in agreement with [ISO 4287:1997(E/F), 1997].

D.3.1 Parameter estimation

Several parameters must be defined to measure surface roughness directly on the machined surface. First, an *estimate of the parameter's value* is calculated using the measured data from only one sampling length. An *average parameter estimate* is calculated by taking the arithmetic mean of the parameter estimates from all the individual sampling lengths. The standard number of sampling lengths is five for roughness profile parameters. For parameters defined over the evaluation length, an *estimate of parameter's value* is calculated from an evaluation length.

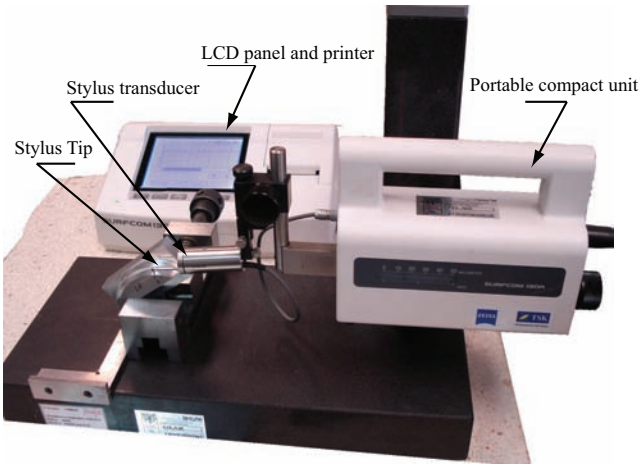

Figure D.1: Main parts of the portable Surfcom type $130A$.

D.3.2 Evaluation length and measurement of the roughness profile parameters

When the direction of measurement is not specified, the workpiece shall be positioned so that direction of section corresponds to the maximum values of height of the roughness parameters (R_a, and R_z). Measurements shall be carried out on that part of the surface on which critical values can be expected; this can be assessed by visual examination. Separate measurements shall be distributed equally over the part of the surface to obtain independent measurements results. Figure D.2a shows three different patterns over the machined surface for measuring the parameter values. Figure D.2b defines the selected central section for measuring the surface roughness.

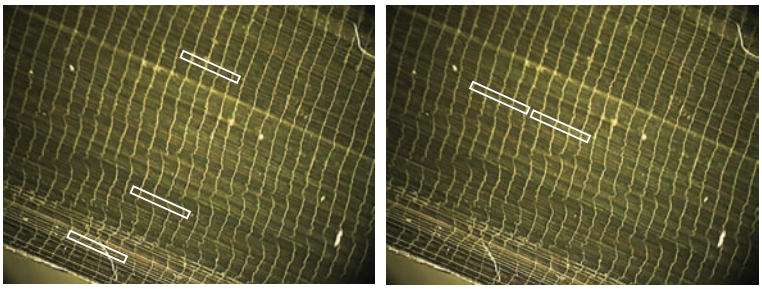

Figure D.2: Identification of the proposal areas for assessment the profile parameters. a) Different patterns identified over the machined surface; b) Specific place for measuring the surface roughness with two evaluation lengths.

The surface texture of the workpiece under inspection can appear homogeneous or be quite different over various areas. In areas where the surface texture appears homogeneous, parameter values determined over the entire surface

shall be used for comparison with the technical product documentation. If there are separate areas with obviously different surface texture, the parameter values which are determined on each area shall be used separately for comparison with the requirements in the technical product documentation. Now, it is necessary to estimate the size of the sampling length and evaluation length that will be used for the assessment of the roughness profile parameters. First, an estimation of the R_a or R_z values are defined by visual inspection, roughness comparison specimens, or a direct measurement over the machined surface. The sampling length can be selected by using Tables D.1 and D.2 (taken from [ISO 4287:1997(E/F), 1997]). The representative values of R_a and R_z obtained during the first

Table D.1: Roughness sampling lengths for the measurement of R_a for non-periodic profiles.

R_a (μm)	Roughness sampling length (l), mm	Roughness evaluation length (L), mm
$0.006 < R_a \leq 0.02$	0.08	0.4
$0.02 < R_a \leq 0.1$	0.25	1.25
$0.1 < R_a \leq 2$	0.8	4
$2 < R_a \leq 10$	2.5	12.5

Table D.2: Roughness sampling lengths for the measurement of R_z for non-periodic profiles.

R_z (μm)	Roughness sampling length (l), mm	Roughness evaluation length (L), mm
$0.025 < R_a \leq 0.1$	0.08	0.4
$0.1 < R_a \leq 0.5$	0.25	1.25
$0.5 < R_a \leq 10$	0.8	4
$10 < R_a \leq 50$	2.5	12.5

measurements, indicate that the sampling length and evaluation length must be 0.8 and 4 mm respectively. Also, the λ_c profile filter which defines the intersection between the roughness and waviness components must be equal to the sampling length (0.8). With these information, the procedure to assess the surface roughness is the following:

1. Define the area where the surface roughness will be measure. Figure D.2b shows that central section of the machined surface presents the best pattern, and this area will be defined for the assessment of R_a.
2. Two evaluation lengths were defined in the central section for the measurements. For each evaluation length, five measurements were made. Therefore, ten values were computed.
3. The measurements were made in two specific areas of the machined surface. Figure D.3 shows the sections for the assessment of the R_a over the machined surface.
4. Five texture parameters were computed for each assessment: R_a, R_q, R_z, R_t, and RSm. Then, an arithmetic mean value (for a specific section) was computed for each parameter by using the ten values.

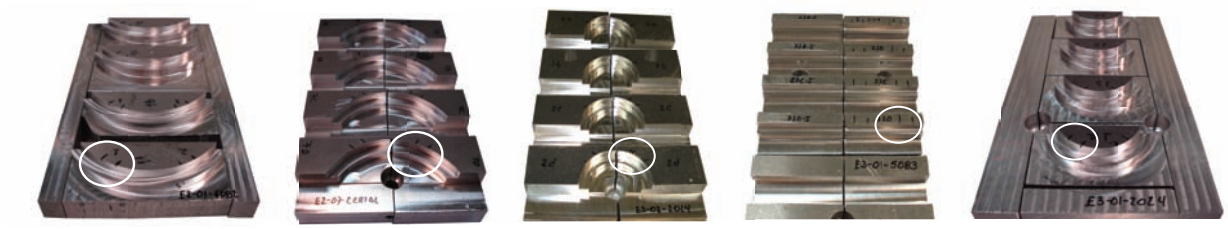

Figure D.3: Identification of the sections for measuring the R_a over the machined surface in the test pieces.

Figure D.4 depicts an example of the measurement made over a machined surface. The measurements results were printed, and recorded in a computer file. Also, a photo was taken of the machined surface.

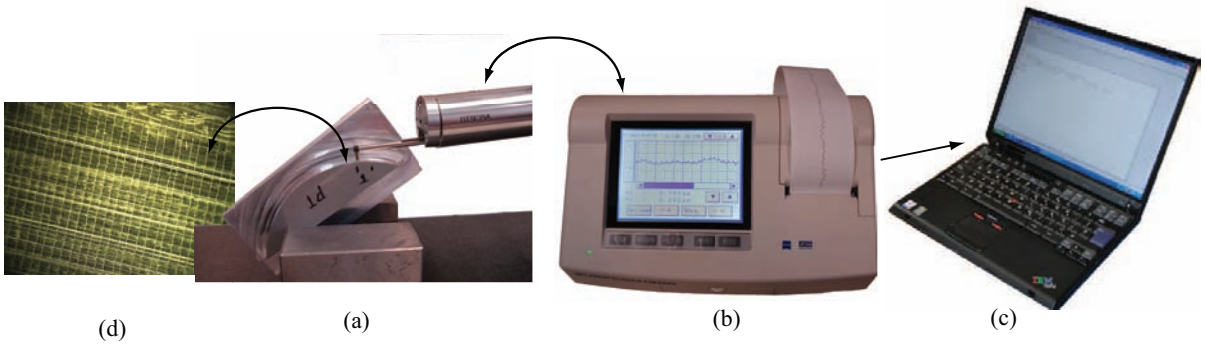

(d) (a) (b) (c)

Figure D.4: Assessment of the surface roughness: (a) Measurement with the stylus tip of the Surfcom $130A$; (b) Register and printer of the information; (c) Storage of the information; (d) and taking of the photo of the machined surface.

D.4 Measurement of the flank wear and run-out

The flank wear of the cutting tool was measured by using a stereoscopic microscope, a digital camera, and the Motic Images software. Figure D.5 shows the complete equipment used for the measurement of the flank wear. The optical characteristics of stereoscopic microscope can be defined as follows: the optical lenses allow a magnification of $20x$, the objective lens a magnification of $2x$, and a manual magnification control of $4x$. The digital camera is fixed over an ocular lens with a magnification of $10x$. All images were taken with a magnification of $40x$, and the software was calibrated to measure the flank wear with this magnification scale. The evolution of the flank wear in the 10 mm cutting tool is shown in Figure D.6.

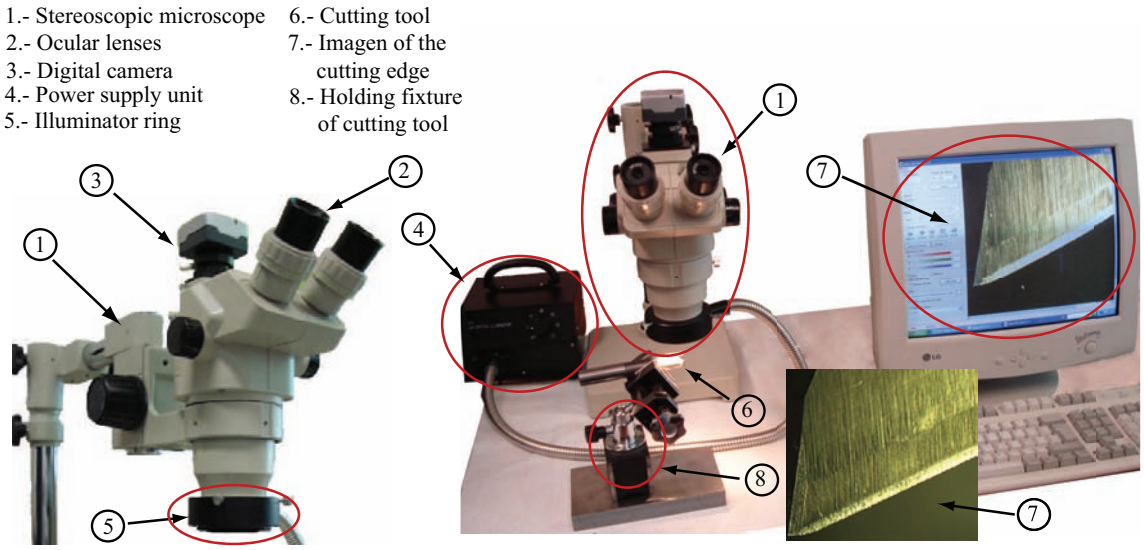

Figure D.5: Equipment for measuring the flank wear of the cutting edge.

The runout of the cutter edges was checked at the beginning of the experimentation. The recommended runout shall not exceed of 0.05 mm for the radial runout condition. Figure D.7 depicts the dial used to assess the radial runout for each cutting tool. Table D.3 presents the radial runout measured for all cutting tool edges. These values were measured during all the cutting tool life, and it is observed that never the limit value (0.05 mm) was exceeded.

Table D.3: Assessment of the radial runout of the cutting tool edges. The radial runout was measured in millimeter.

Tool diameter (mm)	New	Half-new	Half-worn	Worn
8	0.001	0.0098	0.0175	0.0006
10	0.001	0.0107	0.008	0.0073
12	0.01	0.005	0.0135	0.006
16	0.011	0.0017	0.0	0.002
20	0.012	0.0123	0.02	0.02

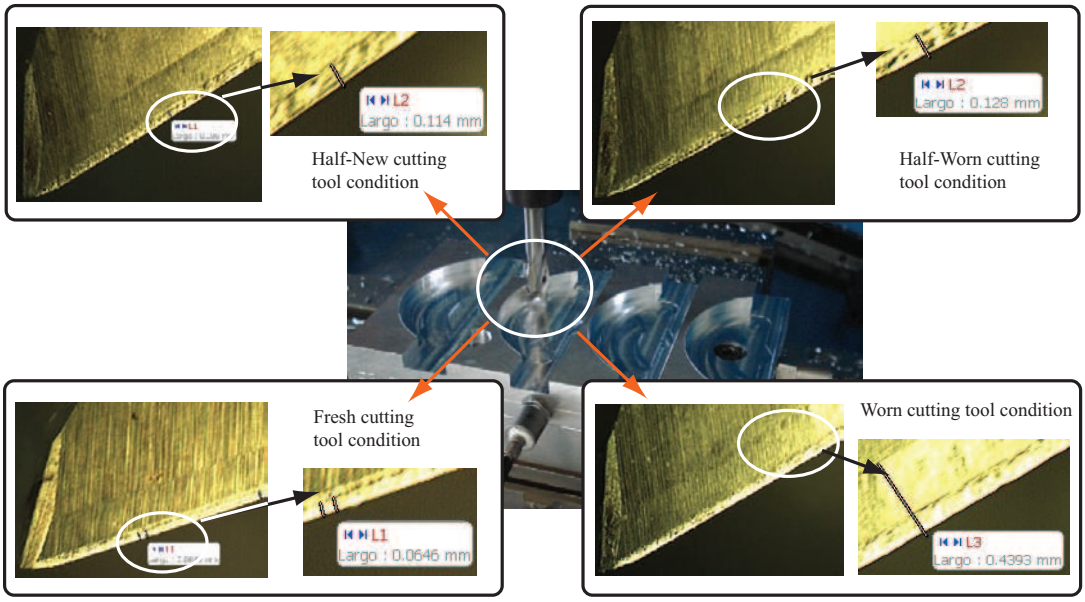

Figure D.6: Evolution of the flank wear for the 10 mm cutting tool.

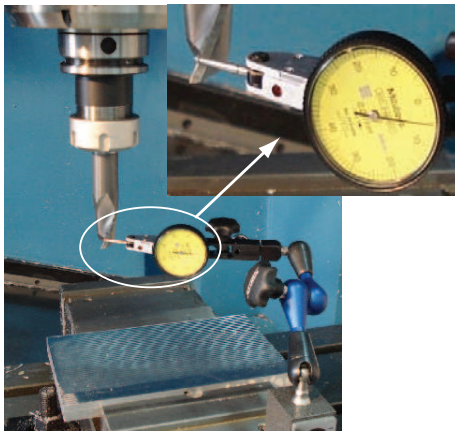

Figure D.7: Assessment of the radial runout of the cutter edges. The cutting tool diameter is 20 mm.

Appendix E

Statistical analysis of the screening factorial design

Fractional factorial design was defined by using MINITAB software. Using MINITAB, the design of experiments was computed by considering eight factors, two levels, $1/8$ fraction, 32 runs, and zero center points. From the experimental results, the next step is to apply an Analysis Of Variance (*ANOVA*). The initial part of this procedure was defined in Chapter 4. Therefore, this appendix presents the results obtained for the refined model. In Chapter 4 was developed the procedure to eliminate the v_c factor, and the next step is to apply the *ANOVA* for refining the model. The results are shown in Table E.1, and E.2.

From the main effects plot was deduced that ap factor does not show a correlation with D_{tool}, ae and HB factors. Therefore, the ap factor will be eliminated with its interactions, and then the ANOVA is applied to compute the effects over R_a. The results are show in Table E.3, and E.4.

From Figure E.1 can be observed that D_{tool} and ae show minimum effect over R_a and they can be eliminated. These factors will be eliminated with its interactions, and once again, the ANOVA is applied to compute the effects over R_a. The results are show in Table E.5, and E.6.

From Table E.6, it is observed that the elimination of D_{tool} and ae factors present a negative impact over the R_a prediction, and the lack of fit presents a low value of the F statistical and a high value of the $p - value$ (the hypothesis is not accepted). For this reason, these factors and their interactions can not be eliminated, because they are important to estimate the R_a value.

Finally, the factors and interactions that are not relevant must be eliminated and by using the *ANOVA* demonstrates that data do not lost the precision for computing the estimated R_a value.

Table E.1: Estimated effects and coefficients for R_a with v_c eliminated (coded units).

Term	Effect	Coef	SE Coef	T	$p-value$
Constant		0.29330	0.004794	61.18	0.000
f_z	0.19675	0.09838	0.004794	20.52	0.000
ap	0.04668	0.02334	0.004794	4.87	0.000
D_{tool}	-0.00603	-0.00302	0.004794	-0.63	0.530
ae	0.00761	0.00380	0.004794	0.79	0.429
HB	-0.06519	-0.03259	0.004794	-6.80	0.000
R	-0.05899	-0.02950	0.004794	-6.15	0.000
I/C	0.10250	0.05125	0.004794	10.69	0.000
$f_z * ap$	0.03919	0.01960	0.004794	4.09	0.000
$f_z * D_{tool}$	0.04539	0.02269	0.004794	4.73	0.000
$f_z * HB$	-0.02576	-0.01288	0.004794	-2.69	0.008
$ap * R$	-0.07208	-0.03604	0.004794	-7.52	0.000
$ap * I/C$	0.01372	0.00686	0.004794	1.43	0.156
$D_{tool} * I/C$	0.04382	0.02191	0.004794	4.57	0.000
$ae * HB$	0.06747	0.03373	0.004794	7.04	0.000
$ae * R$	0.01344	0.00672	0.004794	1.40	0.164
$ae * I/C$	-0.05727	-0.02864	0.004794	-5.97	0.000
$HB * I/C$	-0.02685	-0.01343	0.004794	-2.80	0.006
$R * I/C$	-0.07456	-0.03728	0.004794	-7.78	0.000

Table E.2: Analysis of Variance for R_a with V_c eliminated (coded units).

Source	DF	Seq SS	Adj SS	Adj MS	F	P
Main Effects	7	1.95698	1.68099	0.240141	87.90	0.000
2-Way Interactions	11	0.74955	0.74955	0.068141	24.94	0.000
Residual Error	105	0.28685	0.28685	0.002732		
Lack of fit	12	0.25695	0.25695	0.021413	66.61	0.000
Pure Error	93	0.02990	0.02990	0.000321		
Total	123	2.99337				

Table E.3: Estimated effects and coefficients for R_a with ap eliminated (coded units).

Term	Effect	Coef	SE Coef	T	P
Constant		0.29249	0.006615	44.22	0.000
f_z	0.19514	0.09757	0.006615	14.75	0.000
D_{tool}	-0.00442	-0.00221	0.006615	-0.33	0.739
ae	0.00599	0.00300	0.006615	0.45	0.652
HB	-0.06357	-0.03178	0.006615	-4.81	0.000
R	-0.06061	-0.03030	0.006615	-4.58	0.000
I/C	0.10088	0.05044	0.006615	7.63	0.000
$f_z * D_{tool}$	0.04701	0.02350	0.006615	3.55	0.001
$f_z * HB$	-0.02414	-0.01207	0.006615	-1.82	0.071
$D_{tool} * I/C$	0.04544	0.02272	0.006615	3.43	0.001
$ae * HB$	0.06908	0.03454	0.006615	5.22	0.000
$ae * R$	0.01183	0.00591	0.006615	0.89	0.373
$ae * I/C$	-0.05889	-0.02945	0.006615	-4.45	0.000
$HB * I/C$	-0.02524	-0.01262	0.006615	-1.91	0.059
$R * I/C$	-0.07617	-0.03809	0.006615	-5.76	0.000

Table E.4: Analysis of Variance for R_a with ap eliminated (coded units).

Source	DF	Seq SS	Adj SS	Adj MS	F	$p - value$
Main Effects	6	1.85805	1.65960	0.276600	52.29	0.000
2-Way Interactions	8	0.55875	0.55875	0.069844	13.20	0.000
Residual Error	109	0.57657	0.57657	0.005290		
Lack of fit	16	0.54668	0.54668	0.034167	106.28	0.000
Pure Error	93	0.02990	0.02990	0.000321		
Total	123	2.99337				

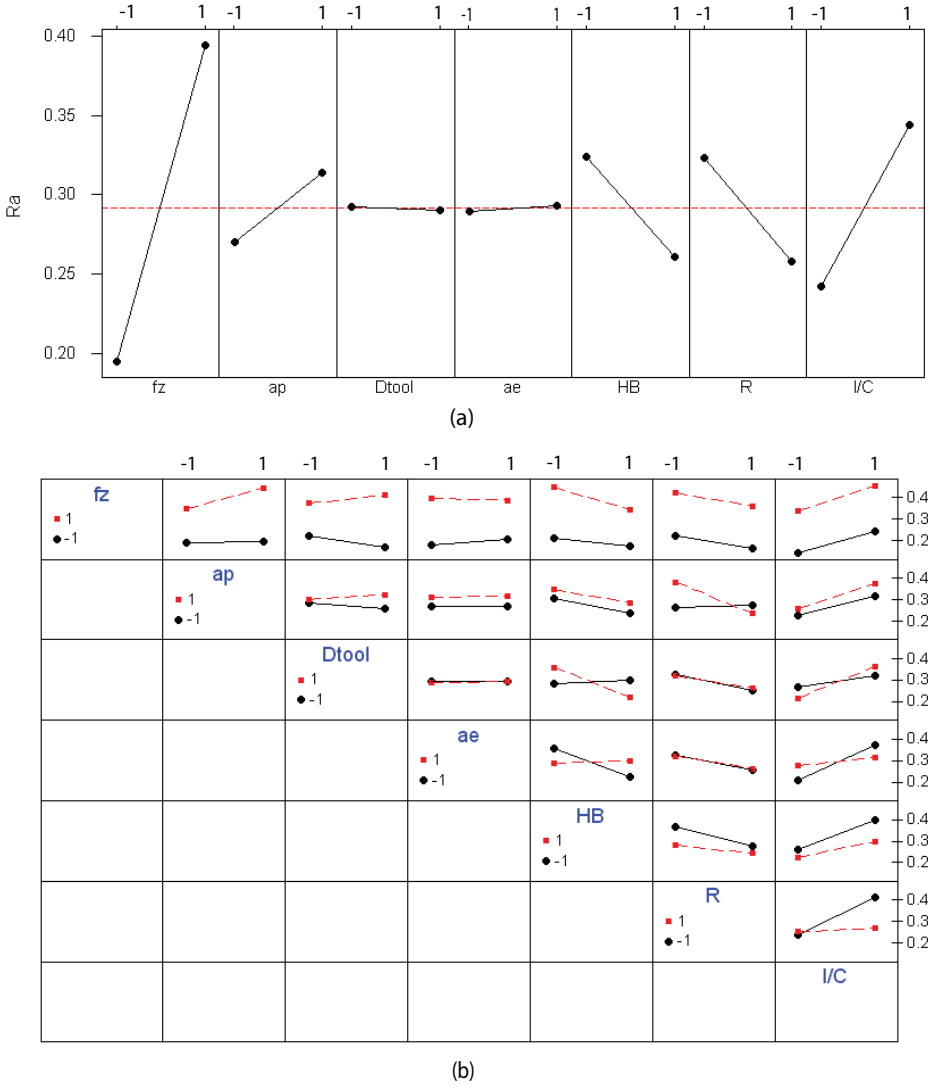

Figure E.1: (a)The seven factors considered with the main effects plot for R_a. (b) Interactions plot for R_a.

Table E.5: Estimated effects and coefficients for R_a with D_{tool} and ae eliminated (coded units).

Term	Effect	Coef	SE Coef	T	P
Constant		0.29662	0.008082	36.70	0.000
fz	0.20339	0.10170	0.008082	12.58	0.000
HB	-0.07183	-0.03591	0.008082	-4.81	0.000
R	-0.05235	-0.02618	0.008082	-3.24	0.002
I/C	0.10914	0.05457	0.008082	6.75	0.000
$fz * HB$	-0.03240	-0.01620	0.008082	-2.00	0.047
$HB * I/C$	-0.03349	-0.01675	0.008082	-2.07	0.040
$R * I/C$	-0.06792	-0.03396	0.008082	-4.20	0.000

Table E.6: Analysis of Variance for R_a with D_{tool} and ae eliminated (coded units).

Source	DF	Seq SS	Adj SS	Adj MS	F	P
Main Effects	4	1.84534	1.83176	0.457941	57.06	0.000
2-Way Interactions	3	0.21709	0.21709	0.072362	9.02	0.000
Residual Error	116	0.93094	0.93094	0.008025		
Lack of fit	8	0.07178	0.07178	0.008972	**1.13**	**0.351**
Pure Error	108	0.85916	0.85916	0.007955		
Total	123	2.99337				

Appendix F

Modeling analysis with *RSM*

This Appendix presents the analysis of variance of the computed results in the Response Surface Methodology (*RSM*). The analysis was made for all cutting tool conditions.

F.1 *RSM* for the new cutting tool condition

The *DoE* was made with new cutting tool condition, and the measurements of R_a were made in agreement with the procedure described in chapter 4. Table F.1 presents the four parameters that were measured to characterize the R_a for each test piece. Using the results of the experimentation with the new cutting tool condition, the next step was to apply an *ANOVA* by considering the four replicates. The following considerations were evaluated:

- The effects due to the several factor combinations.
- The percentage contribution of each factor, denoted by statistical "F" factor. This factor reflects the portion of the total variation observed in an experiment attributed to each factor.
- The factors, and their combinations with a $p - value < 0.05$ (i.e., the hypothesis is true and the effect of the factor is representative).

The *ANOVA* results are shown in Table F.2, where the variability of Ra is explained by the model with $R^2 = 90.6\%$ and the estimated parameters of model are significant in $R^2_{adj} = 89.5\%$. From this table, the factors with a $p - value < 0.05$ were selected to fit the final model. After to select only the relevant factors, the analysis of variance was applied to confirm an acceptable squared error $R^2 = 0.8858$ and adjusted squared error $R^2_{adj} = 0.876$. The final fitted model is given by

$$\begin{aligned} R_a \;=\; & 0.1139 + 0.06513 \times fz + 0.01913 \times fz^2 - 0.0808 \times D_{tool} + 0.04961 \times D^2_{tool} + 0.00896 \times HB^2 - \\ & - 0.0437 \times fz \times D_{tool} - 0.0138 \times fz \times HB + 0.01647 \times D_{tool} \times HB + \\ & + 0.01185 \times ae \times Curv + 0.00937 \times Curv^2 \end{aligned} \tag{F.1}$$

Table F.1: Values of the considered factors for the experiments, and the measurements of the parameters that allow to characterize the R_a for the sections. The cutting tool condition is sharp edge.

						Section 01				Section 02			
Exp	f_z	D_{tool}	ae	HB	$Curv$	R_a	RSm	R_q	R_z	R_a	RSm	R_q	R_z
1	0.050	10	2	93	0.025	0.115	152.6	0.142	0.70	0.147	157.9	0.184	0.91
2	0.100	10	2	93	−0.025	0.448	226.2	0.531	2.19	0.525	219.2	0.624	2.54
3	0.050	16	2	93	−0.025	0.126	275.0	0.155	0.70	0.104	271.8	0.128	0.65
4	0.100	16	2	93	0.025	0.190	226.2	0.228	1.02	0.230	309.4	0.273	1.16
5	0.050	10	4	94	−0.025	0.191	146.6	0.229	1.19	0.179	140.6	0.229	1.19
6	0.100	10	4	94	0.025	0.524	181.5	0.632	2.82	0.464	218.4	0.567	2.71
7	0.050	16	4	94	0.025	0.118	172.5	0.148	0.69	0.125	239.1	0.160	0.86
8	0.100	16	4	94	−0.025	0.224	350.8	0.264	1.15	0.155	261.9	0.190	0.96
9	0.050	10	2	136	−0.025	0.111	158.4	0.147	0.79	0.117	157.9	0.159	0.94
10	0.100	10	2	138	0.025	0.312	201.4	0.395	1.84	0.299	221.6	0.382	1.71
11	0.050	16	2	138	0.025	0.125	248.3	0.157	0.76	0.126	142.1	0.158	0.80
12	0.100	16	2	136	−0.025	0.160	224.8	0.202	1.03	0.140	229.4	0.177	0.88
13	0.050	10	4	134	0.025	0.145	122.9	0.190	0.98	0.165	92.1	0.215	1.19
14	0.100	10	4	135	−0.025	0.351	184.9	0.467	2.45	0.309	208.4	0.423	2.21
15	0.050	16	4	135	−0.025	0.094	201.6	0.122	0.65	0.077	120.1	0.113	1.02
16	0.100	16	4	134	0.025	0.149	213.9	0.195	1.02	0.154	193.0	0.208	1.06
17	0.025	12	3	111	0.000	0.097	188.8	0.121	0.64	0.088	335.2	0.113	0.65
18	0.130	12	3	111	0.000	0.320	232.7	0.399	1.75	0.365	265.9	0.452	2.00
19	0.075	8	3	110	0.000	0.414	184.6	0.497	2.04	0.526	190.1	0.069	0.26
20	0.075	20	3	110	0.000	0.163	271.3	0.198	0.87	0.148	240.7	0.184	0.81
21	0.075	12	1	111	0.000	0.156	227.7	0.193	0.98	0.129	215.9	0.165	0.86
22	0.075	12	5	111	0.000	0.142	177.2	0.178	0.95	0.156	226.9	0.204	1.06
23	0.075	12	3	70	0.000	0.172	193.3	0.215	1.18	0.195	239.2	0.241	1.30
24	0.075	12	3	154	0.000	0.282	151.2	0.356	1.67	0.404	148.9	0.479	1.91
25	0.075	12	3	110	−0.05	0.247	368.7	0.289	1.17	0.157	232.4	0.187	0.87
26	0.075	12	3	111	0.05	0.138	213.5	0.173	0.96	0.172	211.7	0.214	1.10
27	0.075	12	3	111	0.000	0.125	214.6	0.159	0.78	0.128	167.2	0.160	0.77
28	0.075	12	3	111	0.000	0.145	205.6	0.182	0.90	0.133	183.4	0.167	0.85
29	0.075	12	3	111	0.000	0.125	214.6	0.159	0.78	0.128	167.2	0.160	0.77
30	0.075	12	3	111	0.000	0.145	205.6	0.182	0.90	0.133	183.4	0.167	0.85
31	0.075	12	3	111	0.000	0.125	214.6	0.159	0.78	0.128	167.2	0.160	0.77
32	0.075	12	3	111	0.000	0.145	205.6	0.182	0.90	0.133	183.4	0.167	0.85

Table F.2: Results of the ANOVA analysis: $R^2 = 0.906$, $R^2_{adj} = 0.895$ with 128 runs, and fresh cutting tool condition. Response Surface Regression: R_a versus f_z,D_{tool},ae,HB,$Curv$.

Estimated Regression Coefficients for R_a				
Term	Coef	SE Coef	T	$p-value$
$Constant$	0.1139	0.006802	16.748	0.000
f_z	0.0651	0.003661	17.790	0.000
D_{tool}	-0.0808	0.003978	-20.324	0.000
ae	0.0044	0.003666	1.214	0.227
HB	-0.0244	0.004195	-5.833	0.000
$Curv$	0.00358	0.003667	0.976	0.331
$f_z f_z$	0.01913	0.003086	6.200	0.000
$D_{tool} D_{tool}$	0.04961	0.003585	13.837	0.000
$HB \times HB$	0.00896	0.004133	2.169	0.032
$CurvCurv$	0.00937	0.003380	2.772	0.007
$f_z D_{tool}$	-0.0437	0.004406	-9.940	0.000
$f_z HB$	-0.0138	0.004454	-3.106	0.002
$D_{tool} HB$	0.01647	0.004447	3.704	0.000
$aeCurv$	0.01185	0.004490	2.639	0.010
$S = 0.03592$	$R^2 = 90.6\%$	$R^2(adj) = 89.5\%$		

ANOVA for R_a						
Source	DF	Seq SS	Adj SS	Adj MS	F	$p-value$
Regression	13	1.3627	1.3627	0.10482	81.26	0.000
Linear	5	0.91715	0.9951	0.19903	154.30	0.000
Square	4	0.27667	0.2820	0.07052	54.67	0.000
Interaction	4	0.16888	0.1688	0.04222	32.73	0.000
Residual error	109	0.14060	0.1406	0.00129		
Lack-of-Fit	31	0.11934	0.1193	0.00385	14.12	0.000
Pure Error	78	0.02127	0.0212	0.00027		
Total	122	1.5033				

F.2 Modeling of the R_a with *RSM* and half-new cutting tool condition

The *DoE* was reproduced with the half-new cutting tool condition, and the measurements of R_a were made in agreement with the procedure described in section 1.4 of this chapter. Table F.3 presents the four parameters that were measured to characterize the R_a for each test piece. The values corresponds only to the first replicate. The *RSM* was applied to build the model for the half-new cutting tool condition. Following the same steps described in the previous section, the *ANOVA* results are shown in Table F.4, where the variability of Ra is explained by the model with $R^2 = 90.0\%$ and the estimated parameters of model are significant in $R^2_{adj} = 88.7\%$.

Table F.4 shows the terms with a $p - value < 0.05$, and they were selected to fit the final model. After to select only the relevant factors, the analysis of variance was applied to confirm the squared error $R^2 = 0.90$ and the adjusted squared error $R^2_{adj} = 0.887$. The final fitted model is given by

$$\begin{aligned} R_a \quad = \quad & 0.13829 + 0.0573 \times f_z + 0.01273 \times f_z^2 - 0.08581 \times D_{tool} + 0.03293 \times D_{tool}^2 - 0.0435 \times HB + \\ & + 0.07571 \times HB^2 - 0.0096 Curv + 0.00935 \times ae - 0.02156 \times f_z \times D_{tool} + \\ & + 0.01401 \times fz \times Curv - 0.02427 \times Dtool \times ae + 0.01059 \times Dtool \times HB + \\ & + 0.01281 \times D_{tool} \times Curv + 0.01775 \times HB \times Curv \end{aligned} \tag{F.2}$$

The model was validated in agreement with the results shown in Figure F.1. Figure F.1a. depicts the normal distribution of the residuals and it is observed that enough data were used to fit the model. Also, Figure F.1b. defines the normal probability plot, and the tendency (straight line) shows the normality of the error distribution. Finally, Figure F.1c. shows an excellent spread of points on either side of zero, with no patterns of increase or decrease.

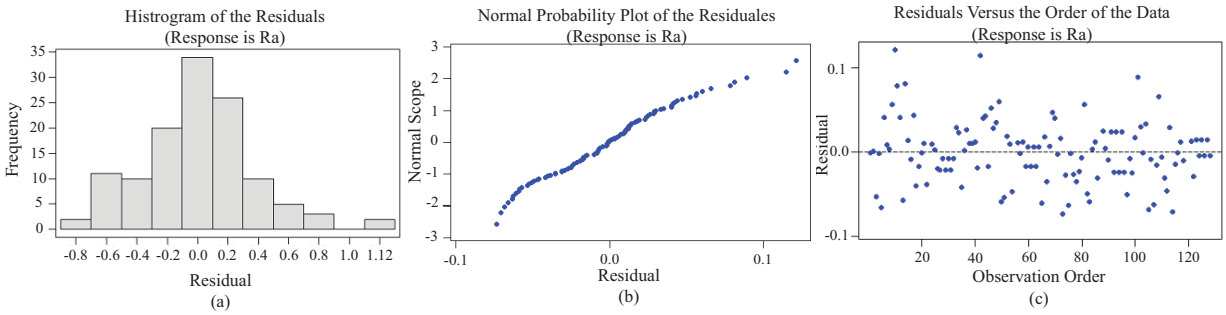

Figure F.1: Validation of the used information to build the Statistical Model by using a half new cutting tool:(a) Normal distribution of the residuals; (b) Normal probability plot; (c) Spread of points.

F.3 Modeling of the R_a with *RSM* and half-worn cutting tool condition

The *DoE* was reproduced with the half-worn cutting tool condition, and the measurements of R_a were made for each test piece. Table F.5 presents the four parameters that were measured for the assessment of the R_a for each

Table F.3: Factors considered for the experiments, and the measurements of the parameters that allow the characterization of the R_a for the two sections. The cutting tool condition is half-new edge.

						Section 01				Section 02			
Exp	f_z	D_{tool}	ae	HB	$Curv$	R_a	RSm	Rq	Rz	R_a	RSm	Rq	Rz
1	0.050	10	2	92	0.025	0.252	126.6	0.311	1.41	0.268	112.7	0.325	1.51
2	0.100	10	2	91	−0.025	0.453	244.3	0.544	2.39	0.494	245.3	0.592	2.56
3	0.050	16	2	91	−0.025	0.167	154.6	0.214	1.32	0.157	134.8	0.198	0.98
4	0.100	16	2	92	0.025	0.280	195.9	0.354	1.71	0.284	186.5	0.359	1.56
5	0.050	10	4	91	−0.025	0.214	175.7	0.258	1.24	0.476	229.1	0.550	2.16
6	0.100	10	4	90	0.025	0.552	212.7	0.654	2.78	0.596	240.0	0.700	2.75
7	0.050	16	4	90	0.025	0.154	177.5	0.193	1.01	0.208	203.7	0.257	1.27
8	0.100	16	4	91	−0.025	0.240	308.7	0.313	1.50	0.225	214.5	0.292	1.36
9	0.050	10	2	133	−0.025	0.254	124.0	0.313	1.38	0.196	125.6	0.252	1.16
10	0.100	10	2	132	0.025	0.470	181.3	0.573	2.34	0.466	182.0	0.561	2.28
11	0.050	16	2	132	0.025	0.196	99.3	0.239	1.14	0.209	89.1	0.251	1.10
12	0.100	16	2	133	−0.025	0.158	236.4	0.197	1.00	0.174	255.4	0.231	1.20
13	0.050	10	4	139	0.025	0.142	111.9	0.185	0.96	0.273	129.0	0.348	1.77
14	0.100	10	4	139	−0.025	0.455	255.4	0.599	2.89	0.483	213.5	0.602	2.58
15	0.050	16	4	139	−0.025	0.090	145.9	0.115	0.63	0.097	179.7	0.126	0.72
16	0.100	16	4	139	0.025	0.206	192.9	0.264	1.41	0.251	179.2	0.321	1.50
17	0.025	12	3	111	0.000	0.153	160.0	0.193	0.93	0.139	128.5	0.179	0.96
18	0.130	12	3	111	0.000	0.333	241.8	0.422	1.91	0.354	251.6	0.441	1.99
19	0.075	8	3	109	0.000	0.358	186.1	0.443	2.16	0.395	189.3	0.468	1.98
20	0.075	20	3	109	0.000	0.126	205.6	0.158	0.75	0.127	227.8	0.162	0.80
21	0.075	12	1	111	0.000	0.153	163.1	0.198	1.03	0.157	163.1	0.200	1.04
22	0.075	12	5	111	0.000	0.170	169.3	0.214	1.16	0.184	160.0	0.238	1.15
23	0.075	12	3	69	0.000	0.286	165.5	0.365	1.84	0.286	168.6	0.363	1.76
24	0.075	12	3	154	0.000	0.341	135.6	0.412	1.79	0.356	147.9	0.431	1.90
25	0.075	12	3	111	−0.05	0.176	196.2	0.212	0.99	0.179	223.4	0.230	1.16
26	0.075	12	3	110	0.05	0.171	146.6	0.223	1.14	0.165	162.3	0.215	1.12
27	0.075	12	3	111	0.000	0.150	157.3	0.188	0.98	0.168	153.8	0.208	1.00
28	0.075	12	3	111	0.000	0.171	158.2	0.211	1.04	0.175	160.3	0.220	1.10
29	0.075	12	3	111	0.000	0.150	157.3	0.188	0.98	0.168	153.8	0.208	1.00
30	0.075	12	3	111	0.000	0.171	158.2	0.211	1.04	0.175	160.3	0.220	1.10
31	0.075	12	3	111	0.000	0.150	157.3	0.188	0.98	0.168	153.8	0.208	1.00
32	0.075	12	3	111	0.000	0.171	158.2	0.211	1.04	0.175	160.3	0.220	1.10

Table F.4: Results of the ANOVA analysis: $R^2 = 0.9$, $R^2_{adj} = 0.887$ with 128 runs, and half-new cutting tool condition. Response Surface Regression: R_a versus f_z,D_{tool},ae,HB,$Curv$.

Estimated Regression Coefficients for R_a						
Term	Coef	SE Coef	T	p-value		
$Constant$	0.13829	0.006773	20.417	0.000		
f_z	0.0573	0.004	14.324	0.000		
D_{tool}	-0.0858	0.004231	-20.278	0.000		
ae	0.00953	0.004058	2.348	0.021		
HB	-0.0435	0.004565	-9.528	0.000		
$Curv$	0.00966	0.004053	2.383	0.019		
$f_z f_z$	0.01274	0.003356	3.796	0.000		
$D_{tool} D_{tool}$	0.03293	0.003781	8.708	0.000		
$HB \times HB$	0.07571	0.005234	14.465	0.000		
$f_z D_{tool}$	-0.0215	0.004833	-4.461	0.000		
$f_z Curv$	0.01401	0.004918	2.849	0.005		
$D_{tool} ae$	-0.0243	0.004828	-5.026	0.000		
$D_{tool} HB$	0.01059	0.00435	2.435	0.017		
$D_{tool} Curv$	0.01281	0.004828	2.653	0.009		
$HB Curv$	0.01775	0.004386	4.047	0.000		
$S = 0.03932$	$R^2 = 90.0\%$	$R^2(adj) = 88.7\%$				
ANOVA for R_a						
Source	DF	Seq SS	Adj SS	Adj MS	F	$P - value$
Regression	14	1.50224	1.50224	0.10730	69.40	0.000
Linear	5	0.88094	1.10216	0.22043	142.56	0.000
Square	3	0.49479	0.49247	0.49247	106.17	0.000
Interaction	6	0.12651	0.12651	0.12651	13.64	0.000
Residual error	108	0.16699	0.16699	0.16699		
Lack-of-Fit	35	0.13758	0.13758	0.13758	9.76	0.000
Pure Error	73	0.02941	0.02941	0.02941		
Total	122	1.66923				

test piece. The ***RSM*** was applied to build the model for the half-worn cutting tool condition. Following the same steps described in the previous sections, the *ANOVA* results are shown in Table F.6, where the variability of Ra is explained by the model with $R^2 = 92.70\%$ and the estimated parameters of model are significant in $R^2_{adj} = 91.60\%$.

Table F.6 shows the terms with a P-value< 0.05, and they were selected to fit the final model. After to select only the relevant factors, the analysis of variance was applied to confirm the squared error $R^2 = 0.927$ and the

Table F.5: Factors considered for the experiments, and the measurements of the parameters that allow the characterization of the R_a for the two sections. The cutting tool condition is half-worn edge.

						Section 01				Section 02			
Exp	f_z	D_{tool}	ae	HB	$Curv$	R_a	RSm	Rq	Rz	R_a	RSm	Rq	Rz
1	0.050	10	2	93	0.025	0.225	106.6	0.284	1.40	0.272	107.3	0.332	1.50
2	0.100	10	2	90	−0.025	0.376	214.7	0.485	2.22	0.440	219.8	0.578	2.02
3	0.050	16	2	90	−0.025	0.233	120.1	0.287	1.47	0.202	121.1	0.255	1.50
4	0.100	16	2	93	0.025	0.334	206.2	0.419	1.94	0.386	175.8	0.473	1.92
5	0.050	10	4	94	−0.025	0.346	185.9	0.425	2.09	0.366	219.5	0.444	2.15
6	0.100	10	4	89	0.025	0.460	204.4	0.600	3.00	0.466	182.5	0.617	3.00
7	0.050	16	4	89	0.025	0.231	94.3	0.285	1.47	0.258	107.1	0.314	1.50
8	0.100	16	4	94	−0.025	0.260	251.9	0.332	1.53	0.240	282.3	0.316	1.74
9	0.050	10	2	145	−0.025	0.182	130.2	0.232	1.24	0.155	134.8	0.204	1.05
10	0.100	10	2	144	0.025	0.414	133.9	0.480	1.93	0.758	178.9	0.912	3.69
11	0.050	16	2	144	0.025	0.206	110.7	0.270	1.41	0.15	95.4	0.197	1.10
12	0.100	16	2	145	−0.025	0.165	228.0	0.204	1.05	0.161	222.2	0.208	1.08
13	0.050	10	4	144	0.025	0.290	99.5	0.368	1.72	0.284	110.7	0.364	1.86
14	0.100	10	4	145	−0.025	0.952	235.9	1.233	6.20	0.569	238.2	0.749	4.34
15	0.050	16	4	145	−0.025	0.121	136.6	0.159	0.88	0.127	135.5	0.162	0.86
16	0.100	16	4	144	0.025	0.218	202.3	0.290	1.43	0.232	186.9	0.309	1.48
17	0.025	12	3	110	0.000	0.153	151.6	0.197	1.06	0.183	200.8	0.233	1.17
18	0.130	12	3	110	0.000	0.448	251.4	0.570	2.64	0.409	259.9	0.505	2.16
19	0.075	8	3	109	0.000	0.387	165.7	0.489	2.41	0.391	169.9	0.498	2.43
20	0.075	20	3	109	0.000	0.137	148.7	0.172	0.90	0.205	200.7	0.258	1.25
21	0.075	12	1	110	0.000	0.152	160.7	0.191	0.95	0.181	158.8	0.228	1.15
22	0.075	12	5	110	0.000	0.188	160.1	0.235	1.16	0.193	144.4	0.241	1.18
23	0.075	12	3	70	0.000	0.315	176.6	0.4	1.88	0.351	149.9	0.433	1.94
24	0.075	12	3	152	0.000	0.294	132.9	0.368	1.83	0.342	133.9	0.424	1.99
25	0.075	12	3	111	−0.05	0.244	176.9	0.313	1.46	0.230	188.3	0.274	1.17
26	0.075	12	3	110	0.05	0.164	197.4	0.208	1.20	0.198	151.2	0.249	1.22
27	0.075	12	3	110	0.000	0.206	172.5	0.262	1.30	0.218	149.5	0.268	1.23
28	0.075	12	3	110	0.000	0.192	154.7	0.247	1.23	0.166	164.3	0.207	1.04
29	0.075	12	3	110	0.000	0.206	172.5	0.262	1.30	0.218	149.5	0.268	1.23
30	0.075	12	3	110	0.000	0.192	154.7	0.247	1.23	0.166	164.3	0.207	1.04
31	0.075	12	3	110	0.000	0.206	172.5	0.262	1.30	0.218	149.5	0.268	1.23
32	0.075	12	3	110	0.000	0.192	154.7	0.247	1.23	0.166	164.3	0.207	1.04

Table F.6: Results of the ANOVA analysis: $R^2 = 0.927$, $R^2_{adj} = 0.916$ with 128 runs, and half-worn cutting tool condition. Response Surface Regression: R_a versus f_z,D_{tool},ae,HB,$Curv$.

Estimated Regression Coefficients for R_a						
Term	Coef	SE Coef	T	p-value		
$Constant$	0.18102	0.006818	26.551	0.000		
f_z	0.07536	0.003866	19.490	0.000		
D_{tool}	−0.0836	0.003906	−21.404	0.000		
ae	0.00893	0.003727	2.397	0.018		
HB	−0.0068	0.003297	−2.061	0.042		
$Curv$	−0.00005	0.003725	−0.014	0.989		
$f_z f_z$	0.0284	0.003452	8.227	0.000		
$D_{tool} D_{tool}$	0.03139	0.003451	9.096	0.000		
$HB \times HB$	0.04364	0.003212	13.585	0.000		
$Curv \times Curv$	0.00869	0.003329	2.609	0.010		
$f_z D_{tool}$	−0.03986	0.004480	−8.896	0.000		
$f_z \times HB$	0.03416	0.003706	9.217	0.000		
$f_z \times Curv$	−0.00886	0.004543	−1.950	0.054		
$D_{tool} ae$	−0.03216	0.004457	−7.215	0.000		
$D_{tool} HB$	−0.02981	0.003644	−8.181	0.000		
$D_{tool} Curv$	0.01686	0.004452	3.787	0.000		
$ae \times HB$	0.00789	0.003702	2.131	0.035		
$ae \times Curv$	−0.03261	0.004549	−7.169	0.000		
$S = 0.03601$	$R^2 = 92.7\%$	$R^2(adj) = 91.6\%$				
ANOVA for R_a						
Source	DF	Seq SS	Adj SS	Adj MS	F	$P - value$
Regression	17	1.76656	1.76656	0.10391	80.13	0.000
Linear	5	0.91810	1.08802	0.21760	167.79	0.000
Square	4	0.41454	0.42201	0.10550	81.35	0.000
Interaction	8	0.43392	0.43392	0.05424	41.82	0.000
Residual error	107	0.13876	0.13876	0.00129		
Lack-of-Fit	19	0.06300	0.06300	0.00331	3.85	0.000
Pure Error	88	0.07576	0.07576	0.00086		
Total	124	1.90532	1.90532			

adjusted squared error $R^2_{adj} = 0.916$. The final fitted model is given by

$$\begin{aligned} R_a \quad = \quad & 0.18102 + 0.07536 \times fz + 0.0284 \times fz^2 - 0.0836 \times D_{tool} + 0.03139 \times D^2_{tool} - 0.0068 \times HB + \\ & + 0.04364 \times HB^2 + 0.00893 ae - 0.03986 \times fz \times D_{tool} + 0.03416 \times fz \times HB - \\ & - 0.03216 \times D_{tool} \times ae - 0.02981 \times D_{tool} \times HB + 0.01686 \times D_{tool} \times Curv + \\ & + 0.0079 \times ae \times HB - 0.03216 \times ae \times Curv + 0.0087 \times Curv^2 \end{aligned} \tag{F.3}$$

The model was validated in agreement with the results show in Figure F.2. Figure F.2a. depicts the normal distribution of the residuals and it is observed that enough data were used to fit the model. Figure F.2. defines the normal probability plot, and the tendency (straight line) shows the normality of the error distribution. Also, Figure F.2c. shows an excellent spread of points on either side of zero, with no patterns of increase or decrease.

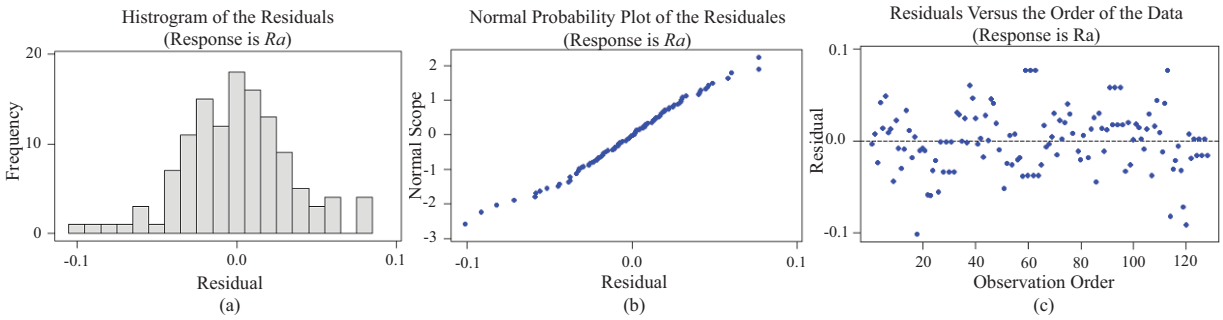

Figure F.2: Validation of the used information to build the Statistical Model for the half worn condition:(a) Normal distribution of the residuals; (b) Normal probability plot; (c) Spread of points.

F.4 Modeling of the R_a with *RSM* and worn cutting tool condition

The *DoE* was reproduced with the worn cutting tool condition, and the measurements of R_a were made for each test piece. Table F.7 presents the four parameters that were measured for the assessment of the R_a for each test piece. The *RSM* was applied to build the model for the worn cutting tool condition. Following the same steps described in the previous sections, the *ANOVA* results are shown in Table F.8, where the variability of Ra is explained by the model with $R^2 = 93.40\%$ and the estimated parameters of model are significant in $R^2_{adj} = 92.50\%$.

Table F.8 shows the terms with a P-value< 0.05, and they were selected to fit the final model. After to select only the relevant factors, the analysis of variance was applied to confirm the squared error $R^2 = 0.934$ and the adjusted squared error $R^2_{adj} = 0.925$. The final fitted model is given by

$$\begin{aligned} R_a \;=\; & 0.21686 + 0.06362 \times fz + 0.02246 \times fz^2 - 0.05339 \times D_{tool} + 0.02217 \times D^2_{tool} - 0.02236 \times HB + \\ & + 0.02962 \times HB^2 + 0.01674 Curv - 0.02925 \times fz \times D_{tool} + 0.01303 \times fz \times HB + \\ & + 0.0208 \times fz \times Curv - 0.00942 \times D_{tool} \times HB + 0.01582 \times D_{tool} \times Curv - 0.01047 \times ae \times HB - \\ & - 0.01047 \times ae \times Curv + 0.0175 \times HB \times Curv^2 \end{aligned} \tag{F.4}$$

The model was validated in agreement with the results show in Figure F.3. Figure F.3a. depicts the normal distribution of the residuals and it is observed that enough data were used to fit the model. Figure F.3b. defines the normal probability plot, and the tendency (straight line) shows the normality of the error distribution. Also, Figure F.3c. shows an excellent spread of points on either side of zero.

Table F.7: Factors considered for the experiments, and the measurements of the parameters that allow the characterization of the R_a for the two sections. The cutting tool condition is worn edge.

						Section 01				Section 02			
Exp	f_z	D_{tool}	ae	HB	$Curv$	R_a	RSm	Rq	Rz	R_a	RSm	Rq	Rz
1	0.050	10	2	94	0.025	0.266	89.5	0.321	1.48	0.27	94.8	0.338	1.58
2	0.100	10	2	94	−0.025	0.392	245.9	0.507	2.34	0.43	220.5	0.573	2.89
3	0.050	16	2	94	−0.025	0.253	112.9	0.314	1.66	0.23	128.3	0.297	1.64
4	0.100	16	2	94	0.025	0.324	181.4	0.410	1.81	0.28	195.8	0.364	1.71
5	0.050	10	4	91	−0.025	0.375	182.4	0.450	1.95	0.34	236.5	0.415	1.80
6	0.100	10	4	90	0.025	0.474	157.4	0.612	2.97	0.48	206.8	0.623	3.14
7	0.050	16	4	90	0.025	0.244	115.4	0.303	1.56	0.25	100.6	0.318	1.52
8	0.100	16	4	91	−0.025	0.258	244.2	0.333	1.58	0.24	218.9	0.323	1.63
9	0.050	10	2	141	−0.025	0.189	137.3	0.242	1.19	0.22	118.4	0.292	1.48
10	0.100	10	2	139	0.025	0.593	177.1	0.720	3.17	0.52	176.9	0.634	2.68
11	0.050	16	2	139	0.025	0.248	99.9	0.312	1.58	0.23	95.3	0.297	1.40
12	0.100	16	2	141	−0.025	0.173	229.1	0.230	1.25	0.16	234.3	0.212	1.06
13	0.050	10	4	139	0.025	0.265	97.8	0.327	1.50	0.21	102.3	0.274	1.30
14	0.100	10	4	140	−0.025	0.526	231.1	0.679	3.24	0.57	236.2	0.736	3.55
15	0.050	16	4	140	−0.025	0.107	261.0	0.134	0.70	0.11	132.6	0.154	0.86
16	0.100	16	4	139	0.025	0.307	183.4	0.385	1.77	0.32	172.6	0.405	1.70
17	0.025	12	3	109	0.000	0.177	154.2	0.225	1.27	0.16	101.9	0.215	1.12
18	0.130	12	3	109	0.000	0.465	238.4	0.587	2.81	0.47	240.6	0.578	2.54
19	0.075	8	3	108	0.000	0.312	182.3	0.395	2.01	0.32	213.6	0.417	2.02
20	0.075	20	3	108	0.000	0.266	155.0	0.334	1.65	0.23	156.1	0.290	1.45
21	0.075	12	1	109	0.000	0.217	167.8	0.271	1.29	0.22	143.7	0.287	1.37
22	0.075	12	5	109	0.000	0.269	167.5	0.343	1.65	0.25	169.7	0.317	1.50
23	0.075	12	3	69	0.000	0.402	165.1	0.504	2.44	0.40	162.6	0.498	2.27
24	0.075	12	3	154	0.000	0.271	145.4	0.336	1.55	0.24	128.6	0.308	1.53
25	0.075	12	3	110	−0.05	0.260	190.5	0.322	1.43	0.26	207.9	0.331	1.60
26	0.075	12	3	110	0.05	0.215	145.0	0.279	1.42	0.22	120.7	0.281	1.44
27	0.075	12	3	109	0.000	0.245	136.0	0.303	1.48	0.25	165.2	0.327	1.66
28	0.075	12	3	109	0.000	0.231	164.1	0.297	1.44	0.25	138.8	0.332	1.65
29	0.075	12	3	109	0.000	0.245	136.0	0.303	1.48	0.25	165.2	0.327	1.66
30	0.075	12	3	109	0.000	0.231	164.1	0.297	1.44	0.25	138.8	0.332	1.65
31	0.075	12	3	109	0.000	0.245	136.0	0.303	1.48	0.25	165.2	0.327	1.66
32	0.075	12	3	109	0.000	0.231	164.1	0.297	1.44	0.25	138.8	0.332	1.65

Table F.8: Results of the ANOVA analysis: $R^2 = 0.934$, $R^2_{adj} = 0.925$ with 128 runs, and worn cutting tool condition. Response Surface Regression: R_a versus f_z,D_{tool},ae,HB,$Curv$.

Estimated Regression Coefficients for R_a						
Term	Coef	SE Coef	T	p-value		
$Constant$	0.21686	0.004303	50.399	0.000		
f_z	0.06362	0.002620	24.278	0.000		
D_{tool}	−0.05339	0.002784	−19.178	0.000		
ae	−0.00083	0.002638	−0.313	0.755		
HB	−0.02236	0.002456	−9.105	0.000		
$Curv$	0.01674	0.002651	6.315	0.000		
$f_z f_z$	0.02246	0.002143	10.482	0.000		
$D_{tool} D_{tool}$	0.02217	0.002433	9.111	0.000		
$HB \times HB$	0.02962	0.002405	12.317	0.000		
$f_z D_{tool}$	−0.02925	0.003178	−9.206	0.000		
$f_z \times HB$	0.01303	0.002867	4.543	0.000		
$f_z \times Curv$	0.02080	0.003247	6.407	0.000		
$D_{tool} HB$	−0.00942	0.002806	−3.356	0.001		
$D_{tool} Curv$	0.01582	0.003178	4.979	0.000		
$ae \times HB$	−0.01047	0.002865	−3.653	0.000		
$ae \times Curv$	−0.01047	0.003251	−3.221	0.002		
$HB \times Curv$	0.01751	0.002875	6.091	0.000		
$S = 0.02549$	$R^2 = 93.4\%$	$R^2(adj) = 92.5\%$				
ANOVA for R_a						
Source	DF	Seq SS	Adj SS	Adj MS	F	$P - value$
Regression	16	1.00822	1.00822	0.06301	96.98	0.000
Linear	5	0.66311	0.70437	0.14087	216.81	0.000
Square	3	0.19460	0.19843	0.06614	101.80	0.000
Interaction	8	0.15051	0.15051	0.01881	28.95	0.000
Residual error	109	0.07082	0.07082	0.00065		
Lack-of-Fit	29	0.04410	0.04410	0.00152	4.55	0.000
Pure Error	80	0.02673	0.02673	0.00033		
Total	125	1.07904				

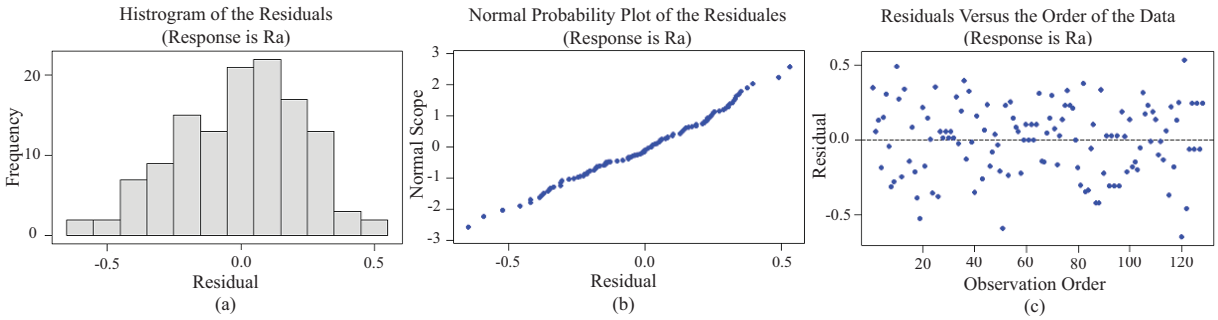

Figure F.3: Validation of the used information to build the Statistical Model for the worn cutting tool condition:(a) Normal distribution of the residuals; (b) Normal probability plot; (c) Spread of points.

F.5 Modeling of the R_a by using *ANN*

The modeling of R_a with *ANN* implies to pre-process the experimental data. First, the mean value of each variable was computed as follows,

$$\bar{x} = \frac{1}{n}\sum_{i=1}^{n}(x_i) \tag{F.5}$$

where the $\bar{x}$ is the mean value of a specific input variable.

Then, the average distance from the mean of the data set to a point must be computed. It represents the standard deviation, and it is defined as,

$$\sigma = \sqrt{\frac{1}{n-1}\sum_{i=1}^{n}(x_i - \bar{x})^2} \tag{F.6}$$

Secondly, the data were normalized with a mean zero and a standard deviation equal at one;

$$\bar{y_i} = \frac{x_i - \bar{x}}{\sigma} \tag{F.7}$$

where $\bar{y_i}$ defines the normalized input variables, and $i = 1, 2..., n$, represents the number of the input variable.

Third, another method for normalizing the data set was used. The *Bipolar sigmoidal* normalization was employed, and it is given by,

$$\bar{z_i} = \frac{1 - e^{-y_i}}{1 + e^{-y_i}} \tag{F.8}$$

where $\bar{z_i}$ defines the new normalized input variable, and $i = 1, 2..., n$, is the number of the input variable.

Appendix G

Tool-life testing procedure and parameters

This appendix presents the concepts, recommendations, and different tool-life parameters computed during the experimentation in the *CNC* Kondia machining center. The Tool-life parameters were obtained for the different Aluminium alloys and for the new, half-new, half-worn, and worn cutting tool condition.

G.1 Tool life testing procedure

This section is in agreement with the *ISO-8688-2* to measure and assessment the tool-life condition. The *ISO-8688-2* norm specifies some procedures for tool-life testing for end milling processes. The cutting conditions in end milling can be considered under two categories:

a) Conditions as a result of which tool deterioration is due to wear.

b) Conditions under which tool deterioration is due to other phenomena such as edge fracture or plastic deformation.

The tool life testing is conducted only for the tool wear condition. During the procedure to wear the cutting tool, important recommendations must be taken:

1. *Tool condition*. The diameter of the tool should not be reduced below 90% of the original diameter.

2. *Tool material*. The recommended tool materials are: uncoated high-speed steel, non-cobalt alloyed or cobalt alloyed, in accordance with *ISO 4957*. If the tool material is the test variable, the material classification and as many characteristics as possible shall be reported.

3. *Mounting the tool*. The cutter shall be securely fastened in the chuck and the runout of the cutter shall be carefully checked at the cutting edges. The maximum value of the runout at any point at the cutting edges shall not exceed of $50\mu m$ for the radial runout condition. The actual runout shall be measured and recorded.

4. *Cutting conditions*. The recommended cutting data must be chosen and combined in order to correspond and emphasize the milling principles. The cutting conditions for tests in which the feed per tooth f_z, the axial depth of cut ap, and the radial depth of cut ae are not the prime test variables, shall be selected from table G.1.

Table G.1: Recommended cutting conditions for end milling.

Cutting conditions	Up milling	Down milling
Axial depth of cut ap in mm	20	20
Radial depth of cut ae in mm	2.5	2.5
Feed f_z in mm/tooth	0.08	0.125

In cases where the cutting conditions indicated in table G.1 cannot be achieved, other values as close as possible to those indicated may be used. Other cutting conditions should be limited to the minimum values given in table G.2.

Table G.2: Minimum limits of cutting conditions.

Cutting conditions	End milling
Minimum feed per tooth f_z in mm per tooth	0.05
Minimum axial depth of cut ap in mm	2^a
Minimum radial depth of cut ae in mm	2^b

[a] For $ap < 0.25D_{tool}$ the value of ae should be at least $0.25D_{tool}$.
[b] For $ae < 0.25D_{tool}$ the value of ap should be at least $0.25D_{tool}$.

In practical workshop situations the time at which a tool ceases to produce workpieces of the desired size or surface quality usually determines the end of useful tool life. It is essential that tool life be defined as the total cutting time of the tool to reach a specified value of tool-life criterion. Here, it is necessary to identify and classify the cutting tool deterioration phenomena, and where it occurs at the cutting edges. The numerical values of tool deterioration are used to determine tool life governs the quantity of testing material required and the cost of testing. Before to explain the deterioration phenomena, some definitions are given.

- Tool wear: Change in shape of the cutting edge part of a tool from its original shape, resulting from progressive loss of tool material during cutting.
- Brittle fracture (chipping): Occurrence of cracks in the cutting part of a tool followed by the loss of small fragments of tool material.
- Tool deterioration measure: Quantity used to express the magnitude of a certain aspect of tool deterioration by a numerical value.

- Tool-life criterion: Predetermined value of a specified tool deterioration measure of the occurrence of a specified phenomenon.
- Tool life T_c: Total cutting time of the cutting part required to reach a specified tool-life criterion.

G.2 Methodology to wear the cutting tool

The process to wear the cutting tool considers two working conditions: (a) the wear of the cutting tool during the Design of Experiments (*DoE*); and (b) the wear of the cutting tool during the machining of the straight path until the flank wear reaches a specific value. The process implies to know the cutting conditions (C_c), cutting parameters (P_c), and the geometric parameters (P_G). This information allows to compute important parameters related with the metal cutting process, and they will be described in this section. The geometries used in the experimentation will be explained, together with the required equations to compute the tool-life parameters.

G.2.1 Convex geometry (Big Island)

The first geometry corresponds to a convex path (big island). Figure G.1 shows the geometry with the information necessary to compute the parameters. Given the measurements b and a, the radius R can be computed for the convex

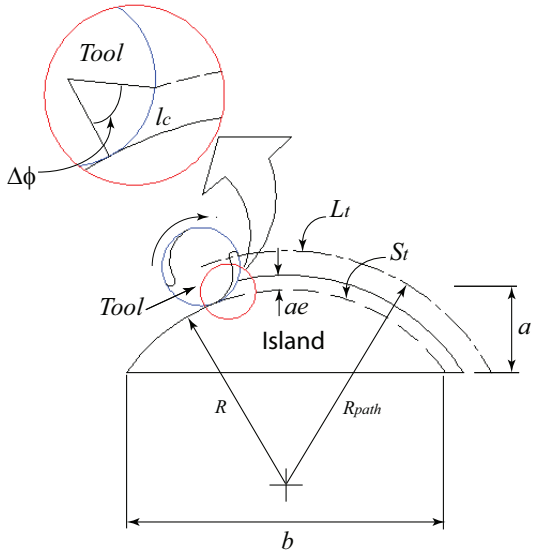

Figure G.1: Machining of the convex geometry.

path. The equation is,

$$R = \frac{a}{2} + \frac{b^2}{8a} \tag{G.1}$$

Given R, D_{tool}, and a values, the length of the arc that follows the cutting tool is defined as,

$$L_t = (R + R_{tool})2cos^{-1}\left(\frac{R-a}{R+R_{tool}}\right) \tag{G.2}$$

where $R_{tool} = D_{tool}/2$. Given the feed rate (v_f) and the length of the cutting tool path, the machining time is defined as,

$$t_m = \frac{L_t}{v_f} \tag{G.3}$$

The immersion angle of the cutting tool is given by

$$\Delta\phi = cos^{-1}\left[1 - \frac{2ae}{D_{tool}}\right] \tag{G.4}$$

The length of cut (l_c) is given by

$$l_c = R_{tool}(\Delta\phi) \tag{G.5}$$

The final length of the convex arc is defined as,

$$S_t = 2Rcos^{-1}\left(\frac{R-a}{R}\right) \tag{G.6}$$

The volume of removal metal is computed as,

$$Vol = ae \times ap \times S_t \tag{G.7}$$

The number of cycles made by the cutting tool edge over the workpiece material is defined as,

$$n_c = \frac{S_t}{f_z 2} \tag{G.8}$$

The cutting edge time during the peripheral process is defined as,

$$t_e = t_m \frac{\Delta\phi}{360} \tag{G.9}$$

G.2.2 Concave geometry (Big Box)

The second geometry corresponds to a concave path (big box). Figure G.2 shows the geometry with the required information to compute the parameters. Given the measurements b, a_1 and a_2, the distance a is equal to $(a_1 - a_2)$, and the radius R, for the concave path, is computed with Eq. (G.1). Given R, D_{tool}, and a values, the length of the arc that follows the cutting tool is defined as,

$$L_t = (R - R_{tool})2cos^{-1}\left(\frac{R-a}{R-R_{tool}}\right) \tag{G.10}$$

where $R_{tool} = D_{tool}/2$. Given the feed rate (v_f) and the length of the cutting tool path, the machining time is computed with Eq. (G.3). The immersion angle of the cutting tool is given by Eq. (G.4), and the length of cut (l_c) is computed with Eq. (G.5). The final length of the concave arc is computed with Eq. (G.6). The volume of the removed metal is computed with Eq. (G.7), and the number of cycles made by the cutting tool edge over the workpiece material is computed with Eq. (G.8). Finally, the cutting edge time during the peripheral process is defined by Eq. (G.9).

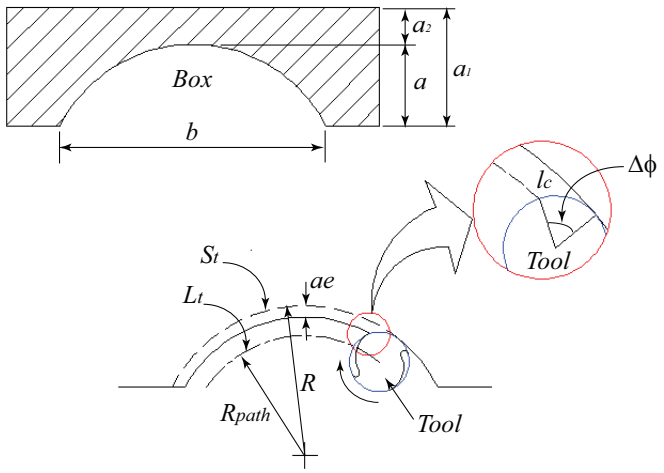

Figure G.2: Machining of the concave geometry.

G.2.3 Convex geometry (Small Island)

The third geometry corresponds to a convex path (small island). Given the measurements b and a, the radius R computed with Eq. (G.1). Given R, D_{tool}, and a values, the length of the arc that follows the cutting tool is obtained with Eq. (G.2). With the feed rate (v_f) and the length of the cutting tool path, the machining time is computed with Eq. (G.3).

The immersion angle of the cutting tool is given by Eq. (G.4), and the length of cut (l_c) is computed with Eq. (G.5). The final length of the convex arc is computed with Eq. (G.6). The volume of the removed metal is deduced with Eq. (G.7). The number of cycles made by the cutting tool edge over the workpiece material is computed with Eq. (G.8), and the cutting edge time during the peripheral process is defined by Eq. (G.9).

G.2.4 Concave geometry (Small Box)

The forth geometry corresponds to a concave path (small box). Given the measurements b, a_1 and a_2, the distance a is equal to $(a_1 - a_2)$, and the radius R is given by Eq. (G.1). Given R, D_{tool}, and a values, the length of the arc that follows the cutting tool is defined as,

$$L_t = (R - R_{tool}) \left(2\pi - 2cos^{-1} \frac{a - R}{R - R_{tool}} \right) \tag{G.11}$$

where $R_{tool} = D_{tool}/2$. With the feed rate (v_f) and the length of the cutting tool path, the machining time is computed with Eq. (G.3). The immersion angle of the cutting tool is given by Eq. (G.4).

The length of cut (l_c) is computed with Eq. (G.5), and the final length of the concave arc is given by Eq. (G.6). The volume of the removed metal is computed with Eq. (G.7), and the number of cycles made by the cutting tool

edge over the workpiece material is given by Eq. (G.8). Finally, the cutting edge time during the peripheral process is computed with Eq. (G.9).

G.2.5 Straight path geometry

The fifth geometry corresponds to a straight path. The machined length (L_t) is defined by the width of the aluminum block. Given the feed rate (v_f) and the machined length, the machining time is given by Eq. (G.3). The immersion angle of the cutting tool is computed with Eq. (G.4), and the length of cut (l_c) is given by Eq. (G.5). The final length of the cutting tool path is equal at,

$$S_t = L_t \tag{G.12}$$

The volume of the removed metal is computed with Eq. (G.7), and the number of cycles made by the cutting tool edge over the workpiece material is computed with Eq. (G.8). Finally, the cutting edge time during the peripheral process is obtained with Eq. (G.9).

G.3 Results of the tool-life tests

The tool-life parameters were computed for each Aluminium alloy and the four cutting tool wear conditions. Table G.3 with the results computed for the 6082 Aluminium alloy and new cutting tool condition.

The complete results of the flank wear evolution are shown in Tables G.4, G.5. The uniform flank wear (VB_{avg}) represents the average value of the two cutting tool edges, and the maximum flank wear (VB_{max}) corresponds to the higher value found in the cutting edges.

Table G.3: Tool-life parameters for the experiments with $6082-T6$ Aluminium alloy and new cutting tool condition. First column defines the workpiece hardness and number of the test piece. The cutting conditions are defined in columns from 2 to 4. The values of the Tool-life parameters are included in columns from 5 to 12.

				Mach.				First Mach.				Second Mach.			
Test piece	f_z	ae	D_{tool}	Time(s)		S_{t1}	S_{t2}	l_c	Vol	n_c	t_e	l_c	Vol	n_c	t_e
E2-01-6082	0.1	2	16	1.8	1.7	83	76	7.2	1250	417	0.26	5.8	764	382	0.19
IG-R45	0.05	2	10	3.3	3.1	83	77	5.8	1248	832	0.61	4.6	766	766	0.46
93 HBN	0.05	2	10	3.3	3.1	83	77	5.8	1248	832	0.61	4.6	766	766	0.46
	0.1	2	16	1.8	1.7	83	76	7.2	1250	417	0.26	5.8	764	382	0.19
E2-02-6082	0.1	2	16	1.8	1.7	83	76	7.2	1246	415	0.26	5.8	765	383	0.19
IG-R45	0.05	2	10	3.3	3.1	83	77	5.8	1250	833	0.61	4.6	766	766	0.46
94 HBN	0.05	2	10	3.3	3.1	83	77	5.8	1250	833	0.61	4.6	766	766	0.46
	0.1	2	16	1.8	1.7	83	76	7.2	1246	415	0.26	5.8	765	383	0.19
E2-03-6082	0.05	4	16	3.8	3.4	89	76	4.0	448	896	0.31	8.4	1530	765	0.57
IG-R45	0.1	4	10	1.8	1.5	89	76	3.2	448	448	0.18	6.8	1530	382	0.34
94 HBN	0.1	4	10	1.8	1.5	89	76	3.2	448	448	0.18	6.8	1530	382	0.34
	0.05	4	16	3.8	3.4	89	76	4.0	448	896	0.31	8.4	1530	765	0.57
E2-04-6082	0.05	4	16	3.8	3.4	89	77	4.0	448	896	0.31	8.4	1532	766	0.57
IG-R45	0.1	4	10	1.8	1.5	89	76	3.2	447	447	0.18	6.8	1529	382	0.34
93 HBN	0.1	4	10	1.8	1.5	89	76	3.2	447	447	0.18	6.8	1529	382	0.34
	0.05	4	16	3.8	3.4	89	77	4.0	448	896	0.31	8.4	1532	766	0.57
E2-05-6082	0.05	2	16	1.8	2.0	81	88	7.2	1224	816	0.26	5.8	879	879	0.24
CG-R35	0.1	2	10	1.1	1.2	81	87	5.8	1219	406	0.20	4.6	875	438	0.18
93 HBN	0.1	2	10	1.1	1.2	81	87	5.8	1219	406	0.20	4.6	875	438	0.18
	0.05	2	16	1.8	2.0	81	88	7.2	1224	816	0.26	5.8	879	879	0.24
E2-06-6082	0.05	2	16	1.8	2.0	80	87	7.2	1206	804	0.26	5.8	867	867	0.23
CG-R35	0.1	2	10	1.1	1.2	80	87	5.8	1199	400	0.20	4.6	867	434	0.18
93 HBN	0.1	2	10	1.1	1.2	80	87	5.8	1199	400	0.20	4.6	867	434	0.18
	0.05	2	16	1.8	2.0	80	87	7.2	1206	804	0.26	5.8	867	867	0.23
E2-07-6082	0.1	4	16	0.8	1.0	75	89	4.0	374	374	0.06	8.4	1774	443	0.17
CG-R35	0.05	4	10	1.9	2.4	75	87	3.2	375	749	0.20	6.8	1751	876	0.52
94 HBN	0.05	4	10	1.9	2.4	75	87	3.2	375	749	0.20	6.8	1751	876	0.52
	0.1	4	16	0.8	1.0	75	89	4.0	374	374	0.06	8.4	1774	443	0.17
E2-08-6082	0.1	4	16	0.8	1.0	75	87	4.0	374	374	0.06	8.4	1748	437	0.17
CG-R35	0.05	4	10	1.9	2.4	74	88	3.2	372	745	0.20	6.8	1760	880	0.52
92 HBN	0.05	4	10	1.9	2.4	74	88	3.2	372	745	0.20	6.8	1760	880	0.52
	0.1	4	16	0.8	1.0	75	87	4.0	374	374	0.06	8.4	1748	437	0.17

Table G.4: Evolution of the flank wear during the experimentation in the *CNC* Kondia machining center. Cutting tool diameters: 8 mm, 10 mm, and 12 mm.

$D_{tool} = 8$ mm							
Cutting Tool Condition	L_t mm	Mach.Time min	Vol mm^3	n_c	t_c min	VB avg	VB max
E2-VB	600	0.220	6000	4000	0.036	0.027	0.033
Tool condition VB-01	41536	23.995	620040	276906	4.526	0.073	0.104
E3-VB	600	0.22	600	4000	0.036		
Tool condition VB-02	69909	34.501	1042635	466060	6.504	0.101	0.123
E4-VB	600	0.22	6000	4000	0.036		
Tool condition VB-03	84360	39.851	1256400	562400	7.509	0.235	0.362
E5-VB	600	0.22	6000	4000	0.036		
Final values	84960	40.071	1262400	566400	7.545	0.332	0.389
$D_{tool} = 10$ mm							
Cutting Tool Condition	L_t mm	Mach.Time min	Vol mm^3	n_c	t_c min	VB avg	VB max
E2-VB	600	0.220	6000	4000	0.036	0.072	0.097
Tool condition VB-01	41536	23.995	620040	431946	4.526	0.096	0.108
E3-VB	5240	0.19	65596	39335	0.357		
Tool condition VB-02	87736	41.355	1300036	744348	7.411	0.116	0.129
E4-VB	5220	2.18	65248	39156	0.356		
Tool condition VB-03	100008	46.147	1471064	830517	8.202	0.235	0.45
E5-VB	5250	2.19	65604	39372	0.357		
Final values	105258	48.337	1536668	869889	8.559	0.43	0.468
$D_{tool} = 12$ mm							
Cutting Tool Condition	L_t mm	Mach.Time min	Vol mm^3	n_c	t_c min	VB avg	VB max
E2-VB	6100	2.62	63682	47232	0.346	0.043	0.086
Tool condition VB-01	33380	12.724	472882	213987	1.87	0.089	0.126
E3-VB	6100	2.62	63810	47274	0.347		
Tool condition VB-02	74558	28.336	1062862	495114	4.177	0.142	0.355
E4-VB	6100	2.62	63566	47141	0.345		
Tool condition VB-03	98202	37.453	1389588	659215	5.503	0.199	0.47
E5-VB	6100	2.62	63726	47232	0.346		
Final values	104302	40.073	1453314	706447	5.846	0.334	0.515

Table G.5: Evolution of the flank wear during the experimentation in the *CNC* Kondia machining center. Cutting tool diameters: 16 mm and 20 mm.

$D_{tool} = 16$ mm							
Cutting Tool Condition	L_t mm	Mach.Time min	Vol mm^3	n_c	t_c min	VB avg	VB max
E2-VB	5260	2.2	65676	39576	0.277	0.065	0.071
Tool condition VB-01	25951	9.863	376041	176502	1.268	0.096	0.105
E3-VB	5250	2.19	65604	39381	0.276		
Tool condition VB-02	72511	27.353	1061295	460683	3.523	0.13	0.139
E4-VB	5230	2.18	65401	39242	0.275		
Tool condition VB-03	98593	37.256	1439476	615770	4.798	0.193	0.471
E5-VB	5250	2.19	65577	39384	0.276		
Final values	103843	39.446	1505053	655154	5.073	0.214	0.573
$D_{tool} = 20$ mm							
Cutting Tool Condition	L_t mm	Mach.Time min	Vol mm^3	n_c	t_c min	VB avg	VB max
E2-VB	600	0.22	4000	4000	0.022	0.029	0.03
Tool condition VB-01	27800	10.294	408000	166222	1.159	0.09	0.147
E3-VB	600	0.22	6000	4000	0.022		
Tool condition VB-02	69610	25.777	1032150	399166	2.937	0.112	0.176
E4-VB	600	0.22	6000	4000	0.022		
Tool condition VB-03	98074	36.317	1456110	557966	4.146	0.22	0.499
E5-VB	600	0.22	6000	4000	0.022		
Final values	98674	36.537	1462110	561966	4.168	0.25	0.612

Appendix H

Theory of the Markov Hidden Models

Real world processes generally produce observable outputs which can be characterized as signals. The signals can be discrete in nature (e.g., characters from a finite alphabet, quantized vectors from a codebook, etc.), or continuous in nature (e.g., speech samples, temperature measurements, vibration signals, music, etc.). The signals can be stationary or non-stationary. The signals can pure or can be corrupted from other signal sources. A problem of fundamental interest is characterizing such real-world signals in terms of signal models. There are many reasons to consider this issue. First, a signal model can provide the basis for a theoretical description of a signal processing system that can be used to process the signal so as to provide a desired output. A second reason why signal models are important is that they are potentially capable of letting us learn a great deal about the signal source. But, the most important reason why signal models are important is that they often work extremely well in practice, and enable us to realize important practical systems (e.g. prediction systems, recognition systems, identification systems, etc.). Signal models can be divided into deterministic and statistical models. Deterministic models generally exploit some known specific properties of the signal, and we only need to determine values of the parameters of the signal model (e.g., amplitude, frequency, phase, etc.). Statistical models use the statistical properties of the signal. Examples of such statistical models include Gaussian processes, Poison processes, Markov Processes, and Hidden Markov processes. In this section, we are going to describe one type of stochastic signal model, Hidden Markov Model (*HMM*). A complete description of the *HMM* can be found in [Rabiner, 1989], and [Mohamed and Garder, 2000].

H.1 Discrete Markov processes

Consider a system which may be described at any time as being in one of a set of *N* distinct states, S_1, S_2, S_3,..., S_N. At regularly spaced discrete times, the system undergoes a change of state (possibly back to the same state) according to a set of probabilities associated with the state. The time instants associated with the state changes as *t = 1, 2,....*, and the actual state at time *t as* q_t. A full probabilistic description of the above system would , in general, requires specification of the current state (at time t), as well as all the predecessor states. For the special case of a discrete, first order, Markov chain, this probabilistic description is truncated to just the current and the predecessor

state, as shown in the following equation,

$$P[q_t = S_j | q_{t-1} = S_i, q_{t-2} = S_k, ...] = P[q_t = S_j | q_{t-1} = S_i] \tag{H.1}$$

Furthermore we only consider those processes in which the right-hand side of Eq.(H.1) are independent of time, thereby leading to the set of state transition probabilities $a_{i,j}$ of the form

$$a_{ij} = P[q_t = S_j | q_{t-1} = S_i], 1 \leq i, j \leq N \tag{H.2}$$

with the state transition coefficients having the properties

$$a_{ij} \geq 0 \tag{H.3}$$

$$\sum_{j=1}^{N} a_{ij} = 1 \tag{H.4}$$

Since, they obey standard stochastic constraints. The above stochastic process could be called an observation Markov model since the output of the process is the set of states at each instant of time, where each state corresponds to a physical event.

H.2 Extension to Hidden Markov Models

In this section, the concept of Markov models is extended to include the case where the observation is a probabilistic function of the state, and the resulting model (which is called a hidden Markov model) is a doubly embedded stochastic process with an underlying stochastic process that is not observable, but can only be observed through another set of stochastic processes that produce the sequence of observations. To figure out this ideas, the following example is presented.

Coin Toss Models. Assume that somebody is in a room behind a wall, and he can not see what is happening. On the other side of the wall there is another person who is performing a coin tossing experiment. The person will not comment anything about what he is doing exactly; he will only tell the result of each coin flip to the first person. Thus a sequence of hidden coin tossing experiments are performed, with the observation sequence consisting of a series of heads and tails, and it would be

$$\begin{aligned} \mathbf{O} &= O_1 O_2 O_3 \cdots O_T \\ &= HHJJJHJJH \cdots H \end{aligned}$$

where *H* stands for heads and *J* stands for tails.

Given the above scenario, the problem of interest is how do we build an *HMM* to explain the observed sequence of heads and tails. The first problem one faces is deciding what the states in the model correspond to, and then deciding how many states should be in the model. One possible choice would be to assume that only a single biased coin was being tossed. In this case, the situation could be modeling as a two-state model, where each state corresponds to a side of the coin (i.e., heads or tails). This model is depicted in Figure H.1a.

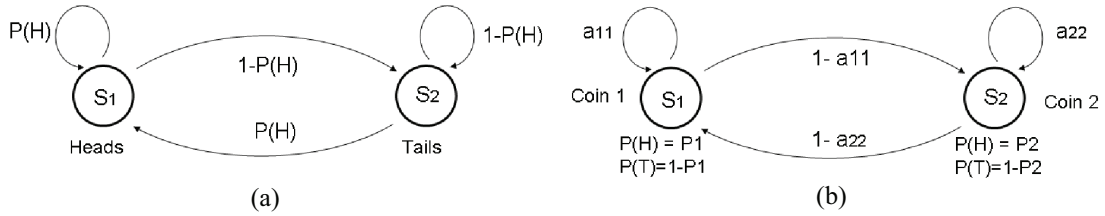

Figure H.1: (a) *HMM* with one coin and two states. (b) *HMM* with two coins and each state with two observations.

A second form of *HMM* for explaining the observed sequence of coin toss outcome is given in Figure H.1b. In this case, there are two states in the model and each state corresponds to a different, biased, coin being tossed. Each state is characterized by a probability distribution of heads and tails, and transitions between states are characterized by state transition matrix. The physical mechanism which accounts for how state transition are selected could itself be a set of independent coin tosses, or some other probabilistic events.

Given the choice among the three models shown in Figure H.1 for explaining the observed sequence of heads and tails, a natural question would be which model best matches the actual observations. It should be clear that the simple 1-coin model of Figure H.1a has only one unknown parameter, and the model of Figure H.1b has four unknown parameters. Therefore, with the greater degrees of freedom, the larger *HMMs* would seem to inherently be more capable of modeling a series of coin tossing experiments than would equivalently smaller models.

An *HMM* is characterized by the following parameters:

- N_s is the number of states in the model. Generally the states are interconnected in such a way that any state can be reached from any other state. The individual states are $S = S_1, S_2, \cdots, S_N$, and the state at time t as q_t.
- M is the number of distinct observation symbols per state. The individual symbols are $V = v_1, v_2, \cdots, v_M$.
- $A = a_{ij}$ is the state transition probability distribution. Where

$$a_{ij} = P[q_t = S_j | q_{t-1} = S_i], 1 \leq i, j \leq N \tag{H.5}$$

- $B = b_j(k)$ is the observation symbol probability distribution in state j. Where

$$b_j(k) = P[v_k att | q_t = S_j], 1 \leq j \leq N 1 \leq k \leq M \tag{H.6}$$

- $\pi = \pi_i$ is the initial state distribution. Where

$$\pi_i = P[q_1 = S_i], 1 \leq i \leq N \tag{H.7}$$

Given appropriate values of N, M, A, B, and π, the *HMM* can be used as a generator to give an observation sequence

$$O = O_1 O_2, \cdots, O_T \tag{H.8}$$

It can be seen from the above discussion that a complete specification of an *HMM* requires specification of two model parameters N_s, and M, specification of observation symbols, and the specification of the three probability measures A, B, and π. For convenience, it is used the compact notation

$$\lambda = (A, B, \pi) \tag{H.9}$$

for the complete parameter set of the model.

H.2.1 Baum-Welch Algorithm

The Baum-Welch algorithm, see [Rabiner, 1989], is used to adjust the model parameters to maximize the probability of the observation sequence given the model. The observation sequence used to compute the model parameters is called a training sequence. The training problem is crucial in the applications of the *HMMs*, because it allows us to optimally adapt model parameters to observed training data. The Baum-Welch algorithm is an iterative process that uses the forward and backward probabilities to solve the problem. The goal is to obtain a new model, $\overline{\lambda} = (\overline{A}, \overline{B}, \overline{\pi})$ to maximize the function,

$$Q(\lambda, \overline{\lambda}) = \sum_{Q} \frac{P(O, Q \mid \lambda)}{P(O|\lambda)} log\left[P(O, Q|\overline{\lambda})\right] \tag{H.10}$$

First, a current model is defined as $\lambda = (A, B, \pi)$, and used to estimate a new model as $\overline{\lambda} = (\overline{A}, \overline{B}, \overline{\pi})$. The new model must present a better likelihood than first model to reproduce the observation sequence. Based on this procedure, if $\overline{\lambda}$ is iteratively used in place of λ and repeat the calculus, then we can improve the probability of O being observed from the model until some limiting point is reached. The result of the recalculation procedure is called a maximum likelihood estimate of the *HMM*. At the end, the new set of parameters (means, variance, and transitions) is obtained for each *HMM*.

H.2.2 Viterbi Algorithm

In pattern recognition applications, it is useful to associate an "optimal" sequence of states to a sequence of observations, given the parameters of model. In pattern recognition, the feature vector, representing the observations, are known, but the sequence of states that defines the model is unknown. A "reasonable" optimality criterion consists in choosing the state sequence (or path) that brings a maximum likelihood with respect to a given model (i.e., best "explains" the observation). This sequence can be determined recursively via the *Viterbi* algorithm. This algorithm allows to find the single best state sequence, $Q = \{q_1\ q_2\ \cdots\ q_T\}$ for the given observation sequence $O = \{O_1\ O_2\ \cdots\ O_T\}$, and it makes use of two variables:

1. The highest likelihood $\delta_t(i)$ along a single path among all the paths ending in state i at time t:

$$\delta_t(i) = \max_{q_1, q_2, \cdots, q_{t-1}} P[q_1\ q_2\ \cdots q_t = i, O_1\ O_2 \cdots O_t|\lambda]$$

2. A variable $\psi_t(i)$ which allows to keep track of the "best path" ending in state j at time t.

Using these two variables, the algorithm implies the following steps:

1. Initialization
$$\delta_1(i) = \pi_i b_i(O_1) \ 1 \leq i \leq N$$
$$\psi_i = 0$$

2. Recursion
$$\delta_t(j) = \max_{1 \leq i \leq N} [\delta_{t-1}(i) a_{ij}] b_j(O_t), \ 2 \leq t \leq T, \ 1 \leq j \leq N$$
$$\psi_t(j) = arg \max_{1 \leq i \leq N} [\delta_{t-1}(i) a_{ij}], \ 2 \leq t \leq T, \ 1 \leq j \leq N$$

3. Termination:
$$P^* = \max_{1 \leq i \leq N} [\delta_T(i)]$$
$$q_T^* = arg \max_{1 \leq i \leq N} [\delta_T(i)]$$

4. Path (state sequence) backtracking:
$$q_t^* = \psi_{t+1}(q_{t+1}^*), \ t = T-1, T-2, \cdots, 1$$

The *Viterbi* algorithm delivers the best states path, which corresponds to the observations sequence. This algorithm also computes a likelihood along the best path.

H.3 Monitoring and diagnose the cutting tool wear condition

This section presents the results that were obtained by applying the Artificial Neural Network (*ANN*) approach for monitoring and diagnosing the cutting tool condition during the peripheral end milling process in *HSM*. A database was built with 441 experiments: 110 experiments with new cutting tool, 112 with half-new cutting tool, 110 with half-worn cutting tool, and 109 with worn cutting tool. A MonteCarlo simulation for the training/testing steps was implemented due to the stochasticity of the approach. The results correspond to the average of 10 runs, where for each run a different training data set (Tr) and testing data set (Ts) was generated.

H.3.1 Assessment of the cutting tool wear condition by using *ANN*

Additionally to the *HMMs*, classical approaches were implemented to compare both results. The cutting tool wear condition was modeled with an *ANN* model. The application of *ANN* to on-line process monitoring systems has attracted great interest due to their learning capabilities, noise suppression, and parallel computability. A complete recompilation of research works in on-line and indirect tool wear monitoring with *ANN* are presented in

[Sick, 2002b]. *ANN* is often defined as a computing system made up of a number of simple elements called neurons, which possesses information by its dynamic state response to external inputs. The neurons are arranged in a series of layers. Multi-layer feed-forward networks are the most common architecture. Furthermore, there are several learning algorithms for training neural networks. Back-propagation has proven to be successful in many industrial applications and it is easily implemented. The proposed architecture implies 12 input neurons, one hidden layer with 12 neurons, and one output neuron. Figure H.2 shows the *ANN* model, where the input neurons represent the following information: feed per tooth, tool diameter, radial depth of cut, workpiece material hardness, curvature, and the *MFCC* vector (7 dimensions).

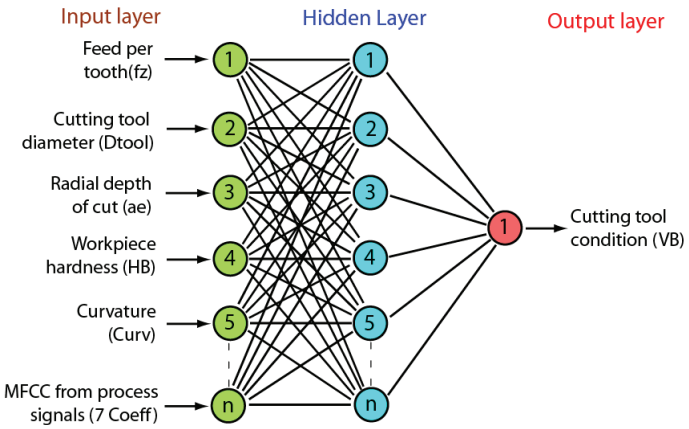

Figure H.2: ANN model implemented for monitoring and diagnosis the on-line cutting tool condition.

Feed-forward ANN model was applied with a "tanh" activation function. The trained algorithm was classical back-propagation. For computing, input data (f_z, D_{tool}, ae, HB, $Curv$, and *MFCC* vector) was normalized and output data was mapped to $[-1, 1]$. All the experimental data sets were normalized to avoid numerical instability. First, the data set was normalized by considering the mean value (μ), and standard deviation (σ) with the following equation,

$$f(x) = \frac{x - \mu}{\sigma} = \overline{x} \tag{H.11}$$

A second normalized method was applied: bipolar sigmoidal. This method was used because the minimum and maximum values are unknown in real-time. The non-linear transformation prevents most values from being compressed into essentially the same values, and it also compresses the large outlier values. The bipolar sigmoidal was applied with the following equation,

$$f(\overline{x}) = \frac{1 - e^{(-\overline{x})}}{1 + e^{(-\overline{x})}} \tag{H.12}$$

With respect to the output neuron, the cutting tool condition, the values were mapped between the normalized tool-wear and tool-wear condition (see Table H.1). Finally, the data set was randomly divided into two sets, training (70%), and testing (30%) sets, in order to measure their generalization capacity.

Table H.1: Tool-wear from *ANN* model is mapped with the cutting tool wear condition.

Normalized cutting tool condition	Cutting tool condition
From $+0.66$ to $+1.00$	New
From 0.0 to 0.66	Half-new
From -0.66 to 0.0	Half-worn
From -1.00 to -0.66	Worn

The performance of the ANN model was computed for ten different sets of data, which were selected in random form. The training and testing processes were programmed by using MatLab software. The obtained results correspond to 8 different *ANN* models, all of them with the same architecture but different *MFCC* vector. The *MFCC* were computed for each of the process signals (accelerometers, forces, and acoustic emission). Table H.2 shows the computed results with different process signals. The obtained performance corresponds to an average value from the ten data sets. Table H.2 shows that *ANN* model with Acoustic Emission signal (*AE*-Spindle) represents the best model for testing data set, with a performance of 89.9% and Mean Squared Error (*MSE*) of 0.10075. Figure H.3 plots the obtained results of the diagnosis system, when the *ANN* model was tested for the prediction of the cutting tool condition.

Table H.2: Performance of the *ANN* model with the training and testing data sets. The first two columns define the success of the accelerometers on the workpiece. The next two, the success of the accelerometers installed on the spindle. The last two columns define the success of the Acoustic Emission sensors.

Data	Workpiece		Spindle		$X4$	Y	*AE*	
sets	$Acc-X$	$Acc-Y$	$Acc-X$	$Acc-Y$	Force	Force	Spindle	Workp.
Training	90.2%	94.5%	97.8%	98.7%	94.2%	97.6%	99.9%	99.2%
Testing	31.3%	33.8%	40.4%	47.2%	48.5%	48.0%	89.9%	69.7%

H.4 Conclusions

This Appendix defines new ideas for monitoring and diagnosis the cutting tool wear condition by using *ANN* model. Feature vectors, based on the Mel Frequency Cepstrum Coefficients, were computed to characterize the process signals during the machining processes. First, with the cutting parameters and *MFCC*, the cutting tool condition was modeled with an *ANN* model. The feedfoward *ANN* model and back-propagation algorithm were used to define the *ANN* model. The proposed architecture implies 12 input neurons and one output neuron (cutting condition). The

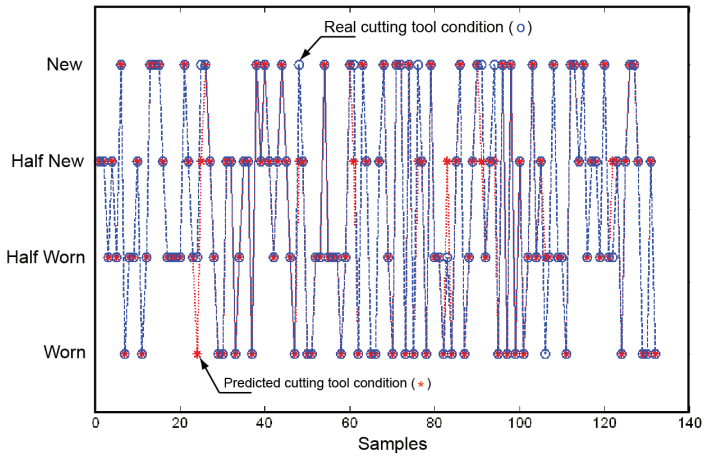

Figure H.3: Monitoring and Diagnosis the cutting tool condition with the *ANN*(12,12,1) model. The *MFCC* were computed for the acoustic emission signal (*AE*spindle).

best results were obtained by using the signals from the Acoustic Emission installed on the machine spindle. The success rate for the *ANN* model was 89.9% for the testing data set. The best performance was obtained with the *HMM* model.

Appendix I

Machining cost

An important task of the intelligent planning module is to recommend an optimal policy (actions) for operating the *CNC* machining center. A methodology based on the Markov Decision Process (*MDP*) was implemented to compute the expected total discount cost and the optimal policy. The application of the *MDP* requires an evaluation of the cost function for each action. The cost function must be defined for all cutting tool wear conditions and actions. For this application, the parameters and cost are shown in Tables I.1, and I.2. These parameters and cost were observed and registered during the experimentation with the cutting tools and materials defined in Chapter 4. The operating cost was obtained off-line and they must be modified according at the specific machining operation in the industry.

Table I.1: Time constants obtained during the experimentation, and used to compute the cost functions.

Concept	Symbol	Time
Time for inspection of the cutting tool	$t_{ins,tool}$	15 min
Time for inspection and changing of the cutting tool	t_{tool}	50 min
Average machining time of each workpiece	$t_{avg,m}$	1.2 min
Time for changing the workpiece of the *CNC*	t_{workp}	20.0 min
Machining time of each cutting tool ($8, 10, 12, 14, 16$ mm)	t_m	$45, 55, 40, 39, 36$ min
Cutting edge time of each cutting tool ($8, 10, 12, 14, 16$ mm)	t_e	$8.6, 9, 5.8, 5, 4.2$ min

The cost function depends of the selected cutting tool diameter and workpiece material. Therefore, the cost was computed for the $6082 - T6$ aluminium alloy and a cutting tool diameter of 16 mm. The experiments with these conditions were used to determine the optimal policy by applying the *MDP*.

- Evaluation of the cost function for the first action.

Table I.2: List of the cost required to compute the cost functions.

Concept	Symbol	Cost
Labor charge rate	L_c	\$0.18254 USD/min
Machining cost	M_c	\$0.833 USD/min
Rate to recover the capital cost of the machine	M_t	\$0.1538 USD/min
Cutting tools cost (8, 10, 12, 16, 20 mm)	$Tool_c$	\$81.3, 114, 145.9, 236, 364.8 USD
Workpiece cost (5083, 6082, 2024, CERTAL, 7075)	WP_c	\$15, 15, 20, 26, 30 USD

a) Evaluation of the operation cost. The constant operation cost is given by

$$Op_{c,cte} = (L_c + M_c) * (t_{avg,m} + t_{workp}) \tag{I.1}$$

During the machining process, the cutting tool edge presents a flank wear, and it increases the friction and cutting forces. Then, a power factor (P_f) must be defined to consider an increment in the *CNC* power due to these factors. The power factor was estimated by considering the observed behaviour in the cutting forces. By using the power factor, the real operation cost is defined as,

$$Op_{c,real} = Op_{c,cte} * P_f \tag{I.2}$$

The total cost of the cutting tool is divided by the machining time, and it is equal to,

$$T_{c,Wp} = t_{avg,m} * Tool_c)/t_m \tag{I.3}$$

Finally, the total operation cost is given by

$$Tot_c = Op_{c,real} + WP_c + T_{c,Wp} \tag{I.4}$$

By using these equations, the total cost, for each cutting tool condition, are defined in Table I.3.

b) The decision theory implies to compute the cost due to the uncertainty decision (see Table I.4).

c) The cost function is computed with the cost shown in Table I.5. The cost function for a_1 action, is given by,

$$f_{a_1} = \{44.15, 46.89, 49.28, 87.84, 320.52\} \tag{I.5}$$

- Evaluation of the cost function for the second action.

a) Evaluation of the operation cost. The operation cost is equal to the cost of the a_1 action, and it is shown in Table I.3.

b) The decision theory implies to use the cost in Table I.4.

Table I.3: Operation cost for the a_1 action.

Cutting tool condition	Constant operation cost	Power factor	Real operation cost	Workpiece cost	Tool cost /Workpiece	Total cost
New	\$21.53	1.016	\$21.89	\$15	\$7.26	\$44.15
Half-new	\$21.53	1.143	\$24.63	\$15	\$7.26	\$46.89
Half-worn	\$21.53	1.254	\$27.02	\$15	\$7.26	\$49.28
Worn	\$21.53	1.174	\$25.29	\$15	\$7.26	\$47.55
Fracture	\$21.53	1.097	\$23.63	\$15	\$7.26	\$45.89

Table I.4: Cost for the decision theory. Actions a_1 and a_2.

Cutting tool condition	Decision cost, (a_1)	Decision cost, (a_2)
New, Half-new, Half-worn	0	0
Worn	$WP_c + Op_{c,real} = \$40.29$	\$16.82
Tool fracture	$WP_c + Op_{c,real} = \$38.63$	\$38.63

Table I.5: Total cost required to compute the a_1 cost function.

	Cutting tool condition				
	New	Half-new	Half-worn	Worn	tool breakage
Decision cost	0	0	0	\$40.29	\$38.63
Operation cost	\$44.15	\$46.894	\$49.283	\$47.553	\$45.891
Tool cost	0	0	0	0	\$236.0
Cost function	\$44.154	\$46.894	\$49.283	\$87.844	\$320.521

Table I.6: Total cost required to compute the a_2 cost function.

	Cutting tool condition				
	New	Half-new	Half-worn	Worn	tool breakage
Decision cost	0	0	0	\$16.82	\$38.63
Operation cost	\$44.15	\$46.894	\$49.283	\$47.553	\$45.891
Tool cost	0	0	0	\$236.0	\$236.0
Cost function	\$44.154	\$46.894	\$49.283	\$300.372	\$320.521

c) The cost function is computed with the cost shown in Table I.6. The final cost function, for the a_2 action, is given by,

$$f_{a_2} = \{44.15, 46.89, 49.28, 300.37, 320.52\} \tag{I.6}$$

- Evaluation of the cost function for the third action.

a) Evaluation of the operation cost. The operation cost for the third action is shown in Table I.3.

b) The decision theory implies to use the cost in Table I.7.

Table I.7: Decision theory cost for the a_3 action.

Cutting tool condition	Decision cost
New	$t_{ins,tool} * (L_c + M_t) = \$5.05$
Half-new	\$5.05
Half-worn	\$5.05
Worn	\$5.05
Tool fracture	\$38.63

c) The cost function is computed with the cost shown in Table I.8. The final cost function, for the a_3 action, is given by,

$$f_{a_3} = \{49.2, 51.94, 54.32, 52.60, 320.52\} \tag{I.7}$$

Table I.8: Total cost required to compute the a_3 cost function.

	Cutting tool condition				
	New	Half-new	Half-worn	Worn	tool breakage
Decision cost	\$5.05	\$5.05	\$5.05	\$5.05	\$38.63
Operation cost	\$44.15	\$46.894	\$49.283	\$47.553	\$45.891
Tool cost	0	0	0	0	\$236.0
Cost function	\$49.20	\$51.939	\$54.328	\$52.598	\$320.521

Appendix J

List of publications

The design and implementation of the intelligent monitoring and supervisory control system implied to research, make exhaust experiments, and produce several publications to validate the proposal ideas and algorithms. The publications obtained during the research work were the following:

- Indexed publications.

    1. Vallejo Antonio Jr, Morales-Menéndez Rubén. Cost-Effective Supervisory Control System in Peripheral Milling using HSM. Special Issue in Annual Reviews in Control, 2009.
    2. Vallejo Antonio Jr, Morales-Menéndez Rubén, Elizalde Siller Hugo Ramón. Intelligent Control System for HSM. Journal of Automation, Mobile Robotics and Intelligent Systems, Poland, Volume 3, pp 54-53, July 2009.
    3. Vallejo Antonio Jr., Morales-Menéndez Rubén, Ramirez Cadena Miguel, Alique JR, Garza Castañon Luis E. Multi Sensor Data Fusion for High Speed Machining. Lecture Notes in Computer Science. Germany, pp 1162-1172, October, 2007.
    4. Vallejo Antonio Jr., Morales-Menéndez Rubén, Sucar Succar Enrique, Nolazco Flores J.A., Rodriguez Gonzalez Ciro. Tool-Wear Monitoring Based on Continuous Hidden Markov Models. Lecture Notes in Computer Science. Germany, pp 880-890, November, 2005.

- Publications in international congress.

    1. Vallejo Antonio Jr., Morales-Menéndez Rubén, Ramírez-Mendoza Ricardo, Garza-Castañon Luis. On-line Prediction of Surface Roughness in Peripheral Milling Processes. European Control Conference *ECC'09*. Hungary, August, 2009.
    2. Vallejo Antonio Jr., Morales-Menéndez Rubén, Ramírez-Mendoza Ricardo. Surface Roughness Modeling in Machining Processes. 13TH *IFAC* Symposium on Information Control Problems in Manufacturing. Moscow, pp 325-330, June, 2009.

3. Vallejo Antonio Jr., Morales-Menéndez Rubén, Elizalde Siller Hugo Ramón. Surface Roughness Modeling in Peripheral Milling Processes. 37o Transactions of the North America Manufacturing Research Institute. USA, pp 25-32, May, 2009.
4. Vallejo Antonio Jr., Morales-Menéndez Rubén. Decision Control System for HSM. 9TH *IFAC* Workshop on Intelligent Manufacturing Systems. Polony, pp 117-121, October, 2008.
5. Vallejo Antonio Jr., Morales-Menéndez Rubén, Alique José Ramon. Intelligent Monitoring and Decision Control System for Peripheral Milling Process. IEEE International Conference on Systems, Man and Cybernetics. Singapore pp 1620-1625, October, 2008.
6. Vallejo Antonio Jr., Morales-Menéndez Rubén, Alique José Ramon. Designing a Cost-Effective Supervisory Control System for Machining Processes. *IFAC-CEA07*, México, October, 2007.
7. Vallejo Antonio Jr., Morales-Menéndez Rubén, Nolazco Flores Juan Arturo, García Perera Leibny Paola. Low-Cost Cutting Tool Diagnosis Based on Sensor-Fusion. *IFAC-CEA07*, México, October, 2007.
8. Vallejo Antonio Jr., Morales-Menéndez Rubén, Garza Castañon Luis Eduardo, Alique José Ramon. Pattern Recognition Approaches for Diagnosis of Cutting Tool Wear. 35o Transactions of the North America Manufacturing Research Institute. USA, pp 81-88, May, 2007.
9. Morales-Menéndez Rubén, Vallejo Antonio Jr., Garza Castañon Luis Eduardo, Cantú Ortiz Francisco Javier, Abellán Nebot José Vicente. AI Approaches for Cutting Tool Diagnosis in Machining Processes. 25o Artificial Intelligence Applications 2007. Austria, pp 186-191, February 2007.
10. Abellán Nebot José Vicente, Morales-Menéndez Rubén, Vallejo Antonio Jr, Rodriguez Gonzalez Ciro, Romero Fernando. Comparación de ténicas de modelado para predicción del desgaste y acabado superficial para fresado. 16o XVI Congreso de Maquinas-Herramienta y Tecnologías de Fabricación. España, pp 935-953, October 2006.
11. Abellán Nebot José Vicente, Morales-Menéndez Rubén, Rodriguez Gonzalez Ciro, Vallejo Antonio Jr. Surface Roughness and Cutting Tool-Wear Diagnosis Based on Bayesin Networks. 6TH *IFAC* Symposium on Fault Dtetection Supervision and Safety of Technical Processes. China, pp 439-444, August 2006.
12. Vallejo Antonio Jr., Morales-Menéndez Rubén, Sucar Succar Enrique, Rodriguez Gonzalez Ciro. Diagnosis of a Cutting Tool in a Machining Center. 2006 International Joint Conference on Neural Networks. Vancouver, Canada, pp 7097-7104, July, 2006.
13. Abellán Nebot José Vicente, Rodriguez Gonzalez Ciro, Vallejo Antonio Jr, Morales-Menéndez Rubén, Romero Fernando. Comparison of Modeling Approaches in Surface Roughness and Cutting Tool Wear Condition for Face Milling Operations. 2o *CIRP*. Vancouver, Canada, June, 2006.
14. Vallejo Antonio Jr., Morales-Menéndez Rubén, Rodriguez Gonzalez Ciro, Sucar Succar Enrique. A methodology for tool wear diagnosis based on Hidden Markov Models. 2o *CIRP*. Vancouver, Canada, June, 2006.

- Publications in national and international congress.

    1. Aguilar Martínez Sheyla, Morales-Menéndez Rubén, Vallejo Antonio Jr, Ramirez Cadena Miguel, Rodriguez Gonzalez Ciro. Modelo Predictivo para acabado superficial en mecanizado de alta velocidad. XIV Congreso Internacional de Computación *CIC* 2005. México, Septiembre 2005.

- Publication in book's chapter.

    1. Vallejo Antonio Jr, Morales-Menéndez Rubén, Alique José Ramon. Robotics Automation and Control. On-line Cutting Tool Condition Monitoring in Machining Processes using Artificial Intelligence. *I-Tech.* Croacia, 2008. Pavla Pecherková, Mirsolav Flídr, Jindrich Duník, pp 143-166.

- Arbitrated publications.

    1. Morales-Menéndez Rubén, Aguilar Martínez Sheyla, Vallejo Antonio Jr., Ramirez Cadena Miguel, Cantú Ortiz Francisco Javier. Surface Roughness Modelling in High Speed Machining. Lecture Series on Computer and Computational Sciences. Leiden, The Netherlands, Vol 1, pp 827-830, October, 2005.
    2. Vallejo Antonio Jr, Morales-Menéndez Rubén, Nolazco Flores Juan Arturo, Sucar Succar Enrique, Rodriguez Gonzalez Ciro. New Approach in Monitor the Tool Condition in a CNC Machining Center. Lecture Series on Computer and Computational Sciences. Leiden, The Netherlands, Vol 1, pp 848-851, October, 2005.